

**PHOTOPOLYMERIZATION WITH NEW LED SYSTEMS  
EMITTING IN THE NEAR INFRARED REGION**

Dissertation

to obtain the academic degree of  
Doctor of Natural Sciences  
- Dr. rer. nat. -

by

**Yulian Pang**

born in Shandong, China

Faculty of Chemistry  
University of Duisburg Essen

**Essen, 2021**

The present work was carried out in the period from February 2018 to February 2021 under the supervision of Prof. Dr. Jochen Gutmann at the Institute of Physical Chemistry at the University of Duisburg-Essen in cooperation with the Niederrhein University of Applied Sciences in the working group of Prof. Dr. Bernd Strehmel at the Institute of Coatings and Surface Chemistry.

Date of Defense: 03.03.2021

Thesis Advisor: **Prof. Dr. Jochen Gutmann**  
University of Duisburg-Essen

**Prof. Dr. Bernd Strehmel**  
Niederrhein University of Applied Sciences

**Jun.-Prof. Dr. Eva Blasco**  
Heidelberg University

Chair: **Jun.-Prof. Dr. Michael R. A. Giese**  
University of Duisburg-Essen



# Explanation

I hereby confirm that I am entitled the present work with the title

“PHOTOPOLYMERIZATION WITH NEW LED SYSTEMS EMITTING IN THE NEAR INFRARED REGION”

independently written and have not used other than the sources and resources indicated, and this work submitted in this or similar form has never been done at any other university.

Yulian Pang

## DuEPublico

Duisburg-Essen Publications online

UNIVERSITÄT  
DUISBURG  
ESSEN

*Offen im Denken*

ub

Universitäts  
bibliothek

Diese Dissertation wird via DuEPublico, dem Dokumenten- und Publikationsserver der Universität Duisburg-Essen, zur Verfügung gestellt und liegt auch als Print-Version vor.

**DOI:** 10.17185/duepublico/74100

**URN:** urn:nbn:de:hbz:464-20210323-091158-7

Alle Rechte vorbehalten.



## Foreword

I would like to thank all the people who helped me in this wonderful way of my life as a Ph.D. student studying in Prof. Dr. Strehmel's group.

Foremost, I would like to show my great honour and appreciation to Prof. Dr. Strehmel who is my supervisor professor. I would like to thank him for giving me this opportunity to study in his group, which leads me on the way to climb the mountain of science in photochemistry fields. I appreciate his support and guidance very much, which always brings light to me when I am confused about my work. I also would like to thank him for all his help in my life in Germany, which let me feel very warm. I am grateful forever for his patience, encouragement, enthusiasm, and immense knowledge which let me feel great pleasure to be his student. Additionally, I also would like to thank Prof. Dr. Jochen Gutmann for his guidance, support, and valuable suggestions for my thesis.

I would like to thank all the current and former colleagues from Strehmel's Group. Working with them is a great experience, and the constructive discussion and inspiring ideas from them helped me make progress in my work. A few people who deserve special thanks, includes Dr. Ceren Kütahya, Dennis Oprych, Serbest Sheikmous, Paul Hermes, Qunying Wang, Lukas Appelhoff, Dr. Christian Schmitz, Dr. Micheal Schläpfer. It is my great pleasure to work with them in this special period of my life.

Furthermore, I would like to thank Prof. Dr. Veronika Strehmel for her supports and inspiring thoughts on my thesis. I also would like to thank her group members, Berran Sanay, Markus Heinz, and Dr. Micheal Schmitt for their help in my work.

I also would like to show my great appreciation and honour to Prof. Dr. Yingquan Zou who leads me in the way of science since 2009 and always hopes the best for my scientific career. In the past 11 years, he offered great help to me in my study life. I am deeply grateful for his guidance and encouragement inspiring me to face all the challenges in the way of science. I also would like to thank Prof. Dr. Jun Nie for his support of my study. I also would like to thank Prof. Dr. Weihai Fang, Prof. Dr. Zhonglin Lu, Prof. Dr. Louzhen Fan, Prof. Dr. Ganglong Cui, Prof. Dr. Ling Chen, Prof. Dr. Dongpeng Yan and Dr. Yong He for their help and support to my study.

I would like to thank all the colleagues from Prof. Dr. Zou's Group. Thanks for their support and help in the work and study. A few people who deserve special thanks, includes Mrs. Yiping Yang, Shuheng Fan, Yangyang Xin, Dr. Shiyzhuo Xiao, Dr. Yufei Deng, Yanhua Ding, Jing Wang, Mei Yi.

Last but not the least, I would like to thank my family for their support in my life, which give me great courage to face all the challenges. My father Yuehua Pang and my mother Chunlan Xu are the best parents in this world. They worked so hard to offer the best education to their children. I appreciate them forever for their patience, kindness, integrity, enthusiasm, positive attitudes towards life, which gives me an optimistic outlook on life. I would like to thank my husband Huimin Li who gives me the greatest support in my life after I met him. I appreciate his kindness, patience, responsibility, and love for me. He always is there whenever I need his support. I appreciate his presence in my life as my lover and best friend.

# Table of Contents

<b>Foreword</b> .....	<b>II</b>
<b>Table of Contents</b> .....	<b>III</b>
<b>Abbreviations</b> .....	<b>VI</b>
<b>List of Schemes</b> .....	<b>VIII</b>
<b>List of Figures</b> .....	<b>X</b>
<b>List of Charts</b> .....	<b>XIII</b>
<b>List of Tables</b> .....	<b>XIV</b>
<b>Abstract</b> .....	<b>XV</b>
<b>Kurzfassung</b> .....	<b>XVI</b>
<b>1. Introduction and Motivation</b> .....	<b>1</b>
1.1 Introduction .....	1
1.2 Motivation of the Thesis .....	6
<b>2. State of the Art</b> .....	<b>12</b>
2.1 Light Sources for Photopolymerization.....	12
2.1.1 Ultraviolet LEDs for Photopolymerization.....	14
2.1.2 Visible LEDs for Photopolymerization.....	15
2.1.3 Near-Infrared LEDs for Photopolymerization.....	16
2.1.4 NIR Laser Diodes for Photopolymerization .....	17
2.2 Photochemical Reactions for Generation and Regeneration of Activated Intermediates.....	19
2.2.1 Bond Cleavage upon Photoexcitation.....	20
2.2.2 Spectral Sensitisation Based on Photoinduced Electron Transfer .....	25
2.2.3 Thermal Decomposition.....	31
2.3 Photochemical Active Materials for Initiator Systems with NIR LED Exposure .....	33
2.3.1 Cyanines as NIR Sensitizers.....	33
2.3.2 Co-Initiators Applied for NIR Sensitized Polymerization .....	45
<b>3. Materials and Methods</b> .....	<b>55</b>
3.1 Light Sensitive Materials.....	55
3.1.1 NIR Sensitive Absorbers Derived from Heptamethine Based Cyanines .....	55
3.1.2 Co-initiators in the NIR Photoinitiating System .....	60
3.1.3 Monomers for Radical Photopolymerization .....	63
3.1.4 Monomers for Cationic Photopolymerization .....	65
3.1.5 Material for Quantification of Conjugate Acid Formed.....	67
3.2 Solvents.....	68

3.3 Methods.....	68
3.3.1 UV-Vis-NIR Spectroscopy .....	68
3.3.2 DSC and Photo-DSC.....	68
3.3.3 FTIR and RT-FTIR Spectroscopy.....	69
3.3.4 Cyclic Voltammetry.....	69
3.3.5 Mass Spectrometry and Coupling with Chromatographic Method.....	69
3.3.6 Dynamic Mechanical Analysis (DMA) .....	70
3.3.7 Conductivity Measurement of the Iodonium Salts .....	70
3.3.8 NIR Sensitive Camera .....	70
3.4 Light Sources.....	70
3.4.1 High Power NIR LEDs.....	70
3.4.2 NIR Lasers .....	71
<b>4. Further Experimental Details .....</b>	<b>72</b>
4.1 High Power NIR LED Photoinduced Free Radical and Cationic polymerization with the Initiating System Comprising Heptamethine Based Cyanine and Iodonium salt.....	72
4.1.1 NIR Sensitized Radical Photopolymerization .....	72
4.1.2 Heat-Promoted Free Radical Photopolymerization as Studied by Photo-DSC Measurement.....	72
4.1.3 Photobleaching and Photobleaching Kinetics of Heptamethine Based Cyanine in combination with Iodonium salt.....	74
4.1.4 Thermal Stability of the Initiating Systems Comprising Heptamethine based cyanine and Iodonium salt in TPGDA.....	74
4.1.5 NIR sensitised cationic photopolymerization .....	74
4.1.6 Photoproduct Analysis with LC-MS .....	75
4.1.7 Quantification of Conjugate Acid Formed .....	75
4.2 High-Power NIR LED Photoinduced Cationic and Radical/Cationic Hybrid Polymerization Using the Combination of Heptamethine Cyanine and Iodonium Salt as the Initiating System.....	76
4.2.1 NIR Sensitized Cationic and Hybrid Radical/Cationic Photopolymerization..	76
4.2.2 Photoproduct Analysis with LC-MS .....	76
4.2.3 Dynamic Mechanical Analysis (DMA) .....	77
4.2.4 Generation of Heat on Demand with NIR Absorber .....	77
4.2.5 Quantification of Conjugate Acid Formed .....	78
4.2.6 Conductivity Measurement.....	78
4.2.7 Viscosity Measurement .....	78
4.2.8 UV-Vis-NIR Measurement of Heptamethine Cyanines Solving in OXE-03.....	79
4.2.9 Dark Curing Measurement.....	79

4.3 High Power NIR LED Photoinduced Free Radical Polymerization (II): the Combination of Heptamethine Based Cyanine and Oxime Ester Serving as Initiating System ...	79
4.3.1 Free Radical Photopolymerization with Oxime Ester.....	79
4.3.2 NIR Sensitized Free Radical Photopolymerization with Initiating System Comprising Heptamethine and Oxime Ester.....	80
4.3.3 Generation of Heat on Demand with NIR Absorber .....	81
4.3.4 Beaching and Bleaching Kinetics of the Combination of Initiator Comprising Heptamethine and Oxime Ester.....	81
4.3.5 Thermal Stability of of the Combination of Initiator Comprising Heptamethine and Oxime Ester system.....	81
4.3.6 Laser Exposure.....	82
4.3.7 Cyclic Voltammetry.....	82
<b>5. Results and Discussion.....</b>	<b>83</b>
5.1 High Power NIR LED Photoinduced Free Radical and Cationic polymerization with the Initiating System Comprising Heptamethine Based Cyanine and Iodonium Salt.....	83
5.2 High-Power NIR LED Photoinduced Cationic and Radical/Cationic Hybrid Polymerization Using the Combination of Heptamethine Cyanine and Iodonium Salt as the Initiating System .....	98
5.3 High Power NIR LED Photoinduced Free Radical Polymerization (II): the Combination of Heptamethine Based Cyanine and Oxime Ester Serving as Initiating System.....	112
<b>6. Conclusions and Outlook.....</b>	<b>126</b>
<b>7. References .....</b>	<b>131</b>
<b>Acknowledgements .....</b>	<b>140</b>
<b>Curriculum Vitae .....</b>	<b>141</b>

## Abbreviations

NIR	Near infrared
UV	Ultraviolet
Vis	Visible
LED	Light emitting diode
IPNs	Interpenetrating polymer networks
DMA	Dynamic mechanical analysis
DSC	Differential scanning calorimetry
CTP	Computer to plate
UCNP	Up-conversion nanoparticle
PCB	Printed circuit board
VOCs	Volatile organic compounds
WCAs	Weakly coordinating anions
HOMO	Highest occupied molecular orbital
LUMO	Lowest unoccupied molecular orbital
CIDNP	Chemical induced dynamic nuclear polarisation
CTCs	Charge transfer complexes
FRPCP	Free radical promoted cationic polymerization
Sens	Sensitizer
Sens*	The excited sensitizer
IS	Iodonium salts
TPGDA	Tripropyleneglycol diacrylate
TMPTA	Trimethylolpropane triacrylate
PEGMA	Poly(ethylene glycol) methyl ether methacrylate (Mn 500)
LMA	Lauryl methacrylate
HBVE	4-Hydroxybutyl vinyl ether
ERL-4211	3,4-Epoxycyclohexanemethyl 3,4-epoxycyclohexanecarboxylate
OXT-03	3,3'-(Oxybis(methylene))bis(3-ethyloxetane)
RhB-L	Rhodamine B lactone
RhB-H	Rhodamine B
FTIR	Fourier Transform Infrared Spectroscopy
RT-FTIR	Real Time Fourier Transform Infrared Spectroscopy
CV	Cyclic voltammetry
OXE-01	1-[4-(Phenylthio)phenyl]-1,2-octanedione 2-(O-benzoyloxime)
OXE-02	[1-[9-ethyl-6-(2-methylbenzoyl)carbazol-3-yl]ethylideneamino] acetate
PET	Photoinduced electron transfer
$E_{ox}$	The oxidation potential
$E_{red}$	The reduction potential
$E_{coul}$	The coulomb term
$\Delta G_{PET}$	The free enthalpy of photoinduced electron transfer
$\Delta G_{PET}^{\ddagger}$	The free activation enthalpy
$k_{PET}$	The kinetic constant of photoinduced electron transfer

$S_0$	The ground state
$S_1$	The singlet state
$T_1$	The triplet state
ISC	Intersystem crossing
IC	Internal conversion
OP	Absorption of one photon
IVR	Intramolecular vibrational relaxation
VR	Vibrational relaxation
VC	Vibrational cooling
ISC'	Reverse intersystem crossing
F	Fluorescence
$\Phi_f$	The fluorescence quantum yield
P	Phosphorescence
DF	Delayed fluorescence
$pK_b$	The $-\log$ of base dissociation constant
PS	Photosensitizer
PS*	The excited photosensitizer
$T_g$	Glass transition temperature
$E'$	The storage modulus
$E''$	The loss modulus
CH <sub>2</sub> Cl <sub>2</sub>	Dichloromethane
DMSO	Dimethylsulfoxide
MeOH	Methanol
BuAc	<i>n</i> -Butyl acetate

## List of Schemes

Scheme 1. General principle of photopolymerization, modified from [164].	20
Scheme 2. Reaction path for $\alpha$ , $\beta$ , $\gamma$ -cleavage of carbonyl compounds, modified from [11].	22
Scheme 3. $\alpha$ -cleavage of the carbonyl group, cited from [1, 11, 67, 164].	23
Scheme 4. The photolysis mechanism of some photoacid generators, cited from [182].	24
Scheme 5. Heterolytic cleavage of arene diazonium salts, cited from [183-184].	25
Scheme 6. Heterolytic cleavage of sulfonium salts comprising an alkyl moiety in $\alpha$ -position, modified from [186].	25
Scheme 7. Thermolysis mechanism of alkoxyamine initiators, azo initiators, and peroxides, cited from [51].	31
Scheme 8. Thermal induced polymerization of vinyl ethers employing diaryliodonium salt, cited from [194].	32
Scheme 9. Thermal induced polymerization of vinyl ethers employing sulfonium salt, cited from [194].	32
Scheme 10. Thermolysis of oxime esters.	32
Scheme 11. The reaction mechanism of the combinations of NIR initiating system comprising three components upon NIR exposure, modified from [19].	42
Scheme 12. The influence of heat in the NIR photoinduced polymerization, cited from [19].	42
Scheme 13. Mechanism of the combination of NIR initiators comprising heptamethine cyanines as sensitizers and iodonium salts as coinitiators, cited from [19].	43
Scheme 14. Heptamethine cyanine dye 1,1',3,3,3',3'-hexamethylindotrycarbocyanine iodide (HITC) and postulated radical initiation mechanism accelerated by methyl diethanolamine (MDEA) upon NIR laser exposure, cited from [221].	44
Scheme 15. Photobleaching of heptamethine cyanine absorbers with NIR light under oxygen conditions, cited from [19].	44
Scheme 16. Photobleaching of sensitizer comprising barbiturate moiety after redox reaction with iodonium salt by cleavage at the conjugated double bond position (P2, P3, P4, P5) and recombination with aryl radicals (P6), cited from [19].	45
Scheme 17. Photolysis of iodonium salts, cited from [231].	48
Scheme 18. Strategies for designing long-wavelength cationic photoinitiating systems, cited from [27].	48
Scheme 19. Mechanism of photosensitizers sensitised diaryliodonium salts by PET, modified from [27, 231].	49
Scheme 20. Photolysis mechanism of oxime esters, cited from [77].	52
Scheme 21. The CTCs of amine/phosphine-iodonium salt combination system and the CTCs of amine/phosphine-sulfonium salt combination system as photo-thermal dual functional combination initiators, cited from [254].	54
Scheme 22. Free radical photopolymerization of acrylate monomers upon light exposure: (1) initiation, (2) propagation, (3) chain transfer, (4) termination, cited from [258].	64

Scheme 23. The cationic polymerization mechanism of the vinyl ethers, cited from [260].	66
Scheme 24. The cationic polymerization mechanism of oxiranes, cited from [258].	66
Scheme 25. The cationic polymerization mechanism of the oxetanes, cited from [111].	67
Scheme 26. Mechanism of RhB-L serving as tracer agent of conjugate acid, modified from [41].	68
Scheme 27. The oxidation pathways of the cyanine carrying cyclopentene in meso-position: path a) [86] oxidised by MnO <sub>2</sub> following the general redox reaction; or path b) oxide by iodonium salts following the photochemical redox reaction. The latter competitively causes formation of the photoproduct with fulvene pattern or bond cleavage of the polymethine chain, published in [96].	96
Scheme 28. Proposal of possible reactions mechanism contributing to generation of radicals by NIR-sensitized activated PET or heat released by NIR sensitizers, published in [118].	119



## List of Figures

Figure 1. The classification of light used in the photochemical sciences, cited from [121].	13
Figure 2. Emission spectra of some UV LEDs	14
Figure 3. Emission spectra of some visible LEDs, cited from [143].	15
Figure 4. Emission spectra of some NIR LEDs, modified from [19].	17
Figure 5. NIR laser used in CTP external drum and line shape laser, cited from [35].	18
Figure 6. Bond cleavage styles upon photoirradiation.	21
Figure 7. Energetic relations of PET considering two scenarios. a) Donor D absorbs the light energy. b) Acceptor A absorbs the light energy.	27
Figure 8. Energetic relations of PET with internal barrier causing threshold systems, a) endothermal conditions with $> 0$ , b) thermoneutral conditions with $=0$ , c) exothermal conditions with $<0$ , d) exothermal conditions with $\ll 0$ .	29
Figure 9. Electronic absorption spectra of carbo-cyanines carrying different numbers of methine in $\text{CH}_2\text{Cl}_2$ , cited from [200].	35
Figure 10. The UV-Vis-NIR absorption spectra of two symmetrical cyanines and the corresponding unsymmetrical cyanine in DMSO, cited from [200].	36
Figure 11. Photophysical processes of an excited absorber/photoactive molecule, modified from [37]. Absorption of one photon (OP), vibrational cooling (VC), internal conversion (IC), intramolecular vibrational relaxation (IVR), intersystem crossing (ISC), reverse intersystem crossing (ISC'), and vibrational relaxation (VR) to non-radiative events while fluorescence (F), and phosphorescence (P) radiatively occur. Photochemistry occurs from both the first excited singlet state (S1) and first excited triplet state (T1). Fluorescence (F) and delayed fluorescence (DF) exhibit similar emission wavelength while the decay of DF occurs in the time frame of the T1; that is significantly larger compared to the S1. This scheme does not include delayed phosphorescence showing a similar fluorescence spectrum with similar maximum but the decay occurs in the time frame of the T1.	39
Figure 12. Electron transfer processes of between excited Sens* and acceptor A, and the different pathways to consume Sen*: (a) back electron transfer, (b) decomposition, or (c) electron transfer with donator D, cited from [19].	41
Figure 13. The emission of the high power NIR LEDs	71
Figure 14. Bleaching kinetics of the combination of NIR initiating system including S4, S9, and S18 ( $7.0 \times 10^{-6} \text{ mol} \cdot \text{g}^{-1}$ ) and iodonium salt IS1 ( $3.0 \times 10^{-5} \text{ mol} \cdot \text{g}^{-1}$ ) in PEGMA using the high intensity NIR LED device, published in [96]. More details in Section 4.1.3 explain the experimental conditions.	86
Figure 15. The double bond conversion of TPGDA with different combinations of initiating system including sensitizers (S1-S24, 0.05 wt%) and iodonium salt IS1 (2 wt%) upon NIR LED exposure, published in [96]. More details in Section 4.1.1 explain the experimental conditions.	87
Figure 16. Photo-DSC measurements of the polymerization of TPGDA with the sensitizers (0.05 wt%) a) S4, b) S5, c) S14, and d) S16 and coinitiator IS1 (2.0 wt%) at different operating temperatures (40 °C, 50 °C, 70 °C) upon 805 nm NIR LED exposure, solid line: polymerization rate (RP), dashed line: conversion, published in [96]. More details in Sec-	

- tion 4.1.2 explain the experimental conditions. ....89
- Figure 17. Energetic relations of PET with internal barriers resulting in threshold systems: a) endothermal conditions, b) thermoneutral conditions, c) exothermal conditions, cited from [36]. 90
- Figure 18. Increasing absorption of the acetone solution comprising sensitiser and IS2 at 556 nm because of protonation of the RhB-L by conjugate acid generated from the system upon 805 nm NIR LED exposure (1.2 W·cm<sup>-2</sup>, 10 min). (a) S4/IS2, (b) S18/IS2, published in[96]. More details in Section 4.1.7 explain the experimental conditions. ....91
- Figure 19. RT-FTIR conversion degree-time profiles of cationic photopolymerization of Epikote 828 using the combination of S4 in different concentration and IS2 (2 wt%) upon 805 nm NIR LED exposure (1.2 W·cm<sup>-2</sup>), published in [96]. More details in Section 4.1.5 explain the experimental conditions. ....92
- Figure 20. Change of the UV-Vis-NIR absorption of S15 a), S3 b) and S4 c) upon 805 nm NIR LED exposure using the iodonium salt IS1 as coinitiator in PEGMA, the blue curve and the red dashed curve in c) exhibit the absorption of the photoproduct of S4 (blue) and that of S4-ref (red dashed), published in [96]. More details in Section 4.1.3 explain the experimental conditions. ....94
- Figure 21. (a) LC-signal of the photoproducts of S4 and IS1 after exposure with the NIR LED device (1.2 W·cm<sup>-2</sup>, 10 min) extracted from the polymer film of PEGMA. (b) LC-signal of the oxidised reference material S4\_ref was used without further treatment for the LC-MS experiment, published in [96]. More details in Section 4.1.6 explain the experimental conditions. ....95
- Figure 23. Electrostatic potential surface of the anions. a: [PF6]<sup>-</sup>, b: [PF3(C2F5)3]<sup>-</sup>, c: [PF3(n-C4F9)3]<sup>-</sup>, d: [Al(O-t-C4F9)4]<sup>-</sup>, e: [Al(O(C3F6)CH3)4]<sup>-</sup>, f:[C(O-SO2CF3)3]<sup>-</sup>, g: [TsO]<sup>-</sup>. Calculation results base on density functional theory based of B3LYP/6-31G\* method. Results obtained regarding the volume and surface are as follows: a: 84 Å<sup>3</sup>, b: 259 Å<sup>3</sup>, c: 433 Å<sup>3</sup>, d: 582 Å<sup>3</sup>, e: 501 Å<sup>3</sup>, published in [115]. ....105
- Figure 24. RT-FTIR conversion degree-time profiles of the polymerization of TMPTA and the polymerization of cationic polymerisable groups comprised in epoxide ERL-4211 and oxetane OXT-03, respectively, published in [115]. More details in Section 4.2.1 explain the experimental conditions. ....107
- Figure 25. The temperature-time profiles of the combination of initiating system S27/IS5 ([S27]=6·10<sup>-3</sup> mmol·g<sup>-1</sup>, [IS5] = 3.8·10<sup>-2</sup> mmol·g<sup>-1</sup>) in different monomers upon irradiation with 805 nm NIR LED (1.2 W·cm<sup>-2</sup>), published in [115]. More details in Section 4.2.4 explain the experimental conditions. ....108
- Figure 26. Profiles for generation of conjugate acid as a function of exposure time at 805 nm (Intensity: 1.2 W·cm<sup>-2</sup>) according to a previous procedure using RhB-L to probe quantitatively the amount on acidic species. Measurements were carried out LMA and BuAc ([Sens] = 4.1×10<sup>-5</sup> M, [IS] = 5.6×10<sup>-4</sup> M), published in [115]. More details in Section 4.2.5 explain the experimental conditions. ....109
- Figure 27. DMA data (tan δ) of films (thickness: 120 μm) exposed using 395 nm LED (1.1 W·cm<sup>-2</sup>, 2 min) and 805 nm LED (1.2 W·cm<sup>-2</sup>, 10 min) in the case of the monomers TMPTA, ERL-4211, and the mixture of TMPTA and ERL (TMPTA / ERL-4211, 1:1), published in [115]. More details in Section 4.2.3 explain the experimental conditions. ....110

- Figure 28. The photo-DSC conversion–time profiles of the polymerization of TPGDA comprising different oxime esters (0.05 wt%) applying a 395 nm UV LED (0.1 W·cm<sup>-2</sup>) with Photo-DSC, published in [118]. More details in Section 4.3.1 explain the experimental conditions. ....113
- Figure 29. Radical photopolymerization of TPGDA comprising S18 (0.05 wt%) and the OXE-01 (2 wt%) using different power NIR LEDs, published in [118]. More details in Section 4.3.2 explain the experimental conditions. ....115
- Figure 30. The temperature-time profiles of the samples (thickness is 160 μm) comprising the monomer TPGDA and the combination of NIR initiator systems (a) samples comprising different sensitizers (0.5 wt%) and OXE-01 (2 wt%), irradiated with the 805nm LED (1.2 W·cm<sup>-2</sup>), (b) samples comprising different sensitizers (0.5 wt%) and OXE-01 (2 wt%) irradiated with the 860nm LED (1.5 W·cm<sup>-2</sup>), (c) samples comprising COXE-15 (2 wt%) and S18 in different concentrations, irradiated with the 805nm LED (1.2 W·cm<sup>-2</sup>), published in [118]. More details in Section 4.3.3 explain the experimental conditions.....116
- Figure 31. RT-FTIR conversion degree-time profiles of TPGDA (a) comprising S18 (0.05 wt%) and different oxime esters (2 wt%), (b) comprising S21 (0.05 wt%) and OXE-01 in different concentrations, (c) comprising different sensitizers (0.05 wt%) and OXE-01 (2 wt%), irradiated with the 870 nm LED (1.2 W·cm<sup>-2</sup>), published in [118]. More details in Section 4.3.2 explain the experimental conditions. ....117
- Figure 32. Change of UV-Vis-NIR spectra of S18 (a), S4 (b), and S25 (c) upon exposure with 805nm NIR LED (1.2 W·cm<sup>-2</sup>) and employing OXE-01 as coiniciator in PEGMA. The blue and the red curves in figure 32b and 32c depict the absorption of the respective oxidized product with fuleven structure. For a sake of simplicity, only the cyanine structure was included, published in [118]. More details in Section 4.3.4 explain the experimental conditions. ....121
- Figure 33. The bleaching kinetics of S5 (blue) and S25 (red). LMA solution including sensitizer (3.5×10<sup>-6</sup> mol·L<sup>-1</sup>), OXE-01 (2.0×10<sup>-5</sup> mol·L<sup>-1</sup>) was irradiated with the 805 nm NIR LED device (1.2 W·cm<sup>-2</sup>) at different exposure time, published in [118]. More details in Section 4.3.4 explain the experimental conditions. ....123
- Figure 34. Electron density in the HOMO and LUMO of S25, S25\_ref obtained after a DFT calculation based on the B3LYP//6-31G\* method implemented in Spartan 16 to optimise the ground state, published in [118]. ....124

## List of Charts

Chart 1. The chemical structure of SS1 and SS2, cited from [185, 187].	25
Chart 2. Typical Type II photoinitiators and co-initiators, cited from [24].	28
Chart 3. Quinoline blue-the first dye named by cyanine, cited from [201].	33
Chart 4. General structure of cyanine compounds, cited from [205].	34
Chart 5. Chemical structure of the heptamethine with different methine chain, cited from [37].	35
Chart 6. Different terminal groups in cyanine chemical structures.	36
Chart 7. Substituted 2,3,3-trimethylindolium-, 2,3,3-benzo[e]indolium-, and 2,3,3-benzo[c,d]indolium salts results in the patterns A1/A1', A2/A2' and A3/A3' of the terminal substituent A in Chart 5, respectively, cited from [37].	37
Chart 8. Different substituent groups in meso-position of the heptamethine chain results in pattern B in Chart 5, cited from [37].	38
Chart 9. General structure of iodonium salts, cited from [232].	46
Chart 10. Some general diaryliodonium salts, cited from [46, 236-237].	47
Chart 11. Some radical photoinitiators working in the FRPCP, cited from [167].	50
Chart 12. The structure of the oxime esters: Quantacure PDO, OXE-01, OXE-02, cited from [67].	51
Chart 13. Some new oxime esters with longer absorption wavelength, cited from [28, 69, 79-80, 82, 85].	53
Chart 14. Some examples of thermal free radical initiators, cited from [51].	54
Chart 15. NIR sensitizers of structure 1 comprising different terminal groups a/a', b/b' and substituent R 2 in the meso-position, modified from [96].	85
Chart 16. Chemical structure of the NIR sensitizers 1, 1' and iodonium salts 2 used in this part of work (the structures of the anion X <sup>-</sup> are shown in Chart 17), published in [115].	98
Chart 17. Structures of ion X <sup>-</sup> serving as counter ions for sensitizers, and iodonium salts used in this part of work. a: [PF6] <sup>-</sup> , b: [PF3(C2F5)3] <sup>-</sup> , c: [PF3(n-C4F9)3] <sup>-</sup> , d: [Al(O-t-C4F9)4] <sup>-</sup> , e: [Al(O(C3F6)CH3)4] <sup>-</sup> , f: [C(O-SO2CF3)3] <sup>-</sup> , g: [TsO] <sup>-</sup> , published in [115].	100

## List of Tables

Table 1. NIR sensitizers (S1-S29) used in this thesis [96, 115, 118].	55
Table 2. Iodonium salts (IS1-IS7) used in this thesis [96, 115, 118].	61
Table 3. The oxime esters used in this thesis [118].	63
Table 4. The radical monomers used in the thesis.	64
Table 5. The cationic monomers used in this thesis.	65
Table 6. Summary of $R_{pmax}$ using different sensitizers (S14, S16, S4, and S5) and the iodonium salt IS1 embedded in the TPGDA at different operating temperature, published in [96]. More details in Section 4.1.2 explain the experimental conditions.	89
Table 7. Amount of conjugate acid ( $aH^+$ ) of the NIR initiator system ( $[Sens] = 6.3 \cdot 10^{-5} M$ ; $[IS2] = 5.6 \cdot 10^{-4} M$ ) in acetone under NIR exposure using the 805 nm LED device with an intensity of $1.2 W \cdot cm^{-2}$ for 10 minutes, published [96]. More details in Section 4.1.7 explain the experimental conditions.	91
Table 8. Peak table of the molecular ions detected in the photoproducts analysis measurement with LC-MS, published in [96] More details in Section 4.1.6 explain the experimental conditions.	95
Table 9. Properties of the sensitizers (S1-S24) used in this subchapter, published in [96]. More details in Section 4.1.1, 4.1.3, and 4.1.4 explain the experimental conditions.	97
Table 10. Summary of NIR sensitizers used in this part of work and their respective absorption in OXT-03 taken at $23^\circ C$ , a: $[PF6]^-$ , b: $[PF3(C2F5)3]^-$ , d: $[Al(O-t-C4F9)4]^-$ , g: $[TsO]^-$ . More details in Section 4.2.8 explain the experimental conditions.	100
Table 11. Viscosity of the monomers used (ERL-4211, HBVE, OXT-03) and selected conductivity data for the respective iodonium salts (IS) ( $[IS]=3.8 \times 10^{-2} mmol \cdot g^{-1}$ ), published in [115]. More details in Section 4.2.6, 4.2.7 explain the experimental conditions.	102
Table 12. Concentration of conjugate acid generated by the NIR initiator systems ( $[Sens] 4.1 \times 10^{-5} M$ , $[IS] 5.6 \times 10^{-4} M$ ) in BuAc or LMA under NIR exposure using the 805nm LED device ( $1.2 W \cdot cm^{-2}$ , 20 minutes), published in [115]. More details in Section 4.2.5 explain the experimental conditions.	106
Table 13. Summary of DMA-data ( $T_g$ : glass transition temperature in $^\circ C$ where $\tan \delta$ appeared, $E'$ : storage modulus in MPa) obtained after exposure of 2 min with 395 nm LED ( $1.1 W \cdot cm^{-2}$ ) and 10 min with 805 nm LED ( $1.2 W \cdot cm^{-2}$ ) while the conversion at this time $x_\infty$ was determined for the monomer polymerising according to a cationic polymerization mechanism (cat) and/or radical polymerization mechanism (rad), published in [115]. More details in Section 4.2.3 explain the experimental conditions.	111
Table 14. Properties of sensitizers, oxime esters, and their combination. Optical data ( $\lambda_{max}$ : absorption maximum, $\epsilon$ : extinction coefficient), electrochemical data ( $E_{ox}$ : oxidation potential, $E_{red}$ : reduction potential), initial temperature of intrinsic polymerization of TPGDA comprising NIR-sensitizer and oxime ester OXE-01 (Ti), and final double bond conversion $x_\infty$ of TPGDA followed by RT-FTIR measurement, published in [118]. More details in Section 4.3.1, 4.3.2, 4.3.5, 4.3.7 explain the experimental conditions.	125

## Abstract

The NIR sensitized photopolymerization following a radical and/or cationic polymerization mechanism was investigated using heptamethine cyanine as sensitizer and either iodonium salt or oxime ester as coinitiating component. New high-power LED prototypes emitting between 800 nm - 900 nm served as excitation source. They exhibited an excitation intensity of  $\geq 1 \text{ W}\cdot\text{cm}^{-2}$ . These new high-power LED prototypes have unexpectedly brought new impetus into the photochemistry of heptamethine based cyanine operating as sensitizer in a photoinduced electron transfer (PET) reaction. They even facilitate to overcome internal reaction barriers in the reaction system where low-power NIR LEDs mostly failed. The strong non-radiative deactivation of the sensitizer can be seen as one source to promote the reaction between excited state of the sensitizer and the co-initiator. These new light sources enabled much more heptamethine cyanines as sensitizer in the PET. Overall, these NIR photoinitiator systems initiated well radical polymerization of acrylate monomers such as **TPGDA**, **TPMTA**, and **PEGMA**.

Particularly heptamethine cyanines carrying a cyclopentene moiety in the central point of the cyanine chain and a diphenylamino group at the *meso*-position of the methine chain were found as the first time in this work to initiate cationic polymerization of epoxides such as **Epikote 357** or **Epikote 828** in combination with iodonium salts. The selective oxidation of the cyclopentene resulting in a fulvene moiety enabled to work cationic polymerization. The possibility to initiate cationic polymerization was extended to oxetanes and vinyl ethers resulting in high conversions as well. The vinyl ether derivatives exhibited the best performance in cationic polymerization followed by oxetanes and oxiranes. These studies also included a variation of anions comprised in both the cationic cyanine sensitizers and the iodonium salts selected from those derived from weakly coordinating anions (WACs) such as aluminates ( $[\text{Al}(\text{O}-\text{t}-\text{C}_4\text{F}_9)_4]^-$ ,  $[\text{Al}(\text{O}-(\text{i}-\text{C}_3\text{F}_7)\text{CH}_3)_4]^-$ ), fluorinated phosphates ( $[\text{PF}_6]^-$ ,  $[\text{PF}_3(\text{C}_2\text{F}_5)_3]^-$ ,  $[\text{PF}_3(\text{n}-\text{C}_4\text{F}_9)_3]^-$ ), and methides ( $[\text{C}(\text{O}-\text{SO}_2\text{CF}_3)_3]^-$ ).  $[\text{Al}(\text{O}-\text{t}-\text{C}_4\text{F}_9)_4]^-$  showed better performance compared to  $[\text{Al}(\text{O}-(\text{i}-\text{C}_3\text{F}_7)\text{CH}_3)_4]^-$  while  $[\text{PF}_3(\text{C}_2\text{F}_5)_3]^-$  did not exhibit the expected performance compared with  $[\text{Al}(\text{O}-\text{t}-\text{C}_4\text{F}_9)_4]^-$ .

These initiating systems can also initiate the hybrid polymerization based on free radical and cationic polymerization resulting in formation of interpenetrating polymer networks (IPNs). Dynamic mechanical analysis (DMA) proved formation of IPNs comprising epoxy and acrylate monomers while the use of the same monomer system failed in a typical UV initiating system where thioxanthone served as photosensitizer.

In addition, oxime esters also served as alternative coinitiators together with heptamethine based cyanines applying NIR excitation. Selected heptamethine sensitizers carrying as terminal group either benzo[e]- or benzo-[c,d]indolium substituents facilitated initiation of free radical photopolymerization where several oxime esters served as co-initiators applying different high-power NIR-LEDs emitting either at 805 nm, 860 nm, or 870 nm. The huge amount of heat released by non-radiative deactivation of heptamethine also enabled this system to overcome an internal activation barrier appearing in the PET reaction proceeding in the excited state. Moreover, this heat promoted thus photopolymerization while the application of thermal treatment failed to initiate polymerization. This will bring new directions for development of technologies requesting internal barriers.

## Kurzfassung

Die NIR-sensibilisierte Photopolymerisation, welche nach einem radikalischen und/oder kationischen Polymerisationsmechanismus abläuft, wurde unter Verwendung von Heptamethincyaninen als Sensibilisator und Iodoniumsalzen bzw. Oximestern, welche die Aufgabe des Coinitiators übernehmen, untersucht. Als Anregungsquelle wurden neue Hochleistungs-LED-Prototypen mit einer Emission zwischen 800 und 900 nm eingesetzt. Sie zeigten eine Anregungsintensität von  $\geq 1 \text{ W}\cdot\text{cm}^{-2}$ . Diese neuen Hochleistungs-LED-Prototypen konnten hinsichtlich der Photochemie von Cyaninen auf Heptamethinbasis, welche als Sensibilisatoren bei einer photoinduzierten Elektronentransferreaktion (PET) wirksam werden, unerwartet neue Impulse setzen. Sie erleichtern sogar das Überwinden interner Reaktionsbarrieren im PET Reaktionssystem, wobei NIR-LEDs mit geringer Emissionsleistung nicht in der Lage waren, die Polymerisation zu initiieren. Die intensive nichtstrahlende Desaktivierung des Sensibilisators kann als eine Ursache angesehen werden, um die Reaktion zwischen dem angeregten Zustand des Sensibilisators und dem Coinitiator auszulösen. Insbesondere die neuen Lichtquellen, die in diesem Bereich emittieren, konnten diese Chemie ermöglichen, da festgestellt wurde, dass viele Heptamethincyanine als NIR-Sensibilisatoren beim PET zwischen den photoangeregten Heptamethin und Iodoniumsalzen bzw. Oximestern wirksam werden. Insgesamt initiierten diese Systeme die radikalische Polymerisation von Acrylatmonomeren wie **TPGDA**, **TPMTA** und **PEGMA**.

Insbesondere Heptamethincyanine, die eine Cyclopenteneinheit im zentralen Gerüst der Cyaninkette und eine Diphenylaminogruppe an der Mesoposition der Methinkette tragen, können die kationische Polymerisation von Epoxiden wie **Epikote 357** oder **Epikote 828** initiieren in Kombination mit Iodoniumsalzen. Darüber wird erstmalig in dieser Arbeit berichtet. Die selektive Oxidation des Cyclopentens, was zur Bildung einer Fulvenstruktur führte, ermöglichte die kationische Polymerisation. Die Möglichkeit, eine kationische Polymerisation zu initiieren, wurde auf Oxetane und Vinylether erweitert, was ebenfalls zu hohen Umsätzen führte. Die Vinyletherderivate zeigten die beste Effizienz bei der kationischen Polymerisation, gefolgt von Oxetanen und Oxiranen.

Die durchgeführten Untersuchungen umfassten auch eine Variation des Anions sowohl im kationischen Cyaninsensibilisator als auch im Iodoniumsalz. Diese wurden so ausgewählt, dass sie sich möglichst von schwach koordinierenden Anionen ableiten wie z.B. Aluminaten ( $[\text{Al}(\text{O}-t\text{-C}_4\text{F}_9)_4]^-$ ,  $[\text{Al}(\text{O}-i\text{-C}_3\text{F}_7\text{CH}_3)_4]^-$ ), fluorierten Phosphaten ( $[\text{PF}_6]^-$ ,  $[\text{PF}_3(\text{C}_2\text{F}_5)_3]^-$ ,  $[\text{PF}_3(n\text{-C}_4\text{F}_9)_3]^-$ ) und Methiden ( $[\text{C}(\text{O}-\text{SO}_2\text{CF}_3)_3]^-$ ). ( $[\text{Al}(\text{O}-t\text{-C}_4\text{F}_9)_4]^-$ ) zeigte eine bessere Wirkung im Vergleich zu  $[\text{Al}(\text{O}-i\text{-C}_3\text{F}_7\text{CH}_3)_4]^-$ , während bei  $[\text{PF}_3(\text{C}_2\text{F}_5)_3]^-$  nicht die erwartete Effizienz im Vergleich zu  $[\text{Al}(\text{O}-i\text{-C}_3\text{F}_7\text{CH}_3)_4]^-$  beobachten war. Diese initiierenden Systeme können auch die Hybridpolymerisation basierend auf einem radikalischen und kationischen Mechanismus initiieren, was zur Bildung interpenetrierender Polymernetzwerke (IPNs) führte. Die dynamisch-mechanische Analyse (DMA) bewies die Bildung von IPNs, wobei Epoxy- und Acrylatmonomere das ermöglichten. Bei der Verwendung der gleichen Zusammensetzung war die Bildung von IPNs nicht zielführend, wobei ein typisches UV-initiiertes System basierend auf Thioxanthon zum Einsatz kam.

Weiterhin wurden Oximester als alternative Coinitiatoren in Kombination mit Cyaninen auf Heptamethinbasis unter NIR-Anregung untersucht. Ausgewählte Heptamethine, die als Endgruppe entweder Benzo[e]- oder Benzo-[c, d]indoliumsubstituenten tragen erleichterten die Initiierung der freien radikalischen Photopolymerisation. Unterschiedliche Oximester wurden als Co-Initiatoren eingesetzt. Dabei kamen unterschiedliche Hochleistungs-NIR-LED Module zum Einsatz, die entweder bei 805 nm, 860 nm oder 870 nm emittierten. Die enorme Wärmemenge ermöglichte es auch in diesem System, dass der PET im angeregten Zustand über eine interne Aktivierungsbarriere ablaufen konnte. Durch die strahlungslose Desaktivierung des NIR-Sensibilisators wird die erforderliche Wärme freigesetzt, um die Photopolymerisation zu initiieren. Der Einsatz von Systemen die ausschließlich Wärme generieren führte nicht zur Initiierung der Photopolymerisation. Dass wird neue Wege für die Entwicklung von Technologien bringen, die interne Barrieren erfordern.

# 1. Introduction and Motivation

## 1.1 Introduction

Photopolymerization was introduced as a method to transform unsaturated monomers into the respective polymer by radical polymerization in 1940s[1]. In the next decades, the development of polymerization included many research with focus on fundamental objectives while industry also started to bring new technologies into the market based on photopolymerization[2-4]. Many efforts from industrial sector to academic laboratory were devoted in this field related to many fields such as coatings, inks, adhesives, 3D-printing including stereolithography, photoresists, laser direct imaging, computer to plate (CTP) technology, holographic optical elements, and tooth repair-just to name a few of the many established examples[2-10]. Comparison with traditional thermal polymerization indicates the benefits of photopolymerization. This polymerization method possesses many outstanding advantages such as fast reaction rate resulting in higher productivity because the light used to initiate polymerization can easily control processes in industry. Photopolymerization mostly operates at room temperature. There is no demand to combine this technique with energy wasting heat sources. This results in less energy consumption compared to other oven technology. Moreover, light-initiated polymerization also enables process technologies solvent-free coatings techniques. This gives access of enabling processing with less or no volatile organic compounds (VOCs)[11]. In addition, photopolymerization easily controls the course of the reaction just by switching ON/OFF the light sources[12]. Thus, the process can be easily stopped. Therefore, problems arise in the case of technologies relying on heat, such as oven technology, can be overcome by light initiated polymerization. Just to make a brief statement, photopolymerization can be seen as an 'eco-friendly' polymerization tool complementing in general the field of green technology. In general, photopolymerization can be classified based on the wavelength used for excitation that is either ultraviolet (UV) photopolymerization, visible (Vis) photopolymerization and near infrared (NIR) photopolymerization. This also addresses certain demands on the light source applied for excitation in the polymerization process[11].

Nowadays, the UV photopolymerization has developed much maturer compared to other methods[11, 13]. It can be seen as the most light-sensitive polymerization because available photoinitiators or sensitizers fit well in the spectral range of the editing UV light source (200-400nm). Thus, light sources based on UV light can be seen as well developed[13-16]. However, there also exist several disadvantages regarding the application of UV-light sources, which should not be ignored for UV photopolymerization. These



include 1) harmfulness of short ultraviolet light to skin and eyes, 2) possible ozone release which is harmful to the environment[17], and 3) problems in curing systems with large thickness because UV light cannot penetrate deep into materials caused by the higher scattering coefficient compared to Visible and NIR light[10, 18-19]. Furthermore, many pigments added in applications possess an intrinsic absorption in the UV range that interferes the absorption efficiency, and therefore, capability to generate initiating species such as radicals and conjugate acid needed for photopolymerization. Therefore, a demand has arisen to develop visible and NIR photopolymerization as alternatives because the longer emission of the excitation source facilitates deeper penetration into the materials[10, 15, 20-24]. In the past several years, the visible light (400-700nm) induced polymerization also received a significant progress[12, 18, 25-30]. However, the NIR photopolymerization, which enables deep penetration of the excitation light into the material, did not develop so fast compared with other methods [19]. The lower photon energy of the NIR light and the lower efficiency to initiate polymerization in the NIR range (>800nm) compared to UV and visible photopolymerization systems have limited its development for industrial applications[19, 31].

NIR light-induced polymerization started from last 90s in the graphic industry to pattern lithographic plates applied in digital imaging[32]. Nowadays, such systems have well developed in this field particularly for the production of 830nm laser sensitive computer to plate (CTP) systems applied in the digital imaging sector[23, 33-35]. It possesses great potential for uses in much more industrial applications because of the benefits such as the safer and cheaper light source being less harmful to operators and possibility of deeper penetration into materials to cure thick materials, and the availability of additional thermal energy generated by internal conversion (IC) enables them for many new applications in the aforementioned areas[36-37]. Feasibility studies also showed the opportunity to embed functional materials absorbing either in the UV and/or visible range into the formulation of the coatings to improve the resistance against solar weathering[19, 36-45].

Nevertheless, the great achievement of NIR photopolymerization bases on the development of efficient NIR absorbers[36-37] forming the prerequisite to absorb NIR light resulting in generation of excited states which are capable to sensitise co-initiators to generate reactive species such as radicals and conjugate acid[36-37]. This occurs by photoinduced electron transfer (PET)[7, 36-37]resulting in radical and/or cationic polymerization[23, 39, 41, 46-48]. During sensitisation of co-initiator decomposition, they also generate a huge amount of heat into the surrounding by non-radiative deactivation[36-37]. The heat gener-

ated by NIR sensitizers has been used in NIR laser welding, laser drying printing inks, laser marking of plastics or thermal curing, etc[7, 19, 45, 49-54]. It is one of the efficient methods to generate heat on demand by controlling the ON/OFF mode of NIR light resulting in systems having the capability to substitute conventional oven processes[35, 50, 55]. NIR photopolymerization has received increased potential in many practical applications[7, 19, 45, 49-54]. However, the design of the photoinitiator does not appear as easy because it needs a larger conjugated structure to exhibit absorption in the NIR range and it must possess sufficient compatibility in the surrounding matrix. Almost all NIR initiating systems base on NIR sensitizers in combination with co-initiators such as onium salts or triazines[35]. Moreover, NIR sensitizers derived from cyanines have been the most applied pattern exhibiting an absorption in the NIR range. Some of them were used in biological and medical imaging and theranostic studies because of the high performance to generate heat and fluorescence on demand[36-37]. Many cyanines absorbing in the NIR range of 750-850nm exhibit more than 85% of non-radiative deactivation resulting in huge heat after excited by an appropriate NIR source while the fluorescence yield ( $\Phi_f$ ) depicts with less than 15% a minor fraction[36-37]. Moreover, some absorbers with absorption maximum higher than 900nm deactivate almost radiationless (>99.9%)[36-37] resulting therefore in generating of huge amount of heat. Therefore, heptamethine cyanines exhibit one kind of perfect photo-thermal converters used to generate heat on demand[45, 50]. Although the radiative deactivation yield of the cyanine can be seen as rather low, the lifetime of the excited state residing in the sub-nanosecond range facilitates the excited state to react with other compounds such as the aforementioned coinitiators by photoinduced electron transfer (PET) to generate reactive intermediates such as radicals, acidic cations for which the term conjugate acid seems more appropriate. Cyanines serve as photosensitizers in such systems[36-37]. Only a few references reported about the fundamental investigations of the NIR photopolymerization system where the heptamethine cyanines function as photosensitizers absorbing NIR radiation released by a NIR laser or NIR LED[23, 31, 35-37, 45-47, 50, 56-57]. Again, appropriate co-initiators such as iodonium salts or triazine resulting in negative free reaction enthalpy for the PET are the source to produce initiating radicals while the oxidised intermediate of the sensitizer releases conjugate acid[23, 47-48].

On the other hand, NIR photoinduced thermal polymerization based on NIR absorbers was also studied offering the opportunity to apply NIR light to initiate polymerization in powder coatings or deep curing systems[45, 50-51, 53]. Here, NIR light undertakes a dual func-

tion; that is the promotion of physical events such as melting of a powder and the PET as a chemical process occurring in the molten material[45, 50]. Most of the reported NIR photopolymerization based on the radical polymerization mechanism. With respect to the cationic polymerization, only aziridines were disclosed to occur polymerization by the neutral cyanine comprising a barbiturate substitute group at the *meso*-position in combination with iodonium salts under low power NIR LEDs ( $\leq 0.1 \text{ W}\cdot\text{cm}^{-2}$ )[47]. There existed from our best knowledge no report about NIR-sensitized cationic polymerization of oxiranes, oxetanes, and vinyl ethers.

Weakly coordinating anions (WCAs) were proved as efficient counter ions in cyanines and co-initiators[58-59]. They do not participate in photoredox reactions because their redox potentials reside outside of the electrochemical window between -2 V and 2 V. The reduction potential of the iodonium cation depicts a value of -0.65 V[47] agreeing well with literature data[60-61]. Particularly, the iodonium salt comprising the bis(trifluoromethyl sulphonyl) imide (**NTf<sub>2</sub><sup>-</sup>**) anion showed outstanding performance with respect to the compatibility in the NIR photosensitive resins[46]. It worked well in NIR photosensitive polymerization in combination with cyanines.[46] Another reported competitive anion relates to tris(pentafluoroethyl)trifluoro-phosphate [**PF<sub>3</sub>(C<sub>2</sub>F<sub>5</sub>)<sub>3</sub><sup>-</sup>**] (FAP) which also improved the solubility of iodonium salts[41, 48]. Nevertheless, applications using this anion are widely protected limiting its applications in a broader range by different users[58, 62]. Recently, a new iodonium salt with perfluorinated alkoxyaluminate anion [**Al(OC(CF<sub>3</sub>)<sub>3</sub>)<sub>4</sub><sup>-</sup>**] exhibiting outstanding low nucleophilicity and ion-pairing, good stability against hydrolysis, and electrophilic decomposition was reported as an efficient iodonium salt [59, 63]. All of these three iodonium salts depict considerable alternatives to iodonium salts carrying the anion **PF<sub>6</sub><sup>-</sup>**. Because these three anions do not cause toxic issues; that is formation of hydrofluoric acid (HF) as **PF<sub>6</sub><sup>-</sup>** does[41, 48, 58-59, 62]. Since iodonium salts serve well as co-initiators in NIR photopolymer initiating systems, there has arisen a certain demand to overcome the HF issue caused by the **PF<sub>6</sub><sup>-</sup>**. Thus, **NTf<sub>2</sub><sup>-</sup>**, **FAP** and the aluminate [**Al(OC(CF<sub>3</sub>)<sub>3</sub>)<sub>4</sub><sup>-</sup>**] depict interesting candidates to overcome the HF issue[41, 46, 48, 59]. Although the anions **FAP** or [**Al(OC(CF<sub>3</sub>)<sub>3</sub>)<sub>4</sub><sup>-</sup>**] can improve the solubility of the iodonium salts, they are not easy to get because of the difficult synthesis process. Therefore, development of alternatives for synthesis has been still a challenge in order to combine them with iodonium cations serving as co-initiators in NIR initiating systems.

Alkoxyamine[53], azo derivatives or (hydro)peroxides exhibit alternatives to iodonium salts because they show thermal sensitive response[52]. Thus, NIR absorbers may serve as photo-thermal converters due to the aforementioned huge release of heat caused by internal conversion (IC)[36-37, 52-53] occurring in NIR absorbers. The huge heat generated from NIR absorbers results in decomposition of thermal initiators to generate reactive radicals that initiate free radical polymerization of acrylate monomers. Photoinduced thermal polymerization advances over the conventional thermal process based on old energy-wasting oven techniques because it offers the advantages to turn either ON or OFF of polymerization just by operating the light with one click. There is no warm-up time necessary to start the polymerization and also no additional cooling after processing resulting in saving of time and energy. Thus, operations with light belong to green technologies [11-12]. In other words, photoinduced-thermal polymerization can be seen as an eco-friendly process. Many thermal initiators can be used in this system benefitting from the longer history and widespread application of the thermal polymerization, which would promote the development of the NIR light induced polymerization. However, the big issue of this system is short shelf-life of the initiators, which decompose at slight elevated temperature[51, 53, 64-65].

Oxime esters ( $R-CR'=N-OR''$ ) exhibit one kind of efficient photoinitiators sensitively operating in UV-visible range. Upon irradiation, they would produce initiating radicals  $R-CR'=N\cdot$  and  $\cdot OR''$  belonging to the group of electrophilic radicals that initiate radical polymerization of (meth)acrylic monomers very well[66-69]. They have been used as photoinitiators for photopolymerization around 50 years[3, 70-72]. Nevertheless, they were eliminated from the industrial sectors because of the shelf-life issue[72]. Consequently, many efforts were devoted to improve the thermal stability and the absorption matching the longer wavelength UV light sources[73-74]. Then at the end of the last 90s, one of the oxime ester **OXE-01** carrying diphenylsulfide moiety was developed[66]. Later, the oxime ester **OXE-02** comprising carbazole was introduced[75]. Nowadays, they are the main commercialized oxime esters applied as photoinitiators as widely used in photoresists[14, 66-67, 75]. More studies were employed to understand the details of the decomposition mechanism by photophysical investigations and time-resolved spectroscopy[68, 76-77]. Recently, a series of the oxime esters carrying a chromophore of substituted coumarin were reported to have better thermal stability and longer absorption in the long wavelength range[28, 69, 78-80]. The improvement of the thermal stability and bathochromic shifts of the absorption make them suitable for the UV-visible LED in the range of 385-450 nm[80-85]. These

more stable oxime esters also exhibit a significantly better compatibility with other components in the photosensitive resins, which make them suitable as coinitiators in digital imaging applications[86] as alternatives to iodonium salts. These applications can still tolerate shelf-life issue, which does not appear so strong compared with other derivatives.

## 1.2 Motivation of the Thesis

This thesis focuses to pursue research to broaden knowledge of NIR photopolymerization as complementary photopolymerization method where traditionally UV and visible initiated photopolymerization occupy the major use for many applications. Its eco-friendly aspects appearing less harmful to the operator, lower energy consumption, feasibility to cure thick samples resulting in large curing depth, additional heat for the reaction and more benefits make this field interesting to explore. Moreover, demands of the society to work with more resource saving equipment and new regularities with focus to replace older techniques based on mercury lamps have enforced the development in this direction[19]. However, many of the successful applications with the respect of the NIR light induced polymerization have focused on the *cw*-NIR lasers until today[57]. Big success can be seen regarding the production of CTP system applied in modern digital imaging technologies with *cw*-NIR lasers, which has hold more than nearly 20 years history[7, 23, 31, 35]. Recently, it was used in curing of powder coatings resulting in the successful replacement of conventional oven heating techniques[45, 50, 57, 87]. Furthermore, up-conversion nanoparticles (UCNP) with capability to generate UV-light showed acceptable performance to initiate free radical polymerization of systems in combination with UV-initiators applying a 980 nm laser[40, 78, 88-89]. Moreover, UCNPs disclosed deep curing lengths applying free radical polymerization while the first report of an ATRP mechanism based on a metal free system appeared in 2017[40]. These few examples demonstrate the potential of NIR sensitized photopolymerization. It, therefore, addresses the challenge to explore more opportunities for uses where the combination of heat and photons complement with each other.

Though these NIR laser based systems possess huge potential, NIR-LED based systems are also interesting for the NIR photopolymerization. The intensity of many NIR LEDs is not so high compared to NIR laser[90], which is easier to use by operators[10, 56]. Furthermore, the high intensity of NIR lasers may lead to a destruction of heat sensitive substrates such as wood, paper or plastics[19]. Thus, NIR LEDs exhibit lower intensity compared to NIR lasers but they may offer more opportunities for applications compared with NIR lasers because they are easier to operate. Furthermore, NIR LEDs also offer the

probability to expose large areas of curing systems without the request to combine the source with more technical related modulators[91-92] to expose large areas[36-37, 45]. Moreover, as well known, the UV-visible emitting LEDs have been used in the dentistry many years[11, 15-16, 93-95]. However, there is a big issue if systems comprise additives with absorption in the UV and visible range, which always interferes the penetration depth of excitation light needed for curing. From this point of view, NIR LEDs depict an alternative to UV-visible LEDs because the NIR light resides out of the UV and visible range. Therefore, the additives with absorption in the UV-Vis range shall not interfere absorption of NIR light by the sensitizer. Additionally, the NIR sensitive initiating system comprising cyanines and iodonium salts exhibit acceptable photosensitivity to initiate free radical polymerization with NIR LEDs[46-47]. Particularly, the iodonium salt with the bis (trifluoromethyl sulphonyl) imide (**NTf<sub>2</sub><sup>-</sup>**)[46] and **FAP** anion[41, 48] exhibited outstanding performance regarding the compatibility in different coatings. Nevertheless, these previous works disclosed that NIR sensitized polymerization only worked with the cyanine carrying a barbiturate substitute group at the *meso*-position with low power NIR LED ( $\leq 0.1 \text{ W}\cdot\text{cm}^{-2}$ ) which limited the development of the NIR LED photopolymerization[47]. For promoting the development of the NIR LED photopolymerization, new high-power NIR LEDs and more NIR absorber sensitizers with different patterns were introduced in our studies. Herein, three different high power NIR LEDs with different emitting wavelength at 805nm, 860nm, and 870nm moved into the focus of our research. Their intensities can approach more than  $1 \text{ W}\cdot\text{cm}^{-2}$  that is more than 10 times compared to the low power LED ( $\leq 0.1 \text{ W}\cdot\text{cm}^{-2}$ ) used in previous works[47]. Finally, the new high power LEDs resulted in unexpected results with respect to the NIR photopolymerization and induced more of cyanines to serve as sensitizers in NIR photopolymerization, which significantly extends the initiating system used in nowadays NIR photopolymerization systems[96].

Additionally, the cationic polymerization initiated by sensitizers absorbing in the UV and visible range in combination with iodonium salts have been widely used in industry[97-101]. Monomers comprising vinyl ether, epoxy, or oxetane[98-99, 102-105] moieties complement the pattern of materials used for cationic polymerization. Moreover, epoxy compounds exhibiting good capability including high thermal capability, excellent adhesion, and good chemical resistance can be widely found in practical applications as monomers or oligomers for this purpose. The bisphenol-A-diglycidyl ether depicts one kind of common commercially available epoxides, which occurred photoinduced in cationic polymerization studies at rather slower rates[106-108]. Moreover, oxetanes depict one

kind of competitive monomers compared to epoxies because of their outstanding properties such as lower toxicity, better thermal stability, excellent adhesion, good chemical resistance[103, 109-110]. Moreover, oxetanes also bring the benefit to polymerise over the oxonium ion[111-113], which makes them more tolerant against the attack of alcohols or COOH groups. This might bring them to lithographic applications in their electronic industry where they can be found in nowadays uses particular in Asia[114]. However, the previous work disclosed only aziridines polymerised using this sensitizer forming nucleophilic products upon exposure with low power NIR LED[47]. Therefore, as an alternative to UV-Vis photopolymerization, it is necessary to extend research in this field to open the door for cationic polymerization using more outstanding cationic monomers. Additionally, interpenetrating polymer networks (IPNs) manufactured by polymerization of distinct monomers relying to different mechanisms considering polymer formation exhibit another field where no report has appeared in the field of NIR sensitized polymerization until today except our research[115]. Thus, the epoxy monomer in combination with acrylate monomers results in hybrid polymerization where both radical and cationic polymerization proceed together[116]. No phase separation should occur in order to form IPNs. Monomers individually cross-linked result in materials that exhibit excellent properties. NIR-sensitized polymerization of hybrid systems based on radical and cationic mechanisms may bring new light in this field because NIR systems additionally provide heat generated by internal conversion (IC)[36-37] which might help such system to overcome internal diffusion barriers generated by the cross-linked moieties formed. Herein, the NIR photoinduced cationic and radical/cationic hybrid polymerization moves into the focus of this thesis.

Moreover, the influence of the different weakly coordinating anions (WCAs)[117] to the reactivity of iodonium salts was studied in the NIR-sensitized radical photopolymerization in previous works. The results showed that different anions influenced solubility, conductivity, compatibility of the iodonium salt, and the reactivity of the initiating system in combination with heptamethine cyanines[41, 46, 48]. Thus, it is also necessary to study the influence of the anions comprising in iodonium salts on the efficiency of the NIR sensitised cationic photopolymerization. Herein, several WCAs, which can generate superacid under certain circumstances, were studied to search the best anion for the NIR photoinduced cationic polymerization[115]. This has been a point of view that has been always underestimated since WCAs do not exhibit interesting redox properties but their chemical structure importantly affects solubility in the matrix.

The coinitiators used in NIR light induced polymerization include iodonium salts, triazine, some thermal initiators, and oxime esters[31, 39, 47, 86]. As aforementioned noticed, iodonium salts are the well known coinitiators used in the NIR photoinduced polymerization. The reaction mechanism between NIR absorbers and iodonium salts was studied, which offered a guideline for the application of the NIR absorber in combination with iodonium salt initiating system. However, there are some disadvantages of iodonium salts such as higher toxicity, lower solubility, worse compatibility with the compounds staying in the surrounding, etc as found in the studies reported[32-33, 46].

Thermal initiators could be used as the coinitiators of the NIR absorbers but there is a big issue in practical applications because of the shelf life issue. Thus, oxime esters as coinitiators as just disclosed in the patent used under NIR laser light source with high power intensity depict from this point an interesting alternative[86]. These compounds exhibit lower toxicity, good stability and solubility, and better compatibility with many environmental materials such as monomers, oligomers, and resins used for polymerization reactions. From this point of view, the demand arises to receive more details about this co-initiating system including the respective absorber. Herein, more details about the oxime esters in combination with NIR absorbers/sensitizers were revealed, which can offer some good guidelines to use these co-initiating systems in more practical application related coatings in combination with new modern high-power LEDs[118].

Publications as First Author or shared First Authorship:

1. C. Schmitz, Y. Pang, A. Gülz, M. Gläser, J. Horst, M. Jäger, B. Strehmel, "New High-Power LEDs Open Photochemistry for Near-Infrared-Sensitized Radical and Cationic Photopolymerization." *Angew. Chem., Int. Ed.* 2019, **58**, 4400-4404. "Neue Hochleistungs-LEDs ermöglichen Photochemie für die Nahinfrarot-sensibilisierte radikalische und kationische Photopolymerisation" *Angew. Chemie* **2019**, **131**, 4445-4450.
2. Y. Pang, S. Fan, Q. Wang, D. Oprych, A. Feilen, K. Reiner, D. Keil, Y. L. Slominsky, S. Popov, Y. Zou, B. Strehmel, "NIR-Sensitized Activated Photoreaction between Cyanines and Oxime Esters: Free-Radical Photopolymerization", *Angew. Chem., Int Ed.* **2020**, **59**, 11440-11447.
3. Y. Pang, A. Shiraishi, D. Keil, S. Popov, V. Strehmel, H. Jiao, J. S. Gutmann, Y. Zou, B. Strehmel, "NIR-Sensitized Cationic and Hybrid Radical/Cationic Polymerization and Crosslinking" *Angew. Chem., Int. Ed.* 2021, **60**, 1465-1473.



4. Y. Pang, Y. Zou, S. Fan, M. Gao, Y. Xin, Coumarin Oxime Ester Compound and Preparation and Use Thereof, (Hubei Gurun Technology Co., Peop. Rep. China), US20200148660A1, **2019**.
5. Y. Pang, Y. Zou, S. Fan, Oxime Esters Photoinitiator Containing Five-membered Heterocycle Structure, Their preparation method and applications in UV-LED photocuring system, (Hubei Gurun Technology Co., Ltd., Peop. Rep. China), CN110551098A, **2019**.
6. Y. Pang, Y. Zou, S. Fan, Preparing Method and Application of Long-wavelength Coumarin Oxime Ester Compound, (Hubei Gurun Technology Co., Ltd., Peop. Rep. China), CN110330501A, **2019**.

Publications contributed as coauthor:

1. B. Strehmel, C. Schmitz, C. Kütahya, Y. Pang, A. Drewitz, H. Mustroph, "Photophysics and Photochemistry of NIR Absorbers Derived From Cyanines: Key to New Technologies Based on Chemistry 4.0" Beilstein Journal of Organic Chemistry 2020, 16, 415-444.

Conference Contributions with Oral Presentation:

1. New NIR-LED Device Facilitates photoinitiated Curing with Cyanine Sensitizers for Radical and Cationic Crosslinking. 83. Lacktagung der Fachgruppe Lackchemie, 11.09.2019 - 13.09.2019, Erfurt.
2. Photoinduced Thermal Curing with New NIR-LED Devices. 15th International Conference on Radiation Curing in Asia (RadTech Asia 2019), October 17-20,2019, Hangzhou, China.
3. Photoinitiated Radical and Cationic Curing with New NIR-LED Device, European Coatings Show 2019 Conference, March18-19, 2019, Nuremberg, Germany.

Conference Contributions with Poster Presentation:

1. New NIR Light Source for Photoinitiated Radical and Cationic Polymerization, 26. Lecture Conference on Photochemistry, September 10-12, 2018, Munich, Germany.
2. Photoinitiated Radical and Cationic Polymerization with New LED Device, the 5th European Symposium of Photopolymer Science (ESPS), September 3-6, 2018, Mulhouse, France .

3. High-Power Near-Infrared Light Sources Radical and Cationic Polymerization of Coatings, 27th Photo IUPAC Symposium in Dublin 2018, July 8-13, Dublin, Ireland.
4. NIR light induced free radical and cationic polymerization, Chinese Society for Imaging Science and Technology (CSIST) 2019 conference, October 9-12, 2019, Beijing, China. ('Youth Outstanding Scientific Paper Award')

## 2. State of the Art

Photopolymerization technology has got a significant development from various academic studies to widespread practical applications since it was developed in the last 40s.[1] In this technology, the light sources and the photoinitiating systems are two key parts that influence the properties of the applications based on the photopolymers. The photoinitiating component absorbs light resulting in generation of reactive species such as radicals, cations and/or conjugate acids, which initiate the polymerization of the composition by photochemical reactions[1, 7, 11]. Thus, many efforts are devoted into the development of light sources resulting in many new photo resources, which are safer to environment and operators, carrying stronger intensity, with smaller volume, more flexible to use in different practical applications, etc.[1, 7, 11] Moreover, more and more photoinitiating systems are developed to fulfil the demand of different light sources[15, 18, 56]. Furthermore, the photochemical mechanisms of the photoinitiating system are also studied to understand which is useful to develop more efficient systems.[1, 7, 11, 119-120] This subchapter reports about the state of the art of light sources, photosensitive materials, and the reactions occurring among the materials.

### 2.1 Light Sources for Photopolymerization

Light sources used in photopolymerization include ultraviolet light (100 nm - 400 nm), visible light (400 nm - 780 nm), and near infrared (NIR) light (780 nm - 2000 nm). Furthermore, the ultraviolet (UV) light is always divided into UV-A light (320 nm - 400 nm), UV-B light (280 nm - 320 nm), and UV-C light (200 nm - 280 nm)[1]. Visible light means the light that can be perceived by the human eye, which comprises violet, blue, blue-green, green, green-yellow, yellow, orange and red colours. The infrared (IR) light being longer than 800nm is subdivided in IR-A light (800 nm - 1400 nm), IR-B light (1400 nm - 3  $\mu\text{m}$ ), IR-C light (3  $\mu\text{m}$  - 1 mm)[121]. The classification of the light used in photochemical sciences can be depicted by Figure 1[121]. Generally, the longer emitting wavelength of the light source results in the lower photonic energy and the deeper penetration of the light into the material. Therefore, the sequence of the light penetration into materials follows this order: NIR light > Visible light > UV light[1]. Recently, photopolymerization induced by NIR light has attracted more and more attention in the scientific community to fulfil the demand of the deep curing used in some special applications such as dental materials, 3D or 4D printings, manufacture of composite materials, etc.[9, 122-124]

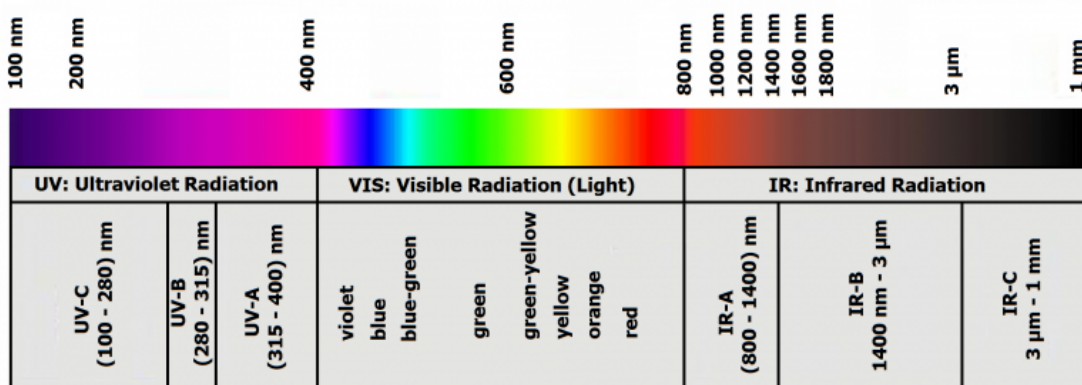


**Figure 1.** The classification of light used in the photochemical sciences, cited from [121].

Mercury lamps, lasers, and LEDs depict the main three kinds of light sources used in photopolymerization. Moreover, the mercury lamp made a great contribution to the development of UV photopolymerization in the past periods[1]. In particular, the medium pressure mercury (MPM) lamp, which exhibits 5 main bands from the UV to visible range, includes 254 nm, 313 nm, 366 nm, 404 nm, and 436 nm. This was widely used in the industrial sector[1]. However, with the development of technology and new demand of the society to operate less harmful equipment, the fatal issues of mercury lamp such as mercury pollution, releasing ozone, and short using life have been revealed. These issues affect the daily life of mankind seriously. Thus, the 'Minamata Convention on Mercury' was signed by 128 countries in 2013 to protect human health and the environment[125]. It prohibits using and producing of mercury productions in widespread respects of human life. This treaty has been carrying out from 01. 02. 2020[125]. Therefore, it urgently demands the society to develop safer light sources and processes appropriate technologies to replace mercury lamps for the future development of photopolymerization.

In recent years, LEDs have received more and more attention as one kind of eco-friendly light sources and competitive candidates to replace mercury lamps. This includes academic studies and industrial applications[126]. Based on the emitting ranges, LED resources can be grouped into UV-LEDs, Visible LEDs, and NIR LEDs. Nowadays, UV and Visible LEDs are more widely used compared to NIR LEDs because there are more initiating systems suitable for UV-visible light irradiation and the technique of the UV-visible LEDs has developed more maturely than NIR LEDs. However, NIR LEDs has received more and more attention because of the unique advantages based on the NIR-light properties as aforementioned noticed.

### 2.1.1 Ultraviolet LEDs for Photopolymerization

Ultraviolet light emitting diodes (UV LEDs) can emit light from 200 nm to 400 nm. Depending on the emission wavelength, they are subdivided in UV-A LEDs ( 315 nm - 400 nm), UV-B LEDs ( 280 nm - 315 nm) and UV-C LEDs ( 200 nm - 280 nm) which can be produced by III-nitride semiconductors, such as InGaN (200 nm - 300 nm), InAlGaN (300 nm - 400 nm), AlGaN (>350 nm)[127-128]. Figure 2 shows the emission of LEDs emitting at 365 nm, 395 nm and 405 nm whose emission ranges from the UV into the blue part.

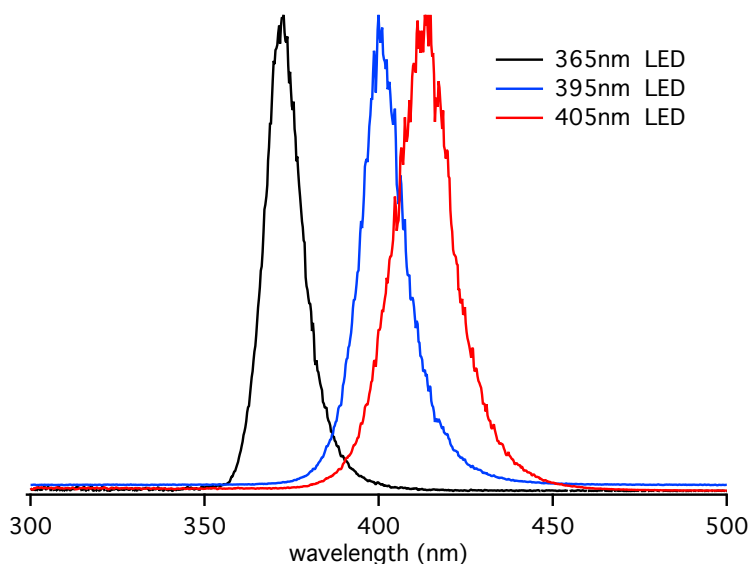


**Figure 2.** Emission spectra of some UV LEDs

Compared with mercury lamps, UV LEDs possess many outstanding advantages such as more flexible opportunities for use in practical applications, longer lifetime (20,000 hours) compared with mercury lamp (from 2,000 to 8,000 hours) and low energy consumption, environmentally friendly treatment because they are mercury free and no ozone release occurs, low heat generation because no IR light emission occurs, no warm-up time, easy control of operation, consistent intensity, and 100% output immediately occurring after turning-on the device[129-130]. These advantages result in a large demand of the market and fast development of the UV LED technology[131]. Nevertheless, there are also some challenges and drawbacks for UV LED; that is limited availability of photoinitiators and formulation suitable for the UV-A LEDs, cooling systems like air while sometimes a water-cooling system is required for some LEDs operation[15]. Additionally, the efficiency and intensity should be improved in future developments.

The main UV LED resources used in photopolymerization are UV-A LEDs (320 nm - 400 nm), which have been widely used in 3D Printing, UV curing of coatings, resins, inks, and adhesives, lithography of photoresist and printed circuit board (PCB), sensing of blanko-

phores and fluorescent labels, medical fields such as bilirubin, blood gas analysis, security fields like banknotes and ID cards, just to name a few examples.[95, 132-136] UV-B and UV-C are mostly used in other fields such as phototherapy, plant lighting[137], gas or biomolecules sensors[138], water purification, sterilisation and disinfection of foods or medical equipments[139-140], non-line-of-sight communication[141] or enabling the charge management systems[142]. However, all of applications base on the development of technology for producing high efficiency and high power LEDs.

### 2.1.2 Visible LEDs for Photopolymerization

Visible Light Emitting diodes (400 nm - 780 nm) include violet LEDs (400 nm - 450 nm), blue LEDs (450 nm - 500 nm), green LEDs (500 nm - 570 nm), yellow LEDs (570 nm - 590 nm), orange LED (570 nm - 600 nm), and red LED (610 nm - 760 nm), see Figure 3[143].

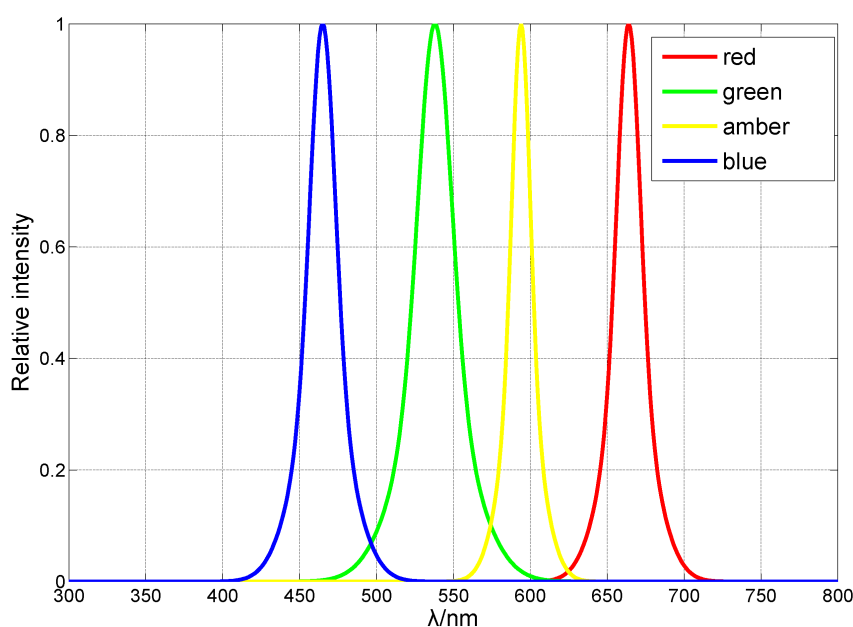


**Figure 3.** Emission spectra of some visible LEDs, cited from [143].

As aforementioned noticed, visible light possesses higher light penetration than UV light in various materials[144]. Moreover, the thickness of resin-based composites interferes with the transmission of light emitting between 350 nm - 425 nm compared to blue light emitting between 425 nm - 550 nm[145-147]. Basically, the longer the wavelength, the less the attenuation of the light transmitted as explained by the scattering coefficient of light. This decreases with increasing wavelength.[145-147] Therefore, the visible LEDs are widely used in deep curing application such as 3D printing and dental photocuring materials as alternatives to UV LED[146, 148-150]. This may be one reason while judicial restrictions sometimes prohibit the use of UV light to protect the human eye as practiced for dental

applications. However, there are some challenges for application of visible LEDs, especially in photocuring field, that are 1) limited amount of photoinitiators for visible range, 2) the blue light hazard to eyes that is greatest at 440 nm[122], 3) lower energy compared with UV LEDs, etc. Great efforts have been achieved regarding the development of the technology. Scientists are doing their best to overcome some of these challenges, which results in more and more photoinitiating systems developed in this field[11, 18, 29, 151]. Moreover, the power of such visible LEDs has also increased[150].

### **2.1.3 Near-Infrared LEDs for Photopolymerization**

Near-Infrared LEDs (NIR LEDs, 700 nm - 2500 nm) possess a narrow emission band as shown in Figure 4[19]. Thus, the shape of emission appears similar compared to UV-Vis LEDs as concluded from the spectra shown in Figures 2-3. Typically, materials possess less intrinsic absorption and exhibit less scattering to NIR LEDs than UV-Vis LEDs. The light emitted from NIR LEDs resides mostly in IR-A region (700 nm - 1400 nm) which does not interfere so strongly with materials such as monomers, resins, oligomers or other compositions comprised in photosensitive formulations. Moreover, mainly the NIR sensitizer contributes to the formulations absorption while functional additives and pigments with absorption in the UV and visible range do not strongly interfere the photo-initiation system in the NIR range[152]. Therefore, NIR light penetrates deep in materials offering great opportunities focusing on deep curing applications[19, 47]. On the other hand, NIR LEDs offer the opportunity for larger areas curing at one time compared to NIR laser because of the large emitting areas of the LEDs. Nowadays, application of NIR LEDs in industrial coatings are limited because of mostly low intensity available LEDs. Recently, the development of NIR LEDs manufacture technology has brought new high power NIR LEDs for research in the lab facilitating NIR photopolymerization while low intensity NIR LEDs did not work in many cases[45, 55, 96, 115, 118]. Particularly, this thesis greatly benefited from this development. Thus, the new high power NIR LED prototypes have brought new impetus in this field. They appear smaller and lighter, the light source generates less heat, much safer usage conditions for the operator compared to NIR laser devices offering great opportunities to promote NIR photopolymerization into more common practical applications. Thus, the research pursued in this thesis with new high power NIR LEDs emitting either at 805 nm or 860 nm has brought new impetus in this field[96, 115, 118] and will give new directions for polymer synthesis as shown by photoinduced polymerization to make interpenetrating polymer networks (IPNs) which failed applying UV exposure[115].

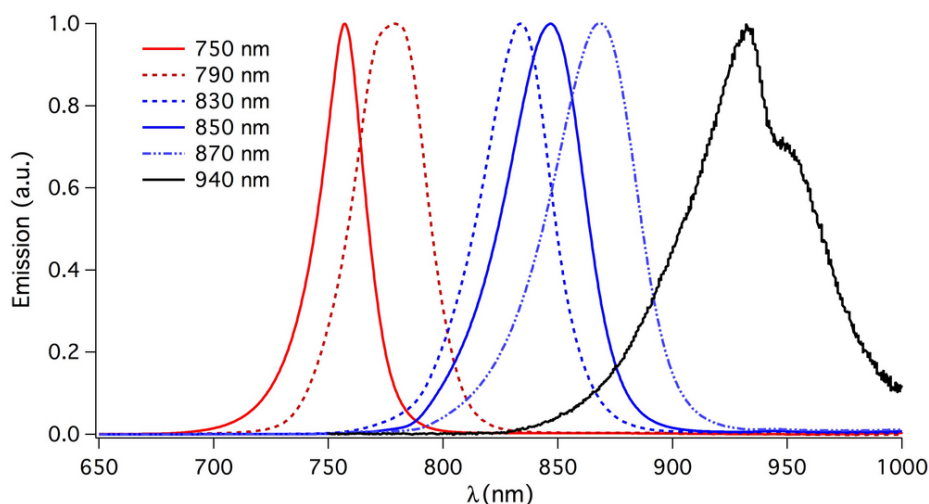


**Figure 4.** Emission spectra of some NIR LEDs, modified from [19].

#### 2.1.4 NIR Laser Diodes for Photopolymerization

NIR laser diodes emitting between 780 nm and 1100 nm depict one kind of lasers that were often made by the same semiconductors used for LEDs. Compared with other light sources, it generates light which is polarised, monochromatic, and often coherent. It also exhibits smaller size, lower costs, and high efficiency compared to other laser devices. Because of the smaller size, the single laser diodes could not produce so much power compared to other lasers operating in the pulsed mode. On the other hand, high power laser diodes, which particularly operate in *cw*-mode, can be obtained by arraying the diodes together as shown in Figure 5. This was successfully used in graphic industry to produce lithographic plates[35, 153]. The emission wavelength of the laser diodes are determined by the materials used to construct them. Generally, the devices made by Al-Ga-As can emit between 700 nm and 900 nm, whereas Ga-As and In-Ga-As-P can emit between 1200 nm and 1600 nm[153]. Thus, laser diodes with different emission wavelength in IR-A range exhibit different intensity; that is from milli-watt to Watt. This makes them useful as powerful tools for NIR photo-induced polymerization resulting in wide applications such as powder coating curing, 3D bio-printing, and manufacture of composite materials[45, 54, 57, 65, 154-156].

NIR laser diodes greatly contributed to the development of the NIR photo-induced polymerization. Birth to this technology was given in 2000 when first patent of a commercialised product appeared in the graphic industry[154]. In the future, one can therefore expect more contributions in a wide range resulting in useful practical application with this new polymerization technique operating in the NIR range.



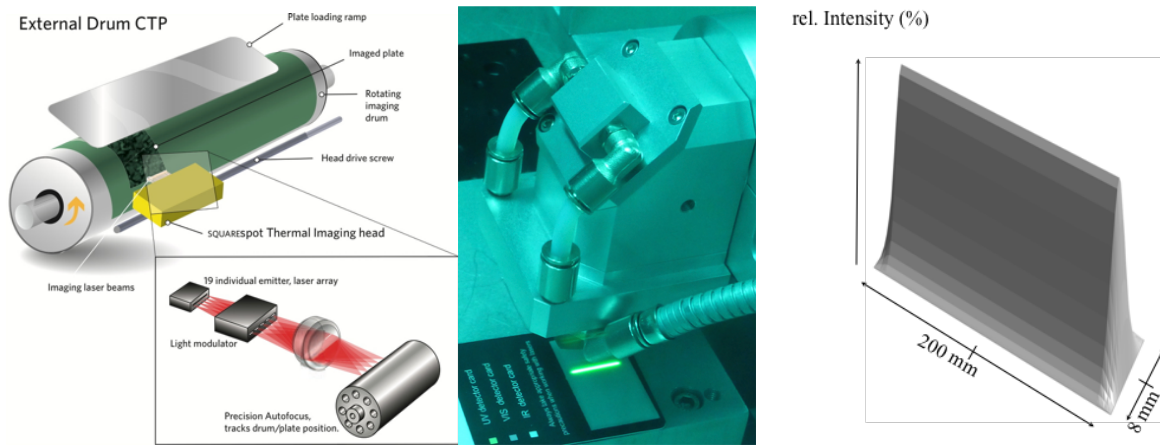
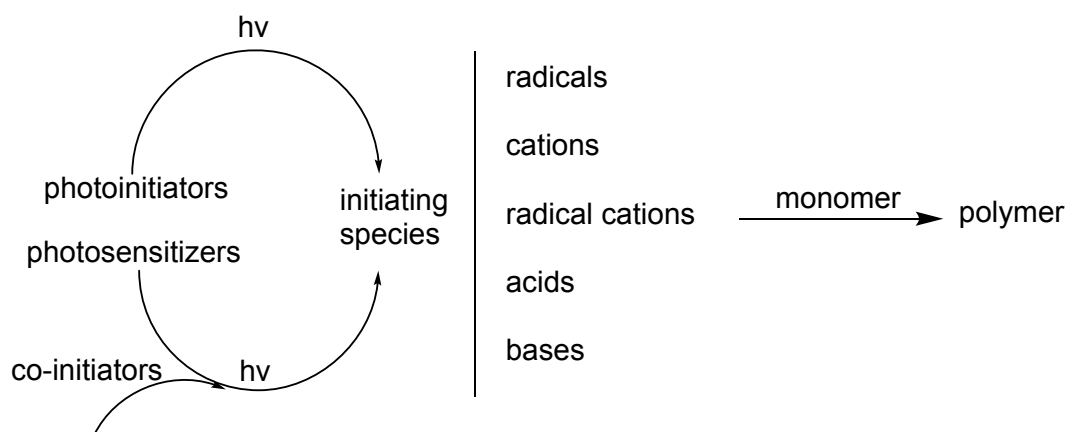


**Figure 5.** NIR laser used in CTP external drum and line shape laser, cited from [35].

## 2.2 Photochemical Reactions for Generation and Regeneration of Activated Intermediates

Photochemical reactions occurring in photopolymerization base on several rules of photochemistry. *The First Law of Photochemistry*[157-158] requests that light must be absorbed by a chemical compound connecting to a chemical reaction. Therefore, photoinitiators or photosensitizers are necessary to absorb light energy while the excited state formed connects to chemistry resulting in generation of initiating species such as radicals and conjugate acid to initiate radical and cationic polymerization, respectively[11]. The *Second Law of Photochemistry*[157] states that each photon absorbed by a molecule results in activation of only one photochemical reaction. Therefore, the higher the amount of absorbed light intensity, the higher the amount of photoproduct considering the same reaction time. Nevertheless, this law is broken in case of multiple-photon absorption where the high intensity source such as a laser causes very high excitation conditions resulting in two or more photons absorption. The *Third Law of Photochemistry* relates to bond cleavage where the energy of the absorbed photon must be greater than the energy of the weakest bond in the molecule[157, 159]. A further example connects to photo-induced electron transfer (PET) reaction where the excitation energy also determines the energetic conditions from a thermodynamic point of view[160-161]. Thus, bond cleavage represents an energy greater than 250 kJ/mol corresponding to  $\lambda_{\max} < 450$  nm. NIR radiation cannot offer this energy and would proceed by other reaction route; that is photoinduced electron transfer (PET)[162].

In photopolymerization, photoinitiators or photosensitizers depict the key components of photopolymerization, which absorb light where the excited state formed converts reactive intermediates such as radicals, cations, radical cations, conjugate acid, or sometimes base to initiate the polymerization of monomers and /or oligomers based on the laws of photochemistry[163-164]. Scheme1 illustrates the general principle of initiation for photopolymerization[164].



**Scheme 1.** General principle of photopolymerization, modified from [164].

There are several paths to generate reactive species:

- Generation by bond cleavage upon photoirradiation, which include homolytic cleavage and heterolytic cleavage;
- Generation by photoinduced electron transfer reaction requesting a co-initiating system comprising sensitiser and co-initiator;
- Generation by bond cleavage caused by heat from surrounding related to a photonic process that is light absorption while the heat released refers to internal conversion (IC).

The first two opportunities base on photoinduced polymerization relying on almost photonics steps while the last point refers to photoinduced thermal initiated polymerization systems[51]. Herein, the details of the photochemical reaction for generation or regeneration of reactive species through these three possibilities are introduced.

### 2.2.1 Bond Cleavage upon Photoexcitation

Photochemical cleavage typically occurs at ambient conditions with the prerequisite to absorb at least so much energy as needed for bond cleavage. This process occurs in a very short time depending whether the reaction occurs from the singlet or triplet state resulting in no energy release to the environment compared to conventional thermal induced bond cleavage caused by thermal treatment as typically observed for the cleavage of azo-compounds[164]. Moreover, the process is controlled by switching on or off the light with no request of additional warm-up or cool-down time decreasing the cost of time and energy power for industrial manufactures[164]. Generally, the bond cleavage upon photoirradiation includes two different types of reactions relating either to homolytic cleavage generating radicals to initiate radical polymerization or heterolytic cleavage generating conjugate

acid or base to initiate ionic polymerization following cationic or anionic polymerization mechanism, in Figure 6. More details about homolytic and heterolytic cleavage are discussed in this section.

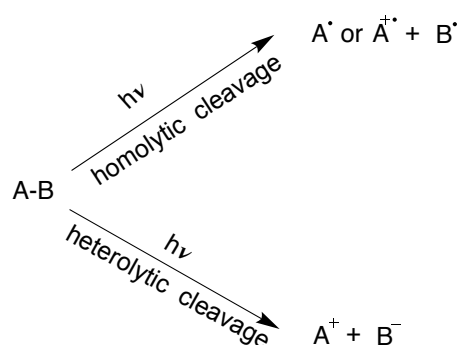
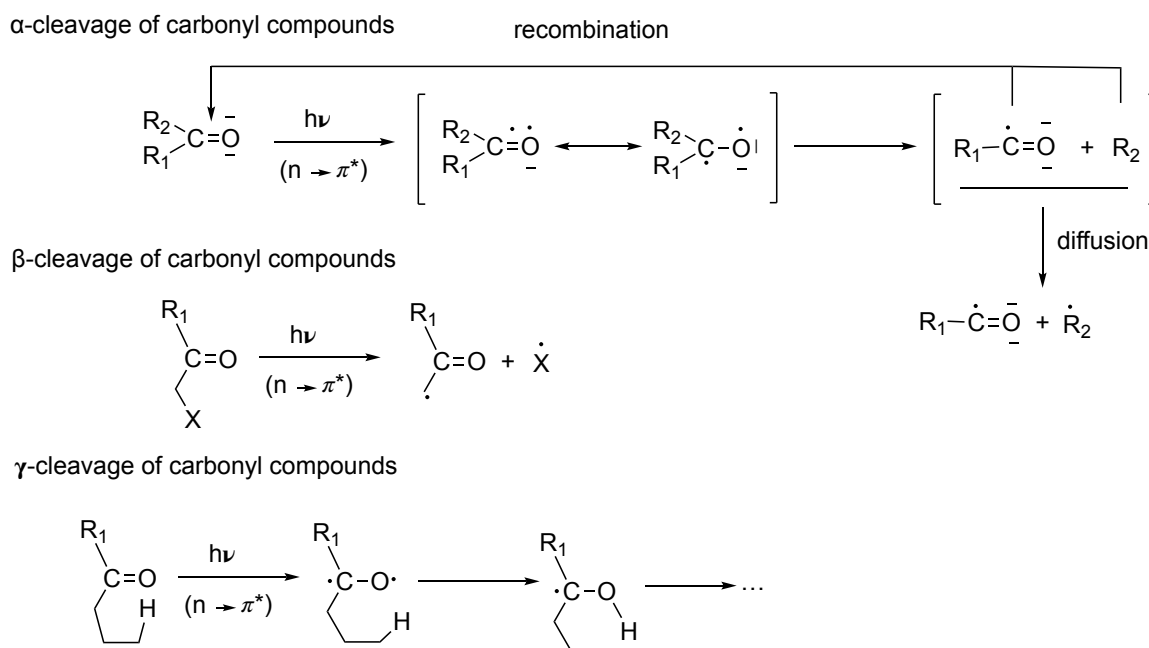


**Figure 6.** Bond cleavage styles upon photoirradiation.

### Homolytic Cleavage of Photoinitiators

Most of the radical photoinitiators and some cationic photoinitiators proceed photolysis according to a homolytic cleavage protocol upon photoirradiation with UV-visible light in photopolymerization systems[1, 11, 164]. For the radical photoinitiators working in the UV-visible range, typical examples of photoinitiators base on derivatives based ketones and aldehydes[11]. These structural features relate to their special mechanistic features. Excitation of these compounds relates to a symmetry forbidden  $n \rightarrow \pi^*$  transition with relatively low extinction coefficient (less than  $10^2 \text{ M}^{-1} \cdot \text{cm}^{-1}$ ) while the lifetime of the excited state remains at longer time frame ( $ns-\mu s$ ) because the triplet state possesses a longer lifetime residing in this range. This photochemical process bases on the transition of the n-electron of the oxygen in a higher located anti-bonding orbital of the  $\pi$ -electron system of the carbonyl group resulting in a structural pattern exhibiting properties of a diradical.[162] This process subsequently results in a series of photochemical reactions such as abstraction of hydrogen,  $\alpha$ -cleavage of the C-C bond adjacently placed to the carbonyl group (*Norrish Type I* cleavage),  $\beta$ -cleavage, or  $\gamma$ -cleavage; see Scheme 2.[11]

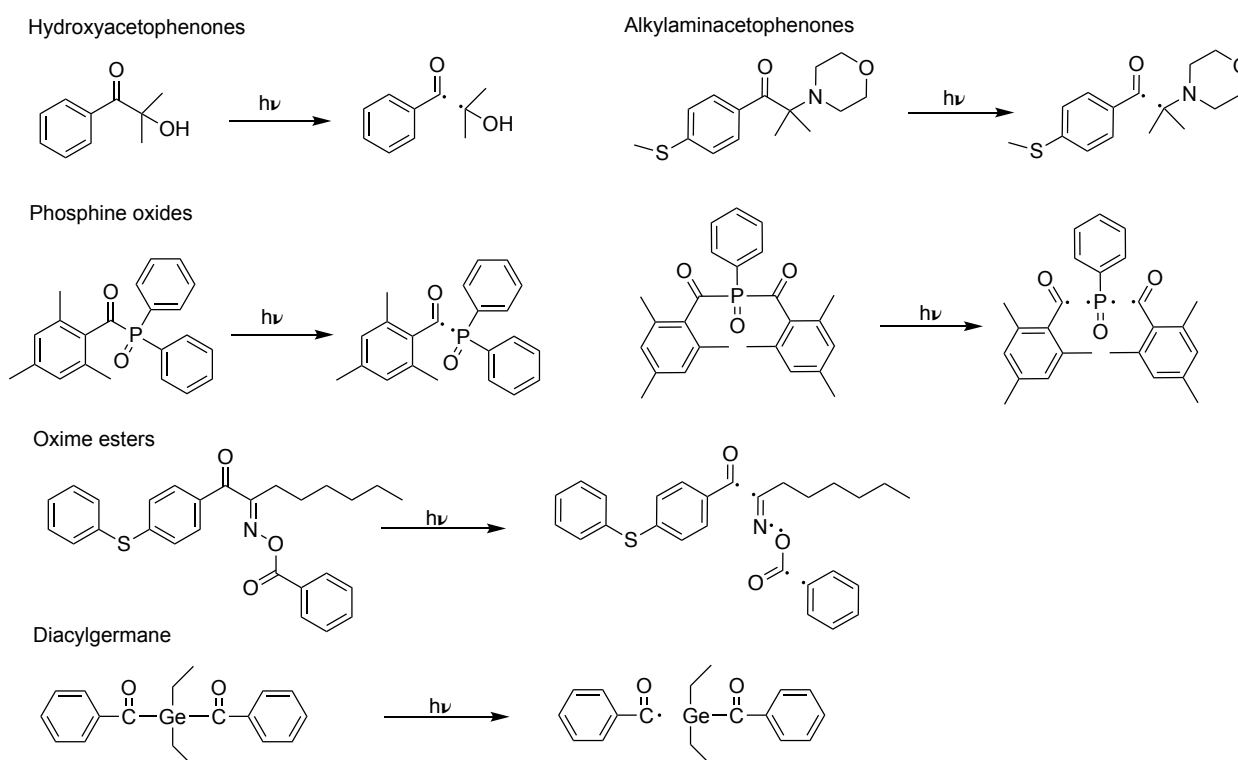


**Scheme 2.** Reaction path for  $\alpha$ ,  $\beta$ ,  $\gamma$ -cleavage of carbonyl compounds, modified from [11].

As well known, cage diffusion processes affect the overall efficiency of the radical polymerization[11]. Generally, the high the viscosity of the solution results in lower capability to diffuse causing a lower efficiency of the system to form radicals for initiation of polymerization. Additionally, another factor affects the efficiency of the radicals related to their electronic properties; that is the electrophilicity causing better efficiency to add on olefins. Generally, electron donating substituents such as alkoxy or amino groups increase the nucleophilicity also of the radical electron resulting in less efficiency to add on olefins carrying electron withdrawing groups such as (meth)acrylic esters[165].

Representative materials exhibiting cleavage of the carbonyl group relate to hydroxyacetophenones, alkylaminoacetophenones, phosphine oxides, oxime esters, or diacylgermane as widely used in industry, Scheme 3[1, 11, 67, 164]. Moreover, hydroxyacetophenones, and alkylaminoacetophenones have been used for several decades as photoinitiators in UV polymerization[1, 11, 164]. Phosphine oxides introduced in the late 80s exhibit higher performance resulting in widespread application in the industrial sector [67]. The phosphine oxide radical generated by  $\alpha$ -cleavage upon irradiation results in addition to olefins. On the other hand, they were reported to exhibit the capability to react with iodonium salts to initiate cationic polymerisation based on photoinduced electron transfer (PET [166-167]. Acylgermanes[168-171], acylsilanes[172], or acylstannanes[173-174] represent additional alternatives showing efficient  $\alpha$ -cleavage. Acylgermanes exhibit a bathochromic shift of absorption facilitating absorption of blue light compared to hydroxyacetophenon,

and alkylaminoacetophenones[171, 175-176]. These changes successfully transferred such photoinitiators to dental applications for restoration of teeth[18, 171, 176]. As a result, incorporation of elements carrying d-orbitals results in higher molar extinction coefficients and bathochromic shifted absorption[173-174]. These studies offer the guideline for develop high performance photoinitiators. Excitation of oxime ester also occurs by  $\alpha$ -cleavage resulting in break of the N-OR bond and generation of two radicals; that are  $R-CR'=N\cdot$  and  $\cdot OR''$ [14, 63, 72]. Both electrophilic radicals facilitate efficient addition to (meth)acrylic monomers resulting in initiation of radical polymerization explaining their outstanding performance as photoinitiators. The next section will discuss more details.

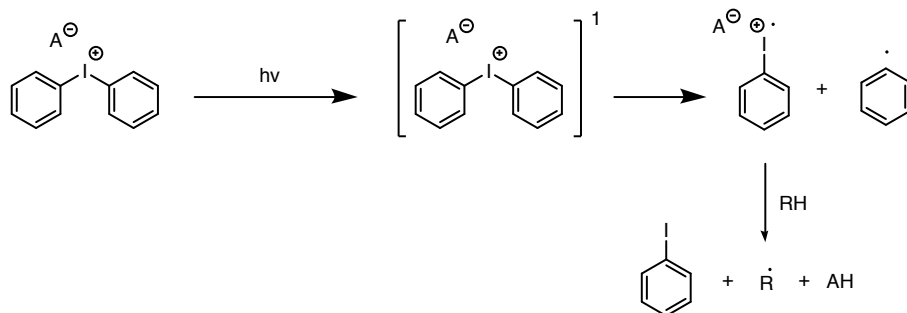


**Scheme 3.**  $\alpha$ -cleavage of the carbonyl group, cited from [1, 11, 67, 164].

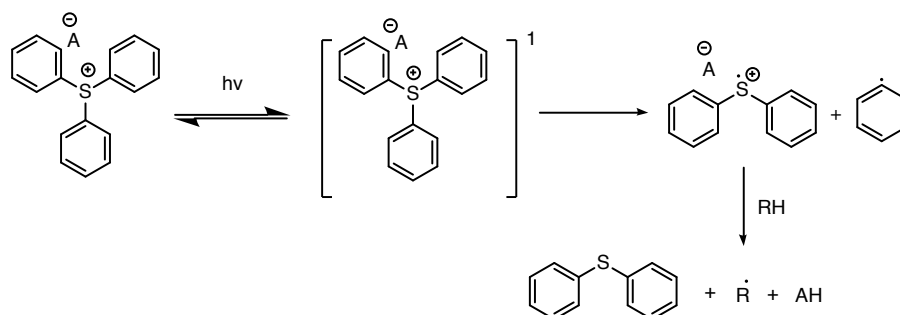
Some photoacid generators used as cationic photoinitiators in the UV-visible range also homolytically cleave upon exposure. These include diaryliodonium salts[177], triarylsulfonium salts[178-179], N-hydroxyimidesulfonate esters[180], and arylsulfonate esters[181]. Herein, the diaryliodonium salts and triarylsulfonium proceed according to a similar mechanism as shown in Scheme 4. It occurs by homolytic cleavage of the Ar-I or Ar-S bond resulting in aryl radical  $Ar\cdot$  and  $ArI^{+\cdot}$  or  $ArS^{+\cdot}$  cation radicals[11]. The latter abstracts hydrogen from the surrounding resulting in generation of conjugate acid[11]. Arylsulfonate follows either homolytic cleavage or heterolytic cleavage depending on the chemical structure[182]. For instance, aryl tosylates prefer homolytically cleave according to path B as

shown in Scheme 4 upon exposure while mesylate and triflate derivatives exhibit heterolytic cleavage of the Ar-O bond as explained in path A shown in the same scheme. Additionally, N-hydroxyimidesulfonate esters homolytically cleave the N-O bond resulting in release of the respective sulfonyloxy radical abstracting hydrogen from the surrounding to produce the corresponding sulfonic acid, see Scheme 4[182].

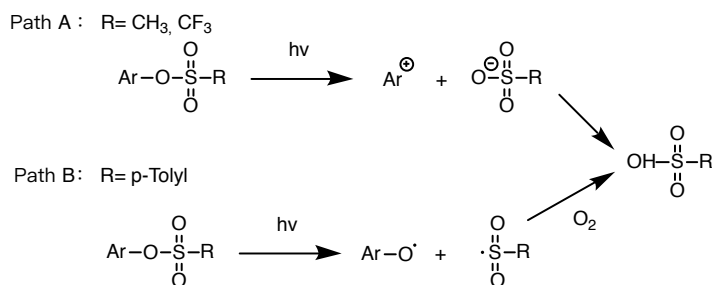
#### Diphenyliodonium salts



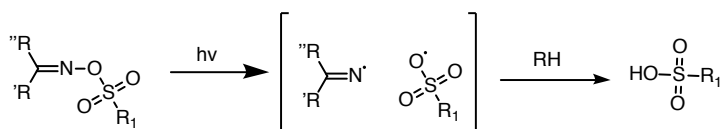
#### Triarylsulfonium salts



#### Arylsulfonate esters



#### N-hydroxyimidesulfonate

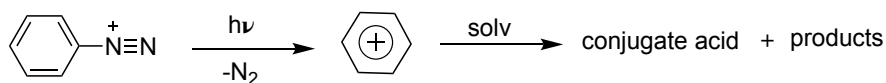


**Scheme 4.** The photolysis mechanism of some photoacid generators, cited from [182].

### Heterolytic Cleavage

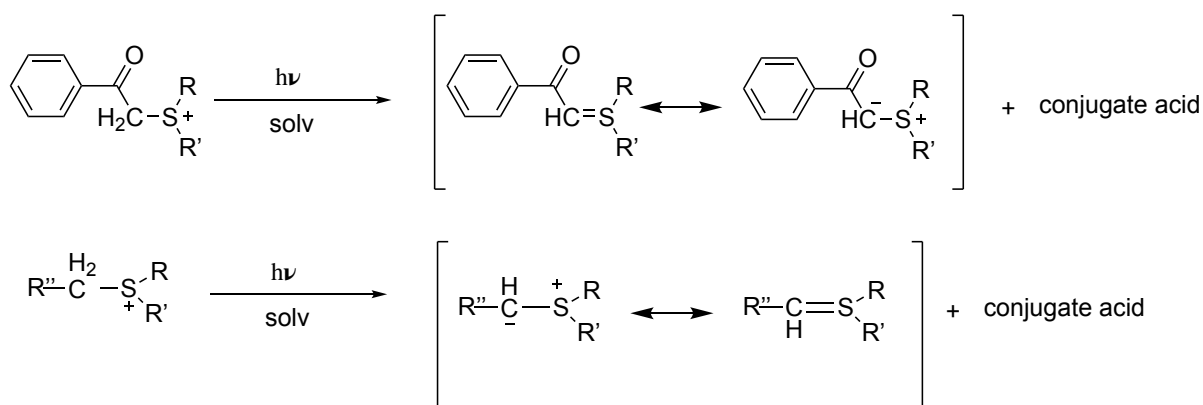
Arene diazonium salts, alkyl- and phenacyl-substituted sulfonium salts depict typical photoinitiators showing heterolytic cleavage[183-184]. Moreover, the cleavage of diazonium

salt results in formation of nitrogen and an aryl cation as reactive intermediate.[183-184]  
The latter fast releases conjugate acid and further products, see Scheme 5.



**Scheme 5.** Heterolytic cleavage of arene diazonium salts, cited from [183-184].

Alkyl- and phenacyl-substituted sulfonium salts exhibit heterolytic cleavage (Scheme 6) competitively occurring to homolytic cleavage [185-186]. Compounds **SS1** and **SS2** (Chart 1) represent two examples where heterolytic cleavage occurs [185]. **SS2** exhibits a longer absorption ( $\lambda_{\max}=392$  nm;  $\epsilon_{\max}=5.5 \times 10^4$  M<sup>-1</sup>cm<sup>-1</sup>) facilitating their application with UV and blue light LEDs[187].



**Scheme 6.** Heterolytic cleavage of sulfonium salts comprising an alkyl moiety in  $\alpha$ -position, modified from [186].

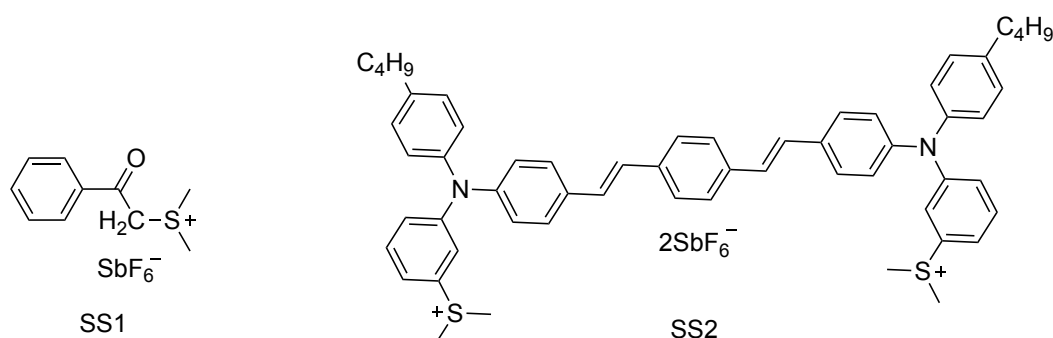


**Chart 1.** The chemical structure of SS1 and SS2, cited from [185, 187].

### 2.2.2 Spectral Sensitisation Based on Photoinduced Electron Transfer

Photoinduced electron transfer (PET) depicts one kind of fundamental reaction occurring in photochemistry, which facilitates the generation of reactive species such radicals, cations and/or conjugate acid to initiate polymerization by absorbing light including UV, the



entire visible range and NIR up to 1100nm[37, 45, 115]. Graphical industry mostly benefited from these developments since PET led to the development of silver halide based information recording materials and later to silver-free materials where photopolymers based on photoinitiated polymerization took a special function.[24, 31, 188-189] PET bases on the energetic levels of the participating components including electron donor **D**, electron acceptor **A**, and photoresource that offers light energy to excite **D** or **A** from stable ground state  $S_0$  to reactive excited state. Based on the frontier molecular orbital theory, the energy of the highest occupied molecular orbital (HOMO) is proportional to the oxidation potential  $E_{ox}$  while the energy of the lowest unoccupied molecular orbital (LUMO) is proportional to the reduction potential  $E_{red}$ . Generally, there are two scenarios to depict PET on an energetic basis as shown Figure 7. Case a): donor **D** absorbs the light energy to promote it to the first excited state  $D^*$ , then **PET** occurs from the first excited state of the donor  $D^*$  reacting with the acceptor **A** where electron transfer occurs. This leads to half-filled upper levels of the donor ( $E_{ox}(D)$ ) and the acceptor **A** ( $E_{red}(A)$ ) resulting in formation of  $D^{+\cdot}$  and  $A^{\cdot-}$ , which results in the free enthalpy of the electron transfer as  $\Delta G_{PET} = E_{red}(D) - E_{red}(A)$ , where half filled levels originally relating to the LUMO of the Donor and Acceptor, respectively. Case b): it discloses circumstances where acceptor **A** absorbs the light energy resulting in  $A^*$ . Here, the half filled orbital originally relating to the HOMO uptakes an electron from the highest from the highest occupied level of **D** into the half-filled lower level of  $A^*$ . This also yields the same species  $D^{+\cdot}$  and  $A^{\cdot-}$  as in case a) which decompose resulting in generation of radicals and conjugate acid. Here, the free enthalpy of the electron transfer is  $\Delta G_{PET} = E_{ox}(D) - E_{ox}(A)$ [160, 190]. These considerations include the excitation energy  $E_{00}$  (case a):  $E_{red}(D) = E_{ox}(D) + E_{00}$ ; case b):  $E_{ox}(A) = E_{red}(A) - E_{00}$

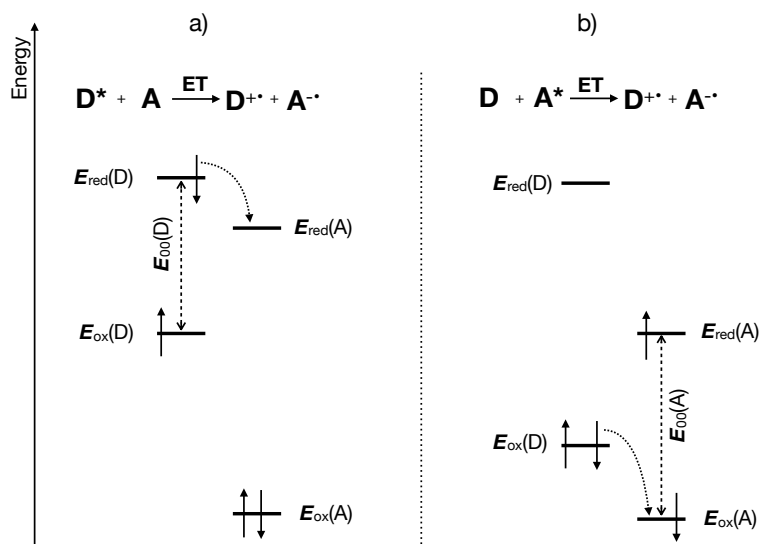


**Figure 7.** Energetic relations of **PET** considering two scenarios. a) Donor **D** absorbs the light energy. b) Acceptor **A** absorbs the light energy.

The free enthalpy of electron transfer can be calculated by Eq.1 where  $F$  stands for the Faraday constant and  $\Delta E_{00}^D$  relates to the excitation energy of the electron donor in Case a). It also comprises a coulomb term ( $E_{coul}$ ), Eq. 3 correcting the energy in the case that two opposite or equal charged species are formed. It also requires knowledge about the oxidation potential of the donor  $E_{ox}^{D/D^+}$ , the reduction potential of the acceptor  $E_{red}^{A/A^-}$  of the reactants, and, of course, the excitation energy of the donor  $\Delta E_{00}^D$ . Eq. 3 relates to case a) which is assigned to an oxidative mechanism.

$$\Delta G_{PET} = F(E_{ox}^{D/D^+} - E_{red}^{A/A^-}) - E_{coul} - \Delta E_{00}^D = E_{red}(D) - E_{red}(A) - \Delta E_{00}^D - E_{coul} \quad (\text{Eq. 1})$$

Where the  $\Delta E_{00}^D$  is:

$$\Delta E_{00}^D = \frac{\hbar c}{\lambda_{max}^D} \cdot N_A \quad [\hbar=6.626 \times 10^{-34} \text{ J}\cdot\text{s}, c=3 \times 10^8 \text{ m/s}, N_A=6.022 \times 10^{23}] \quad (\text{Eq. 2})$$

Where the  $E_{coul}$  is:

$$E_{coul} = \frac{N_A \cdot e_0^2}{4\pi \epsilon_o \cdot \epsilon \cdot \gamma} = \frac{1387}{\epsilon \cdot \gamma} \quad [\text{in kJ}\cdot\text{mol}^{-1} \text{ with } r \text{ in \AA}] \quad (\text{Eq. 3})$$

Case b) in Figure 7 discloses circumstances where excitation of the acceptor **A** results in a negative free reaction enthalpy. Once excitation occurred in the acceptor molecule, there exists the availability to take up an electron from the higher filled orbital of **D** into the lower half filled orbital of **A** resulting finally in completing the photoinduced electron transfer pro-

to col, where relates to a reductive mechanism. The free enthalpy of the photoinduced electron transfer in this case can be expressed by Eq. 4:

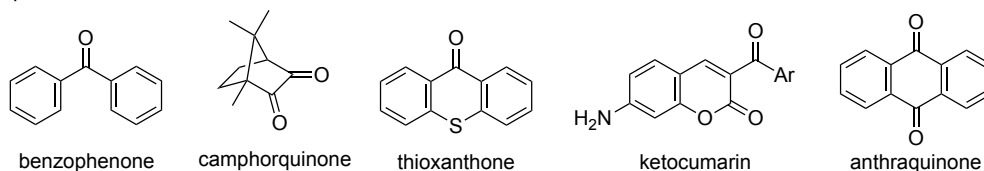
$$\Delta G_{PET} = F(E_{ox}^{D/D^+} - E_{red}^{A/A^-}) - E_{coul} - \Delta E_{00}^A = E_{ox}(D) - E_{ox}(A) - \Delta E_{00}^A - E_{coul} \quad (\text{Eq. 4})$$

Where  $\Delta E_{00}^A$  is:

$$\Delta E_{00}^A = \frac{\hbar c}{\lambda_{max}^A} \cdot N_A \quad (\text{Eq. 5})$$

Such considerations of the photochemical reaction do not include any intrinsic activation barriers,[160, 162] which can also exist even in the case that  $\Delta G_{PET} < 0$ . Some Norrish Type II photoinitiators based on UV-visible initiated photopolymerization in conjunction with various co-initiators result in generation of radicals as typical examples in these considerations. Upon irradiation, the Type II photoinitiator absorbs the light energy and arrives to the excited state. Afterwards, it interacts with the co-initiator to generate radicals via PET[191-192]. The typical Type II photoinitiators normally relate to ketone type photoinitiators such as benzophenone, thioxanthone, camphorquinone, ketocoumarin, anthraquinone, and their derivatives. Typical useful co-initiators are amines, thiols, phosphorus; see Chart 2[11, 24].

#### Type II photoinitiators



#### Coinitiators of Type II photoinitiators

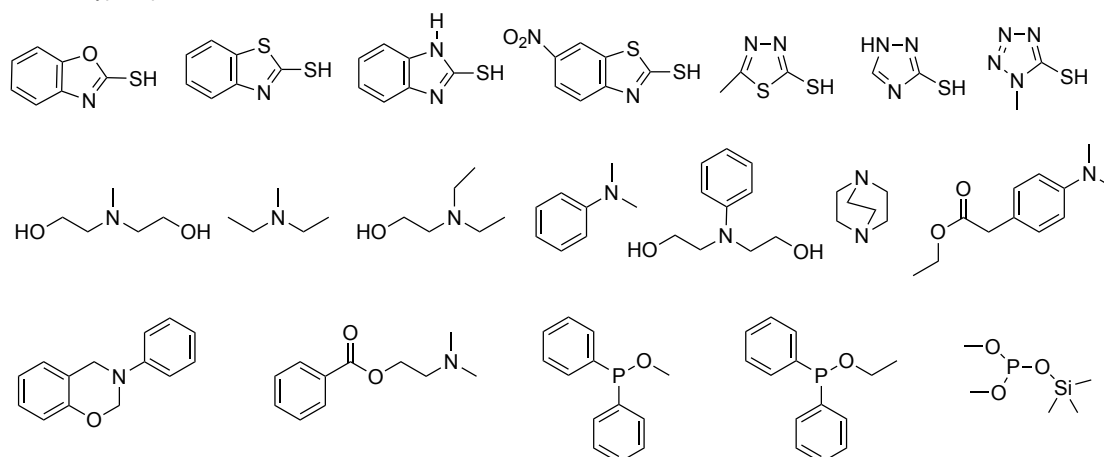


**Chart 2.** Typical Type II photoinitiators and co-initiators, cited from [24].

Another typical example could be nucleophilic radicals produced by Norrish Type I radical photoinitiators upon irradiation exhibiting the capability to transfer an electron to an electron-deficient compound such as diazonium, iodonium or sulfonium salt[11]. Chemical Induced Dynamic Nuclear Polarization (CIDNP) studies confirmed the successful electron transfer between such nucleophilic radicals formed in a Norrish Type I photoinitiators and iodonium salts[166-167].

Nevertheless, Figure 8 depicts different scenarios occurring in the PET reactions where  $\Delta G_{PET}$  can be either positive, zero or negative but the activation free enthalpy  $\Delta G_{PET}^\ddagger$  is greater than zero in some cases explaining the intrinsic barrier and therefore threshold of the reaction in such systems. The position and shape of the potential curves of educts (E) and products (P) determines the size of  $\Delta G_{PET}^\ddagger$ . The shorter the distance between both and the steeper the course, the higher becomes the intrinsic activation barrier. Therefore, the additional energy is necessary to facilitate the reaction occurring. This was overseen for a long time in the case of cyanines working as sensitizers in combination with iodonium salts or Triazine A as acceptors in NIR sensitized photopolymer systems[7, 23, 46-47, 189]. This lack was filled in this thesis by application of high-power NIR LEDs where the PET of photoexcited cyanines resulted in successful electron transfer to oxime esters[160].

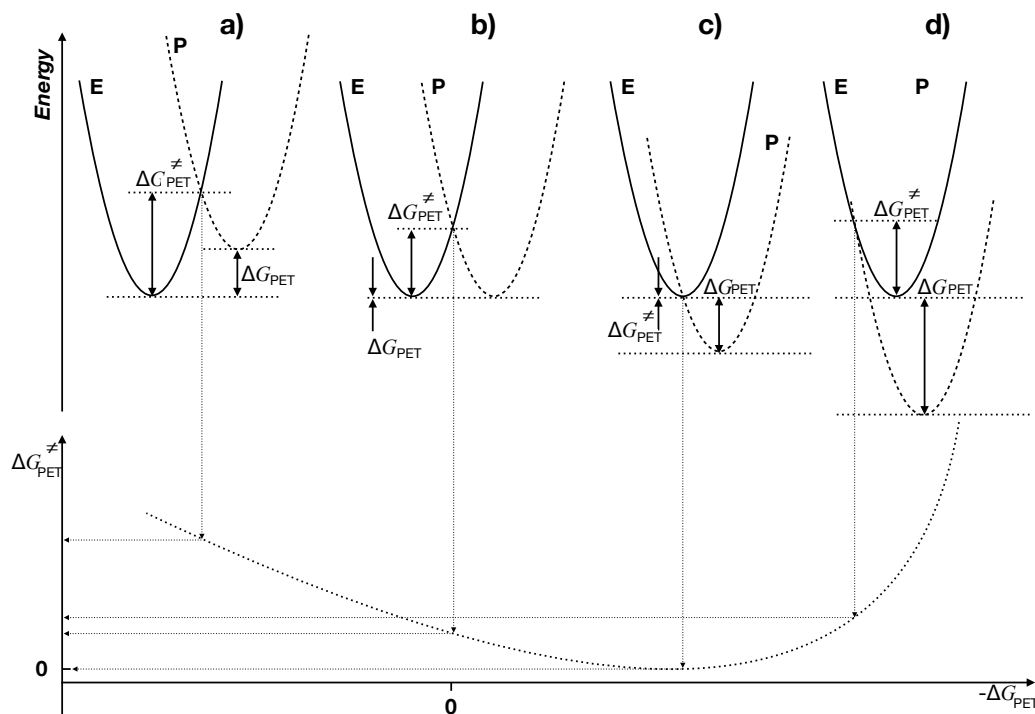


**Figure 8.** Energetic relations of PET with internal barrier causing threshold systems, a) endothermal conditions with  $\Delta G_{PET} > 0$ , b) thermoneutral conditions with  $\Delta G_{PET} = 0$ , c) exothermal conditions with  $\Delta G_{PET} < 0$ , d) exothermal conditions with  $\Delta G_{PET} < 0$ .

Figure 8 depicts the potential energy curves of the educts E and products P demonstrating the necessity to introduce additional heat as released by the heptamethine sensitizers in all systems except in the case c). NIR-sensitive systems possess  $\Delta G_{PET}$  values being either slightly positive, neutral or slightly negative; that is  $\pm 0.5$  eV[47]. Outer-sphere (dielectric constant of the surrounding) and inner-sphere coordinates (change of bond order and lengths) contribute to the reorganisation energy  $\lambda$  as introduced by Marcus in last 50s[160, 162, 190]. His theory was experimentally confirmed a few decades later[160-161] and also explains why the kinetic constant of electron transfer  $k_{PET}$  reduces just by consideration of such parabolic functions explaining the existence of intrinsic activation barriers. This may reside between 1-1.5 eV[160-161]. Non-radiative deactivation of the NIR sensitizer depicts the main deactivation route[37]. It additionally provides enough thermal energy to overcome the activation barrier which is the internal barrier. It can easily achieve temperatures  $>120$  °C in heptamethine cyanine system upon NIR irradiation[36, 45, 50]. Eq. 8 shows the relation between the rate constant  $k_{PET}$ , the activation free enthalpy, the free enthalpy of electron transfer and reorganizational energy  $\lambda$  based on the Marcus theory related to PET reaction[162]. Moreover,  $\lambda$  combines inner sphere coordinates relating to geometry changes and therefore also transfer of vibrational energy, and outer sphere coordinates that relate to properties of the environment such as dielectric constant of the surroundings and refractive index[160-161]. Based on the Marcus theory for electron transfer[160, 190], the activation free enthalpy of PET reaction  $\Delta G_{PET}^\ddagger$  which determines the size of internal activation barrier of the reaction defines as follows:

$$\Delta G_{PET}^\ddagger = (\Delta G_{PET} + \lambda)^2 / 4\lambda \quad (\text{Eq. 6})$$

where  $\lambda$  defines as aforementioned noticed,  $\Delta G_{PET}$  relates to the free enthalpy of electron transfer as expressed by Eq. 7[160]:

$$\Delta G_{PET} = F(E_{ox}^{D/D^+} - E_{red}^{A/A^-}) - E_{coul} - \Delta E_{00}^D \quad (\text{Eq. 7})$$

where  $E_{ox}^{D/D^+}$  is oxidation potential of the electron donor which normally is sensitizer such as heptamethine cyanine, and  $E_{red}^{A/A^-}$  is reduction potential of the electron acceptor which normally is co-initiator such as iodonium salt or oxime ester.  $\Delta E_{00}^D$  depicts the activation energy of the donor. The electron transfer reaction rate constant  $k_{PET}$  defines as follows[160]:

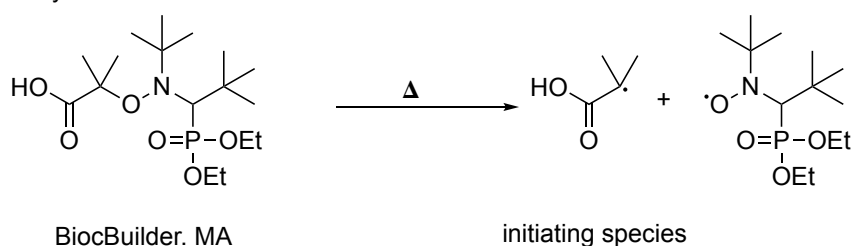
$$k_{PET} = \nu_N \cdot \kappa \times \exp\left(-\frac{\Delta G_{PET}^\ddagger}{RT}\right) = \nu_N \cdot \kappa \times \exp\left(-\frac{(\Delta G_{PET} + \lambda)^2 / 4\lambda}{RT}\right) \quad (\text{Eq. 8})$$

where  $v_N$  is the theoretical maximal available rate, and  $\kappa$  is probability coefficient. Through equation (8), we can see the temperature affects the electron transfer rate constant  $k_{PET}$ [160]. The internal activation barrier caused by the free activation enthalpy  $\Delta G_{PET}^\ddagger$  could be useful in designing technical systems where photochemistry reactions results in the threshold of the system. Under such conditions, it requires to use special hardwares to initiate the reactions while ambient light conditions do not significantly affect the stability of the light sensitive materials. Such systems exist in some computer to plate (CTP) systems carried out at 830 nm laser excitation based on NIR photopolymerization[7, 31-32, 35, 153, 189].

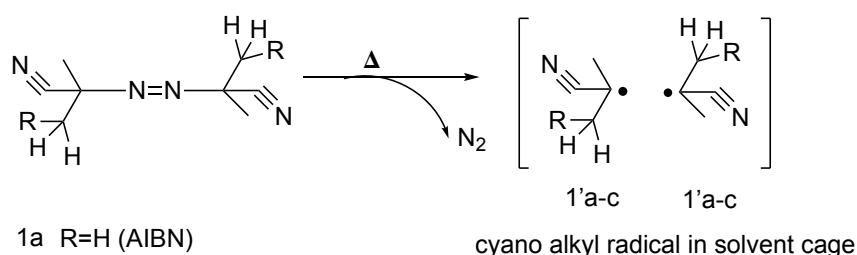
### 2.2.3 Thermal Decomposition

Some available compounds sensitively respond to the heat resulting in generation of radicals by thermal decomposition. These are for example alkoxyamines, azo derivatives, and (hydro)peroxides[51], see Scheme 7 for more details. These compounds are always used as initiators in thermally initiated free radical polymerization. Recently, Lalevee used these initiators in NIR photoinduced polymerization systems applying the heat released by the cyanine to decompose the thermally sensitive initiators[52-53, 65, 193].

alkoxyamine



azo

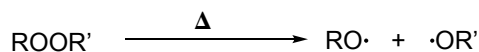


1a R=H (AIBN)

1b R=CH<sub>3</sub> (AMBN)

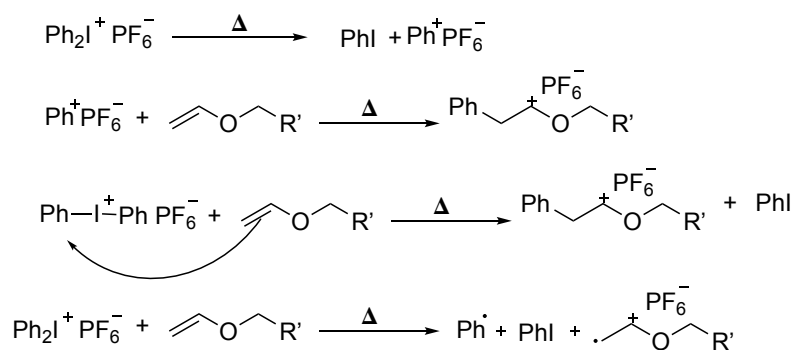
1c R=CH<sub>2</sub>C(CH<sub>3</sub>)<sub>2</sub>COCH<sub>3</sub> (V70)

peroxides

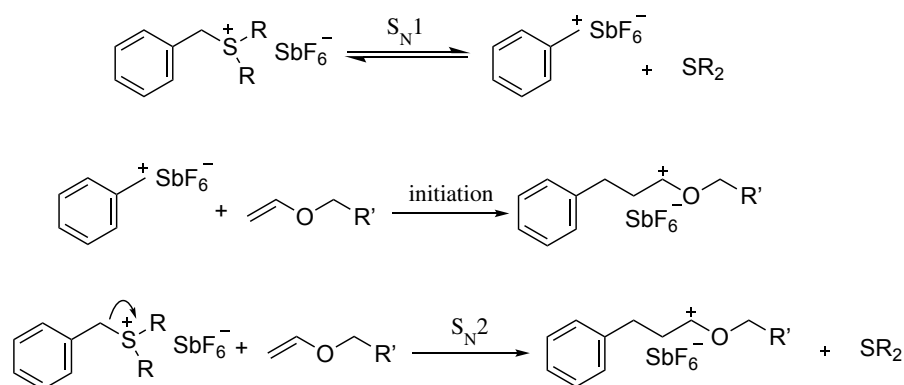


**Scheme 7.** Thermolysis mechanism of alkoxyamine initiators, azo initiators, and peroxides, cited from [51].

Iodonium salts and sulfonium salts can also be used as thermal initiators where the thermal-induced bond cleavage results in generation of radicals and conjugate acid [194-196]. In the case of iodonium salts (Scheme 8) and sulfonium salts (Scheme 9), initiation of the cationic polymerization of vinyl ethers occurs with good efficiency[194-196].

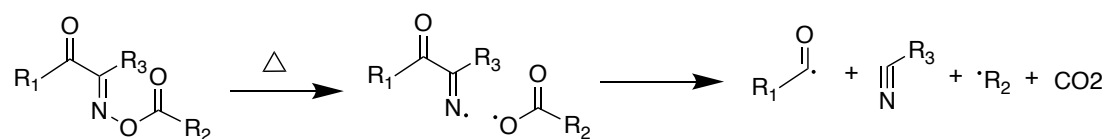


**Scheme 8.** Thermal induced polymerization of vinyl ethers employing diaryliodonium salt, cited from[194].



**Scheme 9.** Thermal induced polymerization of vinyl ethers employing sulfonium salt, cited from [194].

Some of Oxime esters may also exhibit cleavage of the N-O bond after heat treatment (see Scheme 10) . The low bond energy of the N-O, which is only 221.8 kJ/mol[74], may favour such creation pathways. DSC measurement results revealed that this kind of initiator could make polymerisation of acrylate ester monomer with increasing temperature. In other words, some of these photoinitiators can initiate thermal polymerization by thermal decomposition.[28, 197]



**Scheme 10.** Thermolysis of oxime esters.

## 2.3 Photochemical Active Materials for Initiator Systems with NIR LED Exposure

Photochemical active materials including photoinitiators, photosensitizers, and co-initiators depict the key of photopolymerization by converting light to chemistry. For the photoinitiator system in the photoinitiating system, we can subdivide the photoinitiating system into three kinds depending on the number of photochemical active materials; that is unimolecular photoinitiator system (Norrish type I photoinitiators)[11], bimolecular photoinitiator systems[11], and multi-component photoinitiator systems requesting at least three components[42, 198]. We can find all of these different kinds of photoinitiator system in UV-visible curing systems. However, NIR photoinitiating systems mostly relate to bimolecular photoinitiators systems, and multi-molecular photoinitiators systems. The significant lower excitation energy does not facilitate stable unimolecular type I photoinitiators requesting absorption in the NIR range [37]. Different initiating systems exhibiting the capability to initiate the polymerization with NIR light sources were reported in the literature[19, 31, 40, 42, 44, 46, 48, 51-53, 56, 65, 96, 115, 118]. Most of these photoinitiating systems relate to bimolecular photoinitiator systems comprising NIR sensitizers and co-initiators, and multi-component photoinitiator systems which include NIR sensitizers, and several co-initiators[37]. In this section, NIR sensitizers, co-initiators such as iodonium salts, oxime esters, and thermal initiators introduced, that have been used in the NIR photoinitiator systems are introduced.

### 2.3.1 Cyanines as NIR Sensitizers

More than 150 years ago, the word 'cyanine' was used to name a blue dye (Chart 3 ) by the company of Menier on the *London International Exhibition on Industry and Art* in Paris[199]. Starting from that period, the development and application of dyes in industry helped cyanines to receive more importance as class of dyes exhibiting cyan colour[200].

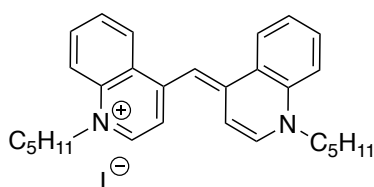


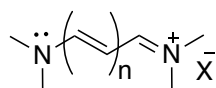
**Chart 3.** Quinoline blue-the first dye named by cyanine, cited from [201].



Cyanines have received huge attention in the last decades[36, 201] because of their special properties related to physical, chemical, photophysical and photochemical aspects[37, 200, 202]. On this subject, numerous studies about novel structures, properties, and applications in various areas have been reported every year[200, 203-206]. Herein, the fundamentals of the cyanines including types, photophysical and photochemical properties, and the applications especially in NIR photopolymerization are reported in detail.

#### Fundamentals of Cyanine as sensitisers

Chart 4 shows the general structure of the cyanine[205]. It relates to a polymethine comprising two nitrogen centers at the two terminal groups carrying an odd number of methane groups, where  $n$  is the number of vinyl groups ( $-\text{CH}=\text{CH}-$ ) in the methine chain[207], which is 0, 1, 2, 3, etc. Depending on the value of  $n$ , the cyanine can be called as monomethine ( $n=0$ ), trimethine ( $n=1$ ), pentamethine ( $n=2$ ), and heptamethine ( $n=3$ ). The number of  $n$  affects the absorption of cyanine significantly because each additional vinyl group results in bathochromic shift of absorption of about 100 nm[37, 200, 208-209], which is illustrated by Figure 9. Based on the theory of vinylene shift, the absorption spectrum of the cyanine could be tailor made by tuning the value of  $n$ . Generally, the higher value of  $n$  the longer appears the cyanine absorption wavelength. However, long wavelength absorbing cyanines exhibit less stability compared to other cyanines with short absorption[42, 51, 200, 206, 210].



X= Br, I, ClO<sub>4</sub>, etc.

n= 0, 1, 2, 3, etc.

**Chart 4.** General structure of cyanine compounds, cited from [205].

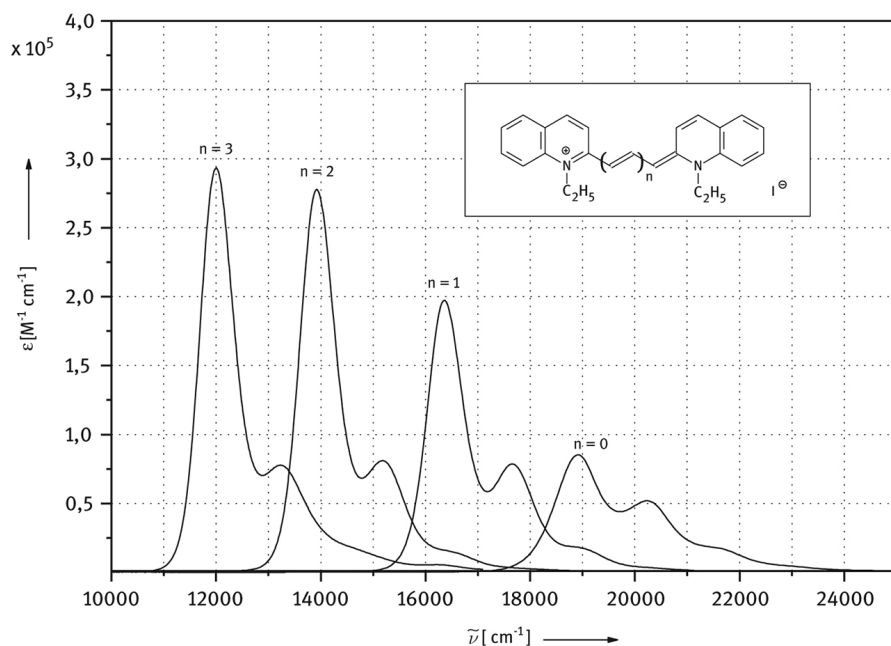


**Figure 9.** Electronic absorption spectra of carbo-cyanines carrying different numbers of methine in  $\text{CH}_2\text{Cl}_2$ , cited from [200].

Heptamethine, whose  $n$  is 3 and absorption is between 750 nm and 1100 nm, was employed as sensitizer in NIR photopolymerization[42, 51, 200, 203, 206, 210-211]. The methine chain of the heptamethine can be either an open chain (pattern I) or a bridged one with pentacyclic (pattern II) or hexacyclic ring (pattern III) chain (Chart 5). Moreover, the cyanine I in Chart 5 comprises a methine with almost flexible geometric structures. The five-membered ring in the central position of pattern II causes an almost planar geometric structure while the six-membered ring in pattern III leads to a non-planar geometry caused by geometry distortion[39]. This makes the latter more flexible. It also diminishes the tendency to aggregate as compared to the five-membered ring in pattern II[39]. Moreover, cyanines carrying pattern III exhibits a much better solubility in organic surroundings such as monomers or oligomers. This is very important for practical applications and gives promising directions to design appropriate cyanines with good solubility[47].

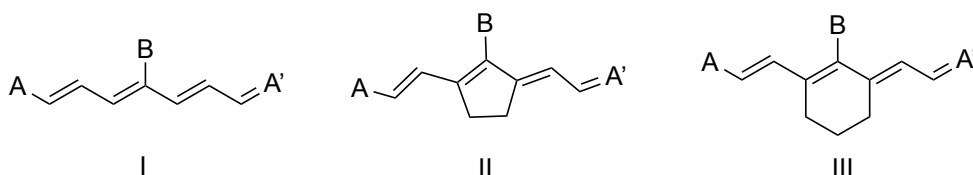


**Chart 5.** Chemical structure of the heptamethine with different methine chain, cited from [37].

There are many kinds of terminal groups ( $A/A'$ ) in the cyanine molecular structure, which include indolenines, benzoindolenines, benzoxazole, benzothiazole, quinoline etc (Chart 6)

[37]. The cyanine can be subdivided into symmetric and unsymmetric compounds depending on the terminal groups. The symmetrical cyanine exhibits narrower absorption bands than the unsymmetrical one because of its smaller carbon-carbon equilibrium bond lengths compared to unsymmetrical cyanine. Figure 10 depicts this situation[200]. Based on the excellent optical and thermal properties, cyanines have been used as photosensitizers for more than one hundred years in information recording systems[37, 200, 202-203, 212].

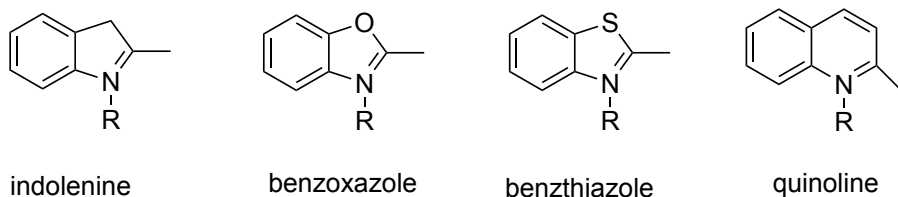


**Chart 6.** Different terminal groups in cyanine chemical structures.

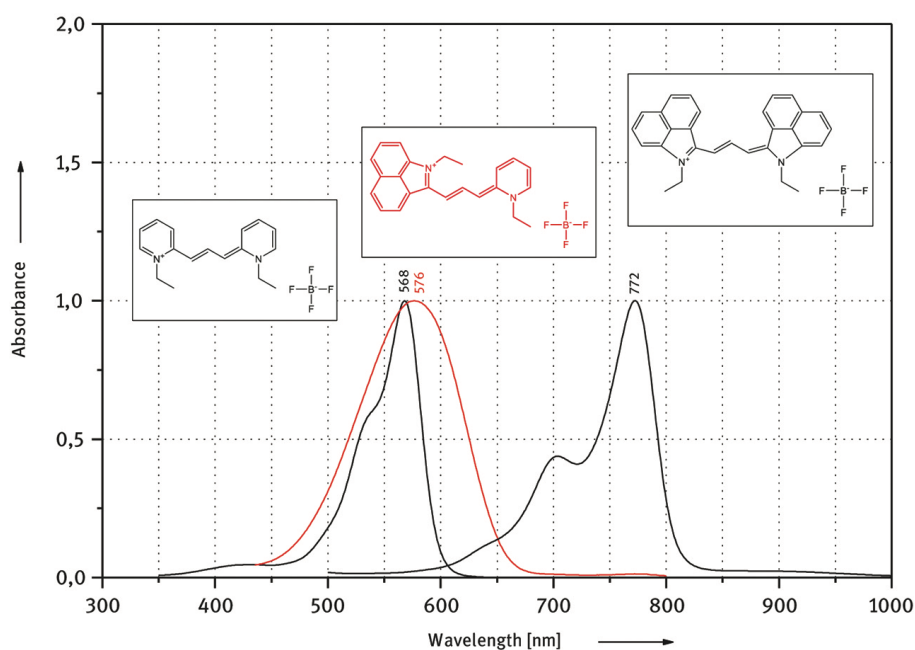


**Figure 10.** The UV-Vis-NIR absorption spectra of two symmetrical cyanines and the corresponding unsymmetrical cyanine in DMSO, cited from [200].

Heptamethines comprising indolium (A1/A1'), benzo[e]indolium (A2/A2') or benzo[c,d]indolium (A3/A3') (Chart 7) as terminal groups are widely used as NIR sensitizers in silver photography, CD-recording materials, NIR computer to plates (CTP), NIR photopolymerization, fluorescent dyes for bioanalysis and medical diagnostics, photodynamic therapy, etc. [36-37, 45, 96, 203, 210-213]. Incorporation of the benzo[c,d]indolium (A3/A3') moiety

possesses the longest bathochromic absorption shift compared to the benzo[e]indolium (A2/A2') moiety carrying the same number of methine groups[37]. In other words, there exist several opportunities to tailor-made the absorption; that is change of the number of methine groups and variation of the terminal groups in the respective cyanine. Furthermore, the absorption and solubility of the cyanine can be tailor made partly by tuning the substitute group  $R_1$ ,  $R_2$ ,  $R_3$  in Chart 7 as well as by variation of the counter ion[37].

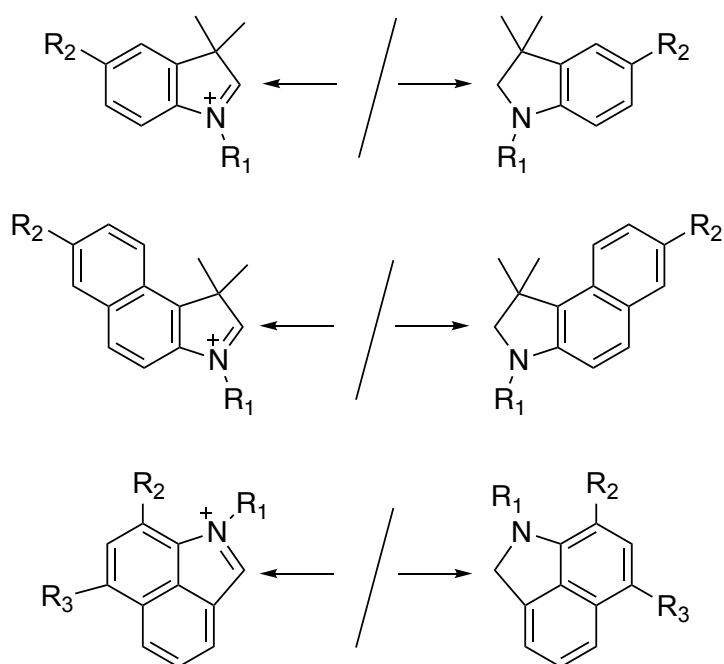


**Chart 7.** Substituted 2,3,3-trimethylindolium-, 2,3,3-benzo[e]indolium-, and 2,3,3-benzo[c,d]indolium salts results in the patterns A1/A1', A2/A2' and A3/A3' of the terminal substituent A in Chart 5, respectively, cited from [37].

Additionally, the absorption of cyanine also can be tailor made by taking different substituents B in the *meso*-position of the heptamethine, which can be electron-donating groups such as Ph-O-, Ph<sub>2</sub>N-, and Ph-S- or electron-withdrawing group like barbiturate and phenyl substituents as shown in Chart 8[23, 37, 214].

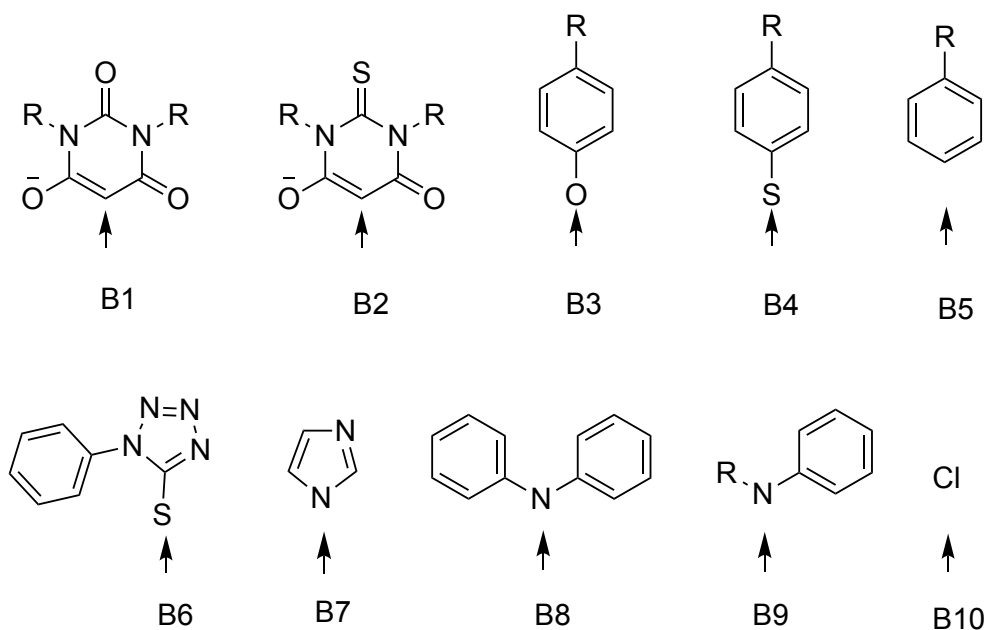


**Chart 8.** Different substituent groups in *meso*-position of the heptamethine chain results in pattern B in Chart 5, cited from [37].

The different structures of B and A result in different cyanine patterns comprising either cationic, zwitterionic, and anionic patterns. For the cationic cyanine, the counter anion includes halide ions ( $\text{F}^-$ ,  $\text{Cl}^-$ ,  $\text{Br}^-$ ,  $\text{I}^-$ ),  $\text{BF}_4^-$ ,  $\text{PF}_6^-$ , tosylate with longer alkyl groups such as  $[\textit{n}\text{-C}_{12}\text{H}_{25}\text{-Ph-SO}_3]^-$ , FAP ( $[\text{PF}_3(\text{C}_2\text{F}_5)_3]^-$ ), NTf<sub>2</sub> ( $[(\text{CF}_3\text{SO}_2)_2\text{N}]^-$ ), aluminates ( $[\text{Al}(\text{t-C}_4\text{F}_9\text{O})_4]^-$ ), and  $\text{SO}_3^-$ [41, 44, 47-48]. Some of these ions unexpectedly improve the solubility such as NTf<sub>2</sub> ( $[(\text{CF}_3\text{SO}_2)_2\text{N}]^-$ ), and aluminates ( $[\text{Al}(\text{t-C}_4\text{F}_9\text{O})_4]^-$ ) resulting in the improvement of the solubility of the corresponding cyanine approaching giant numbers up to 10-30g/L in some acrylate monomers[47, 59] while  $\text{SO}_3^-$  group in the molecular skeleton can promote the cyanine to exhibit an appropriate water solubility[37].

### Photophysics of Cyanines Used as Sensitisers

Figure 11 depicts representative photophysical processes occurring in NIR sensitiser upon NIR excitation. The NIR sensitiser absorbs one-photon assigned as one-photon absorption (OP), which excites the molecule to arrive in a series of higher vibrational levels of the first excited singlet state ( $S_1$ ). The higher vibrational levels relax to the lowest vibrational level. Therefore, the excited molecule arrives into the lowest vibrational level of the  $S_1$  through fast intramolecular vibrational relaxation (VR) depicting one kind of photo-physical processes. From there, it can competitively deactivate by several paths. This includes radiative deactivation by fluorescence, non-radiative deactivation resulting in generation of heat, and photochemical reactions based on photoinduced electron transfer (PET)[37,

214]. Furthermore, radiative and non-radiative deactivation relate to photophysical events. There are several pathways for non-radiative deactivations including IC and fast VR. IC fundamentally forms the basis to transfer the energy from vibrationally hot excited molecules to their cold surrounding (vibrational cooling = VC). The fast VR includes the route from higher vibrational levels of  $S_1$  ( $v' = 2, v' = 1$ ) into its lowest vibrational mode ( $v' = 0$ ) [215-216]. Furthermore, the heat generated by intramolecular vibrational relaxation (IVR) just can take only a minor part related to the non-radiative deactivation scheme. Otherwise, the huge excessive energy would thermally destroy the NIR absorber molecule, which does not occur in practical systems. Therefore, the major part of heat should come from collision with other molecules among the matrix molecules transferring much excessive energy by collision to matrix molecules in the surrounding assigned as vibrational cooling (VC). The heat generated from the NIR absorber is large enough to initiate some physical processes like melting of powder coatings[50] or to activate some thermal reactions as occurring in blocked isocyanates[45]. Depending on the light source intensity, the temperature of the heat can approach more than 100 °C[115, 118]. The system embedded pigments with higher heat capacity was reported to generate heat temperatures more than 350 °C[37, 50].

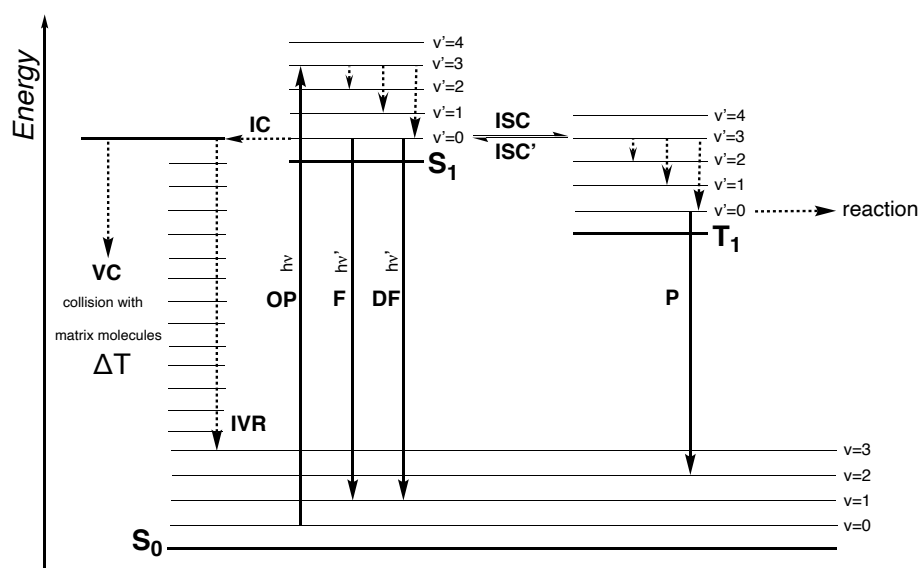


**Figure 11.** Photophysical processes of an excited absorber/photoactive molecule, modified from[37]. Absorption of one photon (OP), vibrational cooling (VC), internal conversion (IC), intramolecular vibrational relaxation (IVR), intersystem crossing (ISC), reverse intersystem crossing (ISC'), and vibrational relaxation (VR) to non-radiative events while fluorescence (F), and phosphorescence (P) radiatively occur. Photochemistry occurs from both the first excited singlet state ( $S_1$ ) and first excited triplet state ( $T_1$ ). Fluorescence (F) and delayed fluorescence (DF) exhibit similar emission wavelength while the decay of **DF** occurs in the time frame of the  $T_1$ ; that is significantly larger compared to the  $S_1$ . This scheme does not include delayed phosphorescence showing a similar fluorescence spectrum with similar maximum but the decay occurs in the time frame of the  $T_1$ .

The cyanine comprising indolium and benzo[e]indolium exhibits an observable fluorescence[37]. The fluorescence yield of cyanine coming from general patten I in Chart 5 can approach up to around 25%[37]. Moreover, the fluorescence quantum yields ( $\Phi_f$ ) of cyanine based on patten II or patten III in Chart 5 can approach up to 20%[37]. Additionally, the substituent in the *meso*-position also affects the value of  $\Phi_f$  significantly. Generally, the sequence for the decrease of  $\Phi_f$  located at the *meso*-position appears as follows: PhO-; Ph-  $\geq$  barbiturate  $\geq$  Ph<sub>2</sub>N- > PhS-> phenylmercapto tetrazole[37]. The cyanine can generate heat and emit fluorescence based on the photophysical process revealed in Figure 11. More than 80-95% of the excited state deactivate via non-radiative deactivation depending on the substitution[37]. Thus, these compounds can work as heat generator on demand by turning on and off the light source. Furthermore, cyanines with absorption larger than 900nm exhibit a  $\Phi_f$  less than 1%, which means more than 99% of the light energy absorbed by the cyanine can be converted into heat. This feature offers the opportunity to design molecular ovens[50].

#### Photochemistry of Cyanines Applied as Sensitiser

The main photochemical reaction of cyanines bases on photoinduced electron transfer between the sensitizer and the acceptor (**A**) and/or donor (**D**) as shown in Figure 12[19]. After irradiation, the sensitizer absorbs the light to arrive in the first excited state  $S_1$  (**Sens\***). Afterward, it transfers the electron to the acceptor (**A**) resulting in generation of the oxidized species **Sens<sup>+</sup>** and anion radical **A<sup>-</sup>**. This follows an oxidative mechanism. Furthermore, three pathway may occur to involve **Sens<sup>+</sup>** in consecutive steps relating to back electron transfer from **A<sup>-</sup>** (a), decomposition of **Sens<sup>+</sup>** (b) or electron transfer from donor **D** resulting in reduction of **Sens<sup>+</sup>** to **Sens** (c). Furthermore, path (a) relating to electron back transfer reduces the efficiency regarding the generation of initiating radicals, which needs to be prevented in practical application by increasing the possibility of path (b) or path (c), respectively[19]. Phosphine was reported as one useful donor (**D**) in path (c) in a three components NIR photoinitiating system[19, 42], where (i) a heptamethine cyanine comprising borate anion was used as sensitizer (**Sens**), (ii) an iodonium salt (**IS**) was used as coinitiator, and (iii) phosphine was additionally applied to take the function as reductant to regenerate **Sens** back and to prevent oxygen inhibition[19, 42]. This three component NIR photoinitiating system exhibited high performance to initiate radical polymerization of acrylate monomers even under the air condition[19, 42, 198].

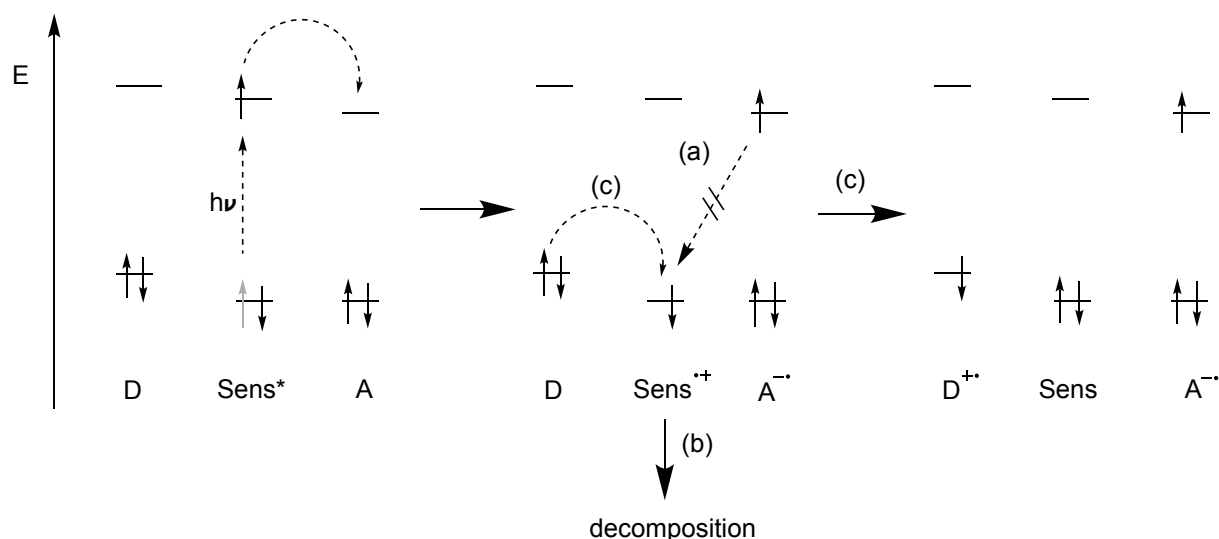
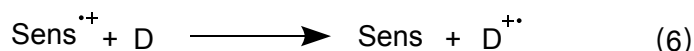
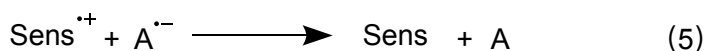
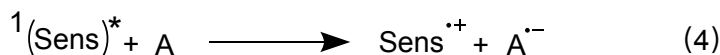
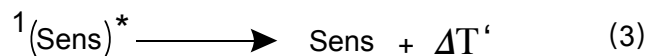
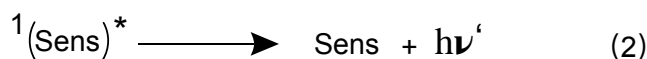
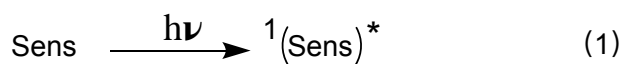


**Figure 12.** Electron transfer processes of between excited **Sens\*** and acceptor **A**, and the different pathways to consume **Sens<sup>•+</sup>**: (a) back electron transfer, (b) decomposition, or (c) electron transfer with donor **D**, cited from [19].

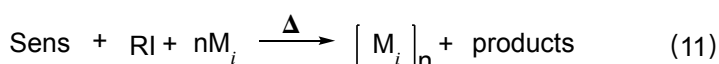
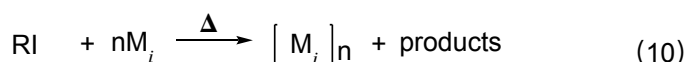
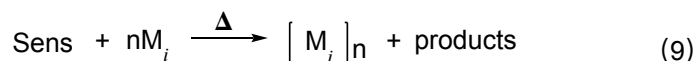
The reactions in a three component system can be also depicted by Scheme 11 where **A** serves as the electron acceptor, which reacts with the excited sensitizer by PET. The typical structure of **A** used in NIR photopolymerization relates either to iodonium salts or triazines, which were used in 830 nm NIR laser CTP systems for many years[31, 34-35, 197, 217-218]. Oxime ester was also reported as one kind of co-initiator reacting with NIR sensitizer taking the function of an acceptor **A**[86]. The electron back transfer is also possible between **Sens** and **A** as shown in process (5) of Scheme 11, which will decrease the efficiency of the NIR photoinduced reaction. However, addition of an electron donor (**D**) can decrease the phenomenon of electron back transfer of the singlet system because the cation radical of Sens (**Sens<sup>•+</sup>**) reacts with **D** and produces **Sens** back while new reactive species **D<sup>•+</sup>** appear in process (6) of Scheme 11. Moreover, as shown in process (7) of Scheme 11, the oxidized species **Sens<sup>•+</sup>** also can cleave to products with lower molecular weight and form conjugate acid, which can initiate cationic polymerization of some compounds like aziridines[47], oxiranes as firstly reported in this thesis[96].





**Scheme 11.** The reaction mechanism of the combinations of NIR initiating system comprising three components upon NIR exposure, modified from [19].

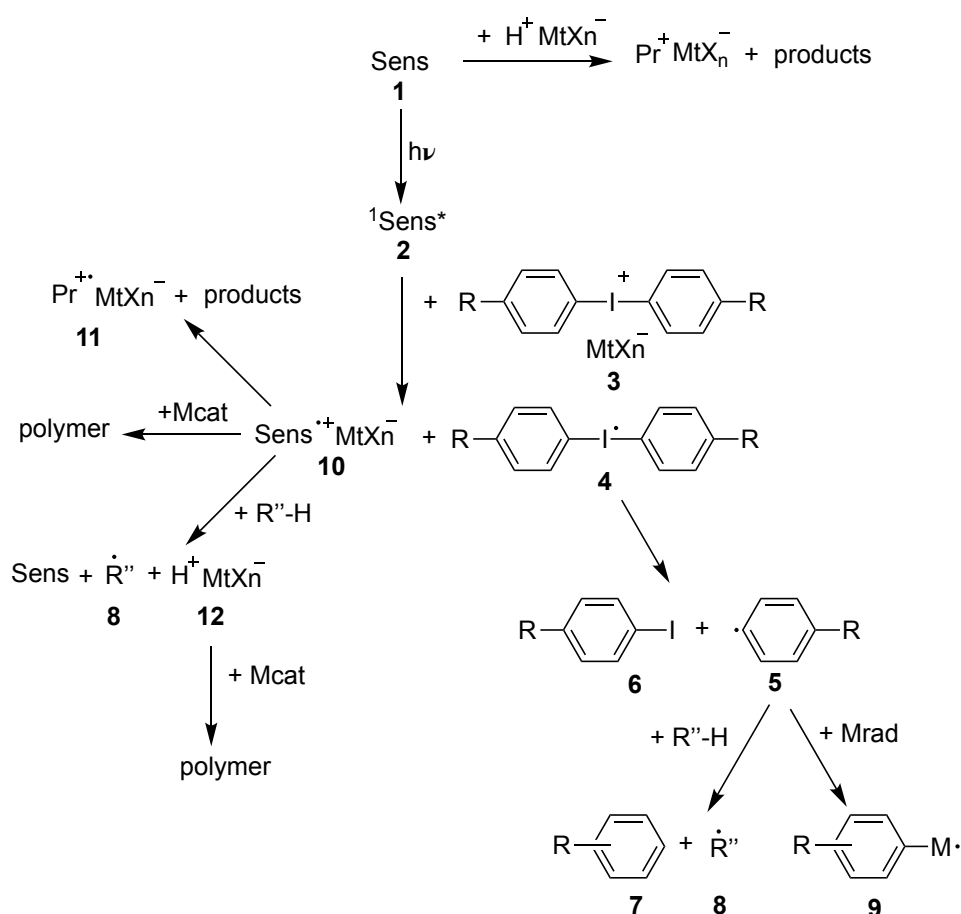
Additionally, the heat released by non-radiative deactivation of the cyanine facilitates the polymerization in many aspects considering the processes 8 to 11 as shown in Scheme 12.[19] Remarkable again, it takes a great function to promote the system to overcome the internal barriers in the PET process.[36-37, 96]



**Scheme 12.** The influence of heat in the NIR photoinduced polymerization, cited from [19].

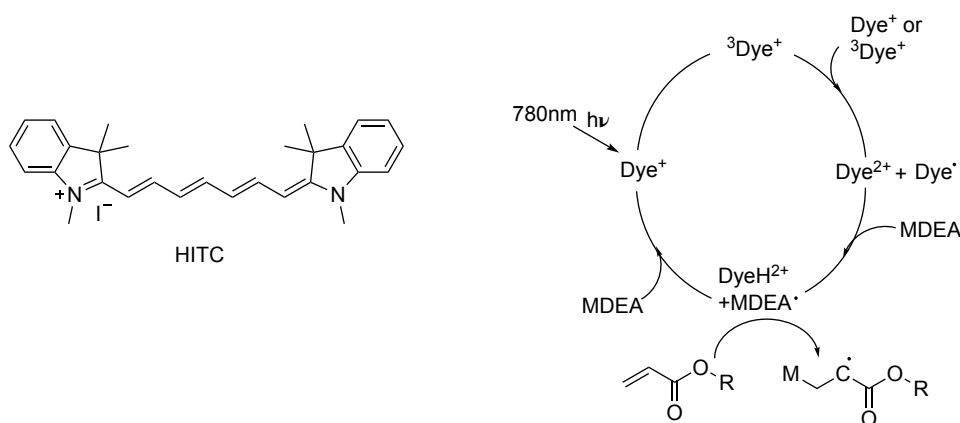
Iodonium salts with a reduction potential in the range from -0.8 to -0.5 V were proved to react with heptamethine cyanine under irradiation with NIR laser or LED, where cyanine works as donor and oxidant[39, 44, 46].  $\Delta G_{PET}$  of the combination initiator systems including heptamethine cyanines and iodonium salts appears slightly negative based on the excitation energy  $\Delta E_{00}^D$  and oxidation potential  $E_{ox}^{D/D^+}$  of the heptamethine cyanine sensitizer serving as a donor (**D**) and the reduction potentials  $E_{red}^{A/A^-}$  of iodonium salts serving as acceptor (**A**). The overview of photochemical reaction between heptamethine cyanine and iodonium salts are depicted by Scheme 13. According to this scheme sensitizer 1 is excited resulting in **Sens**\* 2 upon irradiation, then the electron transfer reaction of **Sens**\* oc-

curred with the iodonium salt 3, which produced  $\mathbf{Ar}_2\mathbf{I}^+$  in 4 and  $\mathbf{Sens}^{++}$  in 10. The reduced iodonium cation  $\mathbf{Ar}_2\mathbf{I}^+$  4 decomposes fast into radical  $\mathbf{Ar}^{\bullet}$  5 and additional products 6. The radical  $\mathbf{Ar}^{\bullet}$  formed initiates radical polymerization (9) or transfers the radical to the surrounding by hydrogen abstraction to generate radicals  $\mathbf{R}''^{\bullet}$  8 and further products 7[101, 219]. On the other hand, the oxidized sensitizer  $\mathbf{Sens}^{++}$  10 either initiates the cationic polymerization or results in formation of conjugate acid 12 while H-abstraction from the surrounding can also lead to species initiating cationic polymerization in the consecutive steps[220]. Conjugate acid responsibly initiate cationic polymerization. Photoproducts formed in step from 10 to 11 could explain bleaching of the absorber. The decomposition rate of 10 influences the electron back transfer and reaction pathway. Furthermore, acid generation in the reactions may accelerate decomposition of sensitizers because some cyanines were reported to decompose in acidic surrounding, which produced the similar photoproducts as the cyanine in the iodonium salt surrounding[39].



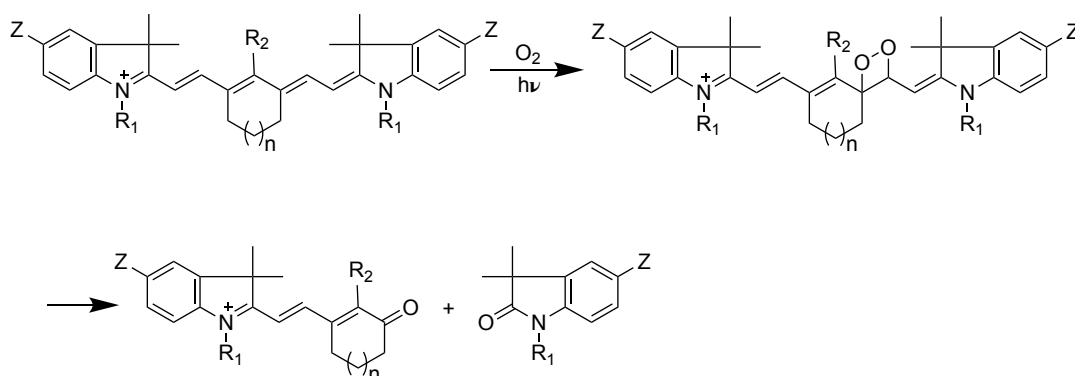
**Scheme 13.** Mechanism of the combination of NIR initiators comprising heptamethine cyanines as sensitizers and iodonium salts as coinitiators, cited from[19].

Nevertheless, the triplet state  $T_1$  of sensitizers was disclosed in a heptamethine cyanine in Scheme 14, where the electron transfer was believed to start from  $T_1$ . The system including this sensitizer and methyl diethanolamine (MDEA) as a coinitiator worked under NIR laser light to initiate free radical polymerization of acrylate monomers[22, 221-222]. However, no report revealed the similar reaction by NIR LED irradiation. In addition, there exists no practical approval that this sensitizer forms triplet states. This may be approved by transient absorption studies, which have not been reported from our best knowledge yet.



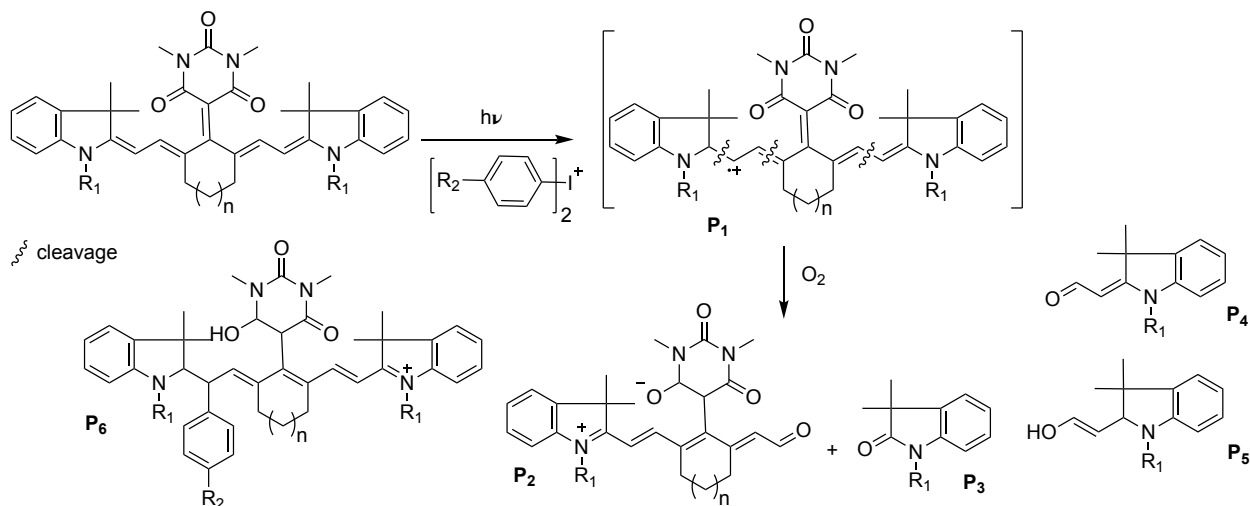
**Scheme 14.** Heptamethine cyanine dye 1,1',3,3,3',3'-hexamethylindotrycarbocyanine iodide (HITC) and postulated radical initiation mechanism accelerated by methyl diethanolamine (MDEA) upon NIR laser exposure, cited from [221]

Photobleaching of heptamethine cyanine absorbers resulted in the decomposition of the sensitizer and generation of smaller molecules as shown in Scheme 15 pursued under aerobic conditions.[223-226] The photoproducts possess a shorter conjugated chain causing the hypsochromic absorption shift and the colour change of the solution from green to yellow or brown. The PET accelerates photobleaching because of the consumption of the  $Sens^{+•}$ . [19]



**Scheme 15.** Photobleaching of heptamethine cyanine absorbers with NIR light under oxygen conditions, cited from [19].

Scheme 16 depicts the bleaching of sensitizer leading to the respective photoproducts in NIR photopolymerization comprising the heptamethine cyanine and iodonium salt. While the color of the film changes from green or blue to yellow, red, or brown appearing photoproducts such as P<sub>3</sub>, P<sub>4</sub>, and P<sub>5</sub> were identified upon NIR irradiation (see Scheme 16)[19]. The nucleophilic products formed result in a decrease of the possibility to initiate the cationic polymerization because chain growth in cationic polymerization bases on the carbocation as intermediates, which can be terminated by nucleophilic moieties.



**Scheme 16.** Photobleaching of sensitizer comprising barbiturate moiety after redox reaction with iodonium salt by cleavage at the conjugated double bond position ( $P_2$ ,  $P_3$ ,  $P_4$ ,  $P_5$ ) and recombination with aryl radicals ( $P_6$ ), cited from [19].

### 2.3.2 Co-Initiators Applied for NIR Sensitized Polymerization

As aforementioned noticed, heptamethine cyanines serve as sensitizers absorbing light and transfer it to some co-initiators such as iodonium salts, triazines, oxime esters, or some thermal initiators resulting in generation of reactive intermediates such as free radicals, cations and conjugate acid, which can initiate free radical or cationic polymerization[35, 42, 46, 86]. Herein, more details about these co-initiators are introduced in this section.

#### Diaryliodonium salts

Diaryliodonium salts (Chart 9) depict one kind of important UV photoinitiators. They were first synthesized more than 130 years ago[97]. However, they were introduced as photoinitiators for cationic photopolymerization until in last 70s[178]. In the past 40 years, the development of cationic polymerization mostly referred to diaryliodonium salts in photosensitized systems used as one class of excellent photoacid generators attracting the in-

terest from both academic and industrial sector[7-8, 25, 27, 35, 41, 46, 59, 97, 227-231]. At present, diaryliodonium salts are commercialised and widely used in many practical applications.

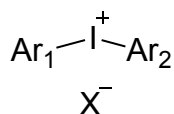
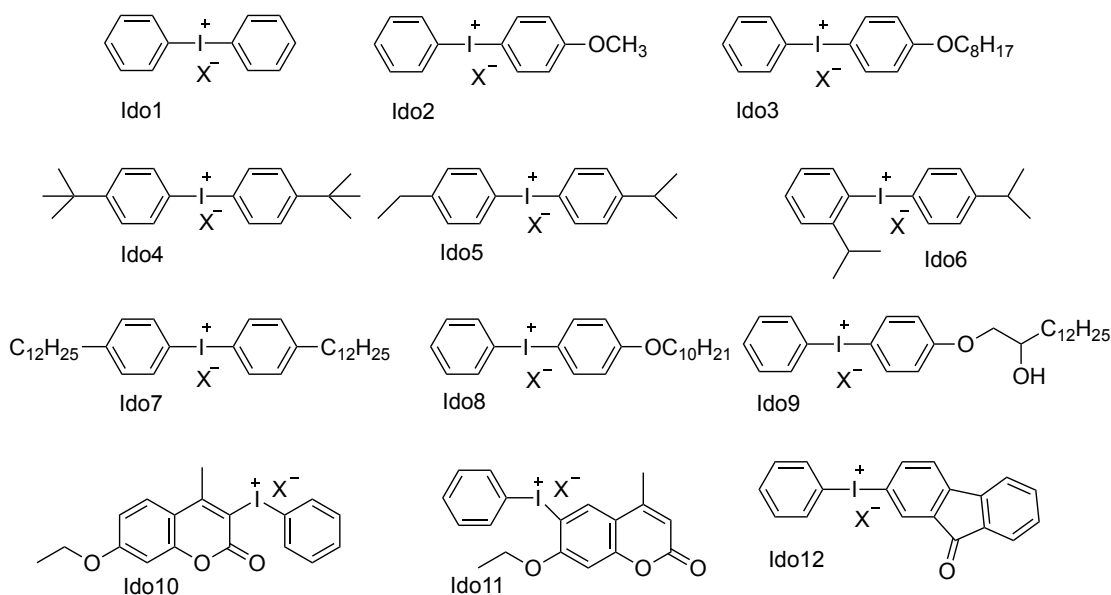


**Chart 9.** General structure of iodonium salts, cited from [232].

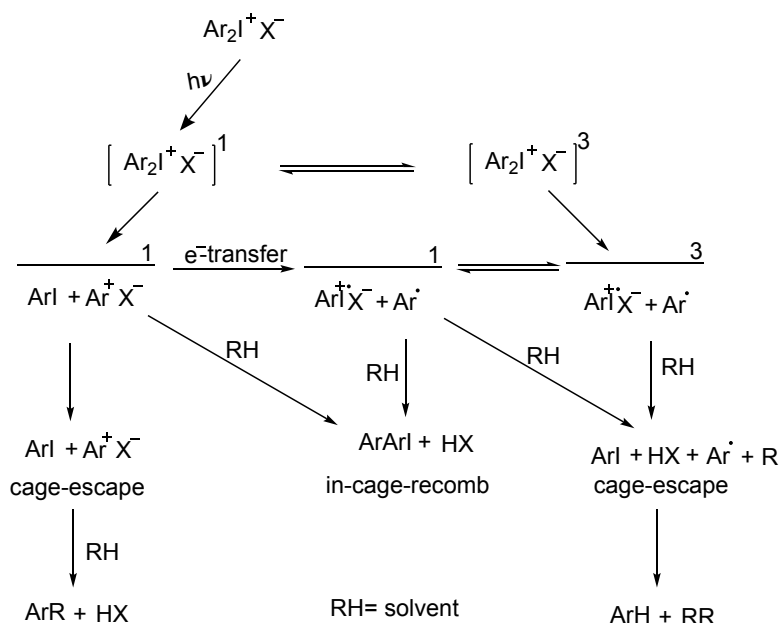
As shown in chart 9, an iodonium salt includes one iodonium cation comprising either the same or different aromatic moieties ( $\text{Ar}_1$  and  $\text{Ar}_2$ ), where iodine atom exhibits positive charge at the central position[46]. The number of the oxidation state relates to +3. Thus, iodonium salts exhibit one kind of hypervalent iodine materials.  $\text{Ar}_1$  and  $\text{Ar}_2$  can comprise either a substituted or non-substituted benzene pattern, naphthalene, heteroaromatic groups, polynuclear aromatic, or other aromatic groups depending on the request of absorption. The substituents may relate to electron-withdrawing or electron-donating groups which can help to tailor make absorption and also improve the solubility of the compounds. The counter anion  $\text{X}^-$  can be  $\text{PF}_6^-$ ,  $\text{SbF}_6^-$ ,  $\text{AsF}_6^-$ ,  $\text{BF}_4^-$ ,  $\text{B}(\text{C}_6\text{F}_5)^-$ ,  $[\text{PF}_3(\text{C}_2\text{F}_5)_3]^-$  (**FAP**),  $[(\text{CF}_3\text{SO}_2)_2\text{N}]^-$  (**NTf<sub>2</sub>**),  $[\text{Al}(\text{t-C}_4\text{F}_9\text{O})_4]^-$  (aluminates),  $\text{CF}_3\text{SO}_3^-$ ,  $\text{C}_8\text{F}_{17}\text{SO}_3^-$ , etc. Some of these ions unexpectedly improve the solubility, like **NTf<sub>2</sub>** ( $[(\text{CF}_3\text{SO}_2)_2\text{N}]^-$ ),[46]  $[\text{PF}_3(\text{C}_2\text{F}_5)_3]^-$  (**FAP**),[48] and aluminates ( $[\text{Al}(\text{t-C}_4\text{F}_9\text{O})_4]^-$ )[59, 63]. Although some iodonium salts can cause issues regarding the solubility in organic solvents and monomers, this problem can be overcome partly by tuning the substituents in the cation of the salt and the respective counter anions. Some of these salts appeared liquid and dissolved 1:1 in the monomer[46]. Furthermore, the short intrinsic absorption of iodonium salts limited their application under longer UV, visible and NIR light source. However, this situation was improved by new iodonium salts based on the coumarin chromophore facilitating excitation with UV LEDs emitting in the UV-A range[233-235]. Moreover, there exist many sensitizers and some Norrish I photoinitiators which generate nucleophilic radicals can sensitise the reduction into the respective radical as shown in Scheme 13  $\text{Ar}_2\text{I}^+$  4 decomposing in initiating radicals[24, 42, 46, 52, 79, 167, 236]. Chart 10 shows some structures of diaryliodonium cations with distinct cationic patterns.



X: PF<sub>6</sub>, SbF<sub>6</sub>, AsF<sub>6</sub>, BF<sub>4</sub>, (C<sub>2</sub>H<sub>5</sub>)<sub>3</sub>PF<sub>3</sub>, (CF<sub>3</sub>SO<sub>2</sub>)<sub>2</sub>N, Al(t-C<sub>4</sub>F<sub>9</sub>O)<sub>4</sub>, CF<sub>3</sub>SO<sub>3</sub>, C<sub>8</sub>F<sub>17</sub>SO<sub>3</sub>, etc

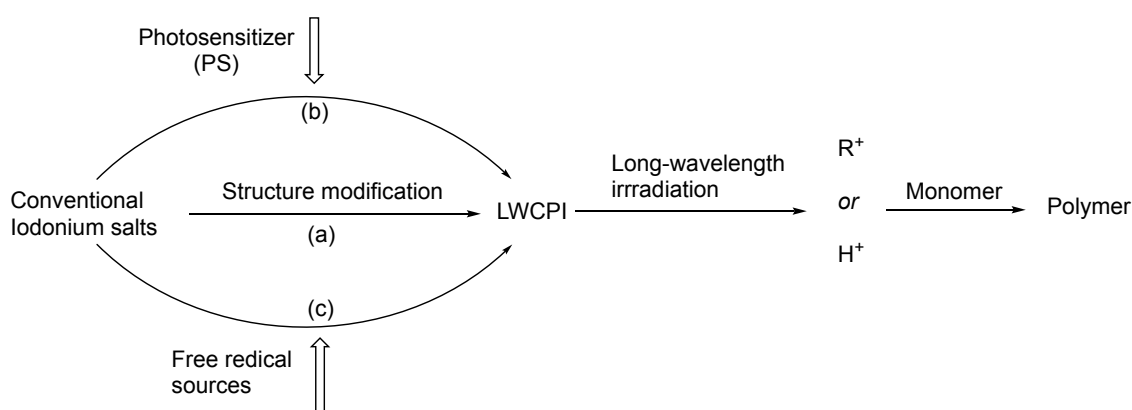
**Chart 10.** Some general diaryliodonium salts, cited from [46, 236-237].

The maximum of UV absorption resides for many iodonium comprising benzene moieties between 200nm to 300nm. They decompose directly upon exposure in its absorption range. Iodonium salts can work by themselves applying UVC and UVB light for exposure. The photolysis mechanism of iodonium salts was studied and analysed by mass spectrometry as depicted by Scheme 17[237-241]. In brief, photo-excited diaryliodonium salts can decompose from the singlet and triplet state upon UV exposure. The excited state causes carbon-iodine bond cleavage by both homolytic and heterolytic methods, see the aforementioned references. The photolysis of iodonium salts produces reactive species such as radicals, radical-cations, and cations. Subsequently, these reactive species react with proton donors in the surrounding such as solvents, monomers, oligomers, polymers. The quantum yields can approach around 0.7 explaining the high performance of the iodonium salts as photoacid generators.[231] However, the short absorption requires to operate them with UV-light. Many matrix molecules possess an intrinsic absorption in this region, which can therefore function as filter materials. There exists consequently a demand to use these materials in combination with UV-A sources. This requires to use them in photosensitized systems enabling UV-A[166], visible[30, 242] and NIR[46-47]sources for exposure.



**Scheme 17.** Photolysis of iodonium salts, cited from [231].

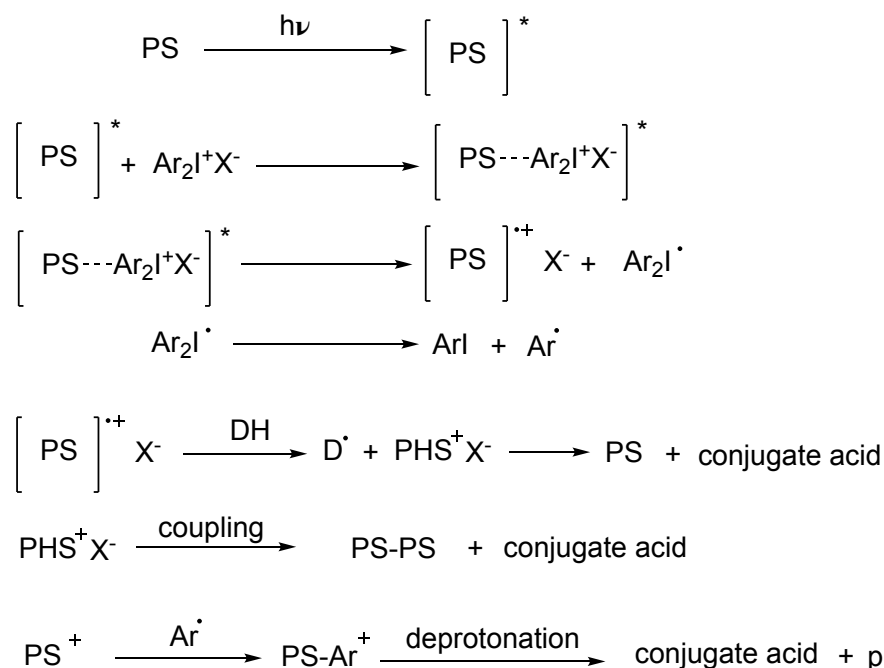
Thus it does not surprise that considerable work has been done to extend the application of iodonium salts to longer wavelength like UV-A, Visible, and NIR range[27, 37]. There are mainly three different strategies for promoting the iodonium salt for use in the longer wavelength region for employment in initiation of cationic photopolymerization, see Scheme 18. The strategy (a) is to design iodonium salts with longer absorption using larger conjugation of phenyl group or incorporation of other moieties carrying the coumarin group or 9-fluorenone group like Ido10, Ido11, Ido12 in Chart 10, which exhibit longer wavelength absorption and good initiating reactivity[97, 234, 236, 243].



**Scheme 18.** Strategies for designing long-wavelength cationic photoinitiating systems, cited from [27].

Strategy (b) uses some photosensitizers in combination with iodonium salts in PET mechanism[27]. There are many sensitizers showing the capability to sensitise decomposition

of the iodonium salts. This can significantly promote the application of these iodonium salts in much wider views and also promote the development of cationic photopolymerization in more practical applications. The mechanism of the photosensitised decomposition of diaryliodonium salts bases on PET as depicted by Scheme 19[27, 231, 236, 244].



**Scheme 19.** Mechanism of photosensitizers sensitised diaryliodonium salts by PET, modified from [27, 231].

As depicted in Scheme 19, the photosensitiser (**PS**) is excited resulting in the excited state **PS\***. Then, it will transfer an electron rather than excitation energy to diaryliodonium salts fast, which causes reduction of the iodonium salt resulting in **ArI<sub>2</sub>•**. Then, the **ArI<sub>2</sub>•** decomposes into **ArI** and **Ar•**[231]. After electron transfer, the excited state **PS\*** oxidizes resulting in **PS<sup>+</sup>** which will abstract hydrogen from the surroundings and releases conjugate acid to initiate cationic polymerization. **PS<sup>+</sup>** also may interact with other intermediates as shown in Scheme 19. A related mechanism called charge transfer complex (CTCs) also must be considered in the photosensitive system comprising iodonium salts[27].

Additionally, some Norrish I free radical initiators are revealed to sensitise reduction of iodonium salts resulting in formation of conjugate acid to initiate cationic polymerization. This facilitates their use in free radical and cationic polymerization (Scheme 18, strategy c)[27]. Therefore choosing longer wavelength absorbing free radical initiators can also give access to long-wavelength cationic photopolymerization, which also extends the application of iodonium salts for uses in combination with longer wavelength LEDs. Norrish I photoinitiators generate radicals by homolytic cleavage upon irradiation.[167] Then, the radicals



spontaneously oxidise the iodonium salt at room temperature as long as their oxidation potentials facilitate the redox reaction, which results in the corresponding carbocations. In the following step, the carbocation can react with either monomer to initiate polymerization or it forms conjugate acid. The latter is assumed to initiate cationic polymerization of respective monomers.[167] Some typical radical photoinitiators working in the free radical promoted cationic polymerization (FRPCP) are shown in the Chart 11.

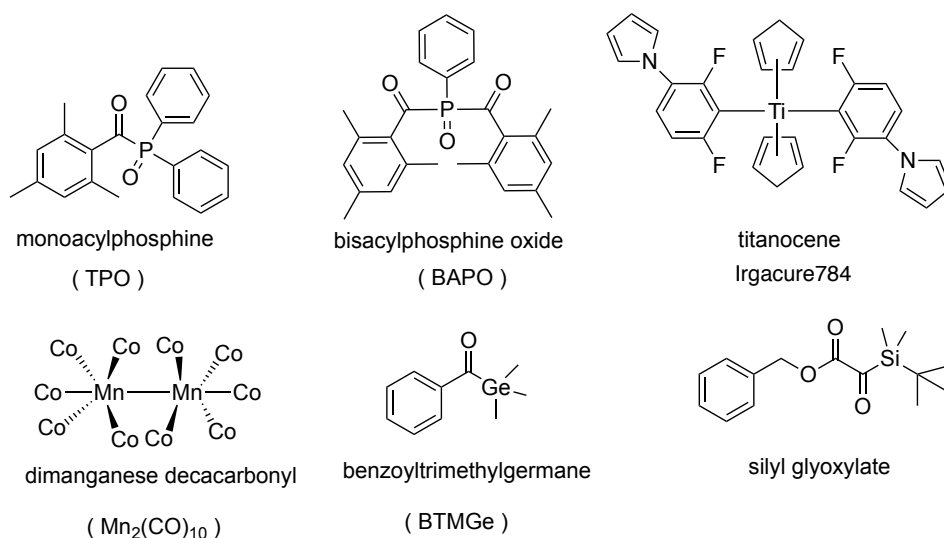


**Chart 11.** Some radical photoinitiators working in the FRPCP, cited from [167].

$Ar\cdot$  assigns to a reactive radical as used to initiate free radical polymerization. A previous work[244-245] approved this view where they used the combinations of sensitizers and iodonium salts system to initiate free radical polymerization with success. Other approaches[19, 31, 42, 44, 46, 48, 56, 65, 96, 115] showed that the cyanine and iodonium salt co-initiator systems can initiate both radical photopolymerization and in some cases cationic polymerization as well. NIR laser and LED systems were applied for excitation. Moreover, the Carbon NanoDots were approved to sensitise reduction of iodonium cations by PET to initiate radical polymerization with visible LEDs[246]. Iodonium salts depict one kind of important photoinitiators or components in systems based on a sensitized mechanism attracting the interest in the community for more uses in the future.

### Oxime esters

Oxime esters as shown in Chart 10 exhibit one kind of high performance photoinitiators, which were widely used in colour or black photoresists because of the outstanding reactivity upon irradiation[14, 66-67]. In 1902, Werner firstly reported that an oxime ester can decompose under daylight by the Beckmann rearrangements[67]. 70 years later, the oxime

ester **Quantacure PDO** was used as photoinitiator in the beginning of photopolymerization[3]. However, it was eliminated soon because of a shelf life issue[247]. Additional 30 years later, the new oxime ester 1-[4(phenylthio)phenyl]-1,2-octandione-2-O-benzoyloxime (**OXE-01**) brought new interest to industry[66]. Because the new pattern comprising phenyl sulfide in the oxime ester structure, UV absorption bathochromically shifted and enabled the use of light sources emitting at 365nm. Additionally, the possibility to release volatile compounds decreased. Furthermore, the thermal stability also improved by introducing a longer alkyl chain with 6 carbons into the molecular structure[67]. Three years later, another more efficient oxime ester; that is 1-[9-Ethyl-6-(2-methylbenzoyl)-9H-carbazol-3-yl]ethanone-1-(O-acetyloxime) (**OXE-02**), was developed[14]. The 2-methylphenyl-carbazole sufficiently resulted in sensitising UV absorption. This occurred bathochromic compared with **OXE-01**. The quantum yield of photodecomposition approached values being nearly twice as high compared to **Quantacured PDO** upon irradiation at 365 nm. This makes them somehow outstanding because of the high sensitivity in some special applications such as black matrix resin, where the light intensity was significantly reduced by embedding of black pigments[67]. Nowadays, **OXE-01** and **OXE-02** appear as main available photoinitiators in colour filter resist formulations[67].

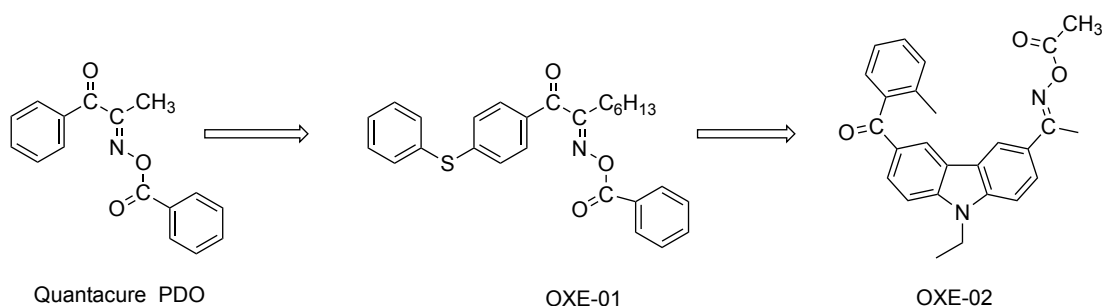
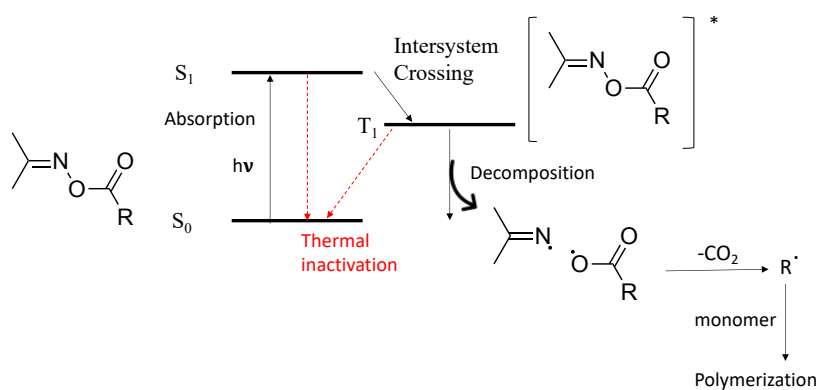


**Chart 12.** The structure of the oxime esters: **Quantacure PDO**, **OXE-01**, **OXE-02**, cited from [67].

Scheme 20 depicts the photolysis process of oxime esters[67]. Upon exposure, oxime ester arrives at the singlet excited state firstly while ISC transfers it to the excited triplet state where the oxime ester decomposes by homolytic cleavage of the of N-O bond resulting in production of two radicals; that is  $R-CR'=N\cdot$  and  $\cdot OR''$ [118]. These radicals assign to electrophilic radicals, which efficiently facilitate addition to (meth)acrylic monomers that initiate the free radical polymerization. Furthermore, the carboxy radicals could generate more efficiently active carbon radicals by decarboxylation. The photolysis mechanism of the oxime ester explains the high performance of the oxime ester as photoinitiator, see Scheme 20.



**Scheme 20.** Photolysis mechanism of oxime esters, cited from [77].

**OXE-01** and **OXE-02** possess significant red-shifted absorption and improved shelf life compared with the first generation of the oxime esters. However, their main absorption mainly covers the range between 300-370 nm, which could not fit in some cases the demand to combine their use with the longer wavelength UV or visible LED emitting at 385 nm, 395 nm, 405 nm, 420 nm, etc. Recently, more and more long wavelength oxime esters were developed to meet the demand of the industrial applications operating with longer wavelength UV-Vis LEDs showing longer wavelength absorption and efficient sensitivity as photoinitiators[28, 69, 79-80, 82, 85, 248-250]. Chart 13 shows some new oxime esters with longer wavelengths.

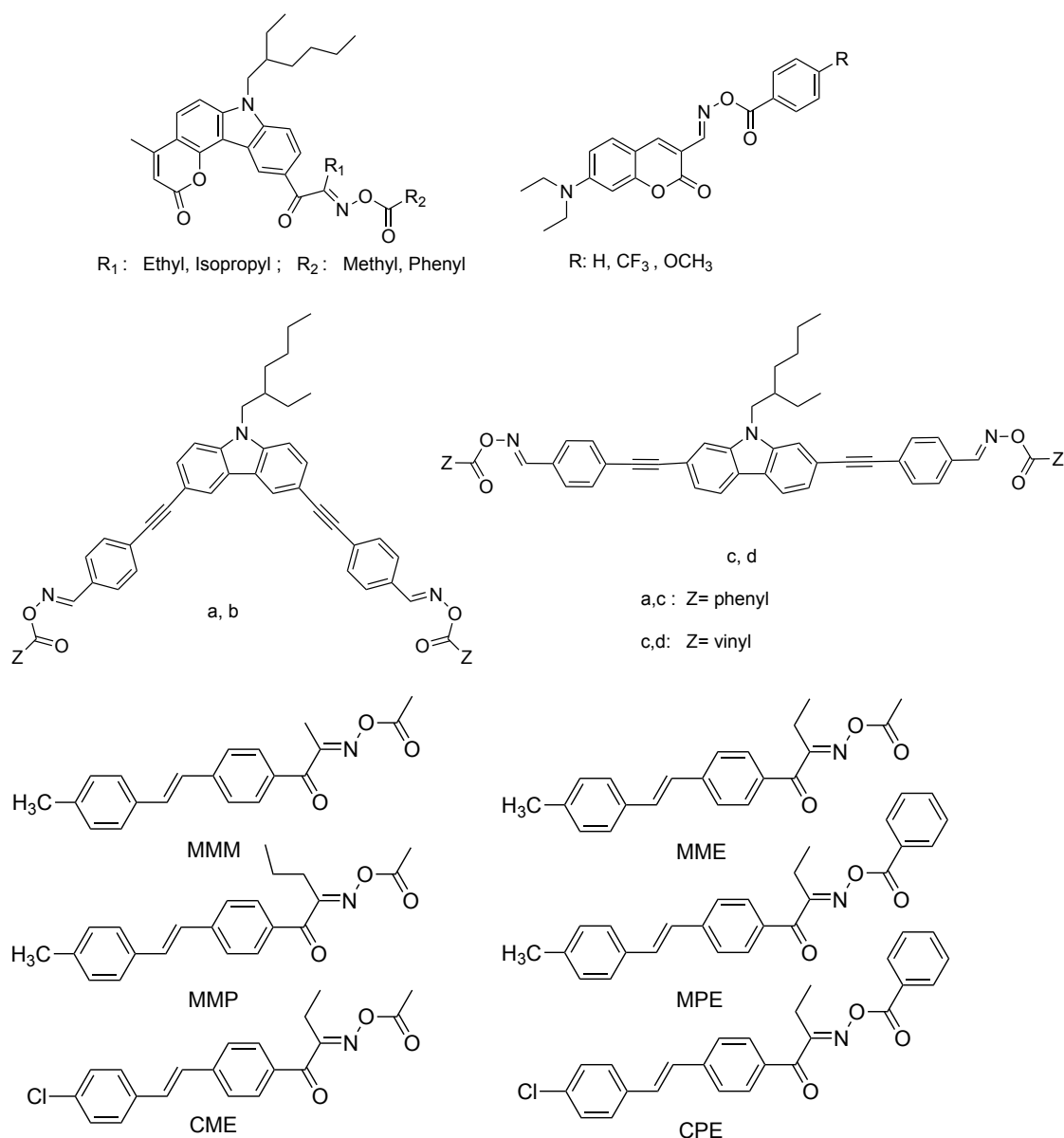


**Chart 13.** Some new oxime esters with longer absorption wavelength, cited from [28, 69, 79-80, 82, 85].

### Thermal initiators

Thermal initiators for polymerization are one kind of compounds, which can generate reactive species such as radicals or conjugate acid upon treatment with heat. The general free radical thermal initiators refer to alkoxyamine, azo derivatives and (hydro)peroxides as shown in Chart 14[51]. These initiators initiated free radical polymerization in combination with the NIR absorbers successfully while the absorber delivered the requested heat as a result occurring non-radiatively[51]. The studies revealed that they decompose to generate radicals by the heat generated by NIR absorber, which can initiate the free radical polymerization with acceptable rate[51-53, 65, 193].

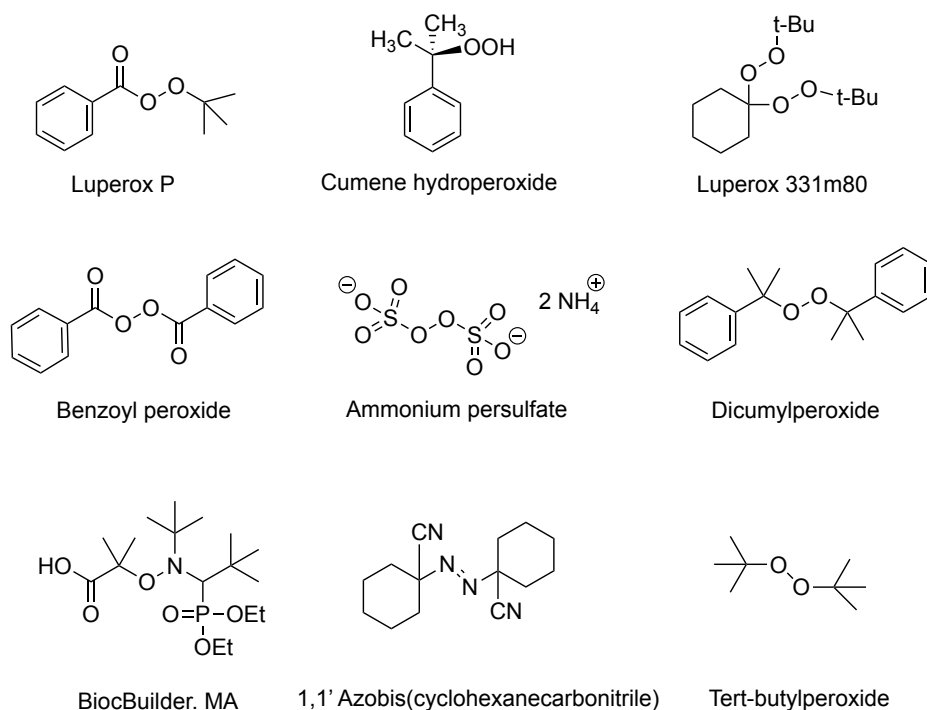
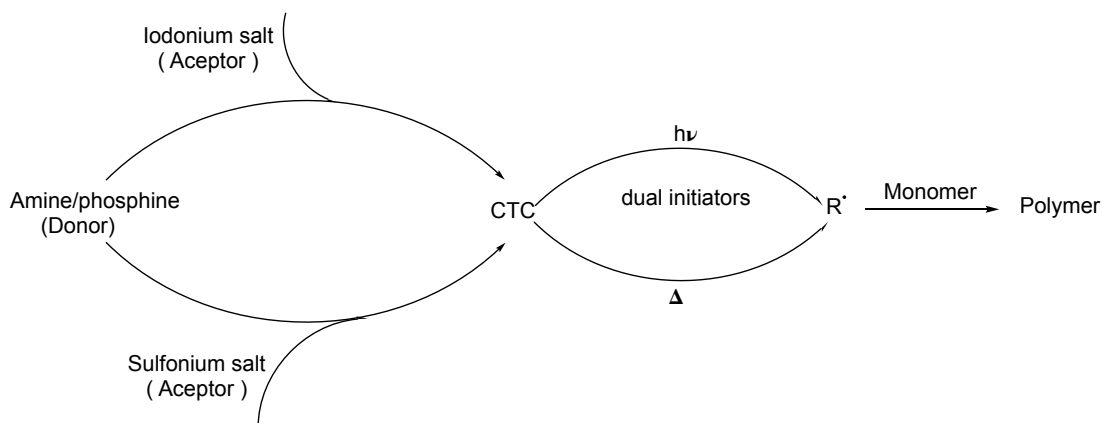


**Chart 14.** Some examples of thermal free radical initiators, cited from [51].

The same lab also reported that the charge transfer complexes (CTCs) of iodonium salts in combination with amines or phosphines, and the CTCs of sulfonium salts in combination with amines or phosphines undertook a dual function of both photo and thermal dual sensitively initiating polymerization[251-256]. It can also be used in NIR photoinduced polymerization to initiate free radical polymerization[54]. The mechanism of these systems are depicted by Scheme 21. They respond sensitively to both the treatment with heat and UV-light. These systems have been used in the NIR light induced polymerization in combination with NIR absorbers[54].



**Scheme 21.** The CTCs of amine/phosphine-iodonium salt combination system and the CTCs of amine/phosphine-sulfonium salt combination system as photo-thermal dual functional combination initiators, cited from [254].

### 3. Materials and Methods

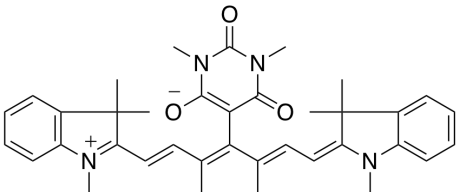
This chapter briefly discloses the materials and methods used in this thesis. More details can be found in own published materials[96, 115, 118].

#### 3.1 Light Sensitive Materials

##### 3.1.1 NIR Sensitive Absorbers Derived from Heptamethine Based Cyanines

In this thesis, heptamethine based cyanines carrying bridged and unbridged chains were selected as NIR absorbers and sensitizers. Furthermore, the sensitizers comprising bridged chains include five-membered ring and six membered ring in the *meso*-position. The sensitizers comprising a five membered ring in the centre keep the planarity of the heptamethine while a six membered ring distorts the planarity of the molecular structure improving the solubility of the sensitizers in the surroundings as disclosed for **S1** and **S18**, respectively[39, 47]. These interesting findings motivated to choose the sensitizers used in this thesis as shown in Table 1. They carry distinct pattern resulting in different electron density based on different substitution with either electron or withdrawing substituents. The different indolence patterns additionally affect physical properties. More details were summarised elsewhere[37]. **S26** was obtained from Spectrum Info Ltd. (Kiev, Ukraine), others were received from FEW Chemicals GmbH. All of them were used directly without further purification because both suppliers claimed sufficient purity. The previous works showed that the heptamethine based cyanine sensitizers can sensitise photoinduced reduction of the iodonium cation by PET based on their redox properties[39, 43, 46-48, 56]. Some of these sensitizers also possess different anions affecting compatibility with the surrounding as well[37].

**Table 1.** NIR sensitizers (**S1-S29**) used in this thesis [96, 115, 118].

Commercial Name	Chemical structure	abbreviation	$\lambda_{\max}$ (nm)	$\epsilon_{\max}$ ( $M^{-1} \cdot cm^{-1}$ )	$E_{ox}$ (V)	$E_{red}$ (V)	$\Phi_f$
<b>S0322</b>		<b>S1</b>	777	$3.58 \times 10^5$	0.40	-0.80	-

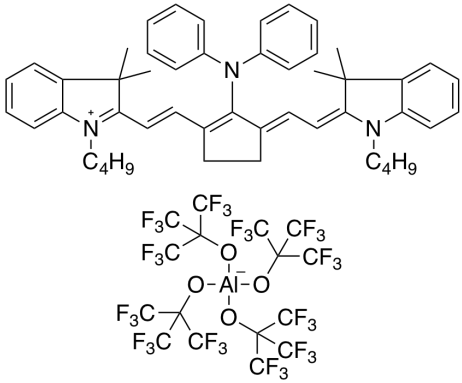
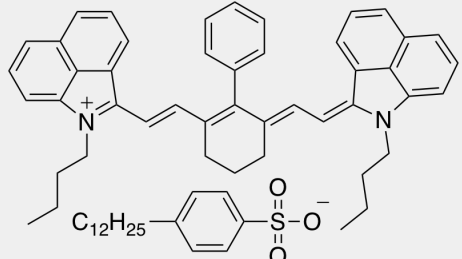


Commercial Name	Chemical structure	abbreviation	$\lambda_{\max}$ (nm)	$\epsilon_{\max}$ ( $M^{-1} \cdot cm^{-1}$ )	$E_{ox}$ (V)	$E_{red}$ (V)	$\Phi_f$
S0507		S9	799	$2.08 \times 10^5$	0.69	-0.34	0.06
S2383		S10	813	$1.62 \times 10^5$	-	-	-
S2389		S11	807	$2.40 \times 10^5$	-	-	-
S2391		S12	809	$2.13 \times 10^5$	-	-	-
S0750		S13	787	$2.04 \times 10^5$	0.75	-0.49	0.07
S2024		S14	793	$2.60 \times 10^5$	0.60	-0.60	0.07
S0253		S15	775	$2.18 \times 10^5$	0.68	-0.50	0.07



Commercial Name	Chemical structure	abbreviation	$\lambda_{\max}$ (nm)	$\epsilon_{\max}$ ( $M^{-1} \cdot cm^{-1}$ )	$E_{ox}$ (V)	$E_{red}$ (V)	$\Phi_f$
S2326		S16	785	$2.86 \times 10^5$	0.67	-0.51	0.19
S0325		S17	812	$3.17 \times 10^5$	0.42	-0.87	0.13
S2265		S18	791	$3.03 \times 10^5$	0.48	-0.97	0.13
S2283		S19	796	$8.15 \times 10^5$	0.48	-0.97	0.13
S2344		S20	793	$2.88 \times 10^5$	0.42	-0.97	0.16
S2468		S21	844	$2.39 \times 10^5$	0.56	-0.57	-
S0821		S22	800	$1.35 \times 10^5$	0.80	-0.59	0.02

Commercial Name	Chemical structure	abbreviation	$\lambda_{\max}$ (nm)	$\epsilon_{\max}$ ( $M^{-1} \cdot cm^{-1}$ )	$E_{ox}$ (V)	$E_{red}$ (V)	$\Phi_f$
S2457		S23	753	$4.63 \times 10^4$	0.67	-0.32	-
S0772		S24	858	$2.05 \times 10^5$	0.73	-0.32	-
S2123		S4_ref	681	$1.36 \times 10^5$	-	-	-
S2026		S25	786	$3.23 \times 10^5$	0.58	-0.56	-
S2178		S25_ref	683	$3.38 \times 10^5$	-	-	-
S10761		S26	835	$2.16 \times 10^5$	0.54	-0.57	-

Commercial Name	Chemical structure	abbreviation	$\lambda_{\max}$ (nm)	$\epsilon_{\max}$ ( $M^{-1} \cdot cm^{-1}$ )	$E_{ox}$ (V)	$E_{red}$ (V)	$\Phi_f$
<b>S2639</b>		<b>S27</b>	-	-	-	-	-
<b>S0991</b>		<b>S28</b>	992	$2.23 \times 10^5$	0.66	-0.34	-

### 3.1.2 Co-initiators in the NIR Photoinitiating System

As aforementioned noticed, co-initiators work together with NIR sensitizers by PET to generate the reactive species such as radicals and/or conjugate acid, which initiate photopolymerization. Herein, iodonium salts were used as co-initiators in this thesis to study NIR sensitized photopolymerization. For the development of more initiating system for uses in NIR photopolymerization, some oxime esters were studied as alternative co-initiators to iodonium salts.

#### Iodonium Salts

Table 2 shows the iodonium salts used in the thesis. All of them carry the same iodonium cation but different counter anions. Furthermore, **IS1** was used in radical polymerization because of its good solubility in some acrylate monomers[46]. Additionally, **IS2-IS7** were used in the cationic polymerization studies to explore the influence of the anion on reactivity in polymerization. All of these anions assign to weakly coordinating anions (WACs) [257], which can generate stronger conjugate acid to facilitate cationic polymerization. The motivation to include alternatives also bases on the fact that the well known hexafluorophosphate ( $PF_6^-$ ) still exhibits the **HF** issue[46]. In other words, iodonium salts comprising  $PF_6^-$  can release this highly toxic material under certain circumstances[46]. **IS1**, **IS5** were

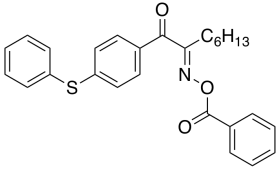
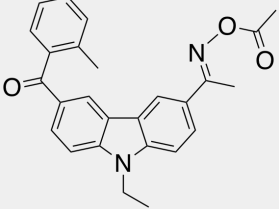
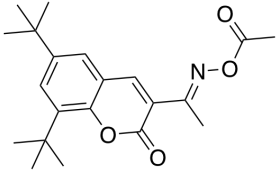
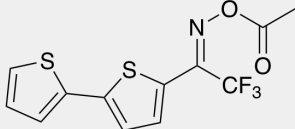
obtained from FEW Chemicals. **IS2** was bought from TCI. **IS3**, **IS4**, **IS6**, **IS7** were synthesised in the lab[41, 48]. They were used directly without further purification.

**Table 2.** Iodonium salts (**IS1-IS7**) used in this thesis [96, 115, 118].

Name	Chemical structure	Name in thesis
<b>S2430</b>		<b>IS1</b>
<b>IS-PF6</b>		<b>IS2</b>
<b>IS-FAP</b>		<b>IS3</b>
<b>IS-FAP-II</b>		<b>IS4</b>
<b>S2617</b>		<b>IS5</b>



**Table 3.** The oxime esters used in this thesis [118].

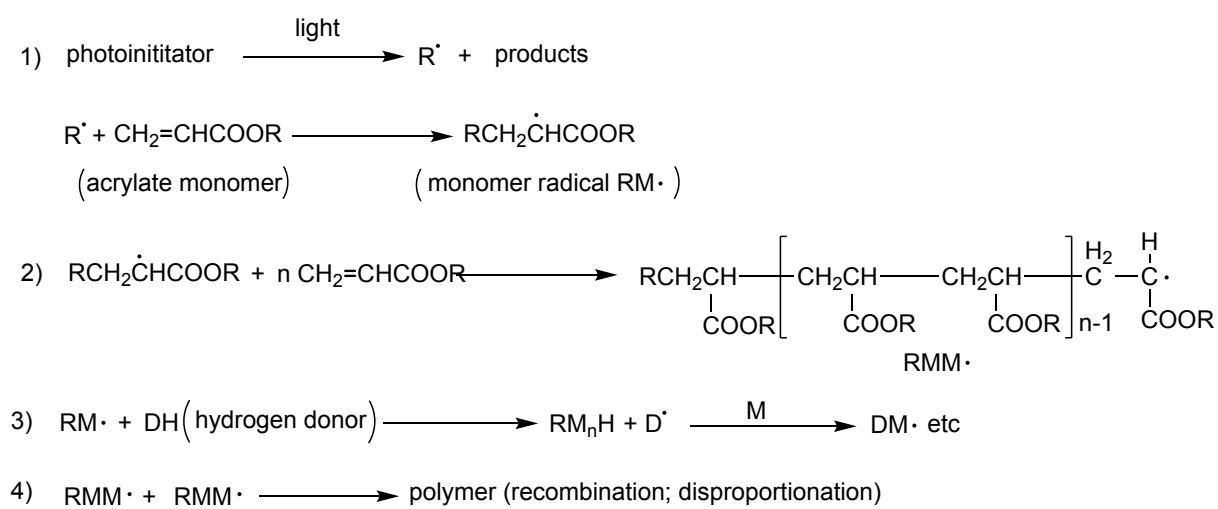
Commercial Name	Chemical Structure	$\lambda_{\max}$ (nm)	$\epsilon_{\max}$ ( $M^{-1}\cdot cm^{-1}$ )	$E_{ox}$ (V)	$E_{red}$ (V)
<b>OXE-01</b>		326	$2.95 \times 10^4$	1.72	-1.36
<b>OXE-02</b>		337	$2.30 \times 10^4$	1.51	-1.26
<b>COXE-15</b>		300	$1.65 \times 10^4$	1.59	-1.30
<b>BTCF-OXE</b>		356	$2.28 \times 10^4$	1.70	-1.26

### 3.1.3 Monomers for Radical Photopolymerization

Acrylates depict one kind of monomers for radical polymerization. They have been widely used in many free radical and hybrid radical-cationic photocuring systems. Herein, different acrylate monomers derived from multifunctional compounds such as **TPGDA** or **TMPTA** and those with one double bond (**LMA**, **PEGMA**), see Table 4 for the structures, were used in the investigations pursued. Furthermore, **TPGDA**, and **TMPTA** were chosen to discover the reactivity of the NIR photoinitiating system comprising the sensitizer and an iodonium salt as initiating system resulting in formation of cross-linked materials. **PEGMA** was used in bleaching measurements because it leads to non-cross-linked materials during polymerization after exposure which easily dissolve as requested by the procedures applied to identify the products later by LC-MS techniques[96]. **LMA** was taken for similar reasons as solvent carrying some features of radical monomers. It was also used as solvent to measure the bleaching of the sensitizers in the surrounding matrix to identify the amount of conjugate acid.

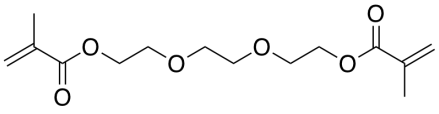
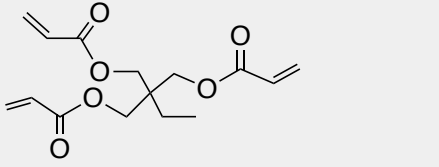
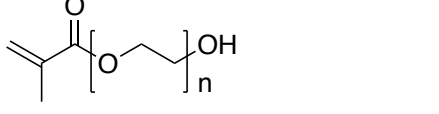
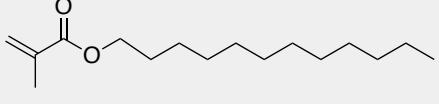
Scheme 22 depicts the process of the free radical polymerization based on four steps, which are initiation, propagation, chain transfer, and termination upon exposure[258]. The

first step, that is initiation, sensitizer relates to the interaction with light and forms therefore the key step of photopolymerization, where the radical  $R^{\bullet}$  generated subsequently adds to the olefin of the acrylate resulting initiation of polymerization. The higher electrophilicity of the radical formed results in the higher efficiency in such polymerization systems. All of these monomers were bought from SigmaAldrich. However, the inhibitors in **TPGDA**, **TMPTA**, and **LMA** were removed by running through basic  $Al_2O_3$  (Carl Roth GmbH) before it was transferred to the experiments. **PEGMA** was used directly without further purification.



**Scheme 22.** Free radical photopolymerization of acrylate monomers upon light exposure: (1) initiation, (2) propagation, (3) chain transfer, (4) termination, cited from [258].

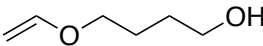
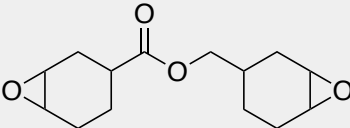
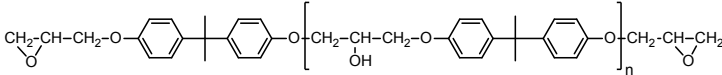
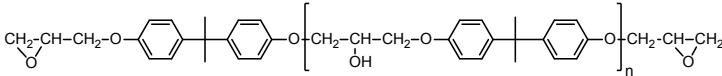
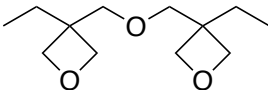
**Table 4.** The radical monomers used in the thesis

Chemical Name	Name	Chemical Structure
Tripropyleneglycol diacrylate	<b>TPGDA</b>	
Trimethylolpropane triacrylate	<b>TMPTA</b>	
Poly(ethylene glycol) methyl ether methacrylate (Mn 500)	<b>PEGMA</b>	
Lauryl methacrylate	<b>LMA</b>	

### 3.1.4 Monomers for Cationic Photopolymerization

Vinyl ether, oxirane, and oxetane are three kinds of general monomers widely used in cationic polymerization. Herein, five respective monomers (see Table 5) originating from these groups were selected to study the cationic polymerization initiated by heptamethine cyanines in combination with iodonium salts under high-power NIR LED exposure. The oxetane **OXT-03** was obtained from Gurun Technology (Hubei Jingmen, P. R. China). The epoxide monomer **ERL-4211** was purchased from IGM Resion as OMNILANE. **Epoxide 357** and **Epoxide 828** were available from Hexion. They were used directly without further purification.

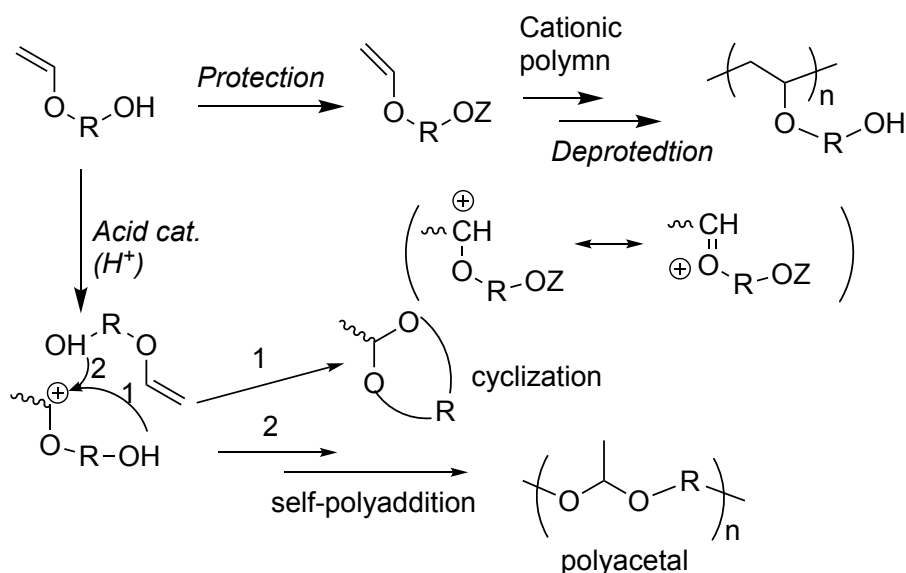
**Table 5.** The cationic monomers used in this thesis

Chemical Name	Short Name	Chemical Structure
4-Hydroxybutyl vinyl ether	<b>HBVE</b>	
3,4-Epoxy cyclohexanemethyl 3,4-epoxycyclohexanecarboxylate	<b>ERL-4211</b>	
Bisphenol A diglycidyl ether, oligomer	<b>Epikote 357</b>	
Bisphenol A diglycidyl ether, oligomer (n=2-3, M: 700 g/mol)	<b>Epikote 828</b>	
3,3'-(Oxybis(methylene))bis(3-ethyloxetane)	<b>OXT-03</b>	

#### Vinyl ethers

Vinyl ethers comprise electron-donating substituents and cannot therefore well function in radical polymerization[102, 259]. However, this pattern generally facilitates their use in cationic polymerization[20, 196]. The adjacent oxygen functions as electron-donating substituent resulting in an increase of the electron density of the vinyl group facilitating the reaction with electrophilic species such as conjugate acid formed upon exposure. However, the hydroxy functionalized vinyl ether can also generate polyacetals when the acid added to the surrounding, see Scheme 23[260].

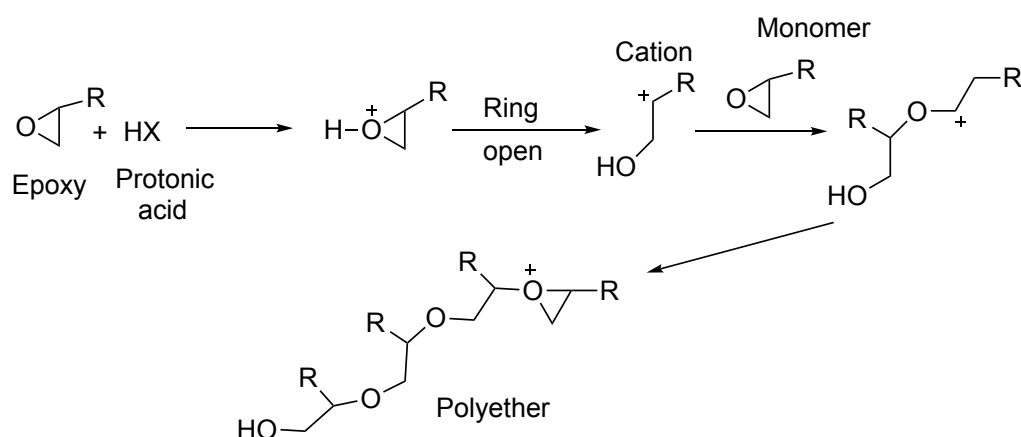




**Scheme 23.** The cationic polymerization mechanism of the vinyl ethers, cited from [260].

### Epoxy Compounds

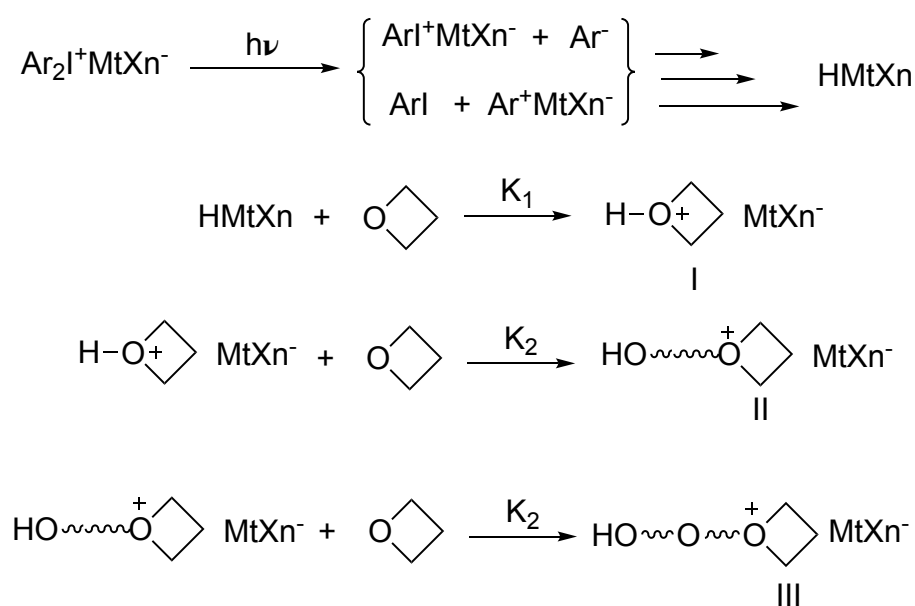
Epoxydes belong to one type of widely used monomers or oligomers for cationic polymerization [261-262] because of high thermal stability, excellent adhesion, and good chemical resistance [103]. Moreover, the bisphenol-A-diglycidyl ethers are one type of common commercially available epoxydes used in photoinduced cationic polymerization occurring at rather slow compared rates compared to radical polymerization. They are available in technical grade as oligomers as shown in Table 5. Their polymerization mechanism is depicted by Scheme 24 [258]. The oxirane ring opens after reaction with conjugate acid. Then the polymer chain propagates based on a mechanism where the carbocation controls chain growth as shown in Scheme 24. This can be easily terminated by nucleophilic reaction partners [258].



**Scheme 24.** The cationic polymerization mechanism of oxiranes, cited from [258].

### Oxetanes

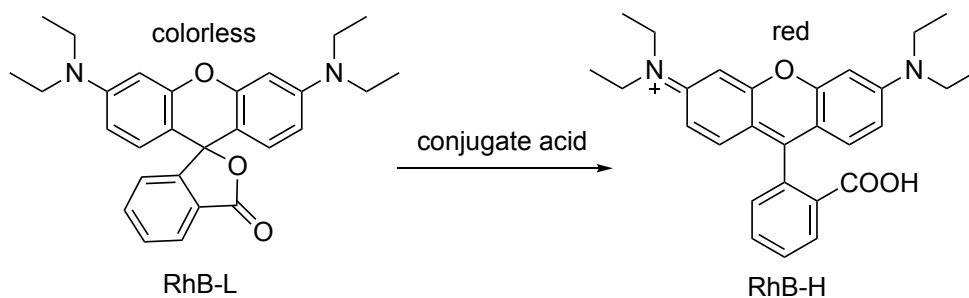
Oxetanes exhibit high thermal stability, excellent adhesion, good chemical resistance, and lower toxicity for applications in photocuring technology[99]. The ring strain of oxetane is 107 kJ/mol while that for ethylene oxide is 114 kJ/mol[263]. The  $pK_b$ -value of oxetane is 3.1 and that epoxide is 7.4, which make oxetane exhibit stronger basicity and be more reactive than epoxides during the photoinitiated cationic ring-opening polymerisation[263]. On the other hand, the higher basicity of oxetane compared to epoxide leads to a higher energy barrier for the ring-opening of the protonated oxetane, which causes oxetanes exhibit a rather long induction period in polymerization compared with epoxides as approved in the early stage of oxetane polymerization.[99, 104, 113] The polymerization mechanism of the oxetane is shown in Scheme 25[111]. The polymer chain propagates based on the oxetanium ion, which appears to be more tolerant in the presence of some nucleophilic groups such as alcohols or carboxylic acid.



**Scheme 25.** The cationic polymerization mechanism of the oxetanes, cited from [111].

#### 3.1.5 Material for Quantification of Conjugate Acid Formed

The Rhodamine B lactone (**RhB-L**) sensitively responds upon treatment with acid[41, 47] resulting in generation of deep coloured Rhodamine B (**RhB-H**) by opening the lactone ring, see Scheme 26. The reaction product appears as magenta coloured solution with an absorption maximum located at 556 nm[41, 47]. Therefore it is used as reagent to monitor the amount of conjugate acid generated in the aprotic organic solution upon irradiation.



**Scheme 26.** Mechanism of **RhB-L** serving as tracer agent of conjugate acid, modified from [41].

## 3.2 Solvents

The following solvents were used. These include methanol (**MeOH**), acetone, acetonitrile, and *n*-butyl acetate (**BuAc**), which are commercially available and were used as received from the respective suppliers. More details can be found in the experimental sections of the publications[96].

## 3.3 Methods

### 3.3.1 UV-Vis-NIR Spectroscopy

UV-Vis-NIR spectra of the sensitizers were measured with a Cary 5000 from Agilent. 1x1 cm quartz cuvettes were applied to take the spectra of the solutions. In some case, monomers comprising the sensitizer were placed between two glass slides carrying spacers providing the requested thickness to take the absorption spectra.

### 3.3.2 DSC and Photo-DSC

The thermal initiation temperature  $T_i$  of the monomer comprising NIR sensitizers and coinitiators such as iodonium salts and oxime esters was determined by differential scanning calorimetry (DSC) experiments. The samples were heated from 25 °C to 200 °C with a rate of 10 K/min and the onset-point of the exothermal peak was determined to define  $T_i$ . The mass of the sample kept around 5 mg[47].  $T_i$  relates to the temperature where significant formation of polymerization heat occurred, see reference[47] for more details.

Additionally, photo-DSC measurements[46] were carried out to determine the photoinitiation efficiency of the NIR photoinitiator systems in the monomers. This measurement also helped to operate at isothermal conditions. The aforementioned 805nm NIR-LED from Phoseon was used for all exposure experiments (output 0.2 W·cm<sup>-2</sup>). The light for exposure was collected with a lens and projected into a y-fiber, which was connected with the

head of the DSC (Q2000 from TA-Instruments). The output of NIR light of each fibre arm was adjusted. The LED-source was synchronised with the DSC by a shutter system placed between the fibre and the lens. The shutter was controlled by an Arduino uno board, which was programmed with the program Arduino 1.05 available from Arduino. This information went to the Arduino uno board controlling the shutter in ON/OFF position by a servomotor. The software of the DSC controls the event-output of this instrument functioning as digital switch. Change of resistance resulted in an ON (no resistance)/OFF (infinite resistance) modulation.[46]

### 3.3.3 FTIR and RT-FTIR Spectroscopy

Fourier transform Infrared Spectroscopy (FTIR) was used to measurement the conversion degree of monomers using the “Alpha-P” device from Bruker. The exposure film was put to the sample area of the “Alpha-P” device and then measured using attenuated total reflection (ATR). To obtain the spectra, 16 scans were carried out in the measuring range from 400 to 4000  $\text{cm}^{-1}$ . The settings and data acquisition were carried out using software "OPUS" (Bruker, Version 6.5).

In addition, real-time FTIR (RT-FTIR) spectra were measured with a VERTEX 70 from Bruker with an acquisition time of 0.2 s for each data point. The samples were prepared by dissolving the NIR sensitizers and coinitiators such as idonium salts or oxime esters in the monomers. The FTIR spectra of the samples on the “Alpha-P” device were collected in real time when exposure was operated using the NIR-LEDs. Spectra were taken in ATR mode.[96, 115, 118]

### 3.3.4 Cyclic Voltammetry

Oxidation and reduction potentials of oxime esters were measured by cyclic voltammetry (VERSASTAT 4-400 from AMETEK served as potentiostats) in acetonitrile ( $10^{-4}$  M) with tetrabutylammonium hexafluorophosphate from Aldrich (0.1 M) as a supporting electrolyte against ferrocene as an external standard. The data were taken with a scanning rate of  $0.015 \text{ V}\cdot\text{s}^{-1}$  using platinum disc as a working electrode and Ag/AgCl as reference electrode.[47]

### 3.3.5 Mass Spectrometry and Coupling with Chromatographic Method

Photoproducts of some sensitizers were analysed with a QTOF-LCMS system (G6530B) from Agilent using Dual AJS ESI as the ion source. As a column Hypersil C4 (125 x 4 mm)

from Thermofischer Scientific was used with acetonitrile/water (80:20) as eluent. After 20 minutes the ratio was changed to 95:5.[96, 115]

### 3.3.6 Dynamic Mechanical Analysis (DMA)

Dynamic Mechanical Analysis (DMA) experiments were carried out to characterise the viscoelastic properties of the films using DMA Q800 (TA Instruments, New Castle, USA) with a three-point bending clamp. The test temperature was varied from  $-50\text{ }^{\circ}\text{C}$  to  $250\text{ }^{\circ}\text{C}$  with a ramping rate of  $3\text{ }^{\circ}\text{C min}^{-1}$ , a frequency of 1 Hz, an amplitude of  $1\text{ }\mu\text{m}$ , and a preload of 0.01 N. The properties measured under this oscillating loading were storage modulus ( $E'$ ) and  $\tan \delta$ . The ratio of the loss modulus ( $E''$ ) to the storage modulus  $E'$  is referred to as the mechanical damping, or  $\tan \delta$ . The glass transition temperature ( $T_g$ ) was determined to be the position of the maximum on the  $\tan \delta$  versus temperature plot.[45, 115]

### 3.3.7 Conductivity Measurement of the Iodonium Salts

Conductivity of the iodonium salts in different monomers was measured with the 856 Conductivity Module comprising 900 Touch Control from Methrohm. The cell constant was determined using an aqueous KCl solution.[46, 115]

### 3.3.8 NIR Sensitive Camera

A NIR sensitive camera (test 0563 0885 V7) was used to measure the temperature generated by sensitizers in the process of the NIR irradiation. Details were previously disclosed[96, 115, 118].

## 3.4 Light Sources

### 3.4.1 High Power NIR LEDs

**805 nm LED:** A NIR-LED prototype emitting at 805 nm with an exposure density of  $1.2\text{ W}\cdot\text{cm}^{-2}$  in a distance of 3 cm was gratefully received from Phoseon Ltd. It exhibits a size 8 cm x 13 cm x 3 cm. The available exposure area covers  $1.4\text{ cm}^2$  in the aforementioned distance[96, 115, 118].

**860 nm LED:** A NIR-LED prototype emitting at 860 nm with an exposure density of  $1.5\text{ W}\cdot\text{cm}^{-2}$  in a distance of 2 cm was gratefully received from EASYTEC GmbH. It exhibits a size 10 cm x 20 cm x 5 cm. The available exposure area covers  $3\text{ cm}^2$  in the aforementioned distance[96, 115, 118].

**870 nm LED:** A NIR-LED prototype emitting at 870 nm with an exposure density of  $1.2 \text{ W}\cdot\text{cm}^{-2}$  in a distance of 1 cm was gratefully received from EASYTEC GmbH and used for real-time FTIR experiments due to the smaller size. The available exposure area covers  $1 \text{ cm}^2$  in the aforementioned distance[115, 118].

The emission spectra of these three LEDs are depicted in figure 13. These new LED devices were available for first measurements in this thesis. Their high intensity enabled photochemistry reaction of sensitizers and co-initiators carrying internal activation barriers to occur successfully[96, 115, 118].

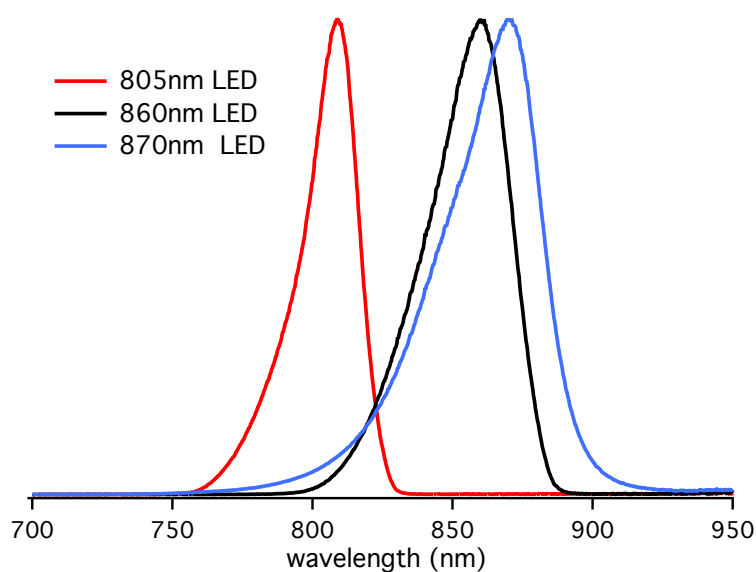


**Figure 13.** The emission of the high power NIR LEDs

### 3.4.2 NIR Lasers

A Fiber-coupled NIR laser emitting at 974 nm (Changchun New Industries Optoelectronics Technology Co., Ltd.; CNI-980-25 W-5-FC-A1-TTL1-MM400SMA, L1) was used to operate Fiber-coupled Laser exposure ( $P_{\text{output}} = 23 \text{ W}$ ,  $I = 125 \text{ W}\cdot\text{cm}^{-2}$ ).

In addition, a Line-shaped focused laser emitting at 980 nm (Laserline LDL 40-400, line width 1.5 mm, line length 31.5 mm) was also used to operate the high power NIR laser exposure (scan speed =  $0.004 \text{ m}\cdot\text{s}^{-1}$ ,  $P_{\text{output}} = 300 \text{ W}$ ).[118]

## 4. Further Experimental Details

This chapter briefly discloses the experimental conditions used in this thesis. More details can be found in published material[96, 115, 118].

### 4.1 High Power NIR LED Photoinduced Free Radical and Cationic polymerization with the Initiating System Comprising Heptamethine Based Cyanine and Iodonium salt

This section briefly discloses the experimental conditions used in this thesis. More details can be found in published material[96].

#### 4.1.1 NIR Sensitized Radical Photopolymerization

The double bond conversion degree  $x$  of acrylate monomer **TPGDA** was analysed by FTIR measurements to study the reactivity of the combination initiating system of NIR sensitizers (**S1-S24**) and iodonium salt (**IS1**). Spectra were taken in ATR mode (Vertex 70 from Bruker). The decrease of the acrylic double bonds at  $810\text{ cm}^{-1}$  was tracked for calculating the double bond conversion degree while the band at  $1720\text{ cm}^{-1}$  relating to the carbonyl group served as reference. The samples including monomer, sensitizer (0.05 wt%) and iodonium salt (2.0 wt%) were prepared as films with a thickness of  $50\text{ }\mu\text{m}$  on the glass. Then, the samples were irradiated with the LED emitting at  $805\text{ nm}$  ( $1.2\text{ W}\cdot\text{cm}^{-2}$ ) under nitrogen atmosphere. The final double bond conversion degree  $x$  of the **TPGDA** was obtained in percentage following Eq.(9)

$$x = \frac{A_0 - A_t}{A_0} \quad \text{Eq.(9)}$$

where  $A_0$  is the absorbance of double bond at  $810\text{ cm}^{-1}$  before irradiation while  $A_t$  relates to the absorbance of double bond at the respective irradiation time. The FTIR setup was the most chosen instrument for the studies of NIR sensitizers[41, 47, 96].

#### 4.1.2 Heat-Promoted Free Radical Photopolymerization as Studied by Photo-DSC Measurement

A regular photo-DSC setup[46] was used to identify the reactivity of the NIR photoinitiator systems in monomers. The photo-DSC offers the opportunity to operate the experiment at different temperatures to approve the function of additional heat to activate the process; that is  $40\text{ }^\circ\text{C}$ ,  $50\text{ }^\circ\text{C}$ , and  $70\text{ }^\circ\text{C}$ . This setup also helped to pursue experiment at isothermal conditions. Therefore operation at different temperatures helped to understand the func-

tion of internal reaction barriers appearing in the PET reaction[96]. Almost no photopolymerization activity was observed at ambient conditions because the heat generated immediately transfers to the DSC equipment and is not available to overcome internal reaction barriers of the PET system[96].

Herein, four sensitizers **S4**, **S5**, **S14**, and **S16** were used. The mass of the sample comprising **TPGDA**, **IS1** (2.0 wt%), and the respective sensitizer (**S4**, **S5**, **S14**, and **S16**, 0.05 wt%) was around 5 mg in the experiment. The aforementioned 805nm NIR-LED from Phoseon was used for all irradiation experiments with an output intensity of 0.2 W·cm<sup>-2</sup>. The light generated from LED was collected with a lens and projected into a y-fiber, which was used to connect with the head of the DSC (Q2000 from TA-Instruments). The intensity of NIR light of each fiber arm was adjusted with a fiber connected with a USB 4000 spectrometer from Ocean Optics. This functioned as radiometric source to adjust the fiber arms needed to expose the sample[47]. Measurements were operated in isothermal mode at the temperature chosen while purging with inert gas (nitrogen flow: 50 mL/min) helped to operate under anaerobic conditions. The polymerization rate and conversion degree of monomer is calculated by the heat flow available as  $\frac{dQ}{dt}$ . This was released during polymerization appearing as exothermal process[264-265]. Conversion degree of the monomer can be calculated by integration of the area under  $\frac{dQ}{dt}$  resulting in the available

exothermic heat  $\Delta Q(t)$  according to Eq. (10) and Eq.(11):

$$\Delta Q(t) = \int_0^{t_1} \frac{dQ}{dt} dt \quad \text{Eq.(10)}$$

$$x = \frac{\Delta Q(t)}{\Delta H_0^{\text{theory}}} \cdot 1/n \quad \text{Eq.(11)}$$

where  $\Delta H_0^{\text{theory}}$  is the molar heat of polymerization.  $n$  relates to the number of double bonds with the unit mol that can polymerise.  $\Delta H^{\text{theory}}$  is available from literature[264-265]. An acrylate group possesses  $\Delta H^{\text{theory}} = 86$  kJ/mol while a methacrylate group exhibits  $\Delta H^{\text{theory}} = 54.6$  kJ/mol [264-265]. The rate of polymerization ( $R_p$  in s<sup>-1</sup>) directly relates to the heat flow  $\frac{dQ}{dt}$  as expressed by Eq. (12) in which relates to the number of reacting double bonds ( $n$ ):

$$R_p = \frac{dQ}{dt} \cdot \frac{1}{\Delta H_0^{\text{theory}}} \cdot \frac{1}{n} \quad \text{Eq.(12)}$$



#### 4.1.3 Photobleaching and Photobleaching Kinetics of Heptamethine Based Cyanine in combination with Iodonium salt

The photobleaching rate of heptamethine sensitizers (**S1-S24**) was measured to study the relation between the structure of the sensitizers and their bleaching properties. The samples comprising the monomer **PEGMA**, the respective sensitizer (**S1-S24**,  $7.0 \times 10^{-6}$  mol·g<sup>-1</sup>), and the iodonium salt **IS1** ( $3.0 \times 10^{-5}$  mol·g<sup>-1</sup>) were prepared to films with a thickness of 50 µm on the glass. Then, samples were irradiated with the 805nm NIR LED device from Phoseon ( $1.2 \text{ W} \cdot \text{cm}^{-2}$ ) under nitrogen atmosphere in 2min. After exposure, the polymer of **PEGMA** was dissolved in methanol (10.0 to 20 mg in 2mL) to get the absorbance of the sensitizer and its photoproducts keeping in the range between 0.3 and 1.5. The UV-Vis-NIR spectra were measured by UV Spectrometer Cary 5000 (Agilent). 1 x 1 cm quartz cuvettes were used for measurements. The concentration of sensitizers residing in the solution was calculated following Beer-Lambert's Law[47, 96].

Additionally, sensitizers **S4**, **S9**, **S18** were chosen to study the bleaching kinetics of the sensitizers in different exposure time when they work together with iodonium salt **IS1** respectively following the same methods as aforementioned explained[47, 96].

#### 4.1.4 Thermal Stability of the Initiating Systems Comprising Heptamethine based cyanine and Iodonium salt in TPGDA

The thermal stability of the initiating system comprising heptamethine based cyanine and iodonium salt was studied by DSC measurement, where the onset thermal initiation temperature  $T_i$  of monomer polymerization was determined. The samples comprise respective sensitizer (**S1-S24**, 0.05 wt%), **IS1** (2.0 wt%). **TPGDA** were heated from 25°C to 200°C with a rate of 10 K/min. This yield the onset-point of heat generated by the polymerization of the monomer. Even small amounts of sensitizer and iodonium salt can lead to the decrease of  $T_i$ [19] while neat monomer exhibits a  $T_i$  of about 180°C. Since this phenomenon has not been well understood in detail, we would like to operate such measurements for our systems to find relations between structure of the sensitizer and  $T_i$ [96].

#### 4.1.5 NIR sensitised cationic photopolymerization

RT-FTIR spectra of the epoxides comprising NIR sensitizer (**S5**) in different concentration and iodonium salt **IS2** (2.0 wt%) upon NIR exposure were measured with a VERTEX 70 from Bruker with an acquisition time of 0.2s for each data point. The samples were prepared by dissolving the NIR sensitizer and **IS2** (2.0 wt%) in the **Epikote 828**. Acetone was

used as auxiliary medium to transfer the sensitizer **S5** and **IS2** into the epoxied. After sample preparation in the spectrometer, the system was first purged with dry nitrogen for 15 min to remove volatile components such as acetone. Purging with nitrogen continued during exposure operating the NIR-LED as aforementioned mentioned in a distance of 3.0 cm. Spectra were taken in ATR mode. The peak area at  $915\text{ cm}^{-1}$  served for monitoring the epoxide conversion degree and the phenylene group band of the **Epikote 828** ( $1230\text{ cm}^{-1}$ ) were used as reference. The conversion degree of the monomer was calculated by Eq.9 in Section 4.1.1[96].

#### 4.1.6 Photoproduct Analysis with LC-MS

The photoproducts of **S4** were prepared by exposure of the combination initiator system including **S4** (0.05wt%) and **IS1** (2.0 wt%) in **PEGMA** with the 805 nm LED prototype ( $1.2\text{ W}\cdot\text{cm}^{-2}$ , 10min) under nitrogen atmosphere. The polymerised **PEGMA** being soluble in MeOH was removed from the photoproducts by column chromatography using methanol as solvent and silica (silica gel 60 from Carl Roth) as column material. Then, the sample was diluted with acetonitrile for further LC-MS measurement. After then, the samples were analyzed with a QTOF-LCMS system (G6530B) from Agilent using Dual AJS ESI as the ion source. Hypersil C4 (125 x 4 mm) from Thermofischer Scientific was used as a column while acetonitrile/water (80:20) was as elution solvent. After 20 minutes the ratio of the elution solvent was changed to 95:5[96].

#### 4.1.7 Quantification of Conjugate Acid Formed

As aforementioned explained, **RhB-L** can monitor the conjugate acid formed in system. Herein, the conjugate acid generated from the combination initiator comprising heptamethine and iodonium salt upon NIR irradiation was monitored by **RhB-H** formed appearing as magenta coloured solution. The respective sensitizer (**S4**, **S18**,  $4.1\times 10^{-5}\text{ M}$ ) and iodonium salt (**IS2**,  $5.6\times 10^{-4}\text{ M}$ ) were dissolved in 10 ml acetone and exposed with 805nm LED light ( $1.2\text{ W}\cdot\text{cm}^{-2}$ ) in a crystallisation dish with 3 cm diameter. The solution was put into a 10 ml volumetric flask and the loss of the solvent because of evaporation was filled to achieve 10 ml solution. The spectra of the **RhB-H** were calculated by subtraction of the spectrum of the sensitizer and its photoproducts from the spectrum containing additionally the **RhB-L** ( $1.0\times 10^{-4}\text{ M}$ ).[41, 46-47] The concentration of the conjugate acid generated from the combination of initiating system are derived from the concentration of **RhB-H** calculated by Beer-Lambert's Law[41, 46-47].

## 4.2 High-Power NIR LED Photoinduced Cationic and Radical/Cationic Hybrid Polymerization Using the Combination of Heptamethine Cyanine and Iodonium Salt as the Initiating System

This section briefly discloses the experimental conditions used in this thesis. More details can be found in published material[115].

### 4.2.1 NIR Sensitized Cationic and Hybrid Radical/Cationic Photopolymerization

A regular RT-FTIR setup as aforementioned explained was used to measure the cationic and radical-cationic hybrid photopolymerization of monomers with the combinations of the NIR initiators comparing different sensitizers **S4**, **S25**, **S26**, and **S27** and iodonium salts **IS2-IS7**[96, 115]. The samples were prepared by dissolving the respective NIR sensitizer ( $6 \times 10^{-3} \text{ mmol}\cdot\text{g}^{-1}$ ) and iodonium salt ( $3.8 \times 10^{-2} \text{ mmol}\cdot\text{g}^{-1}$ ) in different monomers. Moreover, the following combination of initiating system comprising sensitizers and iodonium salts were selected; that are **S5/IS2**, **S26/IS3**, **S26/IS4**, **S27/IS5**, **S27/IS6**, **S25/IS5**, and **S27/IS7**. Herein, the reactivity of the initiator system comprising sensitizer and iodonium salt in different monomer including **TMPTA**, **Epikote357**, **OXT-03** and their mixtures including **TMPTA/Epikote357** (1:1), **TMPTA/ERL** (1:1), **TMPTA/OXT-03** (1:1), **TMPTA/Epikote357** (4:3:3), and **TMPTA/ERL** (4:3:3), was studied. Put the sample to the sample area of the "Alpha-P" device and covered with a piece of microslide which can facilitate to hold the heat generated by sensitizers in the system to minimize the influence of inhibiting oxygen by the surrounding. Exposure was operated with the 805 nm NIR LED ( $1.2 \text{ W}\cdot\text{cm}^{-2}$ ) as aforementioned disclosed at distance of 3.0 cm while the 870 nm NIR LED was placed at a distance of 1.0 cm. Spectra were collected in ATR mode. The peak area at  $810 \text{ cm}^{-1}$  was used to determine the conversion degree of **TMPTA**. The peak area at  $975 \text{ cm}^{-1}$  was used to determine the conversion degree of epoxide **ERL** while  $915 \text{ cm}^{-1}$  was used for monitoring the epoxide conversion degree of **Epikote 357**. The peak area at  $830 \text{ cm}^{-1}$  was used to determine the conversion degree of oxetane **OXT-03**. Furthermore, the peak at  $1650 \text{ cm}^{-1}$  was used to determine the conversion degree of vinyl ether **HBVE**. The conversion degree of the monomers was calculated by Eq.9[115].

Additionally, the conversion degree of the monomers used to form films in DMA measurement (see Section 4.2.3) were taken with FTIR. The setup is the same in Section 4.1.1.

### 4.2.2 Photoproduct Analysis with LC-MS

The photoproduct of **S25** (0.05 wt%) in combination with iodonium salt **IS2** (2 wt%) in **PEGMA** was analyzed by LC-MS[115]. The method is the same as disclosed in Section 4.1.5.

#### 4.2.3 Dynamic Mechanical Analysis (DMA)

The samples used for exposure were prepared by dissolving the sensitizer and iodonium salt in the corresponding monomers. Before exposure, the sample was put on one piece of glass first, then another piece of glass was used to cover the sample on the glass to minimize the influence of inhibiting oxygen from the surrounding and to keep the heat generated from sensitizers in the system. Three pieces of tape were used to make a defined thickness of the films approaching up to 120  $\mu\text{m}$ . The films used for DMA measurement were obtained after exposure. Furthermore, films of the samples comprising the NIR sensitizer **S27** ( $6 \times 10^{-3} \text{ mmol} \cdot \text{g}^{-1}$ ), iodonium salt **IS5** ( $3.8 \times 10^{-2} \text{ mmol} \cdot \text{g}^{-1}$ ) and different monomers were prepared using the 805nm NIR LED ( $1.2 \text{ W} \cdot \text{cm}^{-2}$ , 10 min). Another film of sample comprising **TMPTA** and **ERL-4211** using *i*-propyl thioxanthone (**ITX**, 0.1 wt%) and **IS5** ( $3.8 \times 10^{-2} \text{ mmol} \cdot \text{g}^{-1}$ ) as a combination of initiator was prepared applying the 395 nm UV-LED ( $1.1 \text{ W} \cdot \text{cm}^{-2}$ , exposure time 2 min).

The viscoelastic properties of the films were studied by operating DMA using DMA Q800 (TA Instruments, New Castle, USA) with a three-point bending clamp. The operated temperature ranged from 50 °C to 250 °C with a ramping rate of 3 °C $\cdot$ min $^{-1}$ , a frequency of 1 Hz, an amplitude of 1 $\mu\text{m}$ , and a preload of 0.01 N. The properties measured under this oscillating loading were storage modulus ( $E'$ ) and  $\tan\delta$ . The ratio of the loss modulus ( $E''$ ) to the storage modulus  $E'$  is referred to as the mechanical damping, or  $\tan \delta$ . The glass transition temperature ( $T_g$ ) was determined from the maximum of the  $\tan \delta$  versus temperature plot[115].

#### 4.2.4 Generation of Heat on Demand with NIR Absorber

The heat generated by sensitizers in the process of NIR irradiation was imaged by a NIR sensitive camera (testo 0563 0885 V7) when films were prepared for DMA measurement. The films were prepared as in 4.2.3 disclosed[115].

#### 4.2.5 Quantification of Conjugate Acid Formed

In this section, the method is similar to Section 4.1.6. As aforementioned disclosed, the heptamethine cyanine generates huge amount of heat upon NIR irradiation resulting in higher increase of solution temperature. Therefore, a solvent with high vapour pressure helps to keep the heat generated by the cyanine in the surrounding, which may facilitate the system to generate more conjugate acid. Thus, **LMA** and **BuAc** were used instead of acetone in this section.

The combination of NIR initiator system comprising **S26/IS3**, and **S27/IS5** was respectively dissolved in 10 mL **LMA** or **BuAc** and exposed with the 805 nm LED light ( $1.2 \text{ W}\cdot\text{cm}^{-2}$ ) in a crystallization dish (diameter 3.0 cm). The concentration of sensitizer was  $4.1 \times 10^{-5} \text{ M}$  while iodonium salt was  $5.6 \times 10^{-4} \text{ M}$ . The solution was filled into a volumetric flask and filled up to 10 ml. The spectra were calculated by subtraction of the spectrum of the sensitizer and its photoproducts from the spectrum containing additionally the **RhB-L** ( $1.0 \times 10^{-4} \text{ M}$ ). The concentration of conjugate acid derived from the concentration of **RhB-H** generated from **RhB-L**[41, 47, 115]. This relates to the amount of conjugate acid formed.

#### 4.2.6 Conductivity Measurement

Conductivity of the iodonium salts in different monomers was measured using the 856 Conductivity Module comprising 900 Touch Control from Metrohm as already noticed in Section 3.3.7. Such measurements helped to understand the dissociation behaviour of the iodonium salts in the monomers used in this part of work. Typically a high conductivity results in better dissociation into the single ions and therefore higher reactivity[46]. Aggregated species such as dimers do not contribute to the overall conductivity. The concentration of the iodonium salts (**IS2-IS7**) applied for measurements kept at the same level as in RT-FTIR measurements; that is  $3.8 \times 10^{-2} \text{ mmol}\cdot\text{g}^{-1}$ . The cell constant was determined following a procedure as previously reported.[46, 115]

#### 4.2.7 Viscosity Measurement

The viscosity measurements were carried out using a Stresstech rheometer from ATS Rheosystems (MCR 102 SN81432646) under atmospheric air conditions operated at  $25^\circ\text{C}$  with an oscillation frequency of  $1.0 \text{ s}^{-1}$  at constant stress of 200 Pa. The epoxides **ERL-4211** and **Epikote 357** were measured with the measuring system of CP50-1 SN52361. **HBVE**, **OXT-03** were measured with the measuring system of CP25-1 SN49618. All of

them were measured in the measuring cell P-PTD200+H-PTD200 SN82112134-82331887[115].

#### 4.2.8 UV-Vis-NIR Measurement of Heptamethine Cyanines Solving in OXE-03

The UV-Vis-NIR absorption spectra of the sensitizers **S5**, **S25**, **S26**, and **S27** in **OXT-03** were measured to study the influence of monomer on the absorption of the sensitizer. There was no significant change of absorption profile of the sensitizers in the oxetane monomer **OXT-03** in the same concentration ( $6 \times 10^{-3} \text{ mmol} \cdot \text{g}^{-1}$ ) indicating no significant hint on formation of aggregates applying a sensitizer concentration applied in the photopolymerization experiment. UV-Vis-NIR Spectra were measured with a Cary 5000 from Agilent with putting the sample in the middle of two pieces of the glasses.

#### 4.2.9 Dark Curing Measurement

The initiating system comprising heptamethine cyanine and iodonium salt could generate radicals and conjugate acid, both of which may add to olefin of the vinyl ether. The former trigger free radical polymerization, the later initiate cationic polymerization. Therefore, the dark curing measurement of the **HBVE** comprising **S5** ( $6 \times 10^{-3} \text{ mmol} \cdot \text{g}^{-1}$ ) and iodonium salt **IS2** ( $3.8 \times 10^{-2} \text{ mmol} \cdot \text{g}^{-1}$ ) was carried out to study its polymerization mechanism. A regular FTIR setup (Vertex 70 from Bruker) was used to measure the photopolymerization of the **HBVE** upon irradiation 10 s using 805 nm NIR LED ( $1.2 \text{ W} \cdot \text{cm}^{-2}$ ), and kept in the dark 20 s, 60 s, and 120 s after irradiation 10 s. The peak at  $1650 \text{ cm}^{-1}$  was traced to determine the conversion degree of **HBVE**. Spectra were collected by ATR mode.[115]

### 4.3 High Power NIR LED Photoinduced Free Radical Polymerization (II): the Combination of Heptamethine Based Cyanine and Oxime Ester Serving as Initiating System

This section briefly discloses the experimental conditions used in this thesis. More details can be found in published material[118].

#### 4.3.1 Free Radical Photopolymerization with Oxime Ester

A regular photo-DSC setup[46] was used to determine the photoinitiation efficiency of the oxime ester photoinitiator systems in the monomers giving the opportunity to run the experiment at the same temperatures; that is  $40 \text{ }^\circ\text{C}$ . This setup also helped to operate at isothermal conditions. Thus, each sample comprising **TPGDA** and the respective oxime

ester went through a syringe filter before used in the experiment. The UV-LED emitting at 395nm was used for all exposure experiments (output  $0.1 \text{ W}\cdot\text{cm}^2$ ). The light generated was collected with a lens and projected into a y-fiber, which was connected with the head of the DSC (Q2000 from TA-Instruments). The output of UV light of each fiber arm was adjusted. The LED-source was synchronized with the DSC by a shutter system placed between the fiber and the lens. Details about the shutter system are given in Section 4.1.2. The photo-DSC measurements using **OXE-01**, **OXE-02**, **COXE-15**, and **BTCF-OXE** as the photoinitiator in the concentration of 0.05 wt% in **TPGDA** were carried out at the same isothermal conditions ( $40 \text{ }^\circ\text{C}$ ). The conversion of TPGDA was calculated with the same method used in Section 4.1.2.

#### 4.3.2 NIR Sensitized Free Radical Photopolymerization with Initiating System Comprising Heptamethine and Oxime Ester

The reactivity of the heptamethine in combination with oxime ester initiating system was studied by a regular RTFTIR setup keeping the same circumstance as aforementioned noticed in Section 4.2.1[96]. The samples were prepared by dissolving the respective NIR sensitizer (**S4**, **S7**, **S10**, **S18**, **S21**, **S24**, **S25**, and **S26**, 0.05 wt%) and respective oxime ester (**OXE-01**, **OXE-02**, **COXE-15**, and **BTCF-OXE**, 2.0 wt%) in **TPGDA**. Exposure occurred with the 805nm NIR LED as aforementioned disclosed in a distance of 3.0 cm and 1.0 cm in the case of the 870 nm NIR LED. Spectra were taken in ATR mode. The films had a thickness of  $10 \mu\text{m}$ . The peak area at  $810 \text{ cm}^{-1}$  was used to determine the conversion degree of double bond and the carbonyl group band of the acrylates ( $1720 \text{ cm}^{-1}$ ) severed as reference. Exposure occurred with the LED emitting at 805 nm applying an Intensity of  $1.2 \text{ W}\cdot\text{cm}^{-2}$  while the 870 nm LED provided an intensity of  $1.2 \text{ W}\cdot\text{cm}^{-2}$ .

Additionally, heptamethine cyanine generated considerable amount of heat into the surrounding as a result of non-radiative deactivation. The thicker film can keep more heat in the sample compared to thinner films. Herein, some thick films with a thickness  $160 \mu\text{m}$  were prepared to study the reactivity of the initiating system in the thick coatings. The conversion degree of **TPGDA** was analyzed by FTIR measurements using the band at  $810 \text{ cm}^{-1}$  for the decrease of acrylic double bonds and  $1720 \text{ cm}^{-1}$  of the carbonyl group as the reference. The sample comprised monomer **TPGDA**, the sensitizer **S18** (0.5 wt%), and different oxime esters including **OXE-01**, **OXE-02**, **COXE-15**, or **BTCF-OXE** (2.0 wt%), respectively, as coinitiators. The samples were prepared as films with a thickness  $160\mu\text{m}$

separated with two pieces of glass using tapes ad space. Exposure occurred with the LED emitting at 805nm nm applying an Intensity of  $1.2 \text{ W}\cdot\text{cm}^{-2}$  .[118]

#### 4.3.3 Generation of Heat on Demand with NIR Absorber

The heat generated by sensitizers was measured by NIR sensitive camera as already disclosed in Section 4.2.4. The samples were prepared by solving the respective sensitizer (**S4**, **S7**, **S18**, and **S21**, 0.05 wt%) and **OXE-01** (2 wt%) in **TPGDA**. Additionally, other samples were also prepared by solving sensitizer **S18** in different concentration and the oxime ester **COXE-15** (2 wt%) in **TPGDA**. They were irradiated with the LED device from Phoseon at 805 nm ( $1.2 \text{ W}\cdot\text{cm}^{-2}$ ) and with the device from EASYTECH emitting at 860 nm ( $1.5 \text{ W}\cdot\text{cm}^{-2}$ ) for 600 s. The thickness of the film was  $160 \mu\text{m}$  while the setup was covered with glass. A NIR sensitive camera (testo 0563 0885 V7) was used to record the temperature changes in the process of the irradiation.[96, 115, 118]

#### 4.3.4 Beaching and Bleaching Kinetics of the Combination of Initiator Comprising Heptamethine and Oxime Ester

The photobleaching measurement of heptamethine sensitiser was operated to study the bleaching properties of the sensitizers **S4**, **S18**, and **S25**. The samples comprising the monomer **PEGMA**, the respective sensitizer (**S4**, **S18**, and **S25**, 0.05 wt%) and **OXE-01** (2 wt%) were prepared and measured with the same methods shown in Section 4.1.3[47, 96]. Additionally, bleaching kinetics of **S4** and **S25** ( $3.5\times 10^{-6} \text{ mol}\cdot\text{L}^{-1}$ ) in combination with **OXE-01** ( $2.0\times 10^{-5} \text{ mol}\cdot\text{L}^{-1}$ ) respectively was pursued using **LMA** as monomer and solvent. The 805 nm high-power LED with an exposure density of  $1.2 \text{ W}\cdot\text{cm}^{-2}$  was applied. The method is similar to that in Section 4.1.3[118].

#### 4.3.5 Thermal Stability of of the Combination of Initiator Comprising Heptamethine and Oxime Ester system

The thermal stability of the heptamethine and oxime ester initiating system was studied by DSC. Determination of the  $T_i$  as disclosed in the section 4.1.4 was applied to determine the onset of thermal initiation temperature  $T_i$  of monomer polymerization. The method was the same with Section 4.1.4. Herein, sensitizers **S4**, **S7**, **S10**, **S18**, **S21**, **S24**, **S25**, and **S26** were selected to combine with **OXE-01** respectively for this study. The concentration of the sensitizers was 0.05 wt% while **OXE-01** was 2 wt%. Additionally, the thermal stability



of oxime esters **OXE-01**, **OXE-02**, **COXE-15**, and **BTCF-OXE** in TPGDA was also studied respectively, where the concentration of the oxime esters was 2.0 wt% [118].

#### 4.3.6 Laser Exposure

a) The sample was prepared by solving sensitizer **S28** (0.05 wt%) and **OXE-01** (2.0 wt%) in **TPGDA**. Then, samples were prepared as films with a thickness 160  $\mu\text{m}$  with two pieces of glass and were irradiated using Fiber-coupled laser (see Section 3.4.2) for 10 s ( $P_{\text{output}} = 23 \text{ W}$ ,  $I = 125 \text{ W}\cdot\text{cm}^{-2}$ ). The conversion degree of **TPGDA** was analyzed by FTIR measurements using the band at  $810\text{cm}^{-1}$  for the decrease of acrylic double bonds and  $1720\text{cm}^{-1}$  of the carbonyl group as the reference. A second laser with more power was used to verify this result (see b)).

b) Line-shaped focused laser: Laser exposure was pursued using a NIR laser emitting at 980 nm with line shaped focus (Laserline LDL 40-400, line width 1.5 mm, line length 31.5 mm). The samples were prepared as mentioned above and were irradiated with the laser emitting at 980nm (scan speed =  $0.004 \text{ m}\cdot\text{s}^{-1}$ ,  $P_{\text{output}} = 300 \text{ W}$ , see Section 3.4.2).

#### 4.3.7 Cyclic Voltammetry

The redox potentials of the oxime esters were measured by cyclic voltammetry (VER-SASTAT4-400 from AMETEK served as potentiostat). The samples were prepared by solving the oxime esters **OXE-01**, **OXE-02**, **COXE-15**, **BTCF-OXE**, respectively, in acetonitrile ( $10^{-3} \text{ M}$ ) with tetrabutylammonium hexafluorophosphate from Aldrich (0.1 M) as a supporting electrolyte against ferrocene as an external standard. The data were taken with a scanning rate of  $0.015 \text{ V}\cdot\text{s}^{-1}$  using platinum disc as a working electrode and Ag/AgCl as reference electrode. [47]

## 5. Results and Discussion

The studies in this thesis include three parts relating to (1) high-power NIR LED photoinduced free radical and cationic polymerization with the initiating system comprising heptamethine based cyanine and iodonium salt[96], (2) High-power NIR LED photoinduced cationic and radical/cationic hybrid polymerization using the combination of heptamethine cyanine and iodonium salt used as the initiating system[115], and (3) high-power NIR LED photoinduced free radical polymerization (II): the combination of heptamethine based cyanine and oxime ester serving as initiating system[118]. In the following subsections, the results disclosed some new findings in this field which were beyond the knowledge of literature[47] when our experimental work started in early 2018.

### 5.1 High Power NIR LED Photoinduced Free Radical and Cationic polymerization with the Initiating System Comprising Heptamethine Based Cyanine and Iodonium Salt

Some of the results discussed in this subchapter were previously published[96]. Previous work showed that a low-intensity NIR LED ( $\leq 0.1 \text{ W}\cdot\text{cm}^{-2}$ ) only can initiate radical polymerization if the cyanine bears a barbital group in the *meso*-position to sensitise the reduction of the iodonium cation resulting in formation of initiating aryl radicals initiating for radical polymerisation of acrylate monomers[47]. However, cationic sensitizers only responded upon irradiation applying NIR lasers for exposure while no initiation activity in combination with iodonium salts occurred using low-intensity LEDs although the free energy of photoinduced electron transfer ( $\Delta G_{PET}$ ), see Eq. 1, between photoexcited cyanine and iodonium salt appeared negative for both types of heptamethine cyanines.[7, 31, 35, 41, 46-47, 56] The limitation to heptamethines carrying a barbital group in the *meso*-position has been overcome in this thesis by using a high power NIR LED prototype emitting at 805nm with an intensity of  $1.2 \text{ W}\cdot\text{cm}^{-2}$ [96]. The cationic heptamethine cyanine sensitizers that exhibited no sensitivity in preliminary studies with lower power NIR LED ( $\leq 0.1 \text{ W}\cdot\text{cm}^{-2}$ )[47] showed sufficient sensitivity to react with iodonium salts resulting in initiation of free radical polymerization of acrylates and also cationic polymerization of epoxides, oxetanes, and vinyl ether with this high power NIR LED device[96, 115]. To our knowledge, this was the first report of NIR-sensitized cationic polymerization of epoxides[96].

Generally, cyanines derived from heptamethine with absorption in the NIR range can be used as heat generator resulting in temperature increase of the sample that can approach up to  $140 \text{ }^\circ\text{C}$  upon NIR light exposure[45, 51]. The NIR sensitizers **S1-S21** (Table1)

chosen in this subchapter can exhibit such capability efficiently. These sensitizers (**S1-S21**) derived from heptamethine are depicted by pattern I in Chart 13[96]. Depending on their electronic properties, they can be divided into zwitterionic cyanines and cationic cyanines. They possess different terminal groups  $a/a'$ ,  $b/b'$  (see Chart 15), and different substituents  $R_2$  (see Chart 15) in the *meso*-position affecting their absorption and electronic properties[36-37]. Generally, adjusting the maxima absorption of the sensitizers is mainly due to  $R_2$  which can be either an electron-withdrawing group such as A, B, C, F (see Chart 15) resulting in a blue shift of the absorption or an electron-donating moiety like G or H (see Chart 15) resulting in a bathochromic shift of the absorption. Therefore, **S4** and **S10** exhibit longer absorption wavelength than **S1** and **S7**, respectively. However, the redox potentials of the sensitizers depicted by structure I did not reveal remarkable variations. Therefore, the different combinations of the initiator system comprising iodonium salt **IS1** (see Table 2) used as coinicators and different sensitizers selected from **S1** to **S21** should exhibit similar reactivities based on the PET reaction mechanism system. However, the results revealed in this thesis could not confirm this point of view. The reduction potential of the iodonium salt **IS1**, that is -0.65 V[47, 61] results in a slight negative  $\Delta G_{PET}$  taking the corresponding oxidation potential of sensitizers in Table 1. Eq. 8 (see Section 2.2.2) serves as fundamental basis to calculate  $\Delta G_{PET}$ .

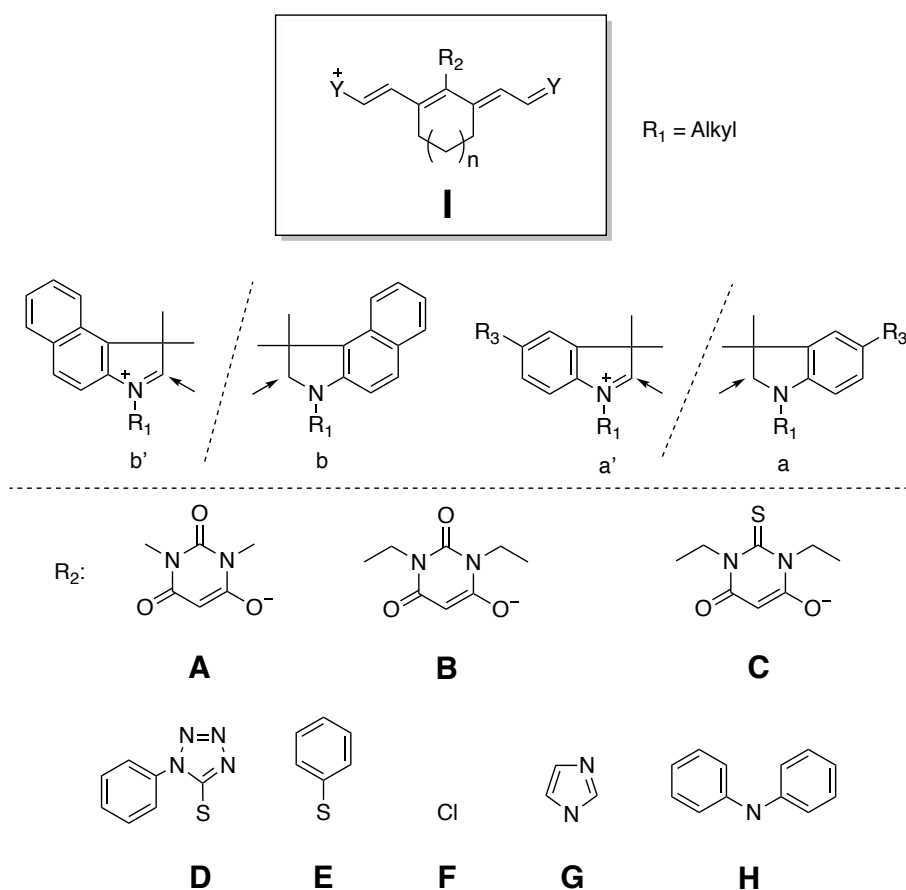


**Chart 15.** NIR sensitizers of structure 1 comprising different terminal groups  $a/a'$ ,  $b/b'$  and substituent  $R_2$  in the *meso*-position, modified from [96].

Sensitizers **S22–S24** (see Table 1) were used as reference because their structures were different compared to **S1–S21** although they also belong to cyanines. In the case of **S22** and **S23**, the structure depicts zwitterionic pattern. The cationic sensitizer **S24** is not a bridged compound carrying the five methine chains influencing photo-physical properties[36-37]. As aforementioned explained in Section 4.1.1, the bleaching of the heptamethine based sensitizers can prevent electron back transfer, which takes a key role in the initiation process of photopolymerization. Thus, it is necessary to carry out some strategies to prevent electron back transfer, which also exhibits negative  $\Delta G_{PET}$ . It is also necessary to study the bleaching properties of the sensitizers to learn more details about the relation between chemical structure and reactivity. Therefore, the bleaching activity of the sensitizers (**S1–S24**) in combination with iodonium salt **IS1** was studied. As aforementioned noticed, the temperature of the samples comprising heptamethine may approach up to 140°C upon irradiation[45, 51]. Then poly(ethylene glycol) methacrylate (**PEGMA**) exhibiting a high boiling point was chosen as the surrounding medium in this study, which would not evaporate under the irradiation conditions with the high power NIR LED while the heat generated from sensitizers keeps in the surrounding. Additionally, **PEGMA** has

similar molecular pattern compared to multifunctional methacrylic monomers but generates linear polymer which possesses sufficient solubility in comparison with the crosslinked polymer in the organic solvent. The bleaching kinetics of three different sensitizers including one zwitterionic sensitizer **S18** and two the cationic sensitizers **S4** and **S9** in combination with iodonium salt **IS1** were studied as documented by the results in Figure 14.

Finally, we found that the 805 nm high power NIR LED resulted in bleaching of all the selected sensitizers (**S1-S24**) in combination with iodonium salt **IS1**[96]. The bleaching rate of this sensitizers are shown in Table 9. This was a new finding at this time caused by the much higher intensity emitting device[96]. Figure 14 describes the bleaching kinetics of three selected sensitizers **S4**, **S9**, and **S18**. As shown in Figure14, the zwitterionic sensitizer **S18** bleached fast in combination with **IS1** as a result of PET. The cationic sensitizer **S9** exhibit less bleaching efficiency. The slowest bleaching efficiency was observed in the case of cationic sensitizer **S4**. The oxidation potential of **S18** (0.48 V) in comparison with **S4** (0.57 V) and **S9** (0.69 V) might partly explain these differences.

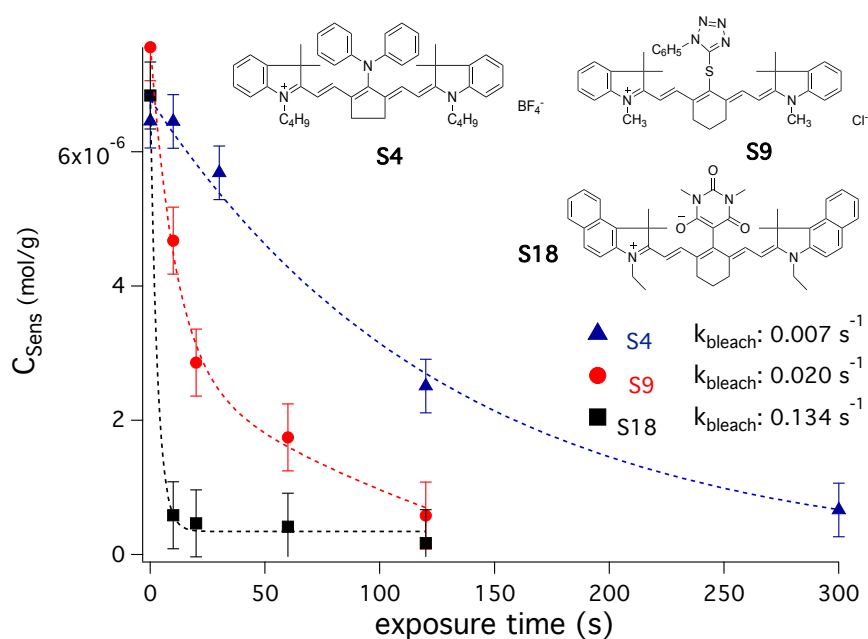


**Figure 14.** Bleaching kinetics of the combination of NIR initiating system including **S4**, **S9**, and **S18** ( $7.0 \times 10^{-6}$  mol·g<sup>-1</sup>) and iodonium salt **IS1** ( $3.0 \times 10^{-5}$  mol·g<sup>-1</sup>) in **PEGMA** using the high intensity NIR LED device, published in [96]. More details in Section 4.1.3 explain the experimental conditions.

Surprisingly, **S1-S21** showed acceptable reactivities in combination with iodonium salt **IS1** under the high-power NIR LED prototype irradiation while no initiation of radical polymerization was observed using cationic sensitizers in combination with iodonium salt applying low-intensity-emitting NIR LEDs[47]. Figure 15 shows double bond conversion of the

monomer **TPGDA** initiated by the selected sensitizer (**S1-S24**) using the aforementioned high intensity NIR LED device emitting at 805 nm[96].

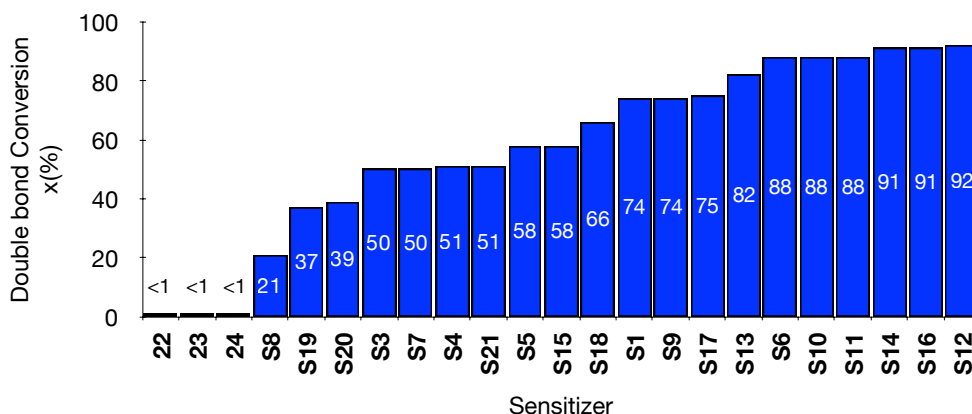


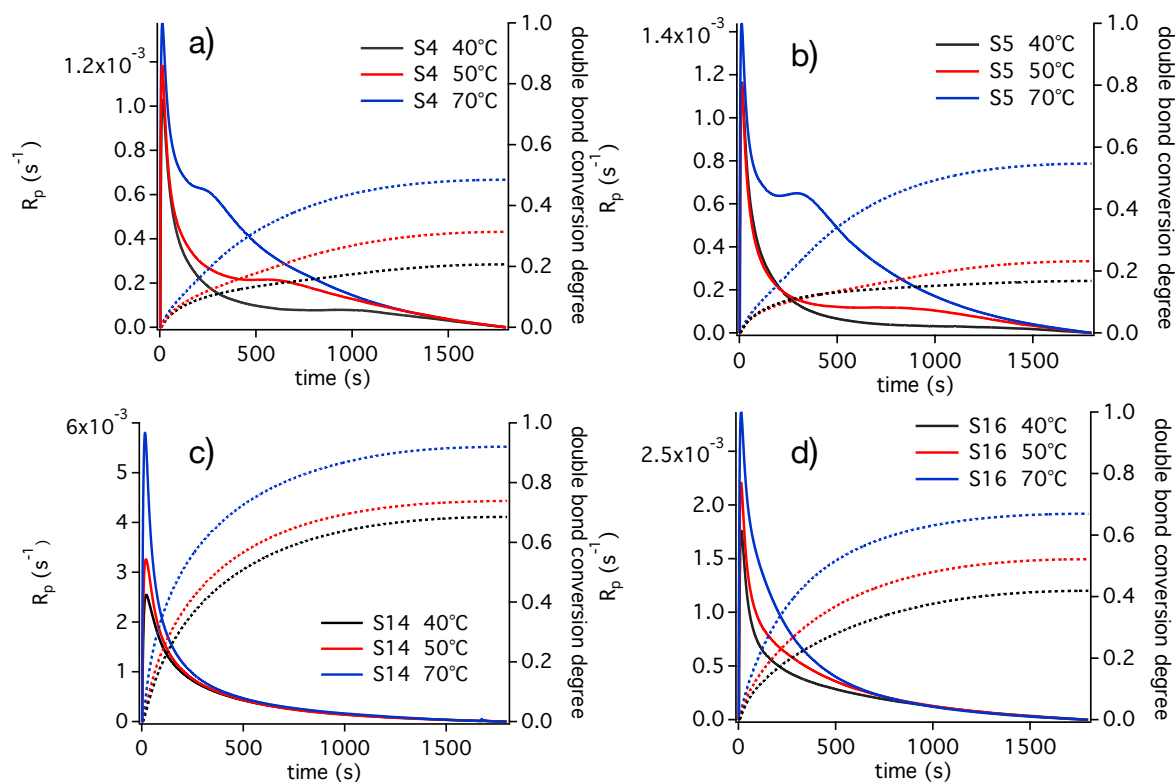
**Figure 15.** The double bond conversion of **TPGDA** with different combinations of initiating system including sensitizers (**S1-S24**, 0.05 wt%) and iodonium salt **IS1** (2 wt%) upon NIR LED exposure, published in [96]. More details in Section 4.1.1 explain the experimental conditions.

Particularly, Figure 15 shows nearly no polymerization applying **S22-S24** as sensitizers and **IS1** as coinitiator, although  $\Delta G_{PET} < 0$ . In addition, **S10-S12**, **S16** carrying phenyl mercaptotetrazole in the *meso*-position resulted in the highest monomer conversion. On the other side, the sensitizers **S10-S12** carrying organic anions exhibited higher monomer conversion compared to **S13** carrying inorganic anions. It shows that it is not possible to explain the reactivity of the sensitizers based on a single isolated molecule. The formation of ionic assemblies also influences the reactivity of the sensitizers. Unexpectedly, the zwitterionic sensitizer **S18** exhibited less **TPGDA** conversion than the cationic sensitizers **S10-S12** and **S16** with the new high-power LED ( $1.2 \text{ W}\cdot\text{cm}^2$ ), which is opposite to the results observed with low-power LEDs ( $\approx 0.1 \text{ W}\cdot\text{cm}^2$ ) where free radical photopolymerization of **TPGDA** was only observed for the zwitterionic cyanine **S18** in combination with **IS1**[47].

Previous studies exhibited that the zwitterionic sensitizers with barbital group showed higher fluorescence quantum yield (about 15%) while the cationic sensitizers selected in this thesis exhibited less fluorescence[47]. Non-radiative deactivation and also the lower bleaching rate of these cyanines caused them to release tremendous heat after absorbing the NIR light explaining the temperature of samples increased up to  $140 \text{ }^\circ\text{C}$ [45, 51]. The heat produced by sensitizers would be adequate for thermal decomposition of the initiator combination comprising sensitizer and iodonium salt **IS1** to generate reactive radicals for polymerization of **TPGDA**. Additionally, the thermal stability measurements of the sample

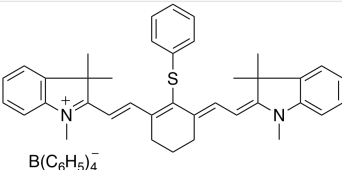
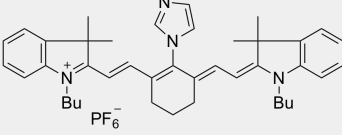
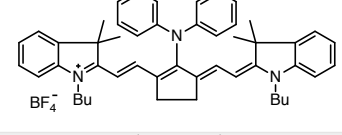
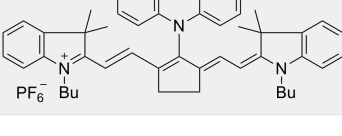
consisting of **TPGDA**, 0.05 wt% **Sens** and 2 wt% **IS1** using DSC showed that the onset of thermal initiation temperature of **TPGDA** polymerization less than 140 °C in all of the initiator system combinations. Thus, the results from DSC measurement might lead to the conclusion that the amount of heat released by sensitizers results in polymerization of **TPGDA**. However, this conclusion was refuted by the results of **S22-S24** which exhibited nearly no capability to initiate polymerization of **TPGDA** although thermal polymerization of **TPDGA** started below 100 °C in the system comprising sensitizer and iodonium salt **IS1**. The intrinsic thermal polymerization temperature ( $T_i$ ) of neat **PEGMA** or **TPGDA** resides at 190 °C[45]. Thus, we can conclude that formation of reactive initiating radicals needs both heat and photons. The former would facilitate the initiator system to proceed over internal barriers which result in threshold systems behaving different for each sensitizer in the PET process, for comparison see Figure 8 in Section 2.2.2. To prove the above conclusions, photo-DSC measurements, which proceed in a setup to operate under isothermal conditions during exposure, were operated at different temperatures. This helped to introduce additional heat in the system and facilitated to move over the existing additional intrinsic barrier easier. Finally, the results from photo-DSC measurement are depicted by Table 6 and Figure 16.

This table shows that increasing operation temperature results in both an increase of the polymerization rate in the maximum ( $R_p^{\max}$ ) and the final conversion of the monomer **TPGDA**. However, no radical photopolymerization of **TPGDA** occurred with a low intensity NIR LED ( $\leq 0.1 \text{ W}\cdot\text{cm}^{-2}$ ) under identical concentrations in the photo-DSC. Additionally, the results in Figure 16 depicted that with increasing temperature the conversion of **TPGDA** in all the systems investigated increased. In brief, the results from photo-DSC demonstrate the necessity to introduce additional heat, which can promote the system to overcome particularly the internal activation barrier easier. Marcus theory[266-267] about the electron transfer reaction rate constant  $k_{\text{PET}}$  (see Eq.8 in Section 2.2.2) also supports this point of view where with the increase of the temperature ( $T$ ) results in an increase of  $k_{\text{PET}}$ . More details can be found in reference[96].



**Figure 16.** Photo-DSC measurements of the polymerization of **TPGDA** with the sensitizers (0.05 wt%) a) **S4**, b) **S5**, c) **S14**, and d) **S16** and coinitiator **IS1** (2.0 wt%) at different operating temperatures (40 °C, 50 °C, 70 °C) upon 805 nm NIR LED exposure, solid line: polymerization rate ( $R_p$ ), dashed line: conversion, published in[96]. More details in Section 4.1.2 explain the experimental conditions.

**Table 6.** Summary of  $R_{p,max}$  using different sensitizers (**S14**, **S16**, **S4**, and **S5**) and the iodonium salt **IS1** embedded in the **TPGDA** at different operating temperature, published in [96]. More details in Section 4.1.2 explain the experimental conditions.

Structure	Sens	$R_{p,max}$ ( $10^{-3} s^{-1}$ )			$T_i$ of <b>TPGDA</b> (°C)
		40° C	50°C	70°C	
	<b>S14</b>	2.5	3.3	5.8	78
	<b>S16</b>	1.8	2.2	2.9	97
	<b>S4</b>	1.0	1.2	1.4	100
	<b>S5</b>	1.2	1.2	1.4	95



Additionally, the free activation enthalpy  $\Delta G_{PET}^\ddagger$  (Eq.6, Section 2.2.2) in PET determines the size of internal activation barrier (see Figure17) of the PET reaction based on the Marcus theory[160, 190, 266-267]. Figure 17 depicts three possible scenarios occurring in PET processes, a) endothermal conditions, b) thermoneutral conditions, and c) exothermal conditions, where the internal barrier exhibit quantity controlling the reactivity. Therefore, the system benefits from the heat released by the sensitizers promoting the reaction to proceed. The combination of NIR initiator systems comprising heptamethine cyanine and iodonium salt mostly belong to scenario c) where  $\Delta G_{PET} < 0$  or that are close to zero. This can be seen as a great result, which allowed to draw the conclusion to this topic according to the results obtained in the experiments pursued. The availability of the internal activation barrier in PET reaction has been considered as a little ‘stepchild’ until now. Hopefully, these results will give new impetus to this technology since this system requests to operate with special hardware in practice. This brings benefits such as improved white light stability of the initiator systems and therefore easier handling of the operating personal.

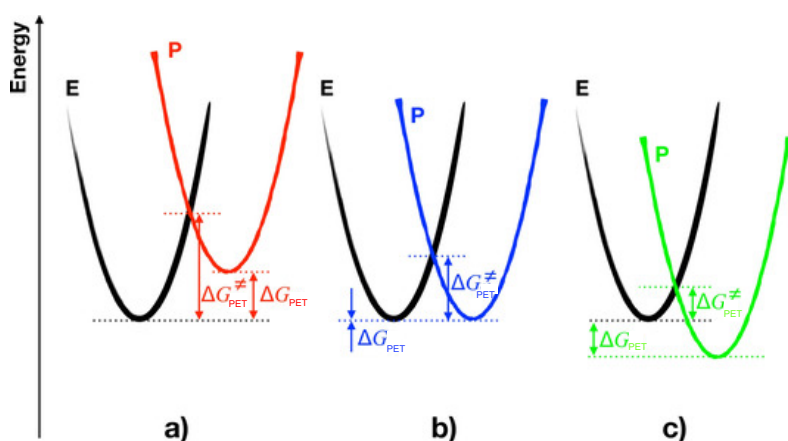


**Figure 17.** Energetic relations of PET with internal barriers resulting in threshold systems: a) endothermal conditions, b) thermoneutral conditions, c) exothermal conditions, cited from [36].

The combination of the initiator system comprising respective sensitizers (**S4**, **S18**) and **IS2** was separately investigated to explore possible formation of conjugate acid under different exposure time. The **RhB-L** was employed to probe the generation of conjugate acid by ring opening reaction, which results in formation of red-colored **RhB-H**, see also Section 4.1.6 for more details in the experimental part[47, 96]. Figure 18 depicts the absorption band changes of **RhB-H** at 550 nm. The amounts of conjugate acid generated in the two different initiating system were summaries in the Table 7. Both Figure 18 and Table 7 exhibit that **S18** can generate more conjugate acid.

**Table 7.** Amount of conjugate acid ( $a_{H^+}$ ) of the NIR initiator system ( $[Sens] = 6.3 \cdot 10^{-5} M$ ;  $[IS2] = 5.6 \cdot 10^{-4} M$ ) in acetone under NIR exposure using the 805 nm LED device with an intensity of  $1.2 W \cdot cm^{-2}$  for 10 minutes, published [96]. More details in Section 4.1.7 explain the experimental conditions.

time/min	$a_{H^+}$ (S18 / IS2)	$a_{H^+}$ (S4 / IS2)
1	$1.3 \cdot 10^{-5} M$	$1.8 \cdot 10^{-6} M$
3	$1.8 \cdot 10^{-5} M$	$4.1 \cdot 10^{-6} M$
5	$1.9 \cdot 10^{-5} M$	$7.2 \cdot 10^{-6} M$
10	$1.7 \cdot 10^{-5} M$	$1.0 \cdot 10^{-5} M$

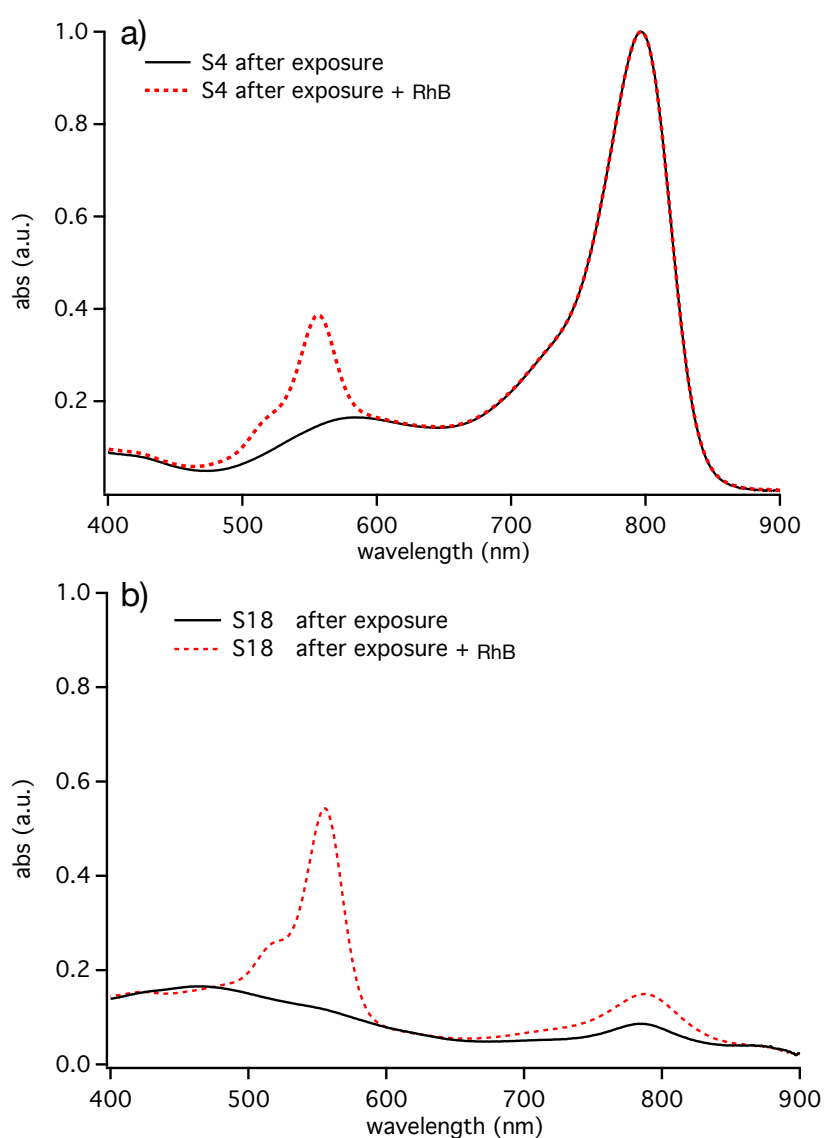


**Figure 18.** Increasing absorption of the acetone solution comprising sensitizer and **IS2** at 556 nm because of protonation of the **RhB-L** by conjugate acid generated from the system upon 805 nm NIR LED exposure ( $1.2 W \cdot cm^{-2}$ , 10 min). (a) **S4/IS2**, (b) **S18/IS2**, published in[96]. More details in Section 4.1.7 explain the experimental conditions.

However, only **S4** and **S5** can initiate polymerization of epoxides based on the bisphenol-A-diglycidylether resin Epikote 828 in combination with **IS2** (see Figure 19). The structural pattern of the sensitizers selected can explain this scenario. The diphenylamino substituent in the *meso*-position does not interfere cationic polymerization because the basicity of the amino nitrogen is  $10^4$  less than that of aliphatic amines as shown for several photoacid generators with diarylamino group[187]. In previous studies, only aziridines were observed to proceed according to cationic polymerization protocol successfully with **IS2** and zwitterionic **S18**[47]. Nevertheless, there was no cationic polymerization of epoxides occurring with **IS2** and zwitterionic **S18** applying the high intensity 805 nm NIR LED because nucleophilic photoproducts formed[39] inhibit cationic polymerization of epoxides. Figure 19 shows the relation between conversion of epoxy groups and sensitizer concentration. A higher concentration of sensitizer always causes a higher amount of conjugate acid formed according to the mechanism for the photosensitized oxidation according to Scheme 14 in Section 2.3.1. Thus, the cation radical formed serves as precursor to form conjugate acid explaining why a higher sensitizer concentration leads to higher amount of conjugate acid. Therefore, it nicely demonstrates the dependence on sensitizer concentration in the cationic polymerization of epoxides. This again approves the generation of conjugate acid by the sensitizer[47].

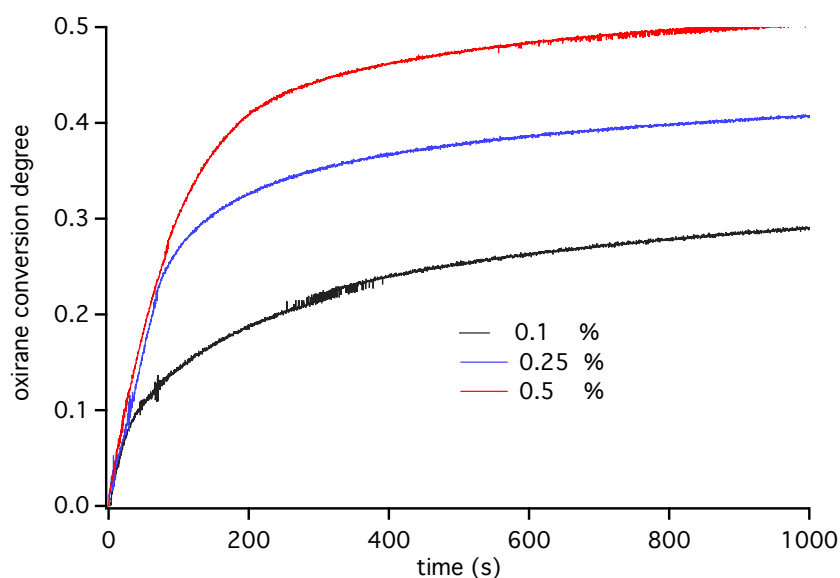


**Figure 19.** RT-FTIR conversion degree-time profiles of cationic photopolymerization of **Epikote 828** using the combination of **S4** in different concentration and **IS2** (2 wt%) upon 805 nm NIR LED exposure ( $1.2 \text{ W}\cdot\text{cm}^{-2}$ ), published in [96]. More details in Section 4.1.5 explain the experimental conditions.

The question still exists why particularly the compound with diphenylamino substitution worked although it forms less conjugate acid while others such as **S18** did not work although the amount of conjugate acid formed was larger (see Figure 18). A view on the absorption spectra obtained in bleaching experiments of **S3** and **S4** provides the answer. It showed a new absorption band generated at around 700nm which means that the photoproducts exhibit around 100 nm hypsochromic shift compared with original sensitizers, Figure 20b)-c). The central moiety belonging to the group with pentacyclic pattern can be seen as the reason. For comparison, **S15** comprising a six-membered carbon ring at the central position only showed bleaching of the cyanine while no new absorption band appeared from 650 nm to 700 nm, Figure 20a. Photoproduct analysis depicted that one of photoproducts of **S4**, which is **S4\_ref**, exhibits an additional double bond in the central position formed because of the reaction between **S4** and iodonium salt **IS2**. The new fulvene pattern explains the difference of the absorption maxima between **S4** and the reference **S4-ref**. It also presumably occurred with **S3** ( $R_2 = \text{Cl}$ ). Generally, **S4-ref** can be synthesised by the redox reaction of **S4** and  $\text{MnO}_2$ [86]. **S4-ref** was kindly provided by Dr. K. Reiner from FEW Chemical GmbH. LC-MS measurements additionally confirmed the formation of the **S4\_ref** which was well separated from **S4** in the mass spectra (see Figure 21 and Table 8), where the molecular weight of photoproduct of **S4** appearing at 6.73 min exhibits 684.4341M/z which is also the molecular weight of **S4\_ref**. Moreover, **S4\_ref** exhibits less nucleophilicity as the photoproducts formed by cleavage of **S15** explaining the capability of **S4** to function as sensitizer in cationic polymerization[96]. This was found for the first time in the experiments pursued in this thesis and was first reported in 2019[96].

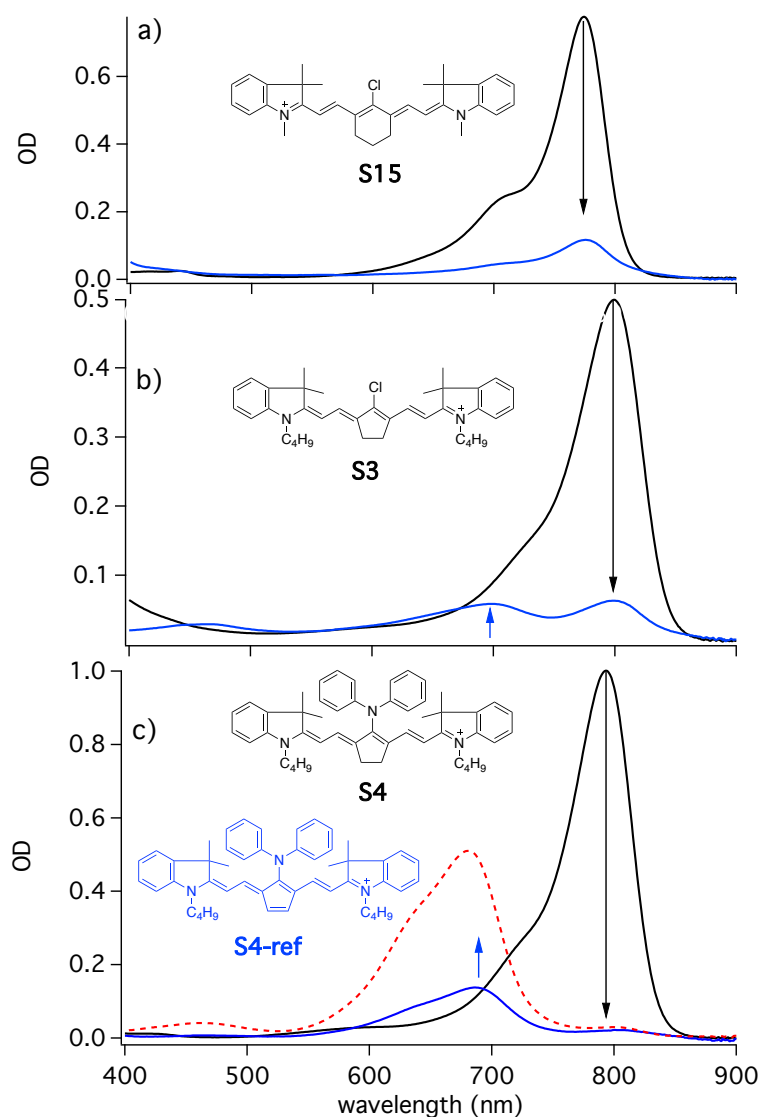


**Figure 20.** Change of the UV-Vis-NIR absorption of **S15** a), **S3** b) and **S4** c) upon 805 nm NIR LED exposure using the iodonium salt **IS1** as coinitiator in **PEGMA**, the blue curve and the red dashed curve in c) exhibit the absorption of the photoproduct of **S4** (blue) and that of **S4-ref** (red dashed), published in [96]. More details in Section 4.1.3 explain the experimental conditions.

As shown in Table 8, some lower molecular weight photoproducts were formed by cleavage of the heptamethine chain as previously reported for other NIR sensitizers. This occurs as competitive process to the formation of the aforementioned fulvene structure. The blue shift of the photoproducts agrees with similar photoproducts reported by previous studies[39]. **S4-ref** ( $\lambda_{\max} = 681 \text{ nm}$ ,  $\epsilon_{\max} = 1.36 \cdot 10^5 \text{ M}^{-1} \cdot \text{cm}^{-1}$ ; in MeOH) was formed with 23% yield[96]. Moreover, we found photoproducts exhibiting lower and higher masses concerning **S4** indicated that bond cleavage of the polymethine chain resulted in photoproducts with shorter masses and recombination products between distinct photoproducts showing in some cases higher masses. This occurred between cleavage products of the iodonium salt and that generated by the NIR sensitizer[39].

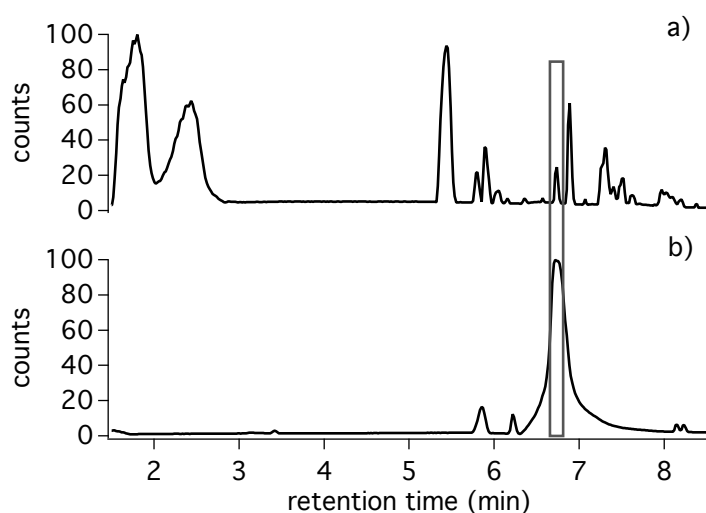


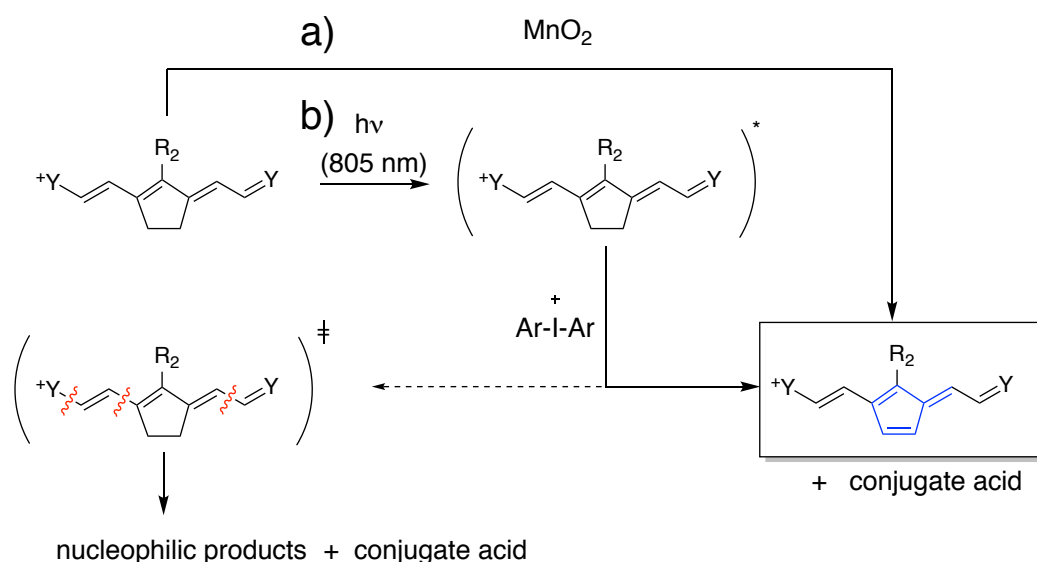
**Figure 21.** (a) LC-signal of the photoproducts of **S4** and **IS1** after exposure with the NIR LED device ( $1.2 \text{ W}\cdot\text{cm}^{-2}$ , 10 min) extracted from the polymer film of **PEGMA**. (b) LC-signal of the oxidised reference material **S4\_ref** was used without further treatment for the LC-MS experiment, published in [96]. More details in Section 4.1.6 explain the experimental conditions.

**Table 8.** Peak table of the molecular ions detected in the photoproducts analysis measurement with LC-MS, published in [96] More details in Section 4.1.6 explain the experimental conditions.

retention time (min)	M/z
1.75	393.1085
6.04	493.2537
6.36	541.2543
6.57	603.3747
<b>6.73</b>	<b>684.4341</b>
6.88	686.4499
7.07	216.1735
7.37	803.3508
7.81	502.287
7.82	376.2643
8.38	282.2217
8.77	734.4372
10.60	338.3424
12.03	394.3483

The possible oxidation mechanism of this kind of sensitizer comprising a five membered ring in the *meso*-position can be summarised by Scheme 27. There are mainly two pathways including cleavage of the heptamethine resulting in generation of short conjugated structures[39] and formation of the product carrying the double bond in the *meso*-position. This photoproduct appears similar to a fulvene structure. The former produces the nucleophilic products which would inhibit cationic polymerization of epoxides because the chain growth in cationic polymerization of epoxides bases on the carbocation, which could be terminated by nucleophilic compounds. The latter prefers to generate the fulvene structure showing lower nucleophilicity as concluded from similar structures derived from hepta-

methine cyanines[86, 268]. As a consequent step, oxidation of the sensitizer resulting in **S4\_ref** results in elimination of hydrogen from the pentacyclic moiety which responsibly contributes to formation of conjugate acid. This may explain the efficient initiation of the cationic polymerization of epoxides in the case of such an initiating system. For comparison, the respective six-membered ring cyanine **S15** exhibited only bleaching and no reactivity in cationic polymerization of epoxides (see Figure. 20).



**Scheme 27.** The oxidation pathways of the cyanine carrying cyclopentene in *meso*-position: path a) [86] oxidised by MnO<sub>2</sub> following the general redox reaction; or path b) oxide by iodonium salts following the photochemical redox reaction. The latter competitively causes formation of the photoproduct with fulvene pattern or bond cleavage of the polymethine chain, published in [96].

In conclusion, the high-power LED prototype facilitated more heptamethine based cyanines to sensitise the iodonium salt decomposition to initiate free radical polymerization, which would help to broaden the NIR photoinitiator systems for NIR photopolymerization. This definitely promotes further development of NIR photopolymerization. Moreover, the cationic photopolymerization of epoxides was found with this high power NIR LED, which would extend the application fields of NIR photopolymerization. This may include the electronic sector as well where patterning of printed circuit boards (PCBs) can be seen as a big challenge. In brief, this part of work approved that the new high power NIR LED opened new opportunities for NIR photopolymerization in practical applications.

**Table 9.** Properties of the sensitizers (**S1-S24**) used in this subchapter, published in [96]. More details in Section 4.1.1, 4.1.3, and 4.1.4 explain the experimental conditions.

Commercial name	Name in thesis	$\lambda_{\max}$ (nm) <sup>a</sup>	$\epsilon_{\max}$ (M <sup>-1</sup> ·cm <sup>-1</sup> )	$\Phi_f$ a)	$E_{ox}$ (V) <sup>b</sup>	$E_{red}$ (V) <sup>b</sup>	Bleach. rate (%/min) <sup>c</sup>	$x_{\infty}$ d)	Ti (°C) e)
S0322	S1	777	3.58·10 <sup>5</sup>	f)	0.40	-0.80	30	0.74	88
S0979	S2	784	3.58·10 <sup>5</sup>	0.15	0.40	-0.80	30	0.74	88
S0337	S3	773	1.94·10 <sup>5</sup>	0.10	0.65	-0.47	94	0.50	94
S2025	S4	792	2.41·10 <sup>5</sup>	g)	0.57	-0.60	98	0.51	100
S2140	S5	794	3.65·10 <sup>5</sup>	0.14	0.57	-0.60	91	h)	h)
S2163	S6	796	1.63·10 <sup>5</sup>	0.11	0.57	-0.60	89	0.88	114
S2459	S7	778	2.62·10 <sup>5</sup>	0.10	0.41	-0.86	97	0.50	87
S2395	S8	764	3.15·10 <sup>5</sup>	i)	0.47	-0.81	2	0.21	88
S0507	S9	799	2.08·10 <sup>5</sup>	0.06	0.69	-0.34	82	0.74	91
S2383	S10	813	1.62·10 <sup>5</sup>	j)	j)	j)	26	0.88	87
S2389	S11	807	2.40·10 <sup>5</sup>	j)	j)	j)	76	0.88	96
S2391	S12	809	2.13·10 <sup>5</sup>	j)	j)	j)	76	0.92	87
S0750	S13	787	2.04·10 <sup>5</sup>	0.07	0.75	-0.49	91	0.82	95
S2024	S14	793	2.60·10 <sup>5</sup>	0.07	0.60	-0.60	87	0.91	78
S0253	S15	775	2.18·10 <sup>5</sup>	0.07	0.68	-0.50	86	0.58	106
S2326	S16	785	2.86·10 <sup>5</sup>	0.19	0.67	-0.51	77	0.91	97
S0325	S17	812	3.17·10 <sup>5</sup>	0.13	0.42	-0.87	95	0.75	83
S2265	S18	791	3.03·10 <sup>5</sup>	0.13	0.48	-0.97	91	0.66	83
S2283	S19	796	8.15·10 <sup>5</sup>	k)	0.48	-0.97	28	0.37	85
S2344	S20	793	2.88·10 <sup>5</sup>	0.16	0.42	-0.97	59	0.39	88
S2468	S21	844	2.39·10 <sup>5</sup>	l)	0.56	-0.56	75	0.51	103
S0821	S22	800	1.35·10 <sup>5</sup>	0.02	0.80	-0.59	65	<0.01	127
S2457	S23	753	4.63·10 <sup>5</sup>	-	0.67	-0.32	33	<0.01	126
S0772	S24	858	2.09·10 <sup>5</sup>	-	0.73	-0.27	22	<0.01	129

a)in methanol, b)in acetonitrile, c)after photopolymerization and dissolving in methanol, d)conversion of photopolymerization of **TPGDA** using **IS1** after 2minutes NIR-LED irradiation, e)onset temperature of the polymerization of **TPGDA**, f)not determined because of structural similarity with **S2**, g)not determined because to structural similarity with **S5**, h)not determined because to structural similarity with **S4**, i)not determined because of structural similarity with barbital comprising sensitizers, j)not determined because of structural similarity with **S9**, k)not determined because of structural similarity with **S18**, l)not determined because of structural similarity with **S9-S12**.



## 5.2 High-Power NIR LED Photoinduced Cationic and Radical/Cationic Hybrid Polymerization Using the Combination of Heptamethine Cyanine and Iodonium Salt as the Initiating System

Some of the results discussed in this subchapter were previously published[115]. As aforementioned disclosed in Section 5.1, the cyanine with the pentacyclic pattern in the *meso*-position (see pattern 1, Chart 14) in combination with **IS2** can initiate the polymerization of epoxides[96]. Because the pentacyclic moiety in the centre of the heptamethine favours to generate the fulvene pattern, which mostly prevents bond cleavage of the polymethine chain resulting in generation of nucleophilic products. This occurred in the case of a six-membered ring compound that typically inhibit cationic polymerization[39, 96]. Another pattern, that is 1', exhibits a longer wavelength absorption because of the benzo[e]indolium group at the terminal positions of the heptamethine chain. Thus, the extension of the conjugated pattern at the indolium moiety from **1** to **1'** (Chart 15) also facilitates absorption to a bathochromic shift, which results therefore in easier access to 850-870 nm NIR-emitters, which are more easily available to setup NIR LED devices with high power and high capability to expose large areas (see Table.10). It was proved to have a similar feature as **1** to initiate cationic polymerization of epoxy monomers in combination with iodonium salts[115].

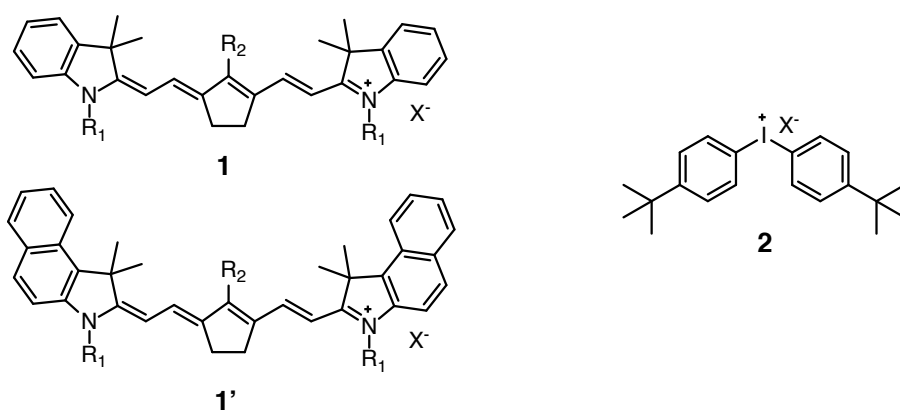


**Chart 16.** Chemical structure of the NIR sensitizers **1**, **1'** and iodonium salts **2** used in this part of work (the structures of the anion X<sup>-</sup> are shown in Chart 17), published in [115].

As aforementioned noticed, the excited state of NIR sensitizer **Sens\*** transfers its electron to iodonium cation (see Chart 16, pattern 2) by PET reaction with an internal activation barrier[35, 39, 46-47, 56, 96]. **1/1'** and **2** should carry same or similar anions X<sup>-</sup> to avoid anion exchange[33]. Thus, we tried to have always the same or similar anion in both the

cationic sensitizer structure and iodonium salt to prevent ion-exchange, which causes less sensitivity of the photoactive materials[33, 86].

Therefore, selection of the anion requests more attention to avoid the appearing anion exchange. Chart 17 shows the anions that were applied in this thesis. These anions comprised in cyanine or iodonium salt were selected from the group of weakly coordinating anions[257] (WCAs) except anion  $[\text{TsO}]^-$  which was used to explore its influence on the overall efficiency of polymerization because the corresponding sensitizer exhibits a low molecular weight resulting in a low mass concentration at the same mole concentration condition. A further motivation to use these anions bases on the fact that hexafluorophosphates  $[\text{PF}_6]^-$  can release toxic HF resulting in environmental and hazardous issues[46]. Therefore, the aluminate anion  $[\text{Al}(\text{O}-t\text{-C}_4\text{F}_9)_4]^-$  and the FAP anion  $[\text{PF}_3(\text{C}_2\text{F}_5)_3]^-$  were introduced as alternative to  $[\text{PF}_6]^-$ [63, 269-270]. From the above views, the following combinations of initiators comprising the sensitizer and the iodonium salt were chosen; that are **S5/IS2 (1a/2a)**, **S26/IS3 (1'b/2b)**, **S26/IS4 (1'b/2c)**, **S27/IS5 (1d/2d)**, **S27/IS6 (1d/2e)** where both the sensitizer and the iodonium salt carry the anion with same or similar structures to avoid anion exchange. WCAs also facilitate good dissociation of the individual ion resulting in higher reactivity[48]. This can be seen as a prerequisite to initiate cationic polymerization. NIR sensitizers used in this section are **S25-S28** as shown in Table 1. Herein, the anion  $[\text{PF}_3(n\text{-C}_4\text{F}_9)_3]^-$  was introduced with an expectation to improve the properties of  $[\text{PF}_3(\text{C}_2\text{F}_5)_3]^-$  because the former comprised an extended fluorinated alkyl group, which helps to minimise the interactions between nucleophilic centers of the anion with growing cationic species. Furthermore,  $[\text{Al}(\text{O}(\text{C}_3\text{F}_6)\text{CH}_3)_4]^-$  was introduced to study the influence of the  $\text{CF}_3$  and  $\text{CH}_3$  on the reactivity of the iodonium salt. Moreover, the anion  $[\text{C}(\text{O}-\text{SO}_2\text{CF}_3)_3]^-$  was used to extend the knowledge in this field by using the combination **S27/IS7** while another combination of **S25 /IS5** was chosen to study whether  $[\text{TsO}]^-$  can function as an affordable anion as an alternative to achieve acceptable reactivity. For a sake to keep further discussion simply, the iodonium structure relates to that in Chart 16 while Chart 17 depicts the respective anions.

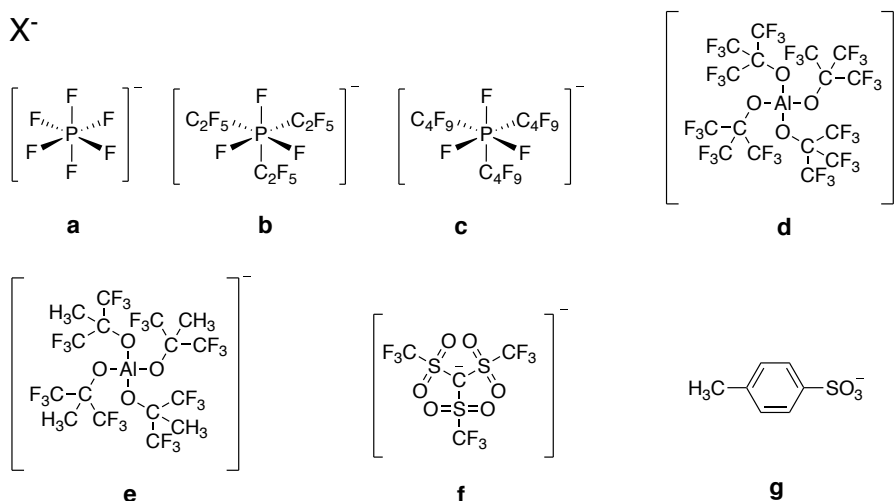


**Chart 17.** Structures of ion  $X^-$  serving as counter ions for sensitizers, and iodonium salts used in this part of work. **a:**  $[PF_6]^-$ , **b:**  $[PF_3(C_2F_5)_3]^-$ , **c:**  $[PF_3(n-C_4F_9)_3]^-$ , **d:**  $[Al(O-t-C_4F_9)_4]^-$ , **e:**  $[Al(O(C_3F_6)CH_3)_4]^-$ , **f:**  $[C(O-SO_2CF_3)_3]^-$ , **g:**  $[TsO]^-$ , published in [115].

**Table 10.** Summary of NIR sensitizers used in this part of work and their respective absorption in **OXT-03** taken at 23°C, **a:**  $[PF_6]^-$ , **b:**  $[PF_3(C_2F_5)_3]^-$ , **d:**  $[Al(O-t-C_4F_9)_4]^-$ , **g:**  $[TsO]^-$ . More details in Section 4.2.8 explain the experimental conditions.

Sensitiser	Struture	Anion	R <sub>1</sub>	R <sub>2</sub>	$\lambda_{max}$ (nm)
<b>S5</b>	<b>1</b>	<b>a</b>	<i>n</i> -C <sub>4</sub> H <sub>9</sub>	N(Ph) <sub>2</sub>	805
<b>S27</b>	<b>1</b>	<b>d</b>	<i>n</i> -C <sub>4</sub> H <sub>9</sub>	N(Ph) <sub>2</sub>	805
<b>S25</b>	<b>1</b>	<b>g</b>	<i>n</i> -C <sub>4</sub> H <sub>9</sub>	Ph	799
<b>S26</b>	<b>1'</b>	<b>b</b>	CH <sub>3</sub>	N(Ph) <sub>2</sub>	849

The monomers used in this section are shown in Table 5. Herein, **TMPTA** was used as monomer for radical polymerization to form interpenetration polymer networks (IPNs) in the hybrid radical/cationic polymerization. Epoxy monomers (**ERL-4211**, **Epoxide 357**), Oxetane (**OXT-03**), and vinyl ether (**HBVE**) were used as cationic monomers to extend the application of the NIR initiating system comprising heptamethine and iodonium salt. Combination of radical and cationic monomers may form interpenetrating polymer networks (IPNs) if both type of cross-linked polymers form one phase. This does not appear so easy because some systems may show phase separation[271-272]. Generally, radical polymerization reacts faster than cationic polymerization[273]. The formation of IPNs according to the cationic mechanism can proceed because propagation of the growing chains through the already network formed by radical polymerization might occur significantly slower. Thus, additional activation is necessary to receive the IPNs successfully. To our best knowledge, the heat released by heptamethine based cyanine NIR sensitizers

can offer additional thermal energy to facilitate the formation of IPNs. Therefore, the NIR photopolymerization system exhibits competitive properties to synthesis of IPNs by generating heat as additional energy, to generate radicals for initiation of free radical polymerization, and to generate conjugate acid for initiation of cationic polymerization[37].

Oxetanes were selected to compare their polymerization properties with oxiranes. The conjugate acid exhibits significant influence on the chain growth of oxiranes which exhibit less tolerance towards nucleophiles[103]. Oxetanes prefer to grow the polymer chain by the oxetanium ion[99-100, 113, 263, 274-275] exhibiting more tolerance in the presence of some nucleophiles carrying functional groups such as alcohols or carboxylic acid. Thus, oxetanes can get more attention in some microelectronic applications because they exhibit more tolerance to the surroundings compared to oxiranes[114, 276-279]. As we know, oxiranes respond more sensitively towards humidity in the surrounding.

Previous investigations revealed that the conductivity of the iodonium salt possesses an important function to generate reactive species like radicals in NIR photopolymerization [46, 48]. It also disclosed that the better dissociation of the respective ions connects with higher reactivity of the iodonium salt while non-conducting ion pairs did not exhibit reactivity[46, 48]. However, a model quantitatively depicting the relation between the reactivity and the ion dissociation has not been successfully established in photochemical reactions occurring in organic surroundings yet[46, 48]. It has been employed as a compromise to explain the relations of structure-reactivity in different operational surroundings. As shown in Table 11, there exists a rough inverse relation between the relation of conductivity and viscosity but it could not fit the quantitative evaluation of data in the Walden-Plot[280] because of the complexity of such systems.

Furthermore, the ion conductivity of iodonium salts in the oxetane **OXT-03** was studied to indicate the relation between ion size and conductivity. Surprisingly, the smaller anion  $[\text{PF}_6]^-$  showed the lowest conductivity while the larger ions like  $[\text{Al}(\text{O}-t\text{-C}_4\text{F}_9)_4]^-$  exhibited higher conductivity which is related to the dissociation degree. Generally, only the well solvated and dissociated ion contributes to conductivity of the iodonium salts while ion pairs show no conductivity[46]. The results also exhibit that a slight change of the anion structure makes a significant influence on conductivity. Higher molecular assemblies may affect conductivity. For instance, extension of the fluorinated group in anion  $[\text{PF}_3(\text{C}_2\text{F}_5)_3]^-$  by two  $\text{CF}_2$  groups resulted in anion  $[\text{PF}_3(n\text{-C}_4\text{F}_9)_3]^-$ . It caused a decrease of conductivity although the size of the anion only slightly changed. The similar phenomenon was found by comparison of the anions  $[\text{Al}(\text{O}-t\text{-C}_4\text{F}_9)_4]^-$  and  $[\text{Al}(\text{O}(\text{C}_3\text{F}_6)\text{CH}_3)_4]^-$ . Partial replacement

of four CF<sub>3</sub> groups by four CH<sub>3</sub> groups exhibited significant drop of the conductivity because of the less tendency to form dissociated ions which facilitate better reactivity.

**Table 11.** Viscosity of the monomers used (**ERL-4211**, **HBVE**, **OXT-03**) and selected conductivity data for the respective iodonium salts (**IS**) ( $[IS]=3.8 \times 10^{-2}$  mmol·g<sup>-1</sup>), published in [115]. More details in Section 4.2.6, 4.2.7 explain the experimental conditions.

Monomer		<b>ERL-4211</b>	<b>HBVE</b>	<b>OXT-03</b>
Viscosity (mPa·s)		739	4.4	12.2
Conductivity (S·cm <sup>2</sup> ·mol <sup>-1</sup> )	<b>IS</b>			
	<b>IS2</b>	0.003	0.7	0.05
	<b>IS3</b>			0.28
	<b>IS4</b>			0.08
	<b>IS5</b>			0.61
	<b>IS6</b>			0.11
	<b>IS7</b>			0.29

**HBVE** is a high performance monomer in the photocuring industry, which prefers to polymerize according to cationic mechanism as shown by the data in Figure 22c rather than free radical polymerization, which was approved by dark curing measurement with FTIR measurement[115]. As shown in Figure 22a-c, **HBVE** exhibits the faster reaction rate of cationic polymerization compared with the cycloaliphatic epoxide **ERL-4211** and oxetane **OXT-03** (Figures 22a and 22b) using the same combination of NIR initiator systems and exposure conditions.

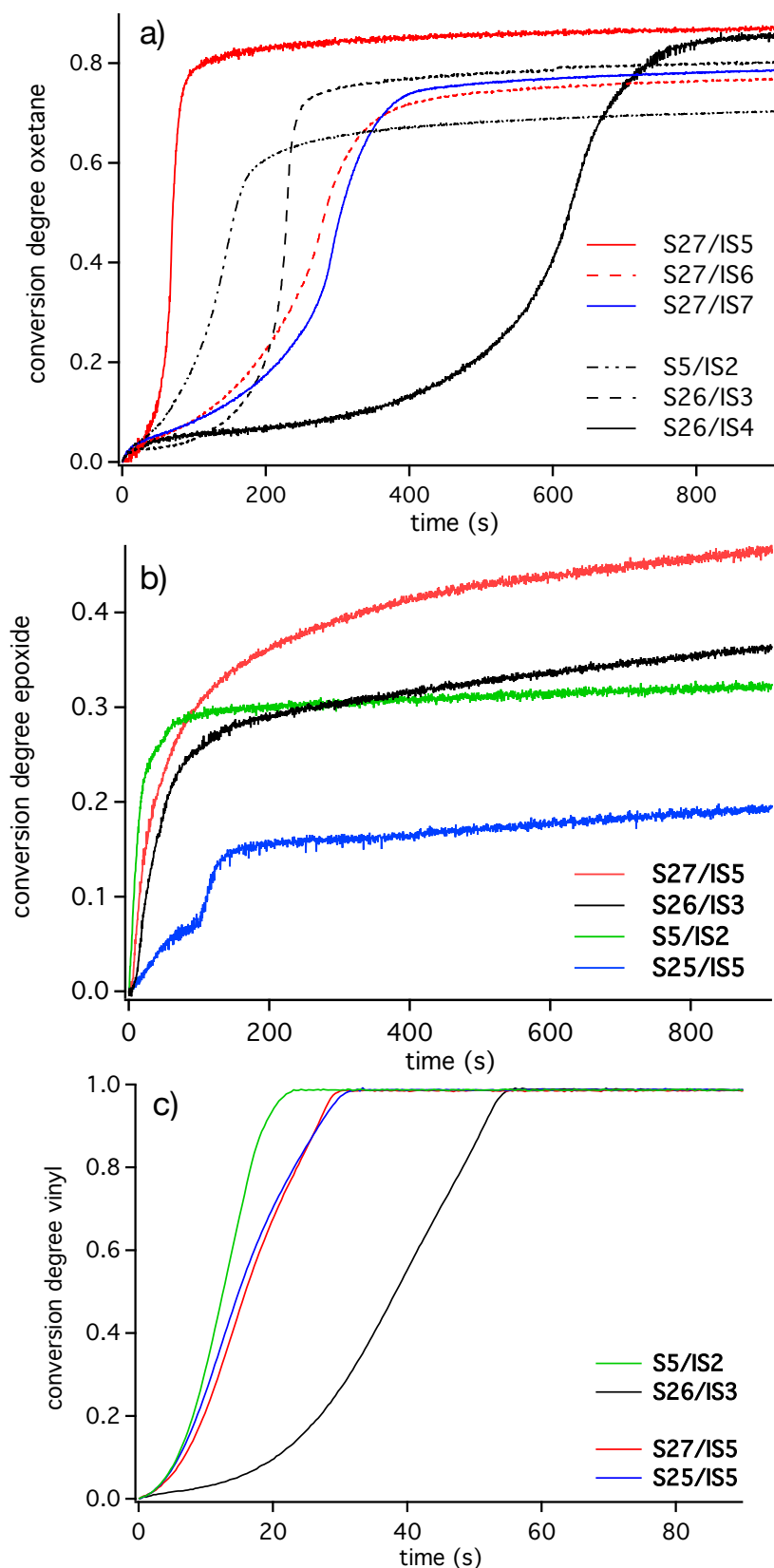


**Figure 22.** RT-FTIR conversion degree-time profiles of cationic polymerisable monomers with different combinations of initiators to study the reactivities of different combinations of **Sens** and **IS** in different cationic monomers, irradiated with 805 nm LED a) **OXT-03**, b) **ERL-4211** c) **HBVE**), published in [115]. More details in Section 4.2.1 explain the experimental conditions.

The combination of the initiator system comprising the aluminate anion  $[\text{Al}(\text{O}-t\text{-C}_4\text{F}_9)_4]^-$  exhibited the best performance in **OXT-03** while the reaction rate was slightly lower compared to  $[\text{PF}_6]^-$  in both the epoxide **ERL-4211** and the oxetane **HBVE**. Unexpectedly, systems comprising the FAP anion  $[\text{PF}_3(\text{C}_2\text{F}_5)_3]^-$  showed less reactivity compared to those comprising  $[\text{Al}(\text{O}-t\text{-C}_4\text{F}_9)_4]^-$  as anion in the iodonium salt. This surprises since the anion  $[\text{PF}_3(\text{C}_2\text{F}_5)_3]^-$  was believed to be an excellent candidate for many applications[269, 281]. Nevertheless, the results in this thesis revealed a different behavior. Moreover, a slight change of  $[\text{PF}_3(\text{C}_2\text{F}_5)_3]^-$  resulting in  $[\text{PF}_3(n\text{-C}_4\text{F}_9)_3]^-$  had significant influence on the reactivity as concluded by comparison of the curves in Figure 22a although the general pattern of this phosphate appears similar. These differences observed were not obviously found in Figure 22b while it exhibited similar tendency as shown in Figures 22a and 22c. Similar results were also obtained with iodonium salts comprising either the anion  $[\text{Al}(\text{O}-t\text{-C}_4\text{F}_9)_4]^-$  or  $[\text{Al}(\text{O}(\text{C}_3\text{F}_6)\text{CH}_3)_4]^-$ . Moreover, a slight change to an anion with lower molecular weight with the goal to decrease the loading with initiating system components while the molar amount remained the same caused a huge change of reactivity by comparison of the curves obtained in the case of **S27/IS5** and **S27/IS6**.

Furthermore, sensitizer **S25** comprising the more nucleophilic anion  $[\text{TsO}]^-$  also exhibited acceptable performance, see Figure 22c. Because of the high extinction coefficient of the cyanine sensitizer, the concentration of this anion is too low to make the system non-reactive. Comparison of Figure 22b and 22c shows that we can draw conclusions of the influence of the nucleophilic anions on the overall polymerization efficiency depending on the monomers used as well.

The electrostatic potentials calculated after geometry optimization based on density functional theory (B3LYP functional; 6-31G\*+ level) might depict one possible interpretation to understand more in detail the differences observed with respect to the polymerization efficiency, see Figure 23[115]. By definition, red colour corresponds to negative partial charges while blue color indicates positive charged areas[282]. While all  $\text{CF}_3$  groups shield well the partial negative charges of  $[\text{Al}(\text{O}-t\text{-C}_4\text{F}_9)_4]^-$ , there exhibits significant difference in comparison with  $[\text{Al}(\text{O}(\text{C}_3\text{F}_6)\text{CH}_3)_4]^-$ . These differences might be one additional reason resulting in different properties such as conductivity and reactivity. However, the electrostatic potential could not explain the different reactivities observed in the case of **IS** comprising either  $[\text{PF}_6]^-$ ,  $[\text{PF}_3(\text{C}_2\text{F}_5)_3]^-$  or  $[\text{PF}_3(n\text{-C}_4\text{F}_9)_3]^-$ . Nevertheless, the data depicts

the volume and surface in the case of  $[\text{Al}(\text{O}-t\text{-C}_4\text{F}_9)_4]^-$ . Surprisingly, a slight change in the structure of  $[\text{Al}(\text{O}-t\text{-C}_4\text{F}_9)_4]^-$  resulting  $[\text{Al}(\text{O}(\text{C}_3\text{F}_6)\text{CH}_3)_4]^-$  had a significant impact on their reactivity. Shielding of the negative charge exhibits more efficient dissociation in the case of  $[\text{Al}(\text{O}-t\text{-C}_4\text{F}_9)_4]^-$  in comparison with  $[\text{Al}(\text{O}(\text{C}_3\text{F}_6)\text{CH}_3)_4]^-$  in cationic polymerization. These calculations were pursued by our coauthor of reference[115].

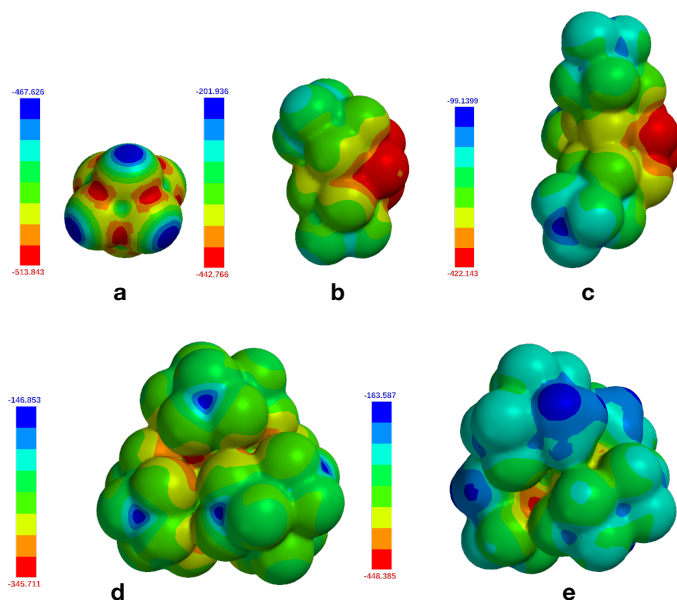


**Figure 23.** Electrostatic potential surface of the anions. **a:**  $[\text{PF}_6]^-$ , **b:**  $[\text{PF}_3(\text{C}_2\text{F}_5)_3]^-$ , **c:**  $[\text{PF}_3(n\text{-C}_4\text{F}_9)_3]^-$ , **d:**  $[\text{Al}(\text{O}-t\text{-C}_4\text{F}_9)_4]^-$ , **e:**  $[\text{Al}(\text{O}(\text{C}_3\text{F}_6)\text{CH}_3)_4]^-$ , **f:**  $[\text{C}(\text{O}-\text{SO}_2\text{CF}_3)_3]^-$ , **g:**  $[\text{TsO}]^-$ . Calculation results base on density functional theory based of B3LYP/6-31G\* method. Results obtained regarding the volume and surface are as follows: a: 84 Å<sup>3</sup>, b: 259 Å<sup>3</sup>, c: 433 Å<sup>3</sup>, d: 582 Å<sup>3</sup>, e: 501 Å<sup>3</sup>, published in [115].

These results depicted huge reactivity changes by the combination of initiator components by slight changes of structural features. Generally, it indicated that **IS5 (2d)** was the best coinitorator for all systems comparing both polymerization rate at the beginning and final conversion. It shows surprisingly outstanding performance compared to the system based on  $[\text{PF}_3(\text{C}_2\text{F}_5)_3]^-$ , which was believed as one of the best anion in iodonium salts[41]. **S27/IS5 (1d/2d)** depicted excellent reactivity in epoxides (**ERL-4211**, **Epikote 357**), vinyl ether (**HBVE**), and oxetanes (**OXT-03**), see Figure 22. On the other hand, quantification measurement of conjugate acid generated from the combinations of NIR initiator system upon NIR LED exposure exhibited a concentration of 10<sup>-5</sup> M after 5min exposure with 805nm NIR LED in lauryl methacrylate (**LMA**) and BuAc as probed by **RhB-L**. Herein, **LMA** was used as solvent carrying some features of radical polymerisable monomers with lower polarity and viscosity. It can better consume the radicals generated from the initiating system upon irradiation according to a radical polymerization mechanism, which could promote the PET reaction to proceed fast, see Scheme 14 in Section 2.3.1. Therefore, as depicted



in Table 12, the initiating system comprising sensitizer and iodonium salt in **LMA** generated more conjugate acid compared to the general solvent BuAc at the same exposure conditions. Moreover, the monomer can promote cationic polymerization in this system because it can facilitate the generation of conjugate acid and prevents consecutive reactions leading to bond cleavage causing formation of nucleophilic products. Table 12 also depicts that with the difference of the anion carried by sensitizers and iodonium salts the quantity of conjugate acid generated from the combination of NIR initiator system. This is different, which responsibly causes the huge reactivity differences depicted in Figure 22.

**Table 12.** Concentration of conjugate acid generated by the NIR initiator systems ([Sens]  $4.1 \times 10^{-5}$  M, [IS]  $5.6 \times 10^{-4}$  M) in **BuAc** or **LMA** under NIR exposure using the **805nm LED** device ( $1.2 \text{ W} \cdot \text{cm}^{-2}$ , 20 minutes), published in [115]. More details in Section 4.2.5 explain the experimental conditions.

Time/ min	$a_{\text{H}^+}$ ( <b>S26/IS3</b> ) in <b>BuAc</b> [M]	$a_{\text{H}^+}$ ( <b>S27/IS5</b> ) in <b>BuAc</b> [M]	$a_{\text{H}^+}$ ( <b>S27/IS5</b> ) in <b>LMA</b> [M]	$a_{\text{H}^+}$ ( <b>S26/IS3</b> ) in <b>LMA</b> [M]
1	$5.0 \cdot 10^{-7}$	$1.3 \cdot 10^{-6}$	$8.7 \cdot 10^{-6}$	$3.8 \cdot 10^{-6}$
5	$5.1 \cdot 10^{-7}$	$3.5 \cdot 10^{-6}$	$3.2 \cdot 10^{-5}$	$1.6 \cdot 10^{-5}$
10	$7.9 \cdot 10^{-6}$	$9.1 \cdot 10^{-6}$	$3.9 \cdot 10^{-5}$	$2.9 \cdot 10^{-5}$
20	$1.9 \cdot 10^{-5}$	$2.2 \cdot 10^{-5}$	$5.0 \cdot 10^{-5}$	$4.5 \cdot 10^{-5}$

Therefore, the combination of initiator system **S27/IS5 (1d/2d)** received outstanding preference for further studies for synthesis of IPNs. Firstly, the hybrid radical/cationic photopolymerization was studied using this pair of initiator combination, where **TMPTA** served as monomer in free radical polymerization while the epoxide **ERL-4211** and the oxetane **OXT-03** functioned as cationic monomer. The results are depicted by Figure 24. **TMPTA** exhibited a faster radical polymerization in the presence of the monomers **ERL-4211** and **OXT-03**. Cationic polymerization typically proceeds slower than radical polymerization [273]. Therefore, the monomer, which is either the oxirane or the oxetane, after adding in **TMPTA** typically a decrease of the  $T_g$  occurred resulting in increase of mobility. It also explains why the polymerization rate of the epoxide in Figure 24a is slower in the mixture consisting of **TMPTA** and **ERL-4211** while it reacts faster in neat **ERL-4211**. The condition becomes more strength in Figure 24b where the oxetane **OXT-03** polymerizes faster in the hybrid radical/cation photopolymerization system. The different cationic polymerization mechanisms of oxirane and oxetane can explain these results (see Scheme 19 and Scheme 20)[99-100, 103]. The huge heat generated by the NIR sensitizers, which is more than 85% with respect of all the absorbed photons, can help to overcome internal activa-

tion barriers and to increase/promote diffusion processes. The latter is necessary for chain growth of the cationic monomers such as oxirane and oxetane in the cross-linking system. As shown in Figure 25, the temperature of the samples comprising NIR sensitizers can easily approach more than 100 °C, which facilitates NIR cationic photopolymerization significantly.

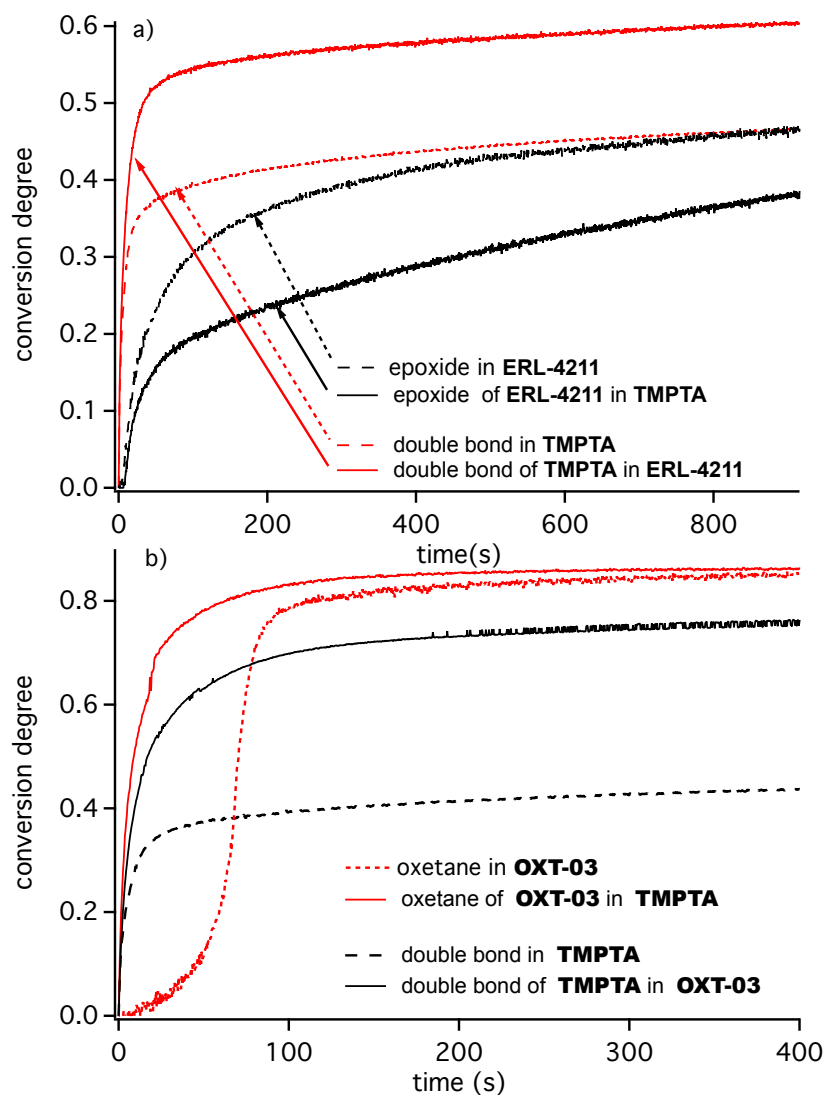


**Figure 24.** RT-FTIR conversion degree-time profiles of the polymerization of **TMPTA** and the polymerization of cationic polymerisable groups comprised in epoxide **ERL-4211** and oxetane **OXT-03**, respectively, published in [115]. More details in Section 4.2.1 explain the experimental conditions.

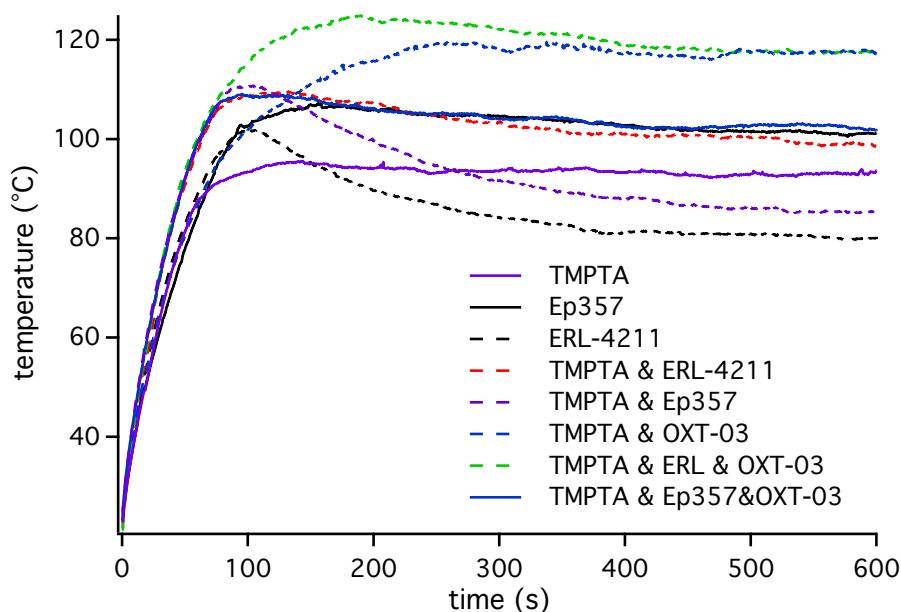


**Figure 25.** The temperature-time profiles of the combination of initiating system **S27/IS5** ( $[S27]=6 \cdot 10^{-3} \text{ mmol} \cdot \text{g}^{-1}$ ,  $[IS5] = 3.8 \cdot 10^{-2} \text{ mmol} \cdot \text{g}^{-1}$ ) in different monomers upon irradiation with 805 nm NIR LED ( $1.2 \text{ W} \cdot \text{cm}^{-2}$ ), published in [115]. More details in Section 4.2.4 explain the experimental conditions.

The different organic surroundings used to operate the experiments also can explain the different reactivities for cationic photopolymerization as shown in Figure 24. The combination of **S27/IS5** generated more conjugate acid in comparison with that of **S26/IS3** applying the same exposure time and same organic surrounding, see Table 12 and Figure 26. The aluminate anion  $[\text{Al}(\text{O}-t\text{-C}_4\text{F}_9)_4]^-$  exhibited more efficient reactivity compared to  $[\text{PF}_3(\text{C}_2\text{F}_5)_3]^-$  confirming previous results [115, 270]. Change the surrounding to **LMA**, which comprises a radical polymerizable vinyl group, caused the increase of the efficiency of conjugate acid generation. The combination of the system comprising  $[\text{Al}(\text{O}-t\text{-C}_4\text{F}_9)_4]^-$  showed better properties compared to that of  $[\text{PF}_3(\text{C}_2\text{F}_5)_3]^-$ . Thus, photo-excitation of the NIR sensitizer **Sens** and reaction of its excited state with the iodonium cation results in formation of  $\text{Sens}^* \cdot \text{M}_{\text{nt}} \text{X}_n^-$ , which would generate radicals and conjugate acid by hydrogen abstraction. **LMA** undertakes the function of a radical scavenger and avoids undesired consecutive side reaction. This can explain the higher rate of conjugate acid formation in the case of systems comprising **LMA** as model monomer than in the solvent BuAc, see Figure 26. These findings can also explain the higher polymerization reactivity of the oxetane group in the mixture of **TMPTA** and **OXT-03** (see Figure 24b). However, the results in epoxides cannot confirm these findings (see Figure 24a). The reaction proceeds slower in epoxides because their cationic polymerization proceeds based on carbocations as aforementioned noticed. On the other hand, conjugate acid prefers protonation of the

oxetane groups resulting in formation of oxetanium as intermediates in cationic polymerization[99].

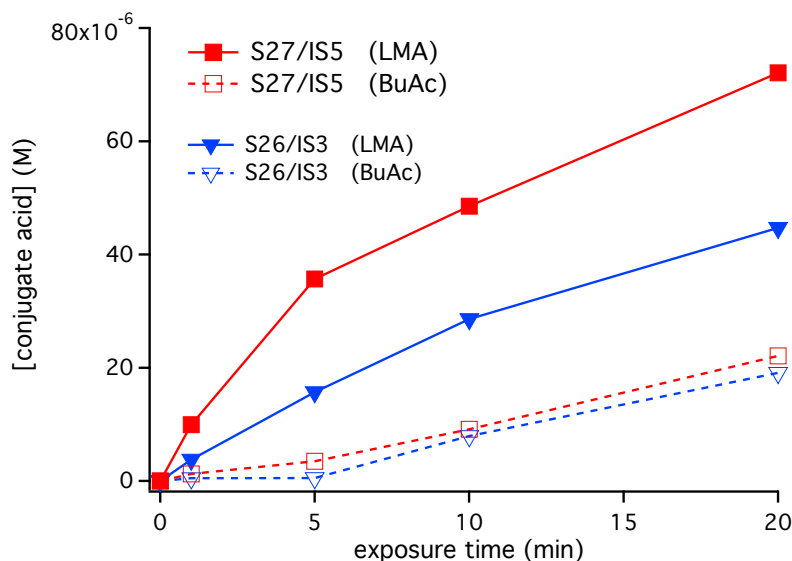


**Figure 26.** Profiles for generation of conjugate acid as a function of exposure time at 805 nm (Intensity:  $1.2 \text{ W}\cdot\text{cm}^{-2}$ ) according to a previous procedure using **RhB-L** to probe quantitatively the amount on acidic species. Measurements were carried out **LMA** and **BuAc** ( $[\text{Sens}] = 4.1 \times 10^{-5} \text{ M}$ ,  $[\text{IS}] = 5.6 \times 10^{-4} \text{ M}$ ), published in [115]. More details in Section 4.2.5 explain the experimental conditions.

Dynamic mechanical analysis (DMA) of the networks synthesized by both UV and NIR sensitized polymerization exhibited different performance (see Figure 27 and Table 13). The maximum of the  $\tan \delta$  curve depicts the glass transition temperature ( $T_g$ ) of the film obtained by photopolymerization. These results exhibit one  $T_g$  occurring at  $113 \text{ }^\circ\text{C}$  upon NIR light exposure while two maxima  $T_g$  were obtained in the case of UV exposure employing the same monomers mixture. The peak at  $86^\circ\text{C}$  corresponds to the radical polymerizable monomer **TMPTA** while the second peak appearing at  $134 \text{ }^\circ\text{C}$  relates to the epoxide **ERL-4211**. However, the neat crosslinked polymer of **TMPTA** and epoxide **ERL-4211** exhibit peak maxima at  $67 \text{ }^\circ\text{C}$  and  $119 \text{ }^\circ\text{C}$ , respectively, proving the formation of two phases in the polymer networks after UV light exposure. The results indicated phase separation during the UV photopolymerization with no IPN formation while NIR sensitized hybrid radical and cationic polymerization facilitated the formation of IPNs as firstly shown in this experiment for this monomer composition[115]. In addition, **TMPTA** itself formed polymer, which broke during the DMA experiment at around  $150 \text{ }^\circ\text{C}$ , see Figure 27 and Table 13.

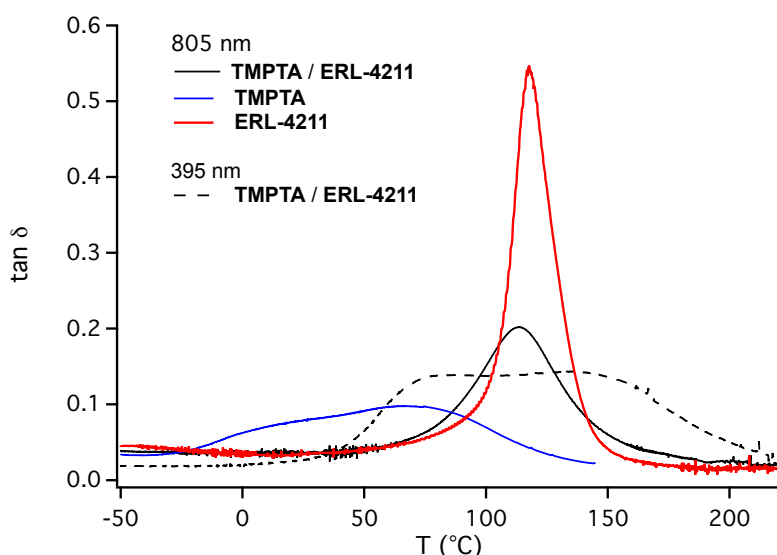


**Figure 27.** DMA data ( $\tan \delta$ ) of films (thickness: 120  $\mu\text{m}$ ) exposed using 395 nm LED (1.1  $\text{W}\cdot\text{cm}^{-2}$ , 2 min) and 805 nm LED (1.2  $\text{W}\cdot\text{cm}^{-2}$ , 10 min) in the case of the monomers **TMPTA**, **ERL-4211**, and the mixture of **TMPTA** and **ERL** (**TMPTA / ERL-4211**, 1:1), published in [115]. More details in Section 4.2.3 explain the experimental conditions.

Table 13 shows the data obtained from DMA measurements comprising different monomer mixtures applied for polymerization. The table also depicts the storage modulus  $E'$  for different polymers relaxed at least 40 K above the corresponding glass transition. This quantity can roughly relate to the network density if it is fully relaxed. The size of the storage modulus relate to the network density[115]. This was applicable for some systems comprising epoxides[116]. However, the system comprising oxetane (**OXE-03**) exhibited different performance. Both of the storage modulus and the  $\tan\delta$  indicated that the system was not completely relaxed at 250 °C. Since this range of temperature appeared quite large, the experiment was not continued at much higher temperatures because any available data obtained would not reliably relate to network density.[115]

The cationic heptamethine based cyanines carrying five membered ring at *meso*-position exhibited outstanding reactivity in combination with iodonium salts to initiate the cationic and hybrid free radical and cationic polymerization with high-intensity NIR LEDs emitting at 805 nm and 870 nm[115]. The influence of the anions to the reactivity was studied. The results showed that the anion  $[\text{Al}(\text{O}-t\text{-C}_4\text{F}_9)_4]^-$  carrying optimal shielding of nucleophilic moieties and large anion radius exhibited the best performance as observed by RT-FTIR spectroscopy, see Figure 23. This will offer new impetus to design outstanding systems in the future showing that the anion undertakes a special function. The fact that the heat released by the NIR sensitizer makes such systems interesting for future development in material research while UV-LED based initiation failed in some cases to form IPNs[115].

The heat generated by non-radiative processes of the sensitizers undertakes a special function in these NIR photopolymerization systems since it facilitated successful formation of IPNs while UV exposure led to the phase separation between the cross-linked acrylate and epoxide. However, oxetane **OXE-03** showed no successful formation of IPNs. Therefore, phase separation still controls the morphology and the mechanical properties of such systems as well.

Table 13. Summary of DMA-data ( $T_g$ : glass transition temperature in °C where  $\tan\delta$  appeared,  $E'$ : storage modulus in MPa) obtained after exposure of 2 min with 395 nm LED ( $1.1 \text{ W}\cdot\text{cm}^{-2}$ ) and 10 min with 805 nm LED ( $1.2 \text{ W}\cdot\text{cm}^{-2}$ ) while the conversion at this time  $x_\infty$  was determined for the monomer polymerising according to a cationic polymerization mechanism (cat) and/or radical polymerization mechanism (rad), published in [115]. More details in Section 4.2.3 explain the experimental conditions.

Monomer (wt %)				805 nm exposure					395 nm exposure				
TMP TA	ERL- 4211	Epik ote 357	OXE -03	$x_\infty$ (cat)	$x_\infty$ (rad)	$\tan \delta_{\max}$	$T_g$	$E'$	$x_\infty$ (cat)	$x_\infty$ (rad)	$\tan \delta_{\max}$	$T_g$	$E'$
100					0.51	0.099	67	a)					
	100			0.96		0.55	119	7					
		100		0.75		0.32	139	57					
			100	0.91		0.067 0.030	77 194	b)	0.96		0.084	96 175 <sup>c)</sup>	
50	50			0.81	0.75	0.20	113	63	0.89	0.90	0.13 0.14	86 <sup>d)</sup> 134 <sup>d)</sup>	60
50		50		0.78	0.47	0.23	103	178					
50			50	0.60	0.69	0.048	91 177 <sup>c)</sup>	b)	0.95	0.86	0.059	91 154 <sup>c)</sup> 183 <sup>c)</sup>	b)
40	30		30	0.67/ 0.75	0.75	0.079	131	b)					
40		30	30	0.81/ 0.52	0.67	0.093	131 220 <sup>c)</sup>	b)					

a) film broken date abatable; b) curve was not fully relaxed.

### 5.3 High Power NIR LED Photoinduced Free Radical Polymerization (II): the Combination of Heptamethine Based Cyanine and Oxime Ester Serving as Initiating System

Some of the results discussed in this subchapter were previously published[118].

The original intention of this study was to introduce more co-initiators as alternatives to iodonium salts used in the NIR photopolymerization. Iodonium salts depict from an economic point an affordable option but they do not belong to cheap raw materials. The NIR-sensitized decomposition of oxime esters, which results in free radical photopolymerization, moved into the focus to sensitise the decomposition of these materials applying NIR radiation based on the knowledge grown in the previous chapters. Surprisingly, new high-power NIR LEDs emitting at 805 nm, 860 nm, and 870 nm also facilitated the decomposition of oxime esters in combination with heptamethine cyanine[118]. Thus, the model discussed based on internal barriers in PETs might be important for these considerations as well. The question also arises whether decomposition of the oxime ester follows an entire photonic mechanism or thermal decomposition mechanism. Cyanines with different structural patterns were chosen to explore whether the PET reaction leads to bond cleavage or not[37, 86, 96].

The chemical structures of the oxime esters used in this thesis are depicted in Table 3. **OXE-01** and **OXE-02** are two typical commercialised oxime ester photoinitiators, while **COXE-15**[250] and **BTCF-OXE**[249] are new oxime esters synthesised in lab. **COXE-15** carries a coumarin as chromophore group resulting in hypsochromic shifted wavelength absorption compared to alternative coumarins[28]. Furthermore, **BTCF-OXE** comprises a thiophene motif resulting in a comparable reactivity and improved thermal stability compared to the commercial photoinitiators **OXE-01** and **OXE-02**. Thermal stability measurement of **BTCF-OXE** in tri(propylene glycol)diacrylate (**TPGDA**) indicated an increase of the thermal initiation temperature,  $T_i$  (Table 13). In other words, this compound can overcome the shelf life issue reported for previous oxime esters investigated[28, 67, 248, 250]. The  $T_i$  of **TPGDA** was below 70 °C taking photoinitiators of **OXE-01** and **OXE-02** while it slightly increased in the case of **COXE-15**. Surprisingly,  $T_i$  of **TPGDA** increased significantly in the case of **BTCF-OXE** comprising thiophene moiety, where the  $T_i$  is close to that of neat **TPGDA** which appeared around 190 °C [47]. Therefore, the thermal stability of the oxime esters investigated in the monomer **TPGDA** follows this order: **BTCF-OXE** » **COE-15** > **OXE-1** > **OXE-2**[118].

Unexpectedly, the DSC measurement showed a significant improved thermal stability after addition of sensitizer to the samples comprising oxime ester **OXE-01** and the monomer **TPGDA**. The  $T_i$  of **TPGDA** increased in general of around 50 °C after addition of the NIR sensitizers **S10**, **S24**, or **S28** while **S4**, **S7**, **S26**, **S21**, or **S18** caused a smaller increase, structure of these sensitizers, see Table 1. Nevertheless, the thermal stability increased after adding the NIR sensitizer figuring out that the thermal instability of oxime ester might be the only reason to result in the reactivity observed under NIR exposure. Herein, the cyanine **S24**, carrying no bridged pattern, was used as reference. It exhibited the best stability in combination with **OXE-01** but less reactivity. On the other hand, initiator of NIR sensitizer and iodonium salt showed a decrease of the initiation temperature ( $T_i$ ) for thermal decomposition.[47, 115] Overall the  $T_i$  data of the **TPGDA** comprising the combination of NIR initiator systems are summarised in Table 13.

The results of photo-DSC measurement showed that the four oxime esters used in this thesis can initiate polymerization of **TPGDA** applying 395 nm LED exposure (Figure 28). Moreover, **OXE-01**, **OXE-02**, and **COXE-15** resulted in a final the conversion ( $x_\infty$ ) of **TPGDA** approaching to 70%, while the **BTCF-OXE** exhibited a better final conversion near 80% although its reaction rate was lower than the other three photoinitiators. Thus, the lower reactivity, which may be caused by the better thermal stability, resulted in a higher overall final monomer conversion because of higher selectivity.

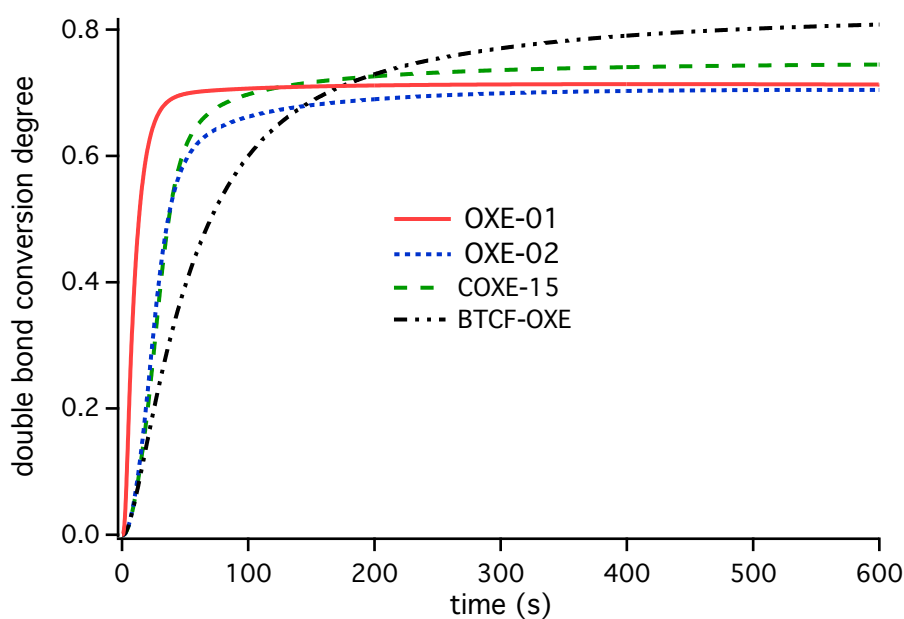


**Figure 28.** The photo-DSC conversion–time profiles of the polymerization of **TPGDA** comprising different oxime esters (0.05 wt%) applying a 395 nm UV LED (0.1 W·cm<sup>-2</sup>) with Photo-DSC, published in [118]. More details in Section 4.3.1 explain the experimental conditions.



The  $T_i$  of **TPGDA** respectively comprising **OXE-01**, **OXE-02** and **COXE-15** was below 80°C, which brings the view that the heat released by sensitizers decomposed the oxime esters to generate reactive radicals in the combination of NIR initiating systems. Therefore, the cyanine **S28** (see Table 1), which nearly quantitatively generates heat upon exposure with a line-shaped focused laser emitting at 980 nm[7, 45, 47], was applied in combination with **OXE-01** to approve the above hypothesis. Actually, **S28** in combination with 980nm laser was successfully applied to initiate NIR light induced melting of powder coatings[50] and to initiate the reaction of blocked isocyanates[45]. However, there was no polymerization of **TPGDA** observed in this experiment using the combination of **S28** and **OXE-01** although the temperature of the sample increased up to 170 °C as monitored by a thermal sensitive camera[118]. This high temperature did not cause thermal initiation of polymerization of **TPGDA** comprising **S28** and **OXE-01**. Thus, the assumption that the heat is the main reason to cause the decomposing of **OXE-01** to initiate **TPGDA** polymerization was not approved. The combination of initiator systems comprising heptamethine based cyanines and oxime esters should mainly work based on PET with internal barriers. Therefore, the cyanines **S4**, **S7**, **S10**, **S18**, **S21**, **S24**, **S26**, and **S28** were selected to study their reactivity with oxime esters serving as coinitiators[118].

The PET free reaction enthalpy of the combination of these cyanines and **OXE-01**,  $\Delta G_{PET}$ , yields a slight positive value which means this relates to an endothermic scenario needing additional activation energy for initiation reaction[160-161]. ( $\Delta G_{PET}$  in eV: **S18** = 0.17; **S4** = 0.27; **S26** =0.4). These energetic conditions give such systems a certain inner threshold which can exceed several dozen  $\text{kJ} \cdot \text{mol}^{-1}$  while PET can still proceed[96]. This combination of NIR initiator system only exhibits reactivity in combination with a strong light source to generate reactive radicals for polymerization explaining their application in graphic industry with a 830nm lasers[32, 34-35]. In this thesis, the high power LED devices emitting at 805 nm, 860 nm, and 870 nm result in efficient generation of the excited state of the sensitizer whose non-irradiative deactivation releases sufficient amount of heat. This helps the system to overcome the internal activation barrier  $\Delta G_{PET}^\ddagger$ . More details can be seen in Figure 17 in Section 5.1. It approved again that these systems only worked with strong emissive sources. The real time-FTIR (RT-FTIR) measurements of the sample comprising **S18** (0.05 wt%), **OXE-01** (2 wt% ) and **TPGDA** were carried out applying both a high-intensity LED and low power LED. The results showed that the low-power LED did not induce photopolymerization compared to high-power LED (see Figure 29).

[118]

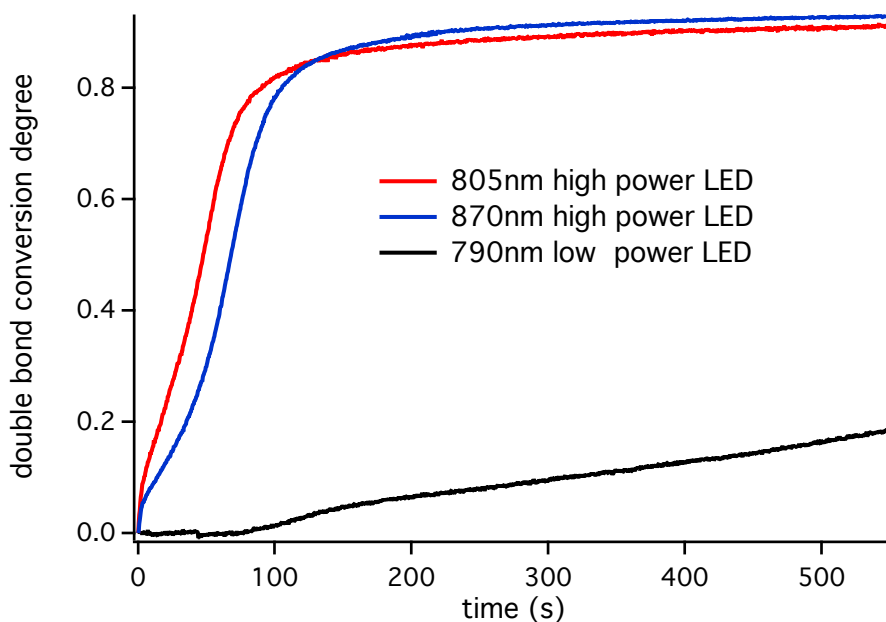


**Figure 29.** Radical photopolymerization of **TPGDA** comprising **S18** (0.05 wt%) and the **OXE-01** (2 wt%) using different power NIR LEDs, published in [118]. More details in Section 4.3.2 explain the experimental conditions.

The temperature of the sample was measured by a thermal sensitive camera. The results showed that the temperature increased to more than 100 °C upon exposure with the high-intensity LED. As shown in Figure 30, the thermal equilibrium is observed between the surroundings and the glass substrate between 100 and 110 °C although it depended on the concentration of the sensitizer (Figure 30). Changing the 805 nm LED device to 860 nm LED caused a slight difference in the pattern. At this emitting wavelength, the sensitizers exhibit a lower absorption which could facilitate the excitation light to penetrate deeper into the samples based on Lambert Beer's law resulting in reaction with the oxime ester that caused loss of absorption. This point of view can explain the decrease of the temperature in the case of **S18**. A photochemical reaction connected with bleaching of the sensitizers causes the consumption of corresponding sensitizer molecules. The higher the concentration of the excited sensitizer molecules in the respective excitation volume, the higher the temperature observed (see Figure 30c)[118].

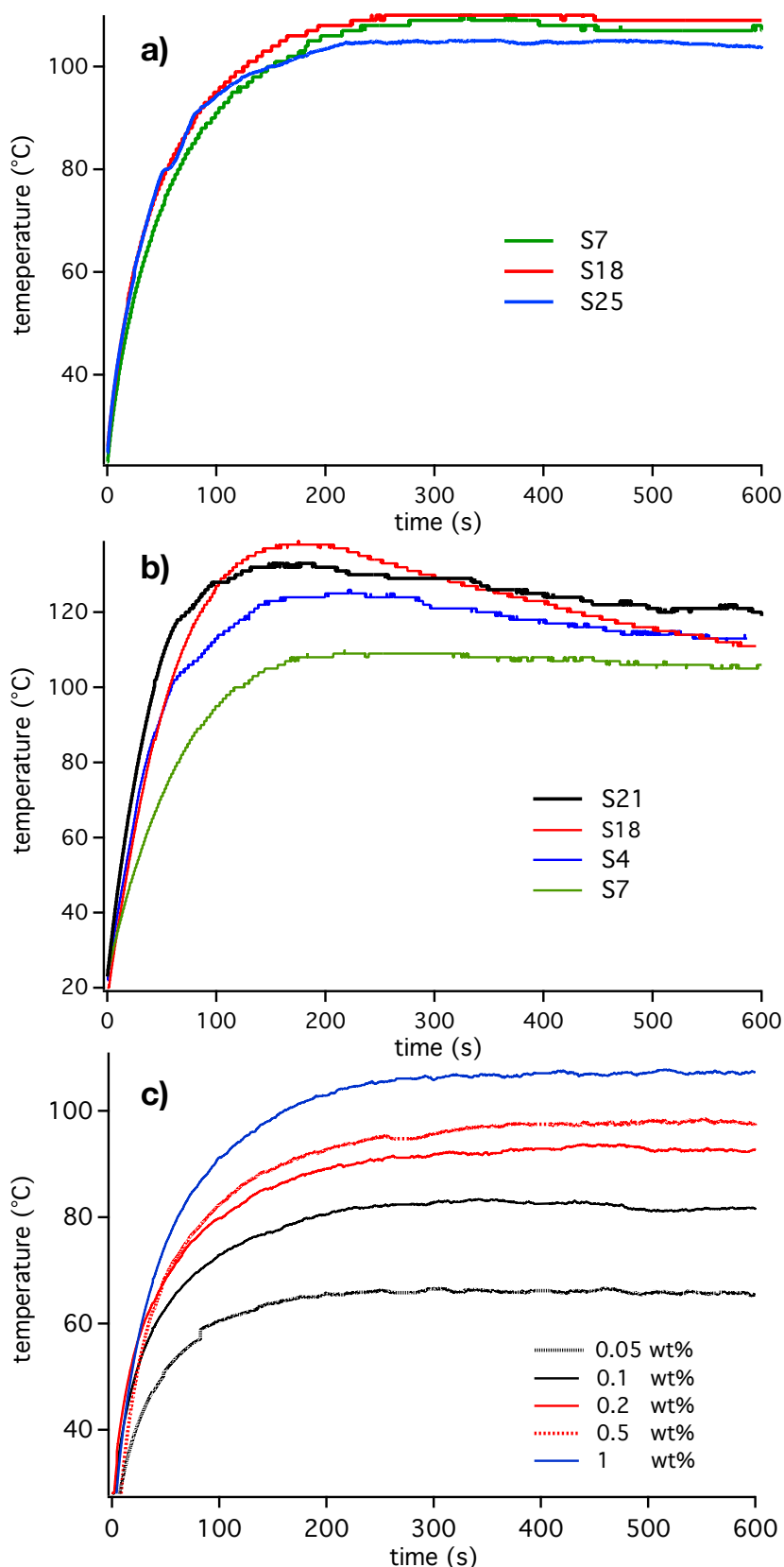


**Figure 30.** The temperature-time profiles of the samples (thickness is  $160\ \mu\text{m}$ ) comprising the monomer **TPGDA** and the combination of NIR initiator systems (a) samples comprising different sensitizers (0.5 wt%) and **OXE-01** (2 wt%), irradiated with the 805nm LED ( $1.2\ \text{W}\cdot\text{cm}^{-2}$ ), (b) samples comprising different sensitizers (0.5 wt%) and **OXE-01** (2 wt%) irradiated with the 860nm LED ( $1.5\ \text{W}\cdot\text{cm}^{-2}$ ), (c) samples comprising **COXE-15** (2 wt%) and **S18** in different concentrations, irradiated with the 805nm LED ( $1.2\ \text{W}\cdot\text{cm}^{-2}$ ), published in [118]. More details in Section 4.3.3 explain the experimental conditions.

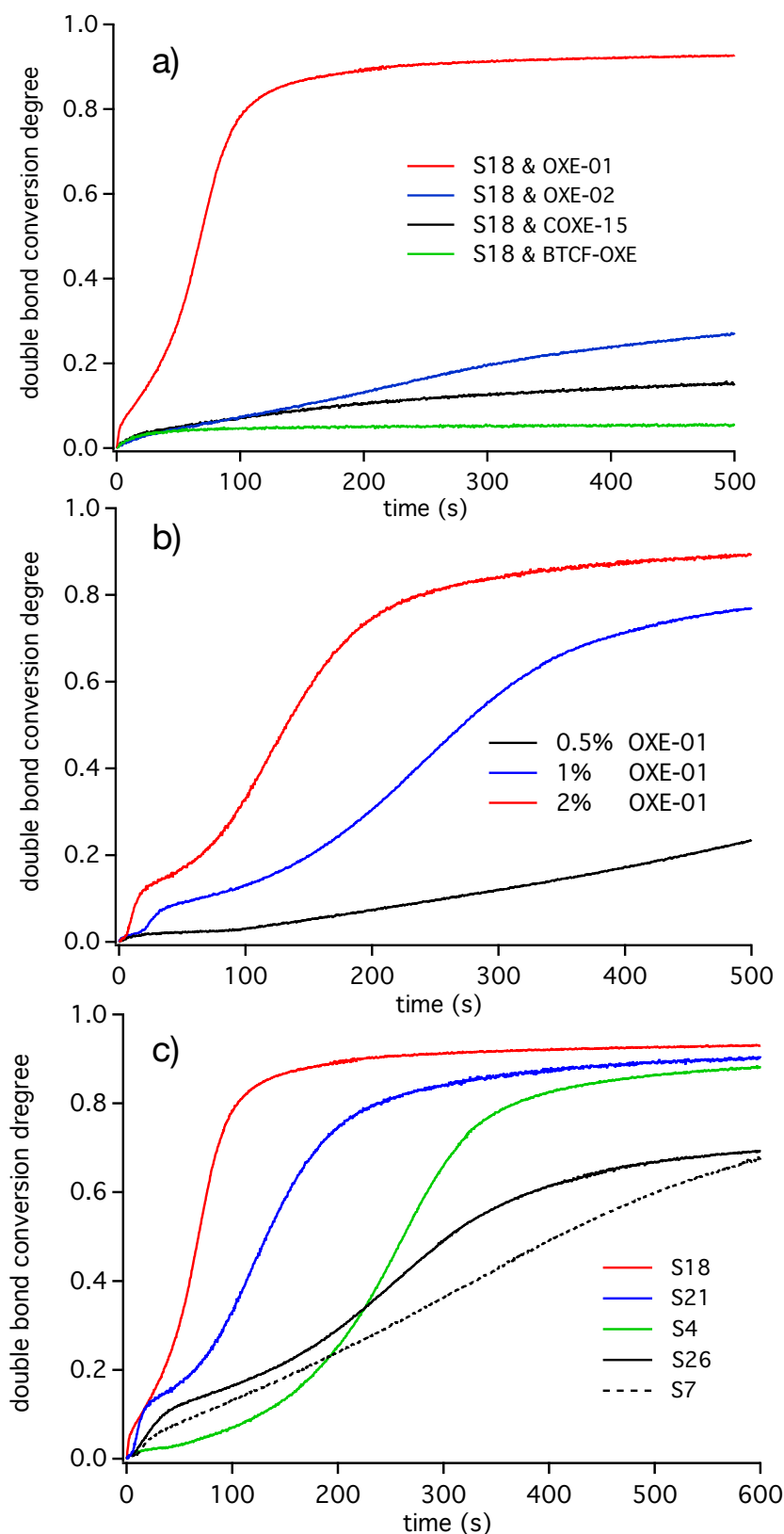
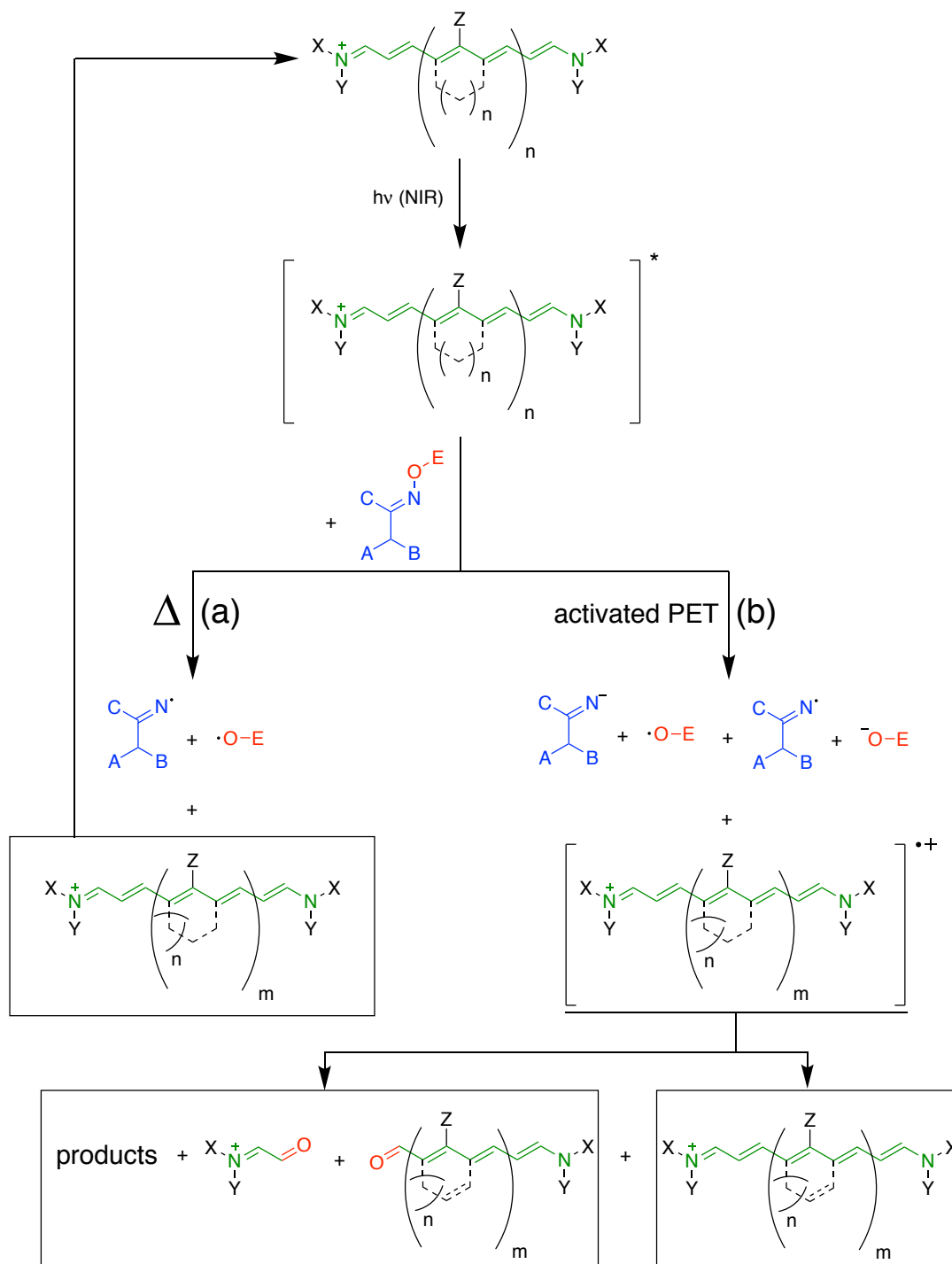


**Figure 31.** RT-FTIR conversion degree-time profiles of TPGDA (a) comprising S18 (0.05 wt%) and different oxime esters (2 wt%), (b) comprising S21 (0.05 wt%) and OXE-01 in different concentrations, (c) comprising different sensitizers (0.05 wt%) and OXE-01 (2 wt%), irradiated with the 870 nm LED ( $1.2 \text{ W}\cdot\text{cm}^{-2}$ ), published in [118]. More details in Section 4.3.2 explain the experimental conditions.

Figure 31 shows the RT-FTIR conversion-time profiles of **TPGDA** comprising cyanine sensitizers and oxime ester. **OXE-01** exhibited the best reactivity in combination with **S18**, see Figure 31a, while **OXE-2**, **COXE-15**, and **BTCF-OXE** showed less performance. Marcus theory[267] about PET can explain the observed results although the free enthalpy of photoinduced electron transfer ( $\Delta G_{PET}$ ) showed positive. This is possible under some circumstances[160-161, 283]. The results showed that only **OXE-01** exhibited the best performance. This surprised because the other oxime esters **OXE-2**, **COXE-15**, and **BTCF-OXE** exhibited similar reduction potentials but different thermal stability in **TPGDA**[118]. Therefore, as aforementioned shown in Figure 30, huge heat released by the NIR-sensitizers promotes also endothermal events under some circumstances. This is concluded in general with an increase of entropy occurring from a complex between the excited state of the sensitizer and the oxide ester. It can proceed in both ways forming either back the ducts or the products. This reaction changes the number of molecules in the reaction resulting in an entropy increase of the system for both directions which must have a lower intrinsic activation barrier in the case of product formation. Again, the additional thermal energy generated helps the initiating initiator system to react resulting in formation of cation radicals **Sens<sup>+</sup> ·** and radicals. The system studied in this thesis exhibit an intrinsic activation barrier differing for each type of sensitizer and oxime ester explaining the different reactivity[118].

Figure 31b shows how increase concentration of **OXE-01** leads to an increase of double bond conversion of **TPGDA**. It means that the initiator system comprising sensitizer and **OXE-01** follows a bimolecular reaction system. Additionally, the different structure of the sensitizer results in a different performance, Figure 31c. However, they did not show clear correlation between electrochemical data and reactivity in combination with **OXE-01** where **S18** exhibited the best efficiency while **S7** showed the lowest reactivity. In this case, the benzo[e]indolium derivative **S18** showed higher efficiency compared to other indolium derivatives. These results resulted in the model of NIR-sensitized decomposition of oxime esters depicted in Table 6. The reaction mechanism of this NIR initiating system based on the combination of heat and protons results in successful bleaching of sensitizers and generating initiating radicals for the polymerization as shown in Scheme 28. Another mechanism based on thermal decomposition may take a part of minor importance because it can not explain the bleaching reaction of sensitizers observed as depicted in Figure 32. The heat generated may lead to decomposition as aforementioned explained in Section 2.3.1 shown in part (a) but the optical density should remain constant. However,

the laser exposure experiment with a system releasing mainly heat showed inefficient reactivity based on route (a). More reaction appears the mechanism based on PET reaction carrying an internal activation barrier.



**Scheme 28.** Proposal of possible reactions mechanism contributing to generation of radicals by NIR-sensitized activated PET or heat released by NIR sensitizers, published in [118].

Additionally, irradiation of the combination consisting of sensitizer and oxime ester with NIR light connects with their chemical reactivity causing generation of the respective reac-

tion of sensitizers as well. This view has been identified by reference materials synthesized by coauthors of this publication[86] and LC-MS measurements[39, 96]. The photoinduced cleavage of the heptamethine chain results in the short conjugated photoproducts bearing terminal carbonyl group. These photoproducts exhibit yellow/brownish colour as approved by the increased absorption between 400-600 nm[39], shown in Figure 32. Exposure of sensitizers comprising a cyclopentene pattern at the *meso*-position generated photoproducts with a fulvene structure exhibiting a 100 nm blue shifted absorption. The respective new structures of the photoproduct of the cyanine cations are depicted in Figure 32b+c, which were approved by LC-MS measurement. Therefore, the absorption also shifted hypsochromically as previously reported for the sensitizer comprising the diphenyl amino group using an iodonium salt as coinitorator[86]. In other words, this phenomenon relates to the same reaction of the sensitizer taking either an iodonium salt or oxide ester as coinitorator resulting in the same photoproduct of the sensitizer. It finally approved that a general pattern of the heptamethine cyanine carrying pentacyclic in the *meso*-position preferred formation of photoproducts comprising fulvene moiety.[118]

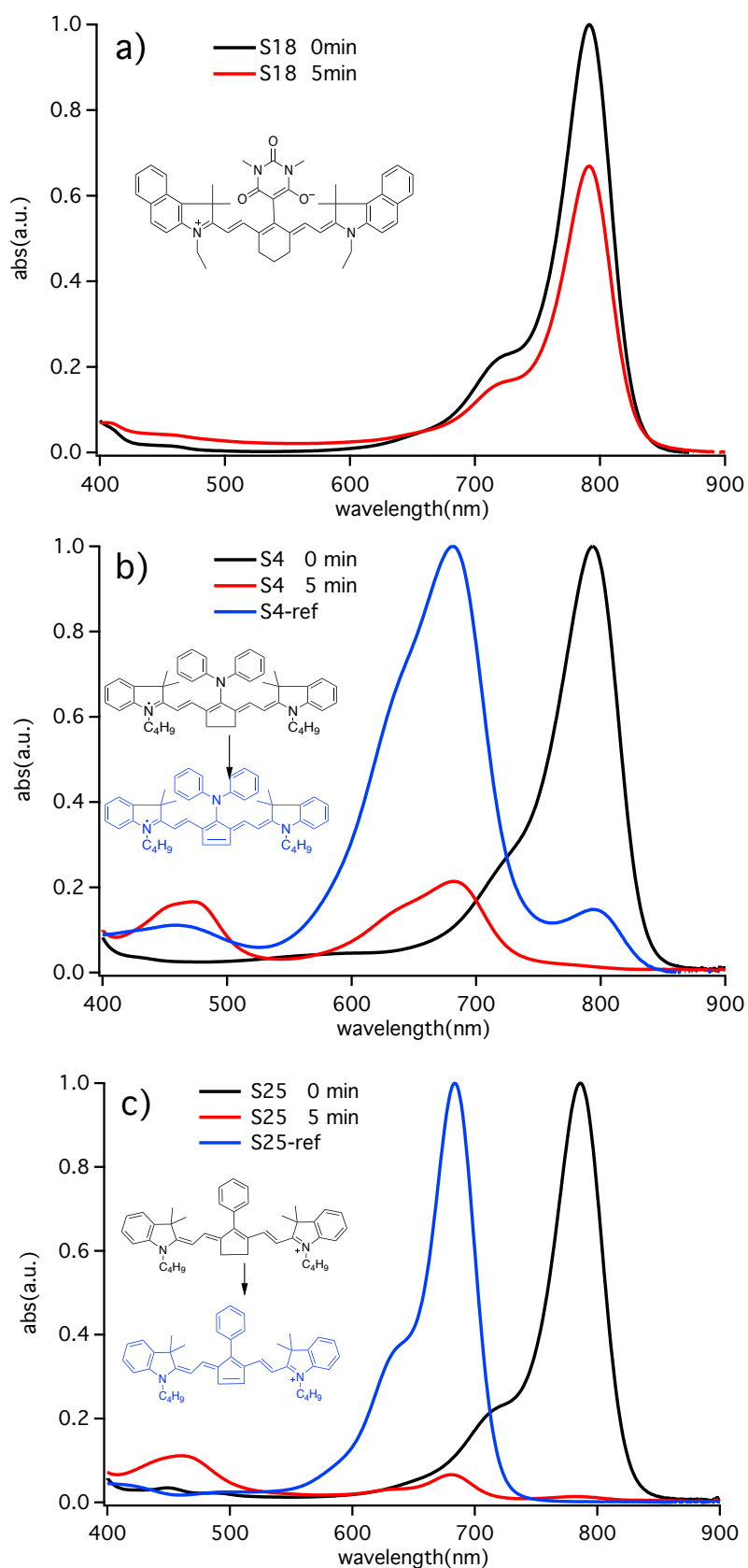


**Figure 32.** Change of UV-Vis-NIR spectra of **S18** (a), **S4** (b), and **S25** (c) upon exposure with 805nm NIR LED ( $1.2 \text{ W}\cdot\text{cm}^{-2}$ ) and employing **OXE-01** as coinitiator in **PEGMA**. The blue and the red curves in figure 32b and 32c depict the absorption of the respective oxidized product with fulvene structure. For a sake of simplicity, only the cyanine structure was included, published in [118]. More details in Section 4.3.4 explain the experimental conditions.



The bleaching kinetics of **S4** and **S25** in the radical polymerizable **LMA**, which operated as radical scavenger, was investigated more in detail. This model shows the better efficiency of the reactivity compared to other traditional solvents. The sensitizer **S25** carrying a phenyl ring at the *meso*-position exhibited a higher bleaching reactivity while **S4** carrying diphenylamino group showed less reactivity upon NIR light exposure, see Figure 33. The results can differ by changing the solvent and also when much more oxygen is available during irradiation. The data obtained apparently appear as first-order kinetics because of no total-absorption. This is explained by the fact that the absorbed light intensity ( $I_{\text{abs}}$ ) is expressed as  $I_{\text{abs}} = I_0(1-10^{-\text{OD}})$ , where  $I_0$  relates the light intensity of the irradiation source, and OD stands the optical density ( $\text{OD} = C \times \epsilon \times d$  according to Lambert-Beer's law). In the case that OD leads to conditions where nearly all photons are absorbed by the sample; that is  $\text{OD} > 2$ , it follows that  $I_{\text{abs}} \approx I_0$  while lower OD ( $\text{OD} < 1$ ) results in  $I_{\text{abs}} \approx I_0 \times \text{OD}$ . The latter is concluded by development of a Taylor series from the expression  $(1-10^{-\text{OD}})$  resulting in  $1-1+\text{OD}/1!-(\text{OD}/2!)^2+\dots$ , which simplifies to OD after discontinuing after the linear term. Thus, the differential change of concentration with respect to the time is now proportional to the concentration or OD. Thus, integration results in an expression that appears to first order kinetics but this is not the case. Just the change of absorption conditions resulted in a switch of the equation where one can write at high concentration the typical differential equation for zero order kinetics  $(-dC/dt) = \phi_{\text{-ln}} \times I_0$  while lower absorption yields the following differential equation:  $-dC/dt = \phi_{\text{-ln}} \times I_0 \times C \times \epsilon \times d$  whose integration yields  $(C_0 - C_t) = \phi_{\text{-ln}} \times I_0 \times t$  for the aforementioned high absorption conditions and  $\ln(C_0/C_t) = \phi_{\text{-ln}} \times I_0 \times t$  for the case that  $\text{OD} \ll 1$ , respectively. In other words, change of the absorption conditions may lead to the impression that kinetic order changed which is not the case. Thus, the slope in Figure 33 is direct proportional to the quantum yield  $\phi_{\text{-ln}}$  of initiator consumption.

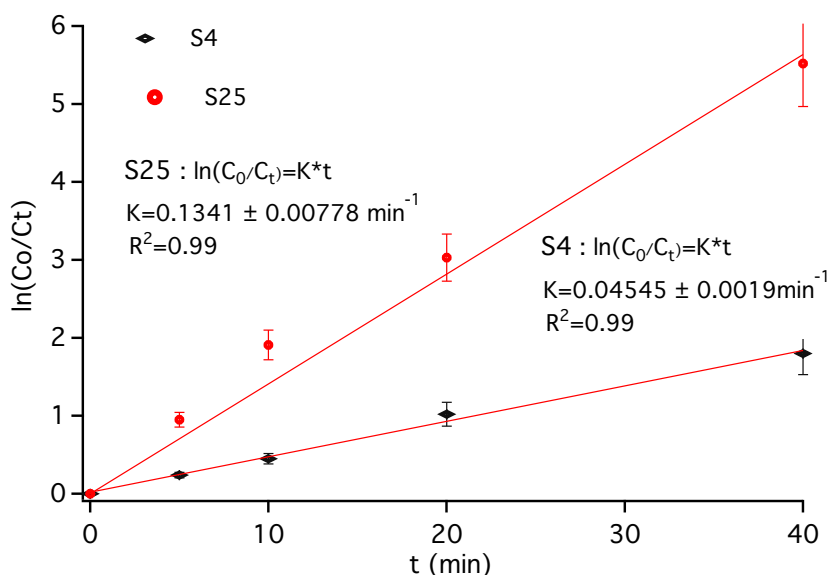


**Figure 33.** The bleaching kinetics of **S5** (blue) and **S25** (red). **LMA** solution including sensitizer ( $3.5 \times 10^{-6} \text{ mol} \cdot \text{L}^{-1}$ ), **OXE-01** ( $2.0 \times 10^{-5} \text{ mol} \cdot \text{L}^{-1}$ ) was irradiated with the 805 nm NIR LED device ( $1.2 \text{ W} \cdot \text{cm}^{-2}$ ) at different exposure time, published in [118]. More details in Section 4.3.4 explain the experimental conditions.

Quantum chemical calculations were additionally used to explain the distinct electron distributions for the **S25** and its photoproduct **S25\_ref**, see Figure 34[118]. The results depict differences in the HOMO where the oxidised product exhibits an unsaturated moiety in the middle of the pattern being rather comparable with that of aromatic structures, Figure 34. Conjugated aromatic patterns typically depict an absorption located at a shorter wavelength compared to the corresponding original cyanines[200], which confirmed the trend observed in the bleaching experiments that photoproducts exhibit shorter absorption wavelength and lower absorption coefficient. These calculations were pursued by one coauthor in ref[118] and mentioned here to complex relationships in such systems.

The results of this part exhibited that NIR sensitized decomposition of the oxime ester based on the mechanism of PET between sensitizers and oxime esters. Heat released by non-radiative deactivation of the NIR-sensitizer takes a huge function in this initiating system because it increases the entropy facilitating the occurrence of PET reactions under endothermal conditions to help such a system to overcome the internal activation barrier. These are two different mechanistic points including thermodynamics and kinetics which explain together the overall observed reactivity of the initiator systems comprising NIR sensitizers and oxime ester as radical initiators.

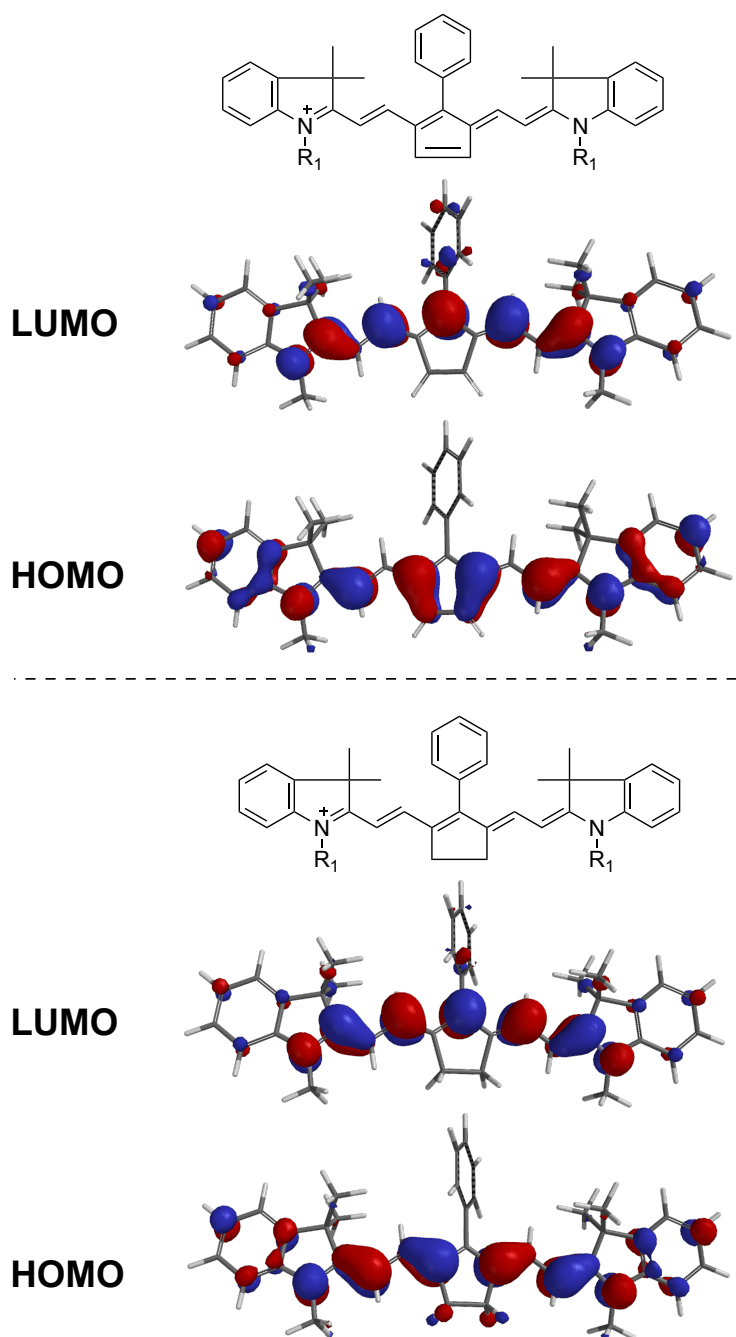


**Figure 34.** Electron density in the HOMO and LUMO of **S25**, **S25\_ref** obtained after a DFT calculation based on the B3LYP//6-31G\* method implemented in Spartan 16 to optimise the ground state, published in [118].

**Table 14.** Properties of sensitizers, oxime esters, and their combination. Optical data ( $\lambda_{\max}$ : absorption maximum,  $\epsilon$ : extinction coefficient), electrochemical data ( $E_{\text{ox}}$ : oxidation potential,  $E_{\text{red}}$ : reduction potential), initial temperature of intrinsic polymerization of **TPGDA** comprising NIR-sensitizer and oxime ester **OXE-01** ( $T_i$ ), and final double bond conversion  $x_{\infty}$  of **TPGDA** followed by RT-FTIR measurement, published in [118]. More details in Section 4.3.1, 4.3.2, 4.3.5, 4.3.7 explain the experimental conditions.

Sens	$\lambda_{\max}$ (nm)[b]	$\epsilon_{\max}$ ( $M^{-1}\cdot\text{cm}^{-1}$ )	$\epsilon(805\text{ nm})$ ( $M^{-1}\cdot\text{cm}^{-1}$ )	$\epsilon(860\text{ nm})$ ( $M^{-1}\cdot\text{cm}^{-1}$ )	$\epsilon(395\text{ nm})$ ( $M^{-1}\cdot\text{cm}^{-1}$ ) [c]	$E_{\text{ox}}$ (V)[c]	$E_{\text{red}}$ (V) [c]	$T_i$ ( $^{\circ}\text{C}$ ) [d]	$x_{\infty}$ (805 nm) (%) [e]	$x_{\infty}$ (870 nm) (%) [f]	$x_{\infty}$ (395 nm) (%) [g]
<b>S29[a]</b> <b>(S0991)</b>	992	$2.23\times 10^5$	-	-		0.66	-0.34		0	0	
<b>S24</b> <b>(S0772)</b>	858	$2.09\times 10^5$	$7.23\times 10^4$	$2.08\times 10^5$		0.73	-0.27	142	0	0	
<b>S4</b> <b>(S2025)</b>	792	$2.41\times 10^5$	$1.94\times 10^5$	$3.37\times 10^3$		0.57	-0.60	80	90	88	
<b>S25</b> <b>(S2026)</b>	786	$3.23\times 10^5$	$1.92\times 10^5$	$1.87\times 10^3$		0.58	-0.56	107	81	69	
<b>S7</b> <b>(S2459)</b>	757	$2.62\times 10^5$	$7.89\times 10^5$	<0.1		0.41	-0.86	92	78	68	
<b>S10</b> <b>(S2383)</b>	813	$1.62\times 10^5$	$1.25\times 10^5$	$1.01\times 10^4$		0.77	-0.38	138	0	38	
<b>S26</b> <b>(S10761)</b>	835	$2.16\times 10^5$	$1.52\times 10^5$	$1.27\times 10^5$		0.54	-0.57	83	-	82[h]	
<b>S21</b> <b>(S2468)</b>	844	$2.39\times 10^5$	$9.92\times 10^4$	$1.32\times 10^5$		0.56	-0.57	80	0	90	
<b>S18</b> <b>(S2265)</b>	791	$3.03\times 10^5$	$1.59\times 10^5$	$6.2\times 10^2$		0.48	-0.97	91	91	93	
<b>OXE-01</b>	326	$2.95\times 10^4$	0	0	$6.43\times 10^2$	1.72	-1.36	65[i]	100[j]		71
<b>OXE-02</b>	337	$2.30\times 10^4$	0	0	$2.48\times 10^2$	1.51	-1.26	68[i]	100[j]		70
<b>COXE-1</b> <b>5</b>	300	$1.65\times 10^4$	0	0	$4.00\times 10^2$	1.59	-1.30	78[i]	67[j]		74
<b>BTCF-</b> <b>OXE</b>	356	$2.28\times 10^4$	0	0	$3.76\times 10^2$	1.70	-1.26	173[i]	<10[j]		81

[a] from ref.[47]. [b] in methanol, [c] in acetonitrile, [d] onset temperature of the polymerization of **TPGDA**, [e] final conversion of photopolymerization of **TPGDA** in the RT-FTIR measurement with 805 nm NIR LED irradiation, [f] final conversion of photopolymerization of **TPGDA** in the RT-FTIR measurement with 870 nm NIR LED irradiation, [g] final conversion of photopolymerization of **TPGDA** in the Photo-DSC measurement with 395 nm UV LED irradiation, [h] conversion of photopolymerization of **TPGDA** after 10 min with 860 nm NIR LED irradiation, [i] onset temperature of the polymerization of **TPGDA** without NIR sensitizer, [j] the final conversion of **TPGDA** comprising **S18** (0.5 wt%), and different oxime esters including **OXE-01**, **OXE-02**, **COXE-15**, or **BTCF-OXE** (2.0 wt%) respectively, as coinitiators, under 805nm NIR LED exposure, the thickness of the sample was 160 $\mu\text{m}$ .

## 6. Conclusions and Outlook

The first part of this work shows the results obtained using a high-power NIR LED prototype emitting at 805 nm to study the NIR photopolymerization where heptamethine cyanines were used as NIR sensitizer in combination with iodonium salts serving as coinitiators. The reaction of the excited state of the cyanine and the iodonium cation results in initiating radicals and conjugate acid needed as prerequisite to initiate radical and cationic polymerization, respectively. The reactivity study of the NIR initiating system comprising the combination of heptamethine based cyanine and iodonium salt led to the conclusion after measuring the double bond conversion of monomers used for radical polymerization such as **TPGDA** that sensitizers with barbital or phenylmercapto groups exhibited good reactivity to initiate free radical photopolymerization upon this high power NIR LED exposure. Particularly, cationic cyanines, which could not be used as sensitizers in photopolymerization employing a low power LED ( $\leq 0.1 \text{ W}\cdot\text{cm}^{-2}$ ), were first found to initiate free radical polymerization of the acrylate esters with remarkable reactivity using the new NIR LED system exhibiting much higher intensity; that is  $\geq 1 \text{ W}\cdot\text{cm}^{-2}$ . This result can be explained based on the mechanism of PET with an internal barrier based on the Marcus theory. The high-power NIR LED facilitated the cyanines to generate the necessary amount of heat by internal conversion (IC), which helped the system to overcome the internal activation barrier needed to proceed the PET resulting in formation of initiating radicals to initiate successfully photopolymerization with NIR radiation. Comparative photo-DSC measurements, in which the heat formed by the sensitizer is compensated by the instrumental DSC setup, showed increasing reactivity at different operating temperatures as a response to heat provided by an external source. This can be seen as approval that internal barriers exist in systems comprising the aforementioned combination of NIR photoinitiator systems. Thus, gradual increase of the operating temperature resulted in both an increase of the reaction rate and double bond conversion. This has a deep impact on development of technologies. Such barrier systems need a special hardware to initiate the chemical process; that is in this case the high power NIR LED emitting at 805 nm available as prototype in this work. In other words, such systems possess better stability under room light, and they can be easier handled in future production systems. This can include manufacturing systems needed for production of electronic components such as printed circuit boards (PCB). In addition, the cationic cyanine carrying cyclopentene in the *meso*-position exhibits the capability of initiating the cationic polymerization of the epoxies and oxetanes which was firstly reported applying the new high-power NIR LED systems introduced in this work.

The bleaching measurement and photoproducts analysis evidenced formation of a new photoproduct with fulvene structure generated in an unexpected photochemical reaction. This brings the benefit into the system to initiate cationic polymerization of epoxies by avoiding formation of nucleophilic products formed by bond cleavage of the polymethine chain as reported in former studies where cyanines without cyclopentene pattern in the centre of the cation were used. The chain growth during epoxy polymerization bases on the carbocation as intermediate, which can be terminated by nucleophilic compounds formed by bond cleavage of the cyanine. This was avoided in the case of cyanines carrying cyclopentene in the centre of the cyanine cation by generating the new photoproduct with fulvene structure. It will bring new impetus in the field of material science because combination with radical polymerization systems opens the door to make interpenetrating polymer networks (IPNs). NIR sensitized cationic polymerization of epoxies was first reported in this work under the aforementioned experimental conditions. In brief, the new high power NIR LED promoted NIR sensitized radical and cationic photopolymerization based on the combination of photo and thermal activated processes.

In addition, such heptamethines with five-numbered ring in the *meso*-position exhibited an unexpected hypsochromic shift of the absorption caused by the selective oxidation resulting in generation of the above mentioned fulvene structure visually appearing as hypsochromic colour shift. This result exhibits a further interesting feature for systems requiring read-only cycles in the exposed areas, which is the case in fully automatised CTP systems operating in on-press procedures in modern printing shops. Future developments shall put the focus not only on such systems. Electronic industry with focus on printed circuit boards (PCB) or some negative resists may benefit from this reaction because it changes colour on demand. There exist a big need to have such systems in practice.

As a consequence, cationic polymerization and radical/cationic hybrid polymerization based on the heptamethine cyanines with cyclopentene in the *meso*-position and iodonium salts were studied in more detail employing three distinct high-power NIR LEDs emitting either at 805nm, 860nm, or 870nm. These detailed studies evidenced successful work of more epoxies and another monomer used for cationic polymerization; that is vinyl ether. Thus, deeper studies of the cationic polymerization of different cationic monomers using the combination of an initiator system comprising a heptamethine with cyclopentene in the centre of the molecule and iodonium salt were carried out to confirm the findings as mentioned above. Surprisingly, particular these cyanines in combination with iodonium salts functioned well as initiating system for cationic polymerization using also vinyl ethers and

oxetanes to complement these findings. Moreover, the vinyl ether showed the best cationic polymerization performance sequentially followed by oxetanes and oxiranes.

Furthermore, the influence of the anion moved also into the focus of the investigations. Its nucleophilicity must deeply affect the reactivity of the corresponding combination of NIR photoinitiator system in cationic photopolymerization. Thus, different anions functioned as counter ion in both the heptamethine and iodonium cations; that are fluorinated phosphate ( $[\text{PF}_6]^-$ ,  $[\text{PF}_3(\text{C}_2\text{F}_5)_3]^-$ ,  $[\text{PF}_3(n\text{-C}_4\text{F}_9)_3]$ ), aluminate ( $[\text{Al}(\text{O}-t\text{-C}_4\text{F}_9)_4]^-$ ,  $[\text{Al}(\text{O}(\text{C}_3\text{F}_6)\text{CH}_3)_4]^-$ ), methide  $[\text{C}(\text{O}-\text{SO}_2\text{CF}_3)_3]^-$ , and tosylate  $[\text{TsO}]^-$ . They were chosen to study the influence the anion on reactivity. These anions except  $[\text{TsO}]^-$  belong to weakly coordinating anions (WCAs), which can produce Brønsted superacid upon exposure. The anion  $[\text{Al}(\text{O}-t\text{-C}_4\text{F}_9)_4]^-$  showed the best reactivity in all cationic polymerisable monomers used in this work. Another anion,  $[\text{PF}_3(\text{C}_2\text{F}_5)_3]^-$ , also exhibited better reactivity following  $[\text{Al}(\text{O}(\text{C}_3\text{F}_6)\text{CH}_3)_4]^-$ . The iodonium salt carrying  $[\text{Al}(\text{O}-t\text{-C}_4\text{F}_9)_4]^-$  exhibited the best conductivity in monomers. Conductivity relates to dissociation and may explain its outstanding performance. Good conductivity obviously relates to good reactivity where presumably the dissociation of the salt into the individual ions undertakes a major role. Further calculation of the electrostatic potentials after geometry optimisation based on density functional theory evidences that anion  $[\text{Al}(\text{O}-t\text{-C}_4\text{F}_9)_4]^-$  exhibited optimal shielding of nucleophilic moieties in the anion, which offers new impetus to design similar systems in the future showing that the anion takes up a special function. This is concluded by the comparison of reactivity studies using equimolar amounts of iodonium salts. On the other hand, the high molecular weight of the anion requests to use higher mass to obtain similar molar ratio. This is not so practicable since the systems used in industry request as low as possible use of compounds having a lower mass. From this point of view, the phosphates  $[\text{PF}_6]^-$  and  $[\text{PF}_3(\text{C}_2\text{F}_5)_3]^-$  may move into the focus. Nevertheless,  $[\text{PF}_6]^-$  fails due to the well known HF issue. The anion  $[\text{PF}_3(\text{C}_2\text{F}_5)_3]^-$ , which was developed as alternative with no HF issue, showed less reactivity compared to  $[\text{Al}(\text{O}-t\text{-C}_4\text{F}_9)_4]^-$ . From this point of view, this new anion can be seen as a great deal for further uses in NIR-sensitized cationic polymerization. It shall be used in future studies unless acceptable alternatives will exist.

Furthermore, the radical and cationic hybrid polymerization was studied with this initiating system. Surprisingly, methacrylic monomers accelerated the cationic polymerization of oxetanes because such monomers promote the generation of the conjugate acid. This was concluded by acidic cation/conjugate acid generation measurements using **LMA** as monomer, which approved as one kind of acrylate ester, and therefore, also as solvent to

draw this conclusion. **RhB-L** quantitatively probed this reaction and clearly evidenced that the initiating system generated more conjugate acid in **LMA** than in the solvent **BuAc**. Therefore, it shows again that the acrylate monomer possesses a special function in order to generate more conjugate acid.

This work firstly reported the successful formation of IPN by NIR-sensitized photopolymerization based on hybrid radical and cationic cross-linking. On the other hand, the same monomer system failed using a typical UV LED initiating system where thioxanthone absorbed the light at 395 nm. DMA measurements approved the results. This result clearly showed that additional heat was necessary to build IPNs. This additional energy was provided by non-radiative deactivation of the NIR sensitizer, which is the main deactivation part in systems absorbing above 700 nm. Thus, heat generated by the NIR sensitizer essentially facilitates synthesis of IPNs, which makes such systems interesting for future development in material research since UV LED based initiation failed in the same monomer systems to form it.

Finally, oxime esters were studied in combination with heptamethines as alternatives to iodonium salts serving as coinitiators in the NIR photoinitiating system. Four oxime esters (**OXE-01**, **OXE-02**, **COXE-15**, and **BTCF-OXE**), which can initiate free radical photopolymerization upon UV-LED exposure, were used in these studies. The reactivity of the initiating system was studied to find the most efficient oxime ester serving as co-initiator for NIR photopolymerization via RT-FTIR measurement. **BTCF-OXE** exhibited the best thermal stability but it could not work with good efficiency together with heptamethine cyanine. On the other hand, **OXE-01** exhibited the worst thermal stability but the best reactivity with **S18**. Nevertheless, its thermal stability was still acceptable. However, the combination of the initiating system comprising oxime ester and heptamethine does not entirely relate to a thermal sensitive initiating system. Additional laser exposure experiments with the cyanine **S28**, whose deactivation of the excited state occurs almost radiationless upon exposure at 980 nm, showed no polymerization of acrylate monomer in combination with **OXE-01** although the temperature generated was much greater than 100 °C. Therefore, photonics and thermal events are both prerequisites to make the NIR-photoinitiator system comprising oxime ester and heptamethine cyanine initiate free radical photopolymerization. The oxime esters used exhibit less toxicity and shall be therefore used in future studies particular as alternative in applications related to materials used in combination with foods.



In this system, NIR-sensitized decomposition of the oxime ester bases on PET proceeding over an internal activation barrier. Heat released by non-radiative deactivation of the NIR sensitizer undertakes a major function in this system. Therefore, it requires the formation of an inner complex whose thermal decomposition increases the entropy of the system, which can promote also the occurrence of reactions even under endothermic conditions and helps such a system to work. Thus, there are two different points, which are thermodynamics and kinetics, explaining together the overall observed reactivity. This finding might influence the development of future technologies since their use requests strong emissive radiation sources in connection with systems certainly having the aforementioned daylight stability. This aspect makes the handling under certain conditions in practice become easier.

The use of a high-power LED offers new opportunities in NIR free radical, cationic and hybrid free radical/cationic polymerization. This also offers an opportunity to develop future technologies combining thermal and photonic processes to crosslink materials in technological events resulting in partial replacement of oven processes in in-line manufacturing. This can be seen as a tremendous result of this thesis following the general requirements of the society to improve our environment. This may also offer the opportunity to embed additives exhibiting an absorption range from the UV to the visible in coatings because excitation occurs in NIR range outside of their absorption in the UV and visible part. Such coatings can become of different interests with applications also requesting a coating to protect against solar weathering. Thus, future work shall also promote to continue the development of photopolymerization in combination with more strong emissive NIR LED devices whose emission would reside much deeper in the materials, and also promote the use of respective sensitizers. Moreover, this results in a colourless appearing coating and could be seen as a great benefit.

## 7. References

- [1] W. A. Green, *Industrial photoinitiators: a technical guide*, CRC Press, **2010**.
- [2] A. Watanabe, M. Koizumi, *B Chem Soc Jpn* **1955**, *28*, 141-146.
- [3] G. A. Delzenne, U. Laridon, H. Peeters, *Eur Polym J* **1970**, *6*, 933-943.
- [4] N. S. Allen, *J Photoch Photobio A* **1996**, *100*, 101-107.
- [5] A. Shibuya, S. Koizumi, K. Kunita, *J. Prin. Sci. Techno* **2005**, *42*, 214-219.
- [6] M. Sangermano, N. Razza, J. V. Crivello, *Macromol Mater Eng* **2014**, *299*, 775-793.
- [7] B. Strehmel, C. Schmitz, T. Brömme, A. Halbhuber, D. Oprych, J. S. Gutmann, *J Photopolym Sci Tec* **2016**, *29*, 111-121.
- [8] M. Sangermano, I. Roppolo, A. Chiappone, *Polymers* **2018**, *10*.
- [9] A. Bagheri, J. Jin, *ACS Appl. Polym. Mater* **2019**, *1*, 593-611.
- [10] N. Corrigan, J. Yeow, P. Judzewitsch, J. T. Xu, C. Boyer, *Angew Chem Int Edit* **2019**, *58*, 5170-5189.
- [11] J.-P. Fouassier, J. Lalevée, *Photoinitiators for Polymer Synthesis: Scope, Reactivity, and Efficiency*, John Wiley & Sons, **2012**.
- [12] M. A. Tehfe, F. Louradour, J. Lalevee, J. P. Fouassier, *Appl Sci-Basel* **2013**, *3*, 490-514.
- [13] R. Schwalm, *UV Coatings. Basics, Recents Developments and New Applications*, Elsevier, Oxford, **2007**.
- [14] K. Dietliker, T. Jung, J. Benkhoff, H. Kura, A. Matsumoto, H. Oka, D. Hristova, G. Gescheidt, G. Rist, *Macromol Symp* **2004**, *217*, 77-98.
- [15] C. Dietlin, S. Schweizer, P. Xiao, J. Zhang, F. Morlet-Savary, B. Graff, J. P. Fouassier, J. Lalevee, *Polym Chem* **2015**, *6*, 3895-3912.
- [16] J. Heathcote, *Vol. 2019*, UV/EB Technology, <https://uvebtech.com/articles/2019/state-of-uv-led-curing-applications/>, **2019**.
- [17] K. Dietliker, J. Baro, *Handbook of Industrial Inkjet Printing: A Full System Approach* **2017**, 117-128.
- [18] P. Xiao, J. Zhang, F. Dumur, M. A. Tehfe, F. Morlet-Savary, B. Graff, D. Gignes, J. P. Fouassier, J. Lalevee, *Prog Polym Sci* **2015**, *41*, 32-66.
- [19] C. Schmitz, D. Oprych, C. Kutahya, B. Strehmel, *Photopolymerisation Initiating Systems* (Eds.: J. Lalevée, J.-P. Fouassier), Royal Society of Chemistry, **2018**, pp. 431-478.
- [20] J. V. Crivello, M. Sangermano, *J Polym Sci Pol Chem* **2001**, *39*, 343-356.
- [21] D. Burget, C. Mallein, J. P. Fouassier, *Polymer* **2003**, *44*, 7671-7678.
- [22] I. Dika, J. P. Malval, O. Soppera, V. Bardinal, D. Barat, C. Turck, A. Spangenberg, A. Bruyant, *Chem Phys Lett* **2011**, *515*, 91-95.
- [23] B. Strehmel, T. Brömme, C. Schmitz, K. Reiner, S. Ernst, D. Keil, *Dyes and Chromophores in Polymer Science* (Eds.: J. Lalevée, J.-P. Fouassier), John Wiley & Sons, Inc., **2015**, 213-249.
- [24] S. Dadashi-Silab, S. Doran, Y. Yagci, *Chem Rev* **2016**, *116*, 10212-10275.
- [25] M.-A. Tehfe, J. Lalevee, F. Morlet-Savary, N. Blanchard, C. Fries, B. Graff, X. Allonas, F. Louerat, J. P. Fouassier, *Eur. Polym. J.* **2010**, *46*, 2138-2144.
- [26] J. Z. Shao, Y. Huang, Q. U. Fan, *Polym Chem-Uk* **2014**, *5*, 4195-4210.
- [27] S. Q. Shi, C. Croutxe-Barghorn, X. Allonas, *Prog Polym Sci* **2017**, *65*, 1-41.
- [28] Z. Q. Li, X. C. Zou, G. G. Zhu, X. Y. Liu, R. Liu, *Acs Appl Mater Inter* **2018**, *10*, 16113-16123.
- [29] J. Zhang, J. Lalevee, N. S. Hill, K. Launay, F. Morlet-Savary, B. Graff, M. H. Stenzel, M. L. Coote, P. Xiao, *Macromolecules* **2018**, *51*, 8165-8173.
- [30] E. Sari, M. Mitterbauer, R. Liska, Y. Yagci, *Prog Org Coat* **2019**, *132*, 139-143.
- [31] B. Strehmel, S. Ernst, K. Reiner, D. Keil, H. Lindauer, H. Baumann, *Z. Phys. Chem.* **2014**, *228*, 129-153.

- [32] H. Baumann, T. Hoffmann-Walbeck, W. Wenning, H.-J. Lehmann, C. D. Simpson, H. Mustroph, U. Stebani, T. Telser, A. Weichmann, R. Studenroth, *Ullmann's Encyclopedia of Industrial Chemistry*, Wiley-VCH Verlag GmbH & Co. KGaA, **2015**, pp. 1-51.
- [33] C. Simpson, H. Baumann, B. Strehmel, (Eastman Kodak Company, USA), WO2009109579A1, **2009**.
- [34] H. Baumann, *Chemie in unserer Zeit* **2015**, *48*, 14-29.
- [35] T. Brömme, C. Schmitz, D. Oprych, A. Wenda, V. Strehmel, M. Grabolle, U. Resch-Genger, S. Ernst, K. Reiner, D. Keil, P. Lüs, H. Baumann, B. Strehmel, *Chem. Eng. Technol.* **2016**, *39*, 13-25.
- [36] B. Strehmel, C. Schmitz, K. Cremanns, J. Göttert, *Chem. Eur. J.* **2019**, *25*, 12855-12864.
- [37] B. Strehmel, C. Schmitz, C. Kütahya, Y. Pang, A. Drewitz, H. Mustroph, *Beilstein J. Org. Chem.* **2020**, *16*, 415-444.
- [38] G. Wagenblast, H. Reichelt, M. Büschel, S. Haremza, P. Erk, E. Frank, (BASF; Flint Group Germany GmbH, Germany), US7901494B2, **2011**.
- [39] T. Brömme, C. Schmitz, N. Moszner, P. Burtscher, N. Strehmel, B. Strehmel, *ChemistrySelect* **2016**, *1*, 524-532.
- [40] Z. Chen, D. Oprych, C. Xie, C. Kutahya, S. Wu, B. Strehmel, *ChemPhotoChem* **2017**, *1*, 499-503.
- [41] A. Shiraishi, H. Kimura, D. Oprych, C. Schmitz, B. Strehmel, *J. Photopolym. Sci. Technol.* **2017**, *30*, 633-638.
- [42] A. H. Bonardi, F. Dumur, T. M. Grant, G. Noirbent, D. Gigmes, B. H. Lessard, J. P. Fouassier, J. Lalevee, *Macromolecules* **2018**, *51*, 1314-1324.
- [43] C. Kütahya, C. Schmitz, V. Strehmel, Y. Yagci, B. Strehmel, *Angew. Chem., Int. Ed.* **2018**, *57*, 7898-7902.
- [44] A. Kocaarslan, C. Kütahya, D. Keil, Y. Yagci, B. Strehmel, *ChemPhotoChem* **2019**, *3*, 1127-1132.
- [45] C. Schmitz, B. Strehmel, *J Coat Technol Res* **2019**, *16*, 1527-1541.
- [46] T. Brömme, D. Oprych, J. Horst, P. S. Pinto, B. Strehmel, *RSC Advances* **2015**, *5*, 69915-69924.
- [47] C. Schmitz, A. Halbhuber, D. Keil, B. Strehmel, *Prog Org Coat* **2016**, *100*, 32-46.
- [48] A. Shiraishi, Y. Ueda, M. Schlapfer, C. Schmitz, T. Bromme, D. Oprych, B. Strehmel, *J. Photopolym. Sci. Technol.* **2016**, *29*, 609-615.
- [49] C. Schmitz, B. Gökce, J. Jakobi, S. Barcikowski, B. Strehmel, *ChemistrySelect* **2016**, *1*, 5574-5578.
- [50] C. Schmitz, B. Strehmel, *ChemPhotoChem* **2017**, *1*, 26-34.
- [51] A. H. Bonardi, F. Bonardi, F. Morlet-Savary, C. Dietlin, G. Noirbent, T. M. Grant, J. P. Fouassier, F. Dumur, B. H. Lessard, D. Gigmes, J. Lalevee, *Macromolecules* **2018**, *51*, 8808-8820.
- [52] A. Bonardi, F. Bonardi, G. Noirbent, F. Dumur, C. Dietlin, D. Gigmes, J. P. Fouassier, J. Lalevee, *Polym Chem* **2019**, *10*, 6505-6514.
- [53] A. H. Bonardi, F. Bonardi, F. Dumur, D. Gigmes, J. P. Fouassier, J. Lalevée, *Macromol Rapid Commun* **2019**, *40*, 1900495.
- [54] A. Caron, F. Dumur, J. Lalevée, *J Polym Sci A Polym Chem* **2020**.
- [55] H. Mokbel, F. Dumur, J. Lalevée, *Polym Chem* **2020**, *11*, 4250-4259.
- [56] T. Brömme, J. Moebius, S. Schafer, C. Schmitz, B. Strehmel, *Eur. Coat. J.* **2012**, 20-21, 24-26, 27.
- [57] C. Schmitz, B. Strehmel, *Eur. Coat. J.* **2018**, *124*, 40-44.
- [58] N. D. Ignatyev, A. D. Kucheryna, U. D. Welz-Biermann, H. P. D. Willner, (Merck, Germany), DE10357360 A1, **2005**.
- [59] N. Klikovits, P. Knaack, D. Bomze, I. Krossing, R. Liska, *Polym Chem* **2017**, *8*, 4414-4421.
- [60] A. Kunze, U. Müller, K. Tittes, J.-P. Fouassier, F. Morlet-Savary, *J. Photochem. Photobiol. A* **1997**, *110*, 115-122.
- [61] P. P. Romańczyk, S. S. Kurek, *Electrochimica Acta* **2017**, *255*, 482-485.
- [62] Y. S. Vygodskii, D. A. Sapozhnikov, A. S. Shaplov, E. I. Lozinskaya, N. V. Ignat'ev, M. Schulte, P. S. Vlasov, I. A. Malyshkina, *Polym J* **2011**, *43*, 126-135.
- [63] R. Liska, D. Bomze, I. Krossing, P. Knaack, (Technische Universitaet Wien, (AT); Albert-Ludwigs-Universitaet Freiburg, (DE)), US20180244836A1, **2018**.

- [64] W. Qiu, P. Hu, J. Zhu, R. Liu, Z. Li, Z. Hu, Q. Chen, K. Dietliker, R. Liska, *ChemPhotoChem* **2019**, *3*, 1090-1094.
- [65] A. H. Bonardi, F. Bonardi, G. Noirbent, F. Dumur, D. Gigmes, C. Dietlin, J. Lalevee, *J Polym Sci A Polym Chem* **2020**, *58*, 300-308.
- [66] A. Matsumoto, H. Oka, M. Ohwa, H. Kura, J.-L. Birbaum, K. Dietliker, (Ciba Specialty Chemicals Holding Inc., Switz.), DE19928742A1, **1999**.
- [67] K. Dietliker, R. Hüsler, J. L. Birbaum, S. Ilg, S. Villeneuve, K. Studer, T. Jung, J. Benkhoff, H. Kura, A. Matsumoto, H. Oka, *Prog Org Coat* **2007**, *58*, 146-157.
- [68] D. E. Fast, A. Lauer, J. P. Menzel, A.-M. Kelterer, G. Gescheidt, C. Barner-Kowollik, *Macromolecules* **2017**, *50*, 1815-1823.
- [69] S. X. Chen, M. Jin, J. P. Matval, J. M. Fu, F. Morlet-Savary, H. Y. Pan, D. C. Wan, *Polym Chem* **2019**, *10*, 6609-6621.
- [70] S. I. Hong, Sumyu Konghak Hoeji **1972**, *9*, 97-110.
- [71] M. Yoshida, H. Sakuragi, T. Nishimura, S.-i. Ishikawa, K. Tokumaru, *Chemistry Letters* **1975**, *4*, 1125-1130.
- [72] P. Baas, H. Cerfontain, JJ. Chem. Soc., Perkin Trans. 2 **1979**, 1653-1660.
- [73] K. H. Chae, K. M. Park, W. C. Choi, J. M. Kim, *Pollimo* **1988**, *12*, 740-748.
- [74] F. AMAT-GUERRI, R. MALLAVIA, R. SASTRE, *J Photopolym Sci Technol* **1995**, *8*, 205-232.
- [75] G. Weidenbruck, *IP.com J.* **2003**, *3*, 29.
- [76] Y. Miyake, H. Takahashi, N. Akai, K. Shibuya, A. Kawai, *Chem. Lett.* **2014**, *43*, 1275-1277.
- [77] M. Makino, K. Uenishi, T. Tsuchimura, *J Photopolym Sci Tec* **2018**, *31*, 37-44.
- [78] Z. Li, X. Zou, R. Liu, Z. Li, R. Liu, Y. Yagci, F. Shi, Y. Yagci, *Nat Commun* **2019**, *10*, 3560.
- [79] X. Ma, D. Cao, H. Fu, J. You, R. Gu, B. Fan, J. Nie, T. Wang, *Prog. Org. Coat.* **2019**, *135*, 517-524.
- [80] P. Hu, W. W. Qiu, S. Naumov, T. Scherzer, Z. Y. Hu, Q. D. Chen, W. Knolle, Z. Q. Li, *ChemPhotoChem* **2020**, *4*, 224-232.
- [81] K. Suyama, H. Tachi, *Rsc Advances* **2015**, *5*, 31506-31513.
- [82] X. Ma, R. Gu, L. Yu, W. Han, J. Li, X. Li, T. Wang, *Polym Chem* **2017**, *8*, 6134-6142.
- [83] K. Suyama, H. Tachi, *J Photopolym Sci Tec* **2018**, *31*, 517-522.
- [84] W. W. Qiu, M. Q. Li, Y. N. Yang, Z. Q. Li, K. Dietliker, *Polym Chem* **2020**, *11*, 1356-1363.
- [85] R. Zhou, X. Sun, R. Mhanna, J.-P. Malval, M. Jin, H. Pan, D. Wan, F. Morlet-Savary, H. Chaumeil, C. Joyeux, *ACS Appl. Polym. Mater.* **2020**, *2*, 2077-2085.
- [86] Y. Iwai, K. Kunita, (Fujifilm Corporation, Japan), US20070212643A1, **2007**.
- [87] C. Schmitz, Laser- und LED-initiierte NIR-Photopolymerisation mit Thermischen und Photonischen Prozessen für Beschichtungen (Duisburg Essen), **2016**.
- [88] D. Oprych, C. Schmitz, C. Ley, X. Allonas, E. Ermilov, R. Erdmann, B. Strehmel, *ChemPhotoChem* **2019**, *3*, 1119-1126.
- [89] J. Zhu, Q. Zhang, T. Yang, Y. Liu, R. Liu, *Nat. Commun.* **2020**, *11*, 3462.
- [90] D. Abliz, Y. G. Duan, L. Steuernagel, L. Xie, D. C. Li, G. Ziegmann, *Polym Polym Compos* **2013**, *21*, 341-348.
- [91] M. Moulin, J. Huang, (Kodak Polychrome Graphics LLC, Switz.), 20030151657A1, **2003**.
- [92] M. Moulin, (Kodak Polychrome Graphics LLC, Switz.), US20040047025A1, **2004**.
- [93] P. Lee, Advancements in UV LED Curing Technology and Solutions for Print, UV+EB Technology, **2015**.
- [94] F. M. Christian Dreyer, *III-Nitride Ultraviolet Emitters Technology and Applications, Vol. 227* (Ed.: J. R. Michael Kneissl ), **2016**, 415-431.
- [95] C. Schmitz, T. Poplata, A. Feilen, B. Strehmel, *Prog Org Coat* **2020**, *144*, 105663.
- [96] C. Schmitz, Y. Pang, A. Gülz, M. Gläser, J. Horst, M. Jäger, B. Strehmel, *Angew. Chem., Int. Ed.* **2019**, *58*, 4400-4404.
- [97] J. V. Crivello, *Adv Polym Sci* **1984**, *62*, 1-48.

- [98] F. Castellanos, J. P. Fouassier, C. Priou, J. Cavezzan, *J. Appl. Polym. Sci.* **1996**, *60*, 705-713.
- [99] U. Bulut, J. V. Crivello, *J Polym Sci Pol Chem* **2005**, *43*, 3205-3220.
- [100] J. V. Crivello, U. Bulut, *Des Monomers Polym* **2005**, *8*, 517-531.
- [101] J. V. Crivello, *J Polym Sci Pol Chem* **2009**, *47*, 5639-5651.
- [102] R. Acosta Ortiz, L. Elizalde Herrera, J. V. Crivello, *J. Macromol. Sci., Pure Appl. Chem.* **2004**, *A41*, 757-777.
- [103] U. Bulut, J. V. Crivello, *Macromolecules* **2005**, *38*, 3584-3595.
- [104] J. V. Crivello, *J Polym Sci Pol Chem* **2014**, *52*, 2934-2946.
- [105] J. V. Crivello, *Polymer* **2015**, *64*, 227-233.
- [106] B. Corakci, S. O. Hacioglu, L. Toppare, U. Bulut, *Polymer* **2013**, *54*, 3182-3187.
- [107] G. Liu, X. Zhu, B. Xu, X. Qian, G. Song, J. Nie, *J. Appl. Polym. Sci.* **2013**, *130*, 3698-3703.
- [108] N. Klikovits, R. Liska, A. D'Anna, M. Sangermano, *Macromol Chem Phys* **2017**, *218*.
- [109] J. V. Crivello, *J Photopolym Sci Tec* **2009**, *22*, 575-582.
- [110] J. V. Crivello, *J Polym Sci Pol Chem* **2015**, *53*, 594-601.
- [111] J. V. Crivello, *Polymer* **2005**, *46*, 12109-12117.
- [112] J. V. Crivello, *J Polym Sci Pol Chem* **2007**, *45*, 4331-4340.
- [113] J. V. Crivello, *J Polym Sci Pol Chem* **2015**, *53*, 586-593.
- [114] K. W. Tsai, M. K. Hung, Y. H. Mao, S. A. Chen, *Adv Funct Mater* **2019**, *29*.
- [115] Y. Pang, A. Shiraishi, D. Keil, S. Popov, V. Strehmel, H. Jao, J. S. Gutmann, Y. Zou, B. Strehmel, *Angew. Chem. Int. Ed.* **2020**, <https://doi.org/10.1002/anie.202010746>.
- [116] F. Chen, W. D. Cook, *Eur. Polym. J.* **2008**, *44*, 1796-1813.
- [117] I. Krossing, I. Raabe, *Angew. Chem., Int. Ed.* **2004**, *116*, 2116-2142.
- [118] Y. Pang, S. Fan, Q. Wang, D. Oprych, A. Feilen, K. Reiner, D. Keil, Y. L. Slominski, S. Popov, Y. Zou, B. Strehmel, *Angew. Chem., Int. Ed.* **2020**, *59*, 11440-11447.
- [119] J. P. Fouassier, X. Allonas, D. Burget, *Prog Org Coat* **2003**, *47*, 16-36.
- [120] Y. Yagci, S. Jockusch, N. J. Turro, *Macromolecules* **2010**, *43*, 6245-6260.
- [121] Gigahertz-Optik, <https://www.gigahertz-optik.de/en-us/basics-light-measurement/light-color/opt-rad-wavelength-range/>.
- [122] R. B. Price, *Dental Clinics* **2017**, *61*, 751-778.
- [123] F. A. Rueggeberg, M. Giannini, C. A. G. Arrais, R. B. T. Price, *Braz Oral Res* **2017**, *31*, 64-91.
- [124] C. P. Ernst, R. B. Price, A. Callaway, A. Masek, H. Schwarm, I. Rullmann, B. Willershausen, V. Ehlers, *J Adhes Dent* **2018**, *20*, 41-55.
- [125] Minamata Convention on Mercury Text and Annexes, U. N. E. Programme, <http://www.mercury-convention.org> **2019.09**.
- [126] Y. Muramoto, M. Kimura, S. Nouda, *Semicond Sci Tech* **2014**, *29*.
- [127] K. B. A Khan, *Comprehensive Semiconductor Science and Technology: Online version*, Elsevier B.V., **2011**.
- [128] M. Kneissl, *III-Nitride Ultraviolet Emitters Technology and Applications* (Ed.: J. R. Michael Kneissl ), Springer, **2016**, pp. 1-18.
- [129] F. J. Arques-Orobon, N. Nunez, M. Vazquez, C. Segura-Antunez, V. Gonzalez-Posadas, *Solid State Electron* **2015**, *111*, 111-117.
- [130] G. Tangdionga, UV/EB Technology, <https://uvebtech.com/articles/2020/uv-led-curing-systems-measuring-accurately-and-eliminating-safety-hazards/>, **2020**.
- [131] Allied Markt Research, UV LED Market Report, <https://www.finanznachrichten.de/nachrichten-2019-11/48205421-uv-led-market-to-reach-dollar-1-2-bn-globally-by-2026-at-17-3-cagr-allied-market-research-008.htm>, **2019**.
- [132] C.-K. Huang, J.-G. Sung, 2009 4th International Microsystems, Packaging, Assembly and Circuits Technology Conference, *IEEE*, **2009**, 613-616.
- [133] M. Schreiner, J. Martínez-Abaigar, J. Glaab, M. Jansen, *Optik & Photonik* **2014**, *9*, 34-37.

- [134] V. Landry, P. Blanchet, G. Boivin, J. F. Bouffard, M. Vlad, *Coatings* **2015**, *5*, 1019-1033.
- [135] G. Malucelli, *Current Organic Chemistry* **2017**, *21*, 2314-2321.
- [136] V. Strongone, M. Bartoli, P. Jagdale, R. Arrigo, A. Tagliaferro, G. Malucelli, *Polymers* **2020**, *12*, 796.
- [137] W.-S. Won, W.-T. Park, K.-K. Kim, C. S. Shin, N. Kim, Y.-J. Kim, Y.-J. Yoon, *Int J Pr Eng Man* **2018**, *19*, 1901-1915.
- [138] M. Würtele, T. Kolbe, M. Lipsz, A. Külberg, M. Weyers, M. Kneissl, M. Jekel, *Water research* **2011**, *45*, 1481-1489
- [139] L. Liao, Z. Li, T. Lang, B. M. Sadler, G. Chen, *Laser Communication and Propagation through the Atmosphere and Oceans III*, Vol. 9224, International Society for Optics and Photonics, **2014**, p. 92241A.
- [140] K. Song, M. Mohseni, F. Taghipour, *Water research* **2016**, *94*, 341-349.
- [141] K. Balakrishnan, K.-X. Sun, A. Alfauwaz, A. Aljadaan, M. Almajeed, M. Alrufaydah, S. Althubiti, H. Aljabreen, S. Buchman, R. L. Byer, *arXiv preprint arXiv:1202.0585* **2012**.
- [142] A. Prasad, L. H. Du, M. Zubair, S. Subedi, A. Ullah, M. S. Roopesh, *Food Eng Rev* **2020**, *12*, 268-289
- [143] Y. Zuo, J. Zhang, *Applied Sciences* **2019**, *9*, 1.
- [144] K. Kishi, *Three Bond Technical News*, **1995**, *45*, 1-7.
- [145] C.-J. Carling, J.-C. Boyer, N. R. Branda, *J. Am. Chem. Soc* **2009**, *131*, 10838-10839.
- [146] C. Shimokawa, B. Sullivan, M. L. Turbino, C. J. Soares, R. B. Price, *Oper Dent* **2017**, *42*, 537-547.
- [147] M. Par, I. Repusic, H. Skenderovic, Z. Tarle, *Clin Oral Investig* **2019**, *23*, 4399-4409.
- [148] F. A. Rueggeberg, *Dent Mater* **2011**, *27*, 39-52.
- [149] C. S. Sampaio, P. J. Atria, F. A. Rueggeberg, S. Yamaguchi, M. Giannini, P. G. Coelho, R. Hirata, R. M. Puppini-Rontani, *Dent Mater* **2017**, *33*, 796-804.
- [150] T. Taki, M. Strassburg, *Ecs J Solid State Sc* **2019**, *9*.
- [151] K. Bukovinszky, M. Szaloki, I. Csarnovics, I. Szabo, S. Keki, M. Nagy, C. Hegedus, *Adv Cond Matter Phys* **2018**, *2018*.
- [152] C. Kütahya, N. Meckbach, V. Strehmel, J. S. Gutmann, B. Strehmel, *Chem. Eur. J.* **2020**, *26*, 10444-10451.
- [153] J. H. Kelly, *Ullmann's Encyclopedia of Industrial Chemistry*, Wiley-VCH, **2000**, pp. 1-18.
- [154] G. Hauck, C. Savariar-Hauck, H.-J. Timpe, (Kodak Polychrome Graphics G.m.b.H., Germany). US6309792B1, **2000**.
- [155] S. Zhang, B. Li, L. Tang, X. Wang, D. Liu, Q. Zhou, *Polymer* **2001**, *42*, 7575-7582.
- [156] Y. Chen, J. Zhang, X. Liu, S. Wang, J. Tao, Y. Huang, W. Wu, Y. Li, K. Zhou, X. Wei, *Sci. Adv.* **2020**, *6*, eaba 7406.
- [157] K. K. Rohatgi-Mukherjee, *Fundamentals of Photochemistry*. Wiley Eastern Ltd., New Delhi, Bangalore, Bombay 1978.
- [158] A. Albini, *Photochem. Photobiol. Sci.* **2016**, *15*, 319-324.
- [159] J. R. Bolton, *Ultraviolet Applications Handbook*, 3rd ed., ICC Lifelong Learn Inc., **2010**.
- [160] G. J. Kavarnos, N. J. Turro, *Chem Rev* **1986**, *86*, 401-449.
- [161] G. J. Kavarnos, *Photoinduced Electron Transfer I* (Ed.: J. Mattay), Springer Berlin Heidelberg, Berlin, Heidelberg, **1990**, 21-58.
- [162] N. J. Turro, V. Ramamurthy, J. C. Scaiano, *Principles of Molecular Photochemistry*, University Science Books, Sausalito, **2009**.
- [163] K. Dietliker, J. Baro, *Handbook of Industrial Inkjet Printing: A Full System Approach (Eds.: W Zapka)*, Wiley VCH, **2017**, 59-116.
- [164] N. Arsu, J. Kabatc, J. Ortyl, D. Avci, P. Xiao, J. Lalevee, F. Dumur, T. Junkers, M. Sangermano, E. Andrzejewska, *Photopolymerisation Initiating Systems*, (Eds.: J. Lalevée, J.-P. Fouassier), Royal Society of Chemistry, **2018**.
- [165] C. A. Ballhausen, H. B. Gray, *Molecular Orbital Theory: An Introductory Lecture Note and Reprint Volume*, WA Benjamin, Inc., **1965**.

- [166] C. Dursun, M. Degirmenci, Y. Yagci, S. Jockusch, N. J. Turro, *Polymer* **2003**, *44*, 7389-7396.
- [167] M. A. Tasdelen, J. Lalevee, Y. Yagci, *Polym Chem* **2020**, *11*, 1111-1121.
- [168] B. Ganster, U. K. Fischer, N. Moszner, R. Liska, *Macromol Rapid Commun* **2008**, *29*, 57-62.
- [169] D. Neshchadin, A. Rosspeintner, M. Griesser, B. Lang, S. Mosquera-Vazquez, E. Vauthey, V. Gorelik, R. Liska, C. Hametner, B. Ganster, R. Saf, N. Moszner, G. Gescheidt, *J. Am. Chem. Soc* **2013**, *135*, 17314-17321.
- [170] J. Radebner, A. Eibel, M. Leybold, C. Gorsche, L. Schuh, R. Fischer, A. Torvisco, D. Neshchadin, R. Geier, N. Moszner, R. Liska, G. Gescheidt, M. Haas, H. Stueger, *Angew Chem Int Edit* **2017**, *56*, 3103-3107.
- [171] M. Haas, J. Radebner, A. Eibel, G. Gescheidt, H. Stueger, *Chem-Eur J* **2018**, *24*, 8258-8267.
- [172] M. Mitterbauer, M. Haas, H. Stuger, N. Moszner, R. Liska, *Macromol Mater Eng* **2017**, *302*.
- [173] M. Mitterbauer, P. Knaack, S. Naumov, M. Markovic, A. Ovsianikov, N. Moszner, R. Liska, *Angew Chem Int Edit* **2018**, *57*, 12146-12150.
- [174] J. Radebner, A. Eibel, M. Leybold, N. Jungwirth, T. Pickl, A. Torvisco, R. Fischer, U. K. Fischer, N. Moszner, G. Gescheidt, H. Stueger, M. Haas, *Chem-Eur J* **2018**, *24*, 8281-8285.
- [175] Y. Y. Durmaz, M. Kukut, N. Moszner, Y. Yagci, *J Polym Sci Pol Chem* **2009**, *47*, 4793-4799.
- [176] A. Eibel, J. Radebner, M. Haas, D. E. Fast, H. Freissmuth, E. Stadler, P. Faschauner, A. Torvisco, I. Lamparth, N. Moszner, H. Stueger, G. Gescheidt, *Polym Chem* **2018**, *9*, 38-47.
- [177] J. V. Crivello, J. H. W. Lam, *Macromolecules* **1977**, *10*, 1307-1315.
- [178] J. V. Crivello, J. H. W. Lam, *J Polym Sci Pol Chem* **1979**, *17*, 977-999.
- [179] J. V. Crivello, *J Polym Sci Pol Chem* **1999**, *37*, 4241-4254.
- [180] H. Okamura, Y. Watanabe, M. Tsunooka, M. Shirai, T. Fujiki, S. Kawasaki, M. Yamada, *J Photopolym Sci Tec* **2002**, *15*, 145-152.
- [181] E. Torti, G. Della Giustina, S. Protti, D. Merli, G. Brusatin, M. Fagnoni, *Rsc Advances* **2015**, *5*, 33239-33248.
- [182] N. Zivic, P. K. Kuroishi, F. Dumur, D. Gigmes, A. P. Dove, H. Sardon, *Angew Chem Int Edit* **2019**, *58*, 10410-10422.
- [183] D. Schulte-Frohlinde, H. Blume, *Zeitschrift für Physikalische Chemie* **1968**, *59*, 299-315.
- [184] D. Schulte-Frohlinde, H. Blume, *Zeitschrift für Physikalische Chemie* **1968**, *59*, 282-298.
- [185] K. Kaya, J. Kreutzer, Y. Yagci, *J Polym Sci A Polym Chem* **2018**, *56*, 451-457.
- [186] K. Kaya, J. Kreutzer, Y. Yagci, *ChemPhotoChem* **2019**, *3*, 1187-1192.
- [187] W. Zhou, S. M. Kuebler, K. L. Braun, T. Yu, J. K. Cammack, C. K. Ober, J. W. Perry, S. R. Marder, *Science* **2002**, *296*, 1106-1109.
- [188] A. Mejiritski, A. Y. Polykarpov, A. M. Sarker, D. C. Neckers, *Chem. Mater.* **1996**, *8*, 1360-1362.
- [189] F. Song, X. Peng, E. Lu, Y. Wang, W. Zhou, J. Fan, *Tetrahedron Lett.* **2005**, *46*, 4817-4820.
- [190] R. A. Marcus, N. Sutin, *Biochim Biophys Acta* **1985**, *811*, 265-322.
- [191] H. J. Hageman, *Prog Org Coat* **1985**, *13*, 123-150.
- [192] H. F. Gruber, *Prog Polym Sci* **1992**, *17*, 953-1044.
- [193] A. H. Bonardi, F. Dumur, D. Gigmes, Y. Y. Xu, J. Lalevee, *Acs Omega* **2020**, *5*, 3043-3046.
- [194] P. E. Sundell, S. Jönsson, A. Hult, *J Polym Sci A Polym Chem* **1991**, *29*, 1535-1543.
- [195] J. V. Crivello, J. Ahn, *J Polym Sci Pol Chem* **2003**, *41*, 2570-2587.
- [196] S. Chen, W. D. Cook, F. Chen, *Polym Int* **2007**, *56*, 1423-1431.
- [197] J. Boucart, E. Zibik, S. Renz, B. Sverdlov, M. Kearley, D. Inder, C. Button, N. Lichtenstein, in *Novel In-Plane Semiconductor Lasers X, Vol. 7953*, International Society for Optics and Photonics, **2011**, p. 79531E.
- [198] Y. Chiu, D. Cheng, J. Lin, K. Chen, H. Liu, *IEEE Access* **2020**, *8*, 83465-83471.
- [199] H. Mastroph, S. Ernst, B. Senns, A. D. Towns, *Color. Technol.* **2015**, *131*, 9-26.
- [200] H. Mastroph, *Phys. Sci. Rev* **2020**, 20190145.
- [201] H. A. Shindy, *Dyes Pigm* **2017**, *145*, 505-513.

- [202] M. Heinz, *Phys. Sci. Rev* **2019**, 4, 20190040.
- [203] G. Bach, S. Daehne, *Second Supplements to the 2nd Edition of Rodd's Chemistry of Carbon Compounds*, Elsevier, **1991**, 383-481.
- [204] A. Mishra, R. K. Behera, P. K. Behera, B. K. Mishra, G. B. Behera, *Chem Rev* **2000**, 100, 1973-2011.
- [205] H. A. Shindy, *Mini-Rev Org Chem* **2012**, 9, 352-360.
- [206] M. Heinz, *Phys. Sci. Rev* **2019**, 5, 20190084.
- [207] H. Mustroph, *Ullmann's Encyclopedia of Industrial Chemistry*, Wiley-VCH, **2014**, 1-38.
- [208] W. König, *Angew. Chem. Int. Ed.* **1925**, 38, 743-748.
- [209] J. Fabian, H. Nakazumi, M. Matsuoka, *Chem Rev* **1992**, 92, 1197-1226.
- [210] M. Doja, *Chem Rev* **1932**, 11, 273-321.
- [211] C. H. Shi, J. B. Wu, D. F. Pan, *J Biomed Opt* **2016**, 21.
- [212] H. Mustroph, M. Stollenwerk, V. Bressau, *Angew Chem Int Edit* **2006**, 45, 2016-2035.
- [213] A. P. Gorka, R. R. Nani, J. Zhu, S. Mackem, M. J. Schnermann, *J. Am. Chem. Soc* **2014**, 136, 14153-14159.
- [214] H. Mustroph, *ChemPhysChem* **2016**, 17, 2616-2629.
- [215] D. D. Dlott, *J Lumin* **1990**, 45, 397-400.
- [216] Y. V. Aulin, M. Liu, P. Piotrowiak, *J Phys Chem Lett* **2019**, 10, 2434-2438.
- [217] H. Baumann, B. Strehmel, U. Dwars, U. Müller, (Kodak Polychrome Graphics G.m.b.H., Germany), DE 102006000783 B3, **2007**.
- [218] H. Baumann, B. Strehmel, D. Pietsch, U. Dwars, T. Ebhardt, A. Draber, (Eastman Kodak Company, USA), US20080248424A1, **2011**.
- [219] J. Crivello, J. Lam, *J Polym Sci A Polym Chem* **1978**, 16, 2441-2451.
- [220] D. C. Neckers, Y. Bi, (SpectraGroupLimited,Inc., Maumee,Ohio), US5639803, **1997**.
- [221] V. Bardinal, B. Reig, T. Camps, E. Daran, J. B. Doucet, C. Turck, J. P. Malval, D. J. Lougnot, O. Soppera, *Appl Phys Lett* **2010**, 96, 051114.
- [222] D. Barat, V. Bardinal, I. Dika, O. Soppera, A. Romyantseva, B. Reig, M. Renault, A. Bruyant, J. B. Doucet, T. Camps, *Microelectron Eng* **2013**, 111, 204-209.
- [223] G. W. G. Byers, S; Henrichs, P.M., *Photochem Photobiol* **1976**, 23, 37-43.
- [224] P. Chen, J. Li, Z. Qian, D. Zheng, T. Okasaki, M. Hayami, *Dyes Pigm* **1998**, 37, 213-222.
- [225] M. Henary, M. Mojzych, in *Heterocyclic Polymethine Dyes: Synthesis, Properties and Applications* (Ed.: L. Strekowski), Springer Berlin Heidelberg, Berlin, Heidelberg, **2008**, pp. 221-238.
- [226] A. Samanta, M. Vendrell, R. Das, Y. T. Chang, *ChemComm* **2010**, 46, 7406-7408.
- [227] H. J. Timpe, P. Filo, H. Baumann, B. Strehmel, *Z. Chem.* **1983**, 23, 102-103.
- [228] K. Feng, H. Zang, D. Martin, T. L. Marino, D. C. Neckers, *J Polym Sci A Polym Chem* **1998**, 36, 1667-1677.
- [229] A. Shirai, H. Kubo, E. Takahashi, *J Photopolym Sci Tec* **2002**, 15, 29-34.
- [230] Y. Yagci, *Macromol Symp* **2006**, 240, 93-101.
- [231] J. V. Crivello, *Iodine Chemistry and Applications (Eds.: Tatsuo Kaiho)*, John Wiley & Sons, Inc., **2014**, 459.
- [232] J. V. L. Crivello, T.P.; Lee, J.L., *J Polym Sci A Polym Chem* **1983**, 21, 97-109.
- [233] J. Ortyl, R. Popielarz, *Polimery* **2012**, 57, 510-517.
- [234] H. Mokbel, J. Toufaily, T. Hamieh, F. Dumur, D. Campolo, D. Gignes, J. Pierre Fouassier, J. Ortyl, J. Lalevée, *J Appl Polym Sci* **2015**, 132,1-10.
- [235] P. O. Boeira, C. T. W. Meereis, C. E. C. Suárez, S. M. de Almeida, E. Piva, G. da Silveira Lima, *Appl Adhes Sci* **2017**, 5, 1-11.
- [236] P. Garra, A. Baralle, B. Graff, G. Schrodj, F. Morlet-Savary, C. Dietlin, J. P. Fouassier, J. Lalevee, *Macromolecules* **2018**, 51, 8899-8911.
- [237] J. P. Fouassier, D. Burr, J. V. Crivello, *J Macromol Sci Pure* **1994**, A31, 677-701.



- [238] R. J. Devoe, M. R. V. Sahyun, N. Serpone, D. K. Sharma, *Can J Chem* **1987**, *65*, 2342-2349.
- [239] H. J. Timpe, V. Schikowsky, *J Prakt Chem*. **1989**, *331*, 447-460.
- [240] J. L. Dektar, N. P. Hacker, *J Org Chem* **1990**, *55*, 639-647.
- [241] J. L. Dektar, N. P. Hacker, *J Org Chem* **1991**, *56*, 1838-1844.
- [242] Y. Y. Durmaz, N. Moszner, Y. Yagci, *Macromolecules* **2008**, *41*, 6714-6718.
- [243] J. Crivello, *Dyes and Chromophores in Polymer Science (Eds.: J. Lalevée, J.-P. Fouassier)*, John Wiley & Sons, Inc., **2015**, 45-79.
- [244] J. Kirschner, J. Paillard, M. Bouzrati-Zerelli, J. M. Becht, J. E. Klee, S. Chelli, S. Lakhdar, J. Lalevee, *Molecules* **2019**, *24*.
- [245] X. Zuo, F. Morlet-Savary, B. Graff, N. Blanchard, J.-P. Goddard, J. Lalevée, *Macromol Rapid Commun* **2016**, *37*, 840-844.
- [246] C. Kütahya, P. Wang, S. Li, S. Liu, J. Li, Z. Chen, B. Strehmel, *Angew Chem Int Edit* **2020**, *59*, 3166-3171.
- [247] H.-G. Heine, H.-J. Traenckner, *Prog Org Coat* **1975**, *3*, 115-139.
- [248] Y. Pang, Y. Zou, S. Fan, (Hubei Gurun Technology Co., Ltd., Peop. Rep. China), CN110330501A, **2019**.
- [249] Y. Pang, Y. Zou, S. Fan, (Hubei Gurun Technology Co., Ltd., Peop. Rep. China), CN110551098A, **2019**.
- [250] Y. Pang, Y. Zou, S. Fan, M. Gao, Y. Xin, (Hubei Gurun Technology Co., Peop. Rep. China), US20200148660A1, **2019**.
- [251] P. Garra, A. Caron, A. Al Mousawi, B. Graff, F. Morlet-Savary, C. Dietlin, Y. Yagci, J. P. Fouassier, J. Lalevee, *Macromolecules* **2018**, *51*, 7872-7880.
- [252] P. Garra, B. Graff, F. Morlet-Savary, C. Dietlin, J. M. Becht, J. P. Fouassier, J. Lalevee, *Macromolecules* **2018**, *51*, 57-70.
- [253] D. X. Wang, P. Garra, J. P. Fouassier, B. Graff, Y. Yagci, J. Lalevee, *Polym Chem* **2019**, *10*, 4991-5000.
- [254] D. X. Wang, K. Kaya, P. Garra, J. P. Fouassier, B. Graff, Y. Yagci, J. Lalevee, *Polym Chem* **2019**, *10*, 4690-4698.
- [255] D. Wang, P. Garra, S. Lakhdar, B. Graff, J. P. Fouassier, H. Mokbel, M. Abdallah, J. Lalevée, *ACS Appl. Polym. Mater* **2019**, *1*, 561-570.
- [256] A. Baralle, P. Garra, F. Morlet-Savary, C. Dietlin, J.-P. Fouassier, J. Lalevée, *Macromol Rapid Commun* **2020**, *41*, 1900644.
- [257] I. M. Riddlestone, A. Kraft, J. Schaefer, I. Krossing, *Angew Chem Int Edit* **2018**, *57*, 13982-14024.
- [258] O. Škola, B. Jašúrek, D. Veselý, P. Němec, *Prog Org Coat* **2016**, *101*, 279-287.
- [259] J. V. Crivello, D. A. Conlon, *J Polym Sci A Polym Chem* **1983**, *21*, 1785-1799.
- [260] S. Sugihara, Y. Kawamoto, Y. Maeda, *Macromolecules* **2016**, *49*, 1563-1574.
- [261] M. Younes, S. Wartewig, D. Lellinger, B. Strehmel, V. Strehmel, *Polymer* **1994**, *35*, 5269-5278.
- [262] C. Decker, T. T. N. Viet, H. P. Thi, *Polym Int* **2001**, *50*, 986-997.
- [263] H. Sasaki, J. V. Crivello, *J Macromol Sci Pure* **1992**, *29*, 915-930.
- [264] K. S. Anseth, C. M. Wang, C. N. Bowman, *Macromolecules* **1994**, *27*, 650-655.
- [265] D. S. Esen, F. Karasu, N. Arsu, *Prog Org Coat* **2011**, *70*, 102-107.
- [266] P. Siders, R. A. Marcus, *J. Am. Chem. Soc* **1981**, *103*, 741-747.
- [267] R. A. Marcus, *Angew Chem Int Edit* **1993**, *32*, 11.
- [268] R. S. Lepkowicz, C. M. Cirloganu, J. Fu, O. V. Przhonska, D. J. Hagan, E. W. Van Stryland, M. V. Bondar, Y. L. Slominsky, A. D. Kachkovski, *J Opt Soc Am B* **2005**, *22*, 2664-2685.
- [269] S. Motofuji, S. Higuchi, A. Shiraiishi, T. Mukai, M. Sakakibara, (Sanyo Chemical Industries, Ltd., Japan), US8853290B2, **2010**.
- [270] N. Klikovits, P. Knaack, D. Bomze, I. Krossing, R. Liska, *Polym Chem* **2017**, *8*, 4414-4421.
- [271] L. H. Sperling, *Adv Chem Ser* **1994**, *239*, 3-38.

- [272] J. P. Fouassier, J. Lalevee, *Polymers* **2014**, *6*, 2588-2610.
- [273] G. Odian, *Principles of Polymerization*, John Wiley & Sons, Hoboken, **1981**.
- [274] J. V. Crivello, H. Sasaki, *J Macromol Sci Pure* **1993**, *A30*, 189-206.
- [275] J. V. Crivello, *J Polym Sci Pol Chem* **2015**, *53*, 1854-1861.
- [276] O. Solomeshch, V. Medvedev, P. R. Mackie, D. Cupertino, A. Razin, N. Tessler, *Adv Funct Mater* **2006**, *16*, 2095-2102.
- [277] B. M. I. van der Zande, S. J. Roosendaal, C. Doornkamp, J. Steenbakkens, J. Lub, *Adv Funct Mater* **2006**, *16*, 791-798.
- [278] D. Credgington, O. Fenwick, A. Charas, J. Morgado, K. Suhling, F. Cacialli, *Adv Funct Mater* **2010**, *20*, 2842-2847.
- [279] A. Kohnen, N. Riegel, D. C. Muller, M. Klaus, *Adv Mater* **2011**, *23*, 4301-4305.
- [280] C. Austen Angell, Y. Ansari, Z. Zhao, *Faraday Discussions* **2012**, *154*, 9-27.
- [281] V. Strehmel, S. Berdzinski, H. Rexhausen, *J Mol Liq* **2014**, *192*, 153-170.
- [282] W. Hehre, S. Ohlinger, *Spartan'16*, Wavefunction, Inc., Irvine, **2016**.
- [283] C. Z. Chen, B.; Lu, D.; Xu, G., *J. Photochem Photobiol A* **1995**, *89*, 25-29

## Acknowledgements

I would like to thank Niederrhein University of Applied Sciences giving me the opportunity to pursue this thesis in cooperation with the Duisburg-Essen University. This was a great opportunity for me to extend my knowledge in both fundamental and applied chemistry study. Therefore, I would like to thank the Vize President for Research, Prof. Dr. Dr. Dr. A. Prange, who has managed the Promotionskolleg at Niederrhein University of Applied Sciences. Founding was received by the County of North-Rhine Westphalia. Furthermore, we acknowledge the Project D–NL–HIT carried out in the framework of the INTERREG–Program Deutschland–Nederland. This project helped to extend my viewpoint to receive more experience in cooperation with industrial partners. I also would like to thank FEW Chemicals GmbH with who we published three nice articles together. In addition, my thanks goes also to Phoseon Ltd. and Easytec GmbH who provided the prototypes of the high-power LEDs for my research studies. Furthermore, I very much acknowledge Dr. S. Popov from Spectrum Info Ltd., who provided samples for exposure using the 860 nm LED. I also would like to thank Gurun Technology Ltd who provided monomers for my PhD research. Finally, I would like to show my appreciation to my supervisors, Prof. Dr. Strehmel and Prof. Dr. J. S. Gutmann, who give me a lot of support and encouragement during the time of the thesis.

## **Curriculum Vitae**

The curriculum vitae is not included in the online version for data protection reasons

The curriculum vitae is not included in the online version for data protection reasons

The curriculum vitae is not included in the online version for data protection reasons